Copy No. 9

DEFENCE DÉFENSE

Experimental and Numerical Investigation into Fatigue Crack Propagation Models for 350WT Steel

D.A.Trask

DalTech

DEFENCE RESEARCH ESTABLISHMENT ATLANTIC

Contractor Report
DREA CR/98/436
June 2000

National Defence Défense nationale

Canada

THIS IS AN UNEDITED REPORT ON SCIENTIFIC OR TECHNICAL WORK CONTRACTED BY THE DEFENCE RESEARCH ESTABLISHMENT ATLANTIC OF THE RESEARCH AND DEVELOPMENT BRANCH OF THE DEPARTMENT OF NATIONAL DEFENCE, CANADA.

THE CONTENTS OF THE REPORT ARE THE RESPONSIBILITY OF THE CONTRACTOR, AND DO NOT NECESSARILY REFLECT THE OFFICIAL POLICIES OF THE DEPARTMENT OF NATIONAL DEFENCE.

PLEASE DIRECT ENQUIRIES TO:

THE DIRECTOR GENERAL
DEFENCE RESEARCH ESTABLISHMENT ATLANTIC
P.O. BOX 1012
DARTMOUTH, NOVA SCOTIA, CANADA
B2Y 3Z7

Experimental and Numerical Investigation into Fatigue Crack Propagation Models for 350WT Steel

D A. Trask
DalTech

Defence Research Establishment Atlantic

Contract Report
DREA CR/98/436
June 2000

Author

D. A. Trask

Approved by

Neil Pegg

N. G. Pegg

Scientific Authority

Approved for release by

Walter E Ellis

Walter E. Ellis

Chair, DREA Document Review Panel

© Her Majesty the Queen as represented by the Minister of National Defence, 2000

© Sa majesté la reine, représentée par le ministre de la Défense nationale, 2000

TABLE OF CONTENTS

Page

TABLE OF CONTENTS ii

LIST OF TABLES vii

LIST OF FIGURES ix

LIST OF ABBREVIATIONS AND SYMBOLS xiii

ACKNOWLEDGEMENTS xvi

ABSTRACT xvii

1. INTRODUCTION 1
   - 1.1 Background 1
   - 1.2 Design and Analysis Methods 2
   - 1.3 Objectives 3

2. PART A – THEORETICAL BACKGROUND 6
   - 2.1 Fracture Mechanics 6
     - 2.1.1 Introduction 6
     - 2.1.2 Linear Elastic Fracture Mechanics 7
       - 2.1.2.1 Stress Intensity Factor 8
       - 2.1.2.2 Strain Energy Release Rate 11
       - 2.1.2.3 Plastic Zone Adjustment 13
     - 2.1.3 Elastic Plastic Fracture Mechanics 16
       - 2.1.3.1 The *J* Contour Integral 17
       - 2.1.3.2 Crack Tip Opening Displacement 18
     - 2.1.4 LEFM Versus EPFM 19
   - 2.2 Fatigue 20
     - 2.2.1 Introduction 20
     - 2.2.2 Fatigue Loading 21

2.2.2.1 Constant Amplitude Loading 21
2.2.2.2 Variable Amplitude Loading 23
2.2.3 Fatigue Life Curve 24
2.2.4 Fatigue Rate Curve 26
2.2.4.1 Description of Region I 26
2.2.4.2 Description of Region II 27
2.2.4.3 Description of Region III 27

2. PART – B STATE-OF-THE-ART REVIEW OF FATIGUE CRACK PROPAGATION MODELS 28

2.3 Introduction 28
2.4 Constant Amplitude Loading Models 29
2.4.1 Paris Model 29
2.4.2 Walker Model 30
2.4.3 Forman Model 31
2.4.4 Modified Forman Model 32
2.4.5 Collipriest Model 33
2.4.6 McEvily Model 33
2.4.7 Pook and Frost Model 35
2.4.8 Zheng and Hirt Model 35
2.4.9 Wang Model 38
2.4.10 Miller and Gallagher's Review of Fatigue Crack Growth Models 39
2.4.11 Dowling and Begley Model 45
2.5 Summary of Constant Amplitude Loading Models 45
2.6 Variable Amplitude Loading Models 46
2.6.1 Load Interactions 46

2.6.2 Use Constant amplitude Loading Fatigue Crack Growth Models 49

2.6.3 Wheeler Model 49
2.6.4 Willemborg Model 51
2.6.5 Elber Model 52
2.6.6 Barsom Model 54
2.6.7 McEvily Model 55
2.6.8 Ahn's Model 56
2.6.9 Variable Amplitude Load Fatigue Crack Growth Predictions .. 58
2.6.9.1 C.M. Hudson Model 59
2.6.9.2 J.C. Newman Jr. Model 61
2.6.9.3 W.S. Johnson Model 63
2.6.9.4 J.L. Rudd and R.M. Engle Jr. Model 64
2.6.9.5 Chang et al (Model One) 65
2.6.9.6 Chang et al (Model Two) 65
2.6.9.7 Results and Discussion 65
2.7 Summary of Variable Amplitude Loading Models 68

3. EXPERIMENTAL METHOD 69
3.1 Introduction 69
3.2 Test Material 69
3.3 Test Specimen 70
3.3.1 Configuration and Dimensions 70
3.3.2 Specimen Preparation 71
3.4 Test Apparatus 73
3.5 Test Procedure 78

4. EXPERIMENTAL RESULTS AND DATA ANALYSIS 80
4.1 Introduction 80
4.2 Data Reduction 82
4.3 Constant Amplitude Loading Test Results 83

4.4 Constant Amplitude Loading Data Analysis 88
  4.4.1 Paris Model 88
    4.4.1.1 Parameter Evaluation 88
    4.4.1.2 Predictions for Crack Length a_i to a_f 89
    4.4.1.3 Failure Predictions 96
  4.4.2 Walker Model 99
  4.4.3 Fatigue Models Based on Tensile Properties of Material 101
  4.4.4 Summary of Constant Amplitude Models 107
4.5 Variable Amplitude Loading Test Results 108
4.6 Variable Amplitude Loading Data Analysis 113
  4.6.1 Predictions Using Constant Amplitude Model 113
  4.6.2 Delay Model 118
  4.6.3 Wheeler Model 123
  4.6.4 Willemborg Model 124
  4.6.5 Summary of Variable Amplitude Models 127

5. NUMERICAL ANALYSIS 129
5.1 Introduction 129
5.2 Fracture Parameter Evaluation 129
  5.2.1 Introduction 129
  5.2.2 FAST-I 130
    5.2.2.1 Conventional Twelve-Node Isoparametric Element ... 131
    5.2.2.2 Enriched Twelve Node-Isoparametric Element 133
  5.2.3 ENDURE -- Fracture Mechanics Module 134
  5.2.4 Quantitative Comparison of FAST-I and ENDURE 136
5.3 Fatigue Life Evaluation 140
  5.3.1 Introduction 140
  5.3.2 FAST-II 141
  5.3.3 ENDURE – Fatigue Module 141

5.3.4 Quantitative Comparison of FAST-II and ENDURE 142
5.4 Constant Amplitude Loading Predictions 143
5.4.1 Fracture Parameter Analysis 144
5.4.2 Fatigue Life Analysis 155
5.5 Variable Amplitude Loading Predictions 159
5.6 Summary of Numerical Prediction Methods 160

6. CONCLUSIONS AND RECOMMENDATIONS 162
6.1 Conclusions 162
6.2 Recommendations 164

REFERENCES 165

APPENDIX A 169
APPENDIX B 172
APPENDIX C 176
APPENDIX D 183
APPENDIX E 186
APPENDIX F 193

LIST OF TABLES

		Page
Table 2.1	Fatigue crack growth rate descriptions	40
Table 2.2	Life prediction ratios for the full interval	43
Table 2.3	Life prediction interval for the shortened interval	44
Table 2.4	Life prediction mean and standard deviation	44
Table 2.5	Comparison of experimental and predicted crack growth under spectrum loading	62
Table 2.6	Random spectrum round-robin analysis summary	66
Table 2.7	Summary of prediction ratios for each test case	67
Table 3.1	Chemical composition of 350WT steel	70
Table 3.2	Material properties of 350WT steel	70
Table 4.1	Constant amplitude test summary	84
Table 4.2	Summary of Paris model parameters	89
Table 4.3	Summary of Paris predictions for crack length a_i to a_f	95
Table 4.4	Percent errors of Paris predictions for crack length a_i to a_f	95
Table 4.5	Predictions of crack length when yielding occurs	97
Table 4.6	Predictions for a_i to a_y	98
Table 4.7	Comparison of analysis	98
Table 4.8	Predictions using Walker equation	99
Table 4.9	Predictions for crack growth interval a_i to a_f based on Zheng and Hirt Model	105
Table 4.10	Variable amplitude test summary	108
Table 4.11	Summary of Paris predictions for crack length interval a_i to a_f	113
Table 4.12	Number of delay cycles after overload	120
Table 4.13	Predictions based on delay model for crack length interval a_i to a_f	122
Table 4.14	Wheeler model fatigue predictions	124
Table 5.1	Example problem properties	137

Table 5.2 Comparison of fracture parameter evaluations 139
Table 5.3 Comparison of execution time (in seconds) 139
Table 5.4 Comparison of fatigue life predictions 142
Table 5.5 '*a* versus ΔK' values obtained through NISA/ENDURE for the model described in Table 5.1 145
Table 5.6 Numerical verification of width influence 148
Table 5.7 Numerically obtained '*a* versus ΔK' relationship for experimental test specimens 149
Table 5.8 ENDURE fatigue life predictions using one and two curve Paris model 157
Table 5.9 Percent error of ENDURE fatigue life predictions using one and two curve Paris model 157
Table 5.10 FAST-II fatigue life predictions (2.5 mm crack length intervals) 158
Table 5.11 FAST-II fatigue life predictions (1.0 mm crack length intervals) 159
Table A.1 Specimen dimensions 171
Table A.2 Specimen loading scenarios 171

LIST OF FIGURES

		Page
Figure 2.1	Three possible modes of crack loading	6
Figure 2.2	Conditions when LEFM is valid (a) and invalid (b, c and d)	7
Figure 2.3	A crack in an infinitely wide plate	9
Figure 2.4	Effect of thickness on fracture toughness	10
Figure 2.5	Fracturing at constant displacement	12
Figure 2.6	Estimate of plastic zone size	14
Figure 2.7	Path independent contour for elastic body with a crack	17
Figure 2.8	(a) Displacement at the original crack tip and (b) 90° intercept	18
Figure 2.9	Fracture mechanics flow chart	19
Figure 2.10	Constant amplitude loading	21
Figure 2.11	Common stress amplitude loading patterns	22
Figure 2.12	(a) Repeated, (b) Semi-random and (c) Completely random loading patterns	23
Figure 2.13	Stress-life curve	25
Figure 2.14	Typical da/dN versus ΔK curve	26
Figure 2.15	Assumption of the amount of incremental fatigue crack propagation	36
Figure 2.16	Retardation (a) Multiple overloads and (b) Single overloads	47
Figure 2.17	Crack growth behavior for (a) Tension overload (b) Compression – Tension overload (c) Tension – compression overload and (d) Compression underload	48
Figure 2.18	Crack tip yield zones	50
Figure 2.19	Crack closure results for fatigue crack propagation	52
Figure 2.20	Stress spectra	55
Figure 3.1	Layout of specimens	72
Figure 3.2	Loading apparatus	73
Figure 3.3	(a) Top fixture and (b) Bottom fixture	74
Figure 3.4	(a) Specimen grips and (b) Grip to fixture connection	76

Figure 3.5 Travelling microscope and its supporting frame 77

Figure 3.6 Experimental setup 77

Figure 3.7 Close up of experimental setup 78

Figure 4.1 Typical specimen failure (note yielding at edges) 81

Figure 4.2 Crack length versus number of cycles for specimens CAL 2 and CAL 3 86

Figure 4.3 d*a*/dN versus ΔK for specimens CAL 2 and CAL 3 86

Figure 4.4 d*a*/dN versus ΔK for specimens CAL 2 to CAL 6 87

Figure 4.5 Paris based predictions for specimen CAL 2 (a_i to a_f) 90

Figure 4.6 Paris based predictions for specimen CAL 3 (a_i to a_f) 91

Figure 4.7 Paris based predictions for specimen CAL 4 (a_i to a_f) 92

Figure 4.8 Paris based predictions for specimen CAL 5 (a_i to a_f) 93

Figure 4.9 Paris based predictions for specimen CAL 6 (a_i to a_f) 94

Figure 4.10 log C versus log (1 - R) graph for the one curve model 100

Figure 4.11 log C versus log (1 - R) graph for the two curve model 100

Figure 4.12 Comparison of fatigue models based on material tensile properties 104

Figure 4.13 Evaluation of threshold effect on Zheng and Hirt model prediction accuracy 106

Figure 4.14 Comparison of constant and variable amplitude data for $R = 0.10$ 110

Figure 4.15 Comparison of specimens VAL 5 and VAL 6 fatigue rate curves 111

Figure 4.16 Paris predictions for specimens VAL 1 and VAL 2 114

Figure 4.17 Paris predictions for specimens VAL 3 and VAL 4 115

Figure 4.18 Paris predictions for specimens VAL 5 and VAL 6 116

Figure 4.19 Definition of number of delay cycles 119

Figure 4.20 Number of delay cycles versus overload ratio 121

Figure 4.21 Predictions for number of delay cycles 121

Figure 4.22 Willemborg predictions with $\alpha = 3$, $\alpha = 1$ and $\alpha = 3$ & 1 126

Figure 5.1 Twelve-Node isoparametric element 132

Figure 5.2 NISA's crack tip element 135

Figure 5.3 (a) Mesh layout and (b) Accuracy of ΔK with respect to correct value 138

Figure 5.4 Comparison of 'ΔK versus a' values calculated by ENDURE and Equation 5.9 146

Figure 5.5 Comparison of 'ΔK versus a' values for specimen CAL 2 150

Figure 5.6 Comparison of 'ΔK versus a' values for specimen CAL 3 151

Figure 5.7 Comparison of 'ΔK versus a' values for specimen CAL 4 152

Figure 5.8 Comparison of 'ΔK versus a' values for specimen CAL 5 153

Figure 5.9 Comparison of 'ΔK' versus a' values for specimen CAL 6 154

Figure 5.10 Comparison of 'ΔK' versus a' curves for ENDURE's internal function, user supplied data input file and Equation 5.9 156

Figure A.1 Specimen layout 170

Figure B.1 Typical experimental datasheet 173

Figure B.2 Typical data reduction spreadsheet 174

Figure B.3 Typical *a* versus N graph 175

Figure B.4 Typical d*a*/dN versus ΔK graph 175

Figure C.1 Crack length versus cycles for CAL 1 177

Figure C.2 d*a*/dN versus ΔK for CAL 1 177

Figure C.3 Crack length versus cycles for CAL 2 178

Figure C.4 d*a*/dN versus ΔK for CAL 2 178

Figure C.5 Crack length versus cycles for CAL 3 179

Figure C.6 d*a*/dN versus ΔK for CAL 3 179

Figure C.7 Crack length versus cycles for CAL 4 180

Figure C.8 d*a*/dN versus ΔK for CAL 4 180

Figure C.9 Crack length versus cycles for CAL 5 181

Figure C.10 d*a*/dN versus ΔK for CAL 5 181

Figure C.11 Crack length versus cycles for CAL 6 182
Figure C.12 d*a*/dN versus ΔK for CAL 6 182

Figure D.2 Experimental data and Zheng and Hirt's predictions for R = 0.20 184
Figure D.3 Experimental data and Zheng and Hirt's predictions for R = 0.30 185
Figure D.4 Experimental data and Zheng and Hirt's predictions for R = 0.40 185
Figure E.1 Crack length versus cycles for VAL 1 187
Figure E.2 d*a*/dN versus ΔK for VAL 1 187
Figure E.3 Crack length versus cycles for VAL 2 188
Figure E.4 d*a*/dN versus ΔK for VAL 2 188
Figure E.5 Crack length versus cycles for VAL 3 189
Figure E.6 d*a*/dN versus ΔK for VAL 3 189
Figure E.7 Crack length versus cycles for VAL 4 190
Figure E.8 d*a*/dN versus ΔK for VAL 4 190
Figure E.9 Crack length versus cycles for VAL 5 191
Figure E.10 d*a*/dN versus ΔK for VAL 5 191
Figure E.11 Crack length versus cycles for VAL 6 192
Figure E.12 d*a*/dN versus ΔK for VAL 6 192

LIST OF ABBREVIATIONS AND SYMBOLS

APES	Axisymmetric/Planar Elastic Structures
ASTM	American Society for Testing and Materials
a	Crack length
a_f	Final crack length
a_i	Initial crack length
a_{OL}	Crack length when overload is applied
a_p	Crack length to elastic-plastic zone interface
a_y	Crack length when yielding of the uncracked cross-section begins
B	Specimen thickness
C, m	Paris model curve fitting parameters
C_W, m_W, n_W	Walker model curve fitting parameters
CAL	Constant amplitude loading
CTOD	Crack Tip Opening Displacement
DREA	Defense Research Establishment Atlantic
da/dN	Fatigue crack growth rate
E	Young's modulus
EDM	Electrical Discharge Machining
ENDURE	Fracture mechanics and fatigue module for NISA
EPFM	Elastic Plastic Fracture Mechanics
FAST	Fatigue Analysis of STructures
FAST-I	Fracture mechanics module for FAST
FAST-II	Fatigue module for FAST
FEM	Finite element method
G	Strain energy release rate
J	Elastic plastic fracture parameter
K	Stress intensity factor

K_C	Plain strain fracture toughness
K_{max}	Minimum stress intensity factor during fatigue cycle
K_{min}	Maximum stress intensity factor during fatigue cycle
K_{op}	Stress intensity factor corresponding to a fully open crack
L	Specimen length
LEFM	Linear Elastic Fracture Mechanics
MCC	Multiple correlation coefficient
MCCI	Modified Crack Closure Integral
N	Number of fatigue cycles
N_{CA}	Number of constant amplitude loading fatigue cycles
N_D	Number of delay fatigue cycles
N_{if}	Number of fatigue cycles from crack length a_i to a_f
N_{OL}	Number of overload fatigue cycles
$N(\xi,\eta)$	Element shape function
NISA	Numerical Integrated System Analysis (Finite element package)
NOL	Number of applied overloads
NSERC	Natural Science and Engineering Research Council of Canada
OL	Overload
OLR	Overload ratio
P_{max}	Maximum load value during fatigue cycle
P_{min}	Minimum load value during fatigue cycle
P_{op}	Crack opening load
R	Stress ratio
R_y	Crack tip plastic yield zone
RA	Reduction in area at fracture in a tension test
u, v	Element displacement components
VCE	Virtual Crack Extension theory
W	Specimen width
x, y	Element coordinate system

Y	Geometric correction factor
Z_{OL}	Overload plastic zone (Willemborg model symbol)
α, β	Linear regression parameters for delay model
ΔP	Fatigue cyclic load range
ΔK	Stress intensity factor range
ΔK_{eff}	Effective stress intensity factor range
ΔK_{rms}	Root mean square of the stress intensity factor range
ΔK_{th}	Stress intensity factor threshold value
$\Delta\sigma$	Fatigue cyclic stress range
ε_f	Fracture ductility
ϕ_R	Wheeler retardation coefficient
γ	Wheeler shaping exponent
σ_f	Fracture strength
σ_{max}	Maximum stress value
σ_{min}	Minimum stress value
σ_y	Yield stress
σ_u	Ultimate stress
ν	Poisson ratio

ACKNOWLEDGEMENTS

I wish to express appreciation to my supervisor Dr. F. Taheri for his encouragement, guidance and support throughout the course of this study. I also wish to thank the members of my thesis committee, Dr. G. M. C. Lee and Dr. N. Pegg for their help and advice. Appreciation is extended to Defense Research Establishment Atlantic and the Natural Science and Engineering Research Council of Canada for their financial support, without which this thesis would not have been possible.

Special thanks are extended to Mr. J. F. Porter of the DREA Dockyard Laboratory for his assistance in providing requested information and arranging for the electrical discharge machining of the test specimens. I would also like to thank Dr. G. M. C. Lee for providing the test fixture that was used to perform the experiments and Dr. David Stredulinsky for his advice.

I am also much obliged to the following technicians for their assistance in preparing the test samples as well as modifications to the test fixture - Richard Sarty, Mark MacDonald, Blair Nickerson and Stewart MacPherson.

Finally, I would like to thank my fiancée Melinda MacDonald and my family for their encouragement and understanding throughout the course of this study.

ABSTRACT

Fatigue analysis is a complex and uncertain process due to the numerous factors that may influence the crack growth process. The development of a fatigue model is important for planning inspection intervals, determining required maintenance, conducting a failure analysis and minimizing the problem of crack propagation in future designs. Various models have been proposed; however, no universal or all encompassing model exists.

A state-of-the-art literature review of the available fatigue crack propagation models was conducted to identify their advantages, disadvantages and limitations. Emphasis was placed on models that are simple to evaluate and require few (if any) empirical curve fitting parameters.

An experimental fatigue program was conducted, consisting of both a constant and variable amplitude loading phase on 350WT steel. This is an important structural steel with application to ships, bridges, cranes and towers; all of which are subjected to cyclic loading The objective of the constant amplitude loading phase was to establish some baseline fatigue data at various stress ratios and to calibrate the available constant amplitude models. The objective of the variable amplitude loading phase was to quantify the magnitude of retardation when periodic tensile overloads are applied in a constant amplitude loading scenario. The fatigue models examined in the literature review were evaluated (spreadsheet method) and the results compared to those obtained from the experiments.

Two fracture-parameter and two fatigue-life prediction software packages were examined and their limitations and advantages were compared. The fracture-parameter programs use the finite element method to calculate the required parameters for various crack lengths. The fatigue-life prediction programs use the results of the fracture program in conjunction with pre-programmed fatigue models to predict the structures' fatigue life.

The test specimens were evaluated with the numerical programs and the results compared to those obtained from the experiments.

RÉSUMÉ

L'analyse de fatigue est une démarche complexe et approximative à cause des nombreux facteurs qui peuvent influencer le processus de propagation des fissures. Il est important d'élaborer un modèle de fatigue qui aidera à planifier les intervalles d'inspection, à déterminer les mesures requises pour l'entretien, à effectuer une analyse de défaillance et à minimiser le problème de propagation des fissures lors de futures études de conception. Divers modèles ont été proposés mais il n'existe pas de modèle universel ou complet.

Nous avons effectué une analyse bibliographique sur l'état des connaissances en matière du choix de modèles de propagation des fissures de fatigue, afin d'identifier leurs avantages, désavantages et limites. On a mis l'accent sur les modèles faciles à évaluer et qui exigent peu (ou pas) de paramètres empiriques pour l'ajustement des courbes.

Nous avons exécuté un programme de recherche expérimentale sur la fatigue comprenant deux cas distincts, soit l'application à l'acier 350WT d'une phase de charge à amplitude constante et celle d'une seconde à amplitude variable. Ce matériau est un acier de construction ayant des applications importantes sur les navires, les ponts, les grues et les tours qui sont tous soumis à des charges cycliques. Le but de l'expérience avec la phase de charge à amplitude constante était d'obtenir des données de base sur la fatigue produite avec différents rapports de contrainte et d'étalonner les modèles à amplitude constante disponibles. Le but de l'expérience avec la phase de charge à amplitude variable était de quantifier l'ampleur de la décélération lors de l'application de surcharges de traction périodiques, dans une situation de charge à amplitude constante. Nous avons évalué les modèles de fatigue provenant de l'analyse bibliographique (à l'aide de la méthode des tableurs électroniques) et avons comparé leurs résultats à ceux des expériences.

Nous avons étudié deux progiciels de prévision des paramètres de rupture et deux autres servant à prévoir la durée de vie en fatigue et avons comparé leurs limites et leurs

avantages respectifs. Les programmes de prévision des paramètres de rupture utilisent la méthode des éléments finis pour calculer les paramètres nécessaires à la formation de fissures de différentes longueurs. Les programmes servant à prévoir la durée de vie en fatigue utilisent les résultats du programme de rupture concurremment avec des modèles de fatigue préprogrammés pour prévoir la durée de vie en fatigue des structures. Nous avons évalué les éprouvettes à l'aide des programmes numériques et avons comparé ces résultats à ceux des expériences.

Chapter 1

Introduction

1.1 Background

Prior to the industrial revolution, the primary building material used was brick and mortar which are "… relatively brittle and unreliable for carrying tensile loads. Consequently, pre-industrial revolution structures were usually designed to be loaded in compression" (Anderson, 1995). As a result the arch shape was predominately used, not because it was aesthetically pleasing, but for its ability to transmit compressive rather than tensile stresses throughout the structure.

During the industrial revolution, iron and steel were being mass produced and the increasing availability of these ductile materials made it "… feasible to build structures that carried tensile stresses" (Anderson, 1995). The presence of a crack subjected to a tensile stress may result in a brittle fracture, which is a "… type of catastrophic failure in structural materials that usually occurs without prior plastic deformation and at extremely high speeds" (Barsom et al., 1987). Failures of this type were common during the first part of the industrial era and since they occurred without warning, the results were usually disastrous. One of the earliest and most famous failures was the rupture of a Boston molasses tank that spilled approximately 2.3 million gallons of molasses and resulted in twelve deaths, forty injuries and extensive property damage (Shank, 1953).

Despite the numerous tank failures, railroad accidents, elevator accidents and boiler explosions, the problem of brittle fracture was not fully appreciated until the large number of Liberty ship failures during World War II. The Liberty ships had an all-welded hull as opposed to, at the time, the riveted construction of traditional ship designs.

Roughly 2700 Liberty ships were fabricated and approximately 400 sustained fractures of which some broke completely in half. As a result of these failures, the problem of brittle fracture became the subject of extensive investigations to try and determine its cause and to rectify the problem.

The problem of brittle fracture still remains today; however, due to our present understanding of the subject, the occurrence is less frequent. Modern day structures are designed so that the probability of a brittle fracture during the component's lifetime is minimized. This, in conjunction with strict quality control and routine inspection programs, has resulted in controlling but not eliminating the problem.

1.2 Design and Analysis Methods

The objective of engineering design is to obtain the geometry and dimensions of components such that they perform their intended function in an economical, reliable and safe manner. Traditional methods involve designing the component's cross-section such that the factored applied stresses are less than the factored critical strength of the material.

During the design lifetime of any component it is inevitable that a crack will occur due to material defects, the manufacturing process or as a consequence of everyday use. The presence of a crack subjected to tensile loading is a cause for concern because it may seriously affect the strength and safety of the component by brittle fracture into two or more sections at a stress level lower than that normally expected. It is the responsibility of the engineer to consider this during the design stage.

Designing to prevent brittle fracture involves the "... elimination of those structural details that act as stress raisers and that can be potential fracture-initiation sites, for example, weld discontinuities, mismatch and intersecting plates" (Barsom et al., 1987). For the majority of engineering structures, elimination of all details and discontinuities is practically impossible. The design approach should recognize this fact and focus on minimizing the number of discontinuities and ensure that they do not grow to a critical size during the component's service life.

The manner in which a brittle failure occurs depends upon the type of loading that the structure is subjected to. Failure of a cracked member due to a monotonically increasing and a cyclic load are referred to as fracture and fatigue respectively. For most equipment and engineering structures, such as ships, bridges, vehicles, aircraft, cranes and towers the major concern is with fatigue, which will be the topic for the remainder of this report.

Presently, there are three main approaches to analyze for fatigue. The traditional approach involves using the nominal stresses in the region of the component being analyzed and is known as the stress based approach. That is, "… the nominal stress that can be resisted under cyclic loading is determined by considering mean stresses and by making adjustments for the effects of stress raisers, such as grooves, holes, fillets and keyways" (Dowling, 1993). Another approach is the strain-based approach "… which involves more detailed analysis of the localized yielding that may occur at stress raisers during cyclic loading" (Dowling, 1993). The third approach is fracture mechanics, which specifically considers the presence of a growing crack. Fracture mechanics has become the preferred method and its theory will be discussed in the next chapter.

1.3 Objectives

This report is a result of the author's interest in the subject of fatigue and is supported by Defence Research Establishment Atlantic (DREA) and Natural Science and Engineering Research Council of Canada (NSERC). It involves investigating both experimentally and numerically several approaches to modeling fatigue crack growth in 350WT steel for constant and variable amplitude loading.

Assessing the behavior of fatigue cracks in any structure is a complex and uncertain process due to the large number of parameters that may influence the crack growth process. Numerous models have been developed over the past few decades which take different approaches to modeling fatigue crack growth; however, no universal or all encompassing model exists. Most models are developed for a specific application and incorporate the main parameters influencing fatigue crack growth for the structure in question. A successful model strikes a balance between being able to accurately predict the crack growth rate and its simplicity. Such a model is beneficial in planning inspection intervals, determining required maintenance and minimizing the problem of crack propagation in future designs.

A major parameter that needs to be considered is the influence of load history, which is usually variable in nature. One aspect of this loading is large tensile overloads, which create a residual compressive stress just beyond the crack tip in many materials and retards the crack growth rate for a number of cycles after the overload. The amount of retardation depends upon a number of material and loading factors, which will be examined in more detail. Below is a detailed description of the objectives that will be investigated in this report.

1) Literature Review

A state-of-the-art review of the available fatigue crack propagation models was performed to identify their advantages, disadvantages and limitations with application to various structures.

Traditional, empirical fatigue crack growth models such as Paris, Walker, and Forman have been successfully applied to various metallic structures. However, these models require material fatigue data that may not, at times, be available. Therefore, it is desirable to seek a model that does not rely on any empirical parameters.

2) Experimental Investigation

An experimental fatigue program was developed and undertaken on a simple crack geometry problem and the results were compared to predictions obtained from the various models discussed during the literature review.

The experimental program consisted of a constant and variable amplitude loading phase for a center cracked specimen configuration. The objectives of the constant amplitude phase will be to establish some baseline data for 350WT steel at various stress ratio's (R) and to calibrate the available constant amplitude model parameters. The variable amplitude phase consisted of periodic tensile overloads to quantify the magnitude of retardation in 350WT steel and to help recommend a suitable technique and model for predicting fatigue crack propagation subjected to this type of loading.

3) Numerical Investigation

As a result of recent advances in the finite element method (FEM) and its application to fracture mechanics, various numerical methods exist to calculate the fracture parameters and to evaluate the fatigue crack growth models. One of the advantages of the numerical method is that accurate results can be obtained for complex problems of any geometry and crack configuration in a fraction of the time and cost compared to the alternative of experimentation.

A model of the center cracked experimental specimens was analyzed with various FEM programs and the results were compared to those obtained from the experiments. The applicability of the FEM for calculating the fracture parameters and fatigue crack growth are evaluated and discussed.

Chapter 2

Part A – Theoretical Background

2.1 Fracture Mechanics

2.1.1 Introduction

The theory of fracture mechanics was developed to analyze and predict the failure of structures that have cracks. The origins of fracture mechanics can be traced back to Griffith (Dowling, 1993) who explained the discrepancy between the measured and predicted strength of glass by considering the stability of a small crack.

Present day fracture mechanics includes Linear Elastic Fracture Mechanics (LEFM) and Elastic Plastic Fracture Mechanics (EPFM) which use quantities called 'fracture parameters' to characterize the stress field surrounding the crack tip and serve as a criteria capable of predicting failure. These fracture parameters are accompanied by the subscripts I, II or III which correspond to the appropriate mode of loading illustrated by Figure 2.1.

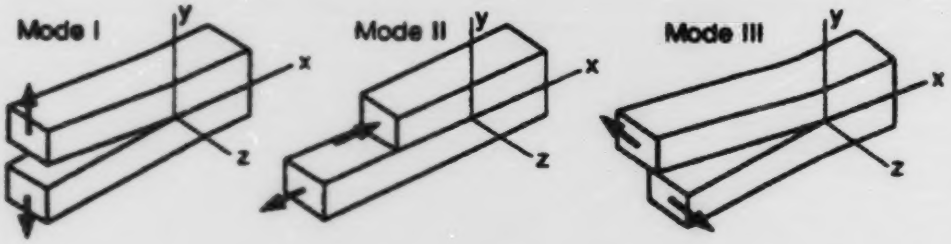

Figure 2.1 - Three possible modes of crack loading (Dowling, 1993)

Mode I, the opening mode, corresponds to the principle load being applied normal to the crack plane causing the crack faces to move apart. Mode II, the sliding mode, corresponds to in-plane shear loading causing the crack surfaces to slide relative to one another in the same plane but in opposite directions. Mode III, the tearing mode, corresponds to out-of-plane shear loading causing the crack surfaces to displace in the plane of the crack and parallel to the leading edge of the crack. A cracked body subjected to any arbitrary loading can be completely described by one or a combination of these modes.

The theory of fracture mechanics will be discussed in the following sections; however, one must be careful not to solely rely on a fracture mechanics analysis to determine when failure of a component with a crack will occur. The failure of a cracked component may occur by either collapse (yielding) of the remaining cross-sectional area or fracture, which are competing conditions, and the one satisfied first will prevail. Therefore, no fracture analysis is complete without the evaluation of collapse conditions.

2.1.2 Linear Elastic Fracture Mechanics

The Linear Elastic Fracture Mechanics (LEFM) approach was originally developed for metallic materials which obey Hooke's law and exhibit little or no plastic deformation at the crack tip. An overall limit on the use of LEFM is represented by Equation 2.1 and illustrated in Figure 2.2.

$$a,(b-a),h \geq \frac{4}{\pi}\left(\frac{K}{\sigma_y}\right)^2 \qquad \text{(LEFM applicable)} \qquad (2.1)$$

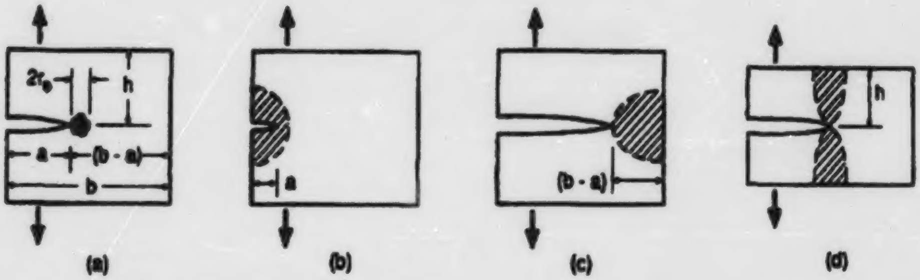

Figure 2.2 - Conditions when LEFM is valid (a) and invalid (b, c and d) (Dowling, 1993)

The commonly used LEFM fracture parameters are the stress intensity factor (*K*) and the strain energy release rate (*G*). For somewhat higher stress levels than permitted by the limitations of Equation 2.1, a plastic zone adjustment method may be used which extends the applicability of LEFM. The following sections will discuss the above topics in more detail.

2.1.2.1 Stress Intensity Factor

When a crack exists in any material subjected to an applied stress, it functions as a stress concentrator that produces a high stress gradient in the vicinity of the crack tip. A relatively simple description of the stress field can be obtained from a stress analysis of the crack tip in accordance with the theory of elasticity. For an infinitely wide plate consisting of a homogeneous isotropic material with a sharp crack of arbitrary size and subjected to mode I loading (Figure 2.3), it can be proven that the stresses at a point (r,θ) are equal to

$$\sigma_x = \frac{K_I}{\sqrt{2\pi r}}\cos\frac{\theta}{2}\left[1-\sin\frac{\theta}{2}\sin\frac{3\theta}{2}\right] + \ldots \qquad (2.2a)$$

$$\sigma_y = \frac{K_I}{\sqrt{2\pi r}}\cos\frac{\theta}{2}\left[1+\sin\frac{\theta}{2}\sin\frac{3\theta}{2}\right] + \ldots \qquad (2.2b)$$

$$\tau_{xy} = \frac{K_I}{\sqrt{2\pi r}}\cos\frac{\theta}{2}\sin\frac{\theta}{2}\cos\frac{3\theta}{2} + \ldots \qquad (2.2c)$$

$$\sigma_z = 0 \qquad \text{(plane stress; } \sigma_z = 0) \qquad (2.2d)$$

$$\sigma_z = \nu(\sigma_x + \sigma_y) \qquad \text{(plane strain; } \varepsilon_z = 0) \qquad (2.2e)$$

$$\tau_{yz} = \tau_{zx} = 0 \qquad (2.2f)$$

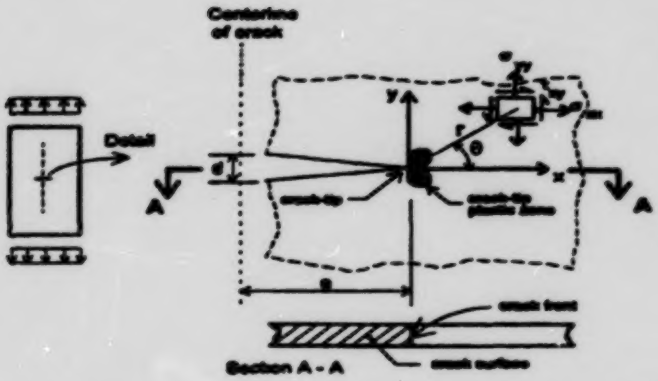

Figure 2.3 - A crack in an infinitely wide plate (Kulak et al., 1993)

The expression K_I in Equation 2.2 is the stress intensity factor for the crack opening mode I and characterizes the severity of the crack situation as affected by crack size, applied stress and specimen geometry. The general form of the stress intensity factor is

$$K_I = \lim_{r,\theta \to 0}\left(\sigma_y \sqrt{2\pi r}\right)$$

$$\text{or} \quad K_I = Y\sigma\sqrt{\pi a} \tag{2.3}$$

where Y is a geometric correction factor, σ is the gross stress of the section and 'a' is the half crack length. The expression for Y is determined by experiment and the results for many common specimen configurations are published in various handbooks. "Expressions for stress distributions for other types of loading and crack geometry's in isotropic materials lead to expressions that are similar to those of Equation 2.2 and the corresponding stress intensity factor can be found in the same way" (Gibson, 1994). That is, the term K_I is replaced by K_{II} = $\text{Y}\,\sigma\sqrt{\pi a}$ for pure mode II loading and K_{III} = $\text{Y}\,\sigma\sqrt{\pi a}$ for pure mode III loading.

Since the stress intensity factor determines the crack tip stress field, "... fracture will occur when K becomes too high for the material. How high the stress intensity can be depends upon the material; it must be determined from a test" (Broek, 1991). This value of K is referred to as the materials fracture toughness and is governed by ASTM Standard No. E399 entitled "*Standard Test Method for Plane-Strain Fracture Toughness of Metallic Materials*".

Typical results from a fracture toughness test are presented in Figure 2.4 for a three point bend specimen of varying thickness.

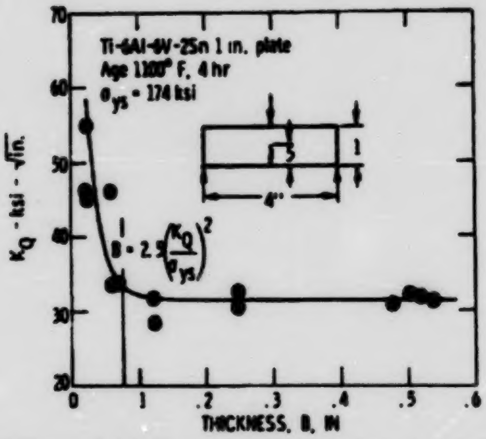

Figure 2.4 - Effect of thickness on fracture toughness (Dowling, 1993)

This trend of decreasing K_Q with increasing specimen thickness is typical for most metals and occurs because the behavior of the plastic zone depends upon specimen thickness. Once the thickness, B, satisfies Equation 2.4, the value of K_Q is considered to be a constant.

$$B \geq 2.5\left(\frac{K_Q}{\sigma_y}\right)^2 \tag{2.4}$$

This constant value of K_Q is called the plane strain fracture toughness (K_C) and represents the worst case scenario. Thus for a given plate of known geometry, applied stress and crack length; the stress intensity factor can be calculated by Equation 2.3 and if this value is less than K_C, the plate will not fail.

2.1.2.2 Strain Energy Release Rate

The basis of the strain energy release rate (G) parameter is that "… elastic strain energy is stored in a body when it is deformed elastically and this energy is released as the crack grows through the body and is used for the creation of new surfaces associated with the crack" (Matthews, 1994). To obtain the expression for G, one must consider a plate with a crack extending through its thickness. Writing the expression for the system's potential energy gives

$$\Pi = U + W - V \tag{2.5}$$

where U represents the internally stored energy, V represents the external energy and W is the work needed to fracture the material over length da. By applying the theory of minimum potential energy to Equation 2.5 one obtains

$$\frac{d\Pi}{da} = 0 = \frac{dU}{da} + \frac{dW}{da} - \frac{dV}{da}$$

$$\text{or} \quad \frac{d}{da}(V - U) = \frac{dW}{da} \tag{2.6}$$

Equation 2.6 represents the conservation of energy principle expression in terms of the changes of the energy per unit thickness.

Figure 2.5 illustrates a typical load displacement record for a change in crack length da under constant displacement.

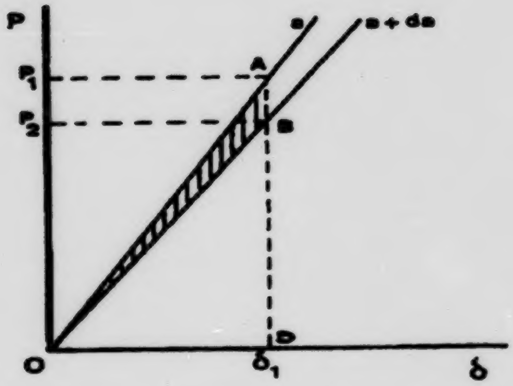

Figure 2.5 - Fracturing at constant displacement (Broek, 1995)

The stiffness of the member decreases and since constant displacement is maintained, the applied load decreases from P_1 to P_2. The load does not move through a distance and therefore it does no work ($dV = 0$). The change in strain energy is equal to area OAB and must be equal to the work required to extend the crack by an amount *da* as one can conclude from Equation 2.6; that is,

$$\frac{dW}{da} = -\frac{dU}{da} \tag{2.7}$$

The expression *dW/da* represents the work needed to fracture the material over length *da* and is equal to the change in the strain energy over crack length *da*. By denoting the expression *dW/da* as *G*, Equation 2.7 becomes

$$G = -\frac{dU}{da} \quad \text{(per unit thickness)} \tag{2.8a}$$

$$\text{or} \quad G = -\frac{1}{t}\frac{dU}{da} \quad \text{(for thickness t)} \tag{2.8b}$$

G represents the energy per unit crack area required to propagate the crack and the expression *dU/da* is evaluated for the specific geometry and loading condition of the problem.

It can be shown that the fracture parameters K and G are related by the following equations

$$G = \frac{K^2}{E} \qquad \text{(plane stress; } \sigma_Z = 0\text{)} \qquad (2.9a)$$

$$G = \frac{(1-\nu)K^2}{E} \qquad \text{(plane strain; } \varepsilon_Z = 0\text{)} \qquad (2.9b)$$

Since K and G are directly related, only one parameter is required when analyzing a material that obeys LEFM. As a result of many researchers reporting their results in terms of K, it has become the preferred fracture parameter.

2.1.2.3 Plastic Zone Adjustment

The elastic stress field equations (Equation 2.2) theoretically predict that the stresses at a sharp crack tip ($r = 0$) are infinite. Realistically materials cannot support these infinite stresses and as a result the crack tip becomes blunted and a region of intense deformation forms due to yielding which is called the plastic zone. The applicability of LEFM requires that the plastic zone be small compared to the components planar dimensions.

An estimate of the plastic zone size may be developed from the elastic stress field equations. Considering plane stress conditions, Equations 2.2 predicts that in the plane of the crack ($\theta = 0$)

$$\sigma_x = \sigma_y = \frac{K}{\sqrt{2\pi r}} \qquad (2.10a)$$

$$\sigma_z = \tau_{xy} = \tau_{yz} = \tau_{zx} = 0 \qquad (2.10b)$$

Both the maximum shear stress and the octahedral shear stress yield criteria estimate yielding at $\sigma_x = \sigma_y = \sigma_{yield}$ and substituting this into Equation 2.10a gives

$$r_{o\sigma} = \frac{1}{2\pi}\left(\frac{K}{\sigma_y}\right)^2 \tag{2.11}$$

This represents "… the distance ahead of the crack tip where the elastic stress distribution exceeds the yield criterion for plane stress"(Dowling, 1993). In this region ($r_{o\sigma}$), the yielded material offers less resistance than expected and thus the yielding zone is extended beyond the value of $r_{o\sigma}$ as illustrated in Figure 2.6.

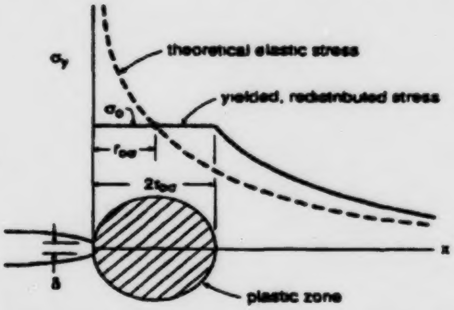

Figure 2.6 - Estimate of plastic zone size (Dowling, 1993)

It has been determined this yielding extends to approximately $2r_{o\sigma}$ and an acceptable estimate of the actual plastic zone size for plane stress conditions is

$$2r_{o\sigma} = \frac{1}{\pi}\left(\frac{K}{\sigma_{yield}}\right)^2 \tag{2.12}$$

Similarly, an estimate of the actual plastic zone size for plane strain conditions is

$$2r_{o\varepsilon} = \frac{1}{3\pi}\left(\frac{K}{\sigma_{yield}}\right)^2 \tag{2.13}$$

Equation 2.13 is known as Irwin's estimate for the plane strain plastic zone and it estimates a zone one-third as large as that of plane stress. This is because $\sigma_z \neq 0$ (for plane strain) which results in higher σ_x and σ_y values required to cause yielding which thus decreases the plastic zone size relative to that for plane stress.

An overall limit on the applicability of LEFM is described by Equation 2.1. By modifying the value of *K*, the validity of LEFM can be extended to somewhat higher stress levels beyond this limit. The procedure used to modify *K* involves making a plastic zone adjustment.

The redistributed stresses outside the plastic zone of Figure 2.6 are "… similar to those for the elastic stress field equations for a hypothetical crack of length …" (Dowling, 1993)

$$a_e = a + r_{o\sigma} \tag{2.14}$$

This modifies *K* by increasing its value to account for the excessive yielding by using a_e instead of the actual crack length. Therefore Equation 2.3 becomes

$$K = Y\sigma\sqrt{\pi(a + r_{o\sigma})} \tag{2.15}$$

Substituting the value of $r_{o\sigma}$ from Equation 2.12 into Equation 2.15, the modified plane stress expression for *K* becomes

$$K_e = Y\sigma\sqrt{\frac{\pi a}{1-\frac{1}{2}\left(\frac{Y\sigma}{\sigma_y}\right)^2}} \tag{2.16}$$

The plane strain expression for K_e is calculated in a similar manner and is equal to

$$K_e = Y\sigma\sqrt{\frac{\pi a}{1-\frac{1}{6}\left(\frac{Y\sigma}{\sigma_y}\right)^2}} \tag{2.17}$$

The plastic zone adjustment modifies the value of *K* so that LEFM is valid at a higher stress level than permitted by Equation 2.1. This approach is not valid for large amounts of yielding and it is recommended that "… the use of plastic zone adjustments be limited to loads below 80% of the fully plastic value" (Dowling, 1993). The usefulness of this method is limited because of the development of elastic plastic fracture parameters.

2.1.3 Elastic-Plastic Fracture Mechanics

As previously discussed, LEFM is valid for material that obeys Hooke's law and exhibits limited plastic deformation at the crack tip. In many important engineering applications, especially for nuclear pressure vessel's, the limits of LEFM are exceeded. An attempt to use LEFM beyond its region of validity will result in the engineering calculations to be nonconservative; that is, to be on the unsafe side. Thus, alternative fracture mechanics parameters capable of handling materials with large plastic zones at the crack tip are required and this branch of fracture mechanics is referred to as Elastic-Plastic Fracture Mechanics (EPFM).

The two commonly used elastic plastic fracture parameters are the *J* contour integral and the crack tip opening displacement (CTOD) which will be discussed in the following sections. It should be noted that the use of the *J* and CTOD parameters are not valid for large plastic zones which correspond to yielding of the remaining uncracked portion of the member. This situation does not correspond to fracture failure but rather plastic collapse.

2.1.3.1 The *J* Contour Integral

The fracture parameter *J* is based on the same energy principle as *G*, except it is capable of handling large amounts of yielding and nonlinear stress-strain relationships. For the special case of a linear stress-strain curve and small scale yielding, the value of *J* is equal to *G*. Therefore, *J* can be thought of as a generalization of the strain energy release rate to cases of nonlinear stress-strain response of materials and as with *K* and *G*, if the value of J is greater than its critical value (J_C) fracture will occur. The fracture toughness parameter for mode I loading is governed by ASTM E813 entitled "*Standard Test Method for J_{Ic}, A Measure of Fracture Toughness*".

Historically, "Rice presented a path independent integral for analysis of cracks and showed that the value of this integral, which he called J, is equal to the energy release rate in a nonlinear elastic body that contains a crack" (Anderson, 1995). The expression for Rice's J contour integral (valid for any loading conditions, geometry and crack) is commonly defined in literature as

$$J = \oint (U_o dy - T_i \frac{du_i}{dx} ds) \tag{2.18}$$

where U_o is the strain energy density, S (as illustrated in Figure 2.7a) is a closed contour, T_i is the tension perpendicular to S (or the traction), u is the displacement vector components and ds is an element of S.

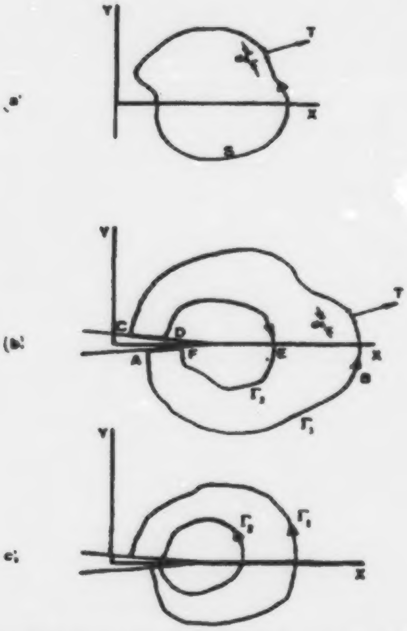

Figure 2.7 – Path independent contour for elastic body with a crack (Broek, 1995)

The first term of the integral (Equation 2.18) represents the strain energy (U) while the second term of the integral is the work done (V) by the force T_i displaced through a distance $(du_i/dx)ds$. Evaluating the expression of Equation 2.18 along a closed contour ABCDEF as illustrated by Figure 2.7b;

$$\int_{\Gamma_1} + \int_{CD} + \int_{\Gamma_2} + \int_{FA} = 0 \tag{2.19}$$

The second and fourth integral are equal to zero since $T = 0$ and $dy = 0$ along path CD and FA. Therefore

$$\int_{\Gamma_1} + \int_{\Gamma_2} = 0 \quad \text{or} \quad \int_{\Gamma_1} = -\int_{\Gamma_2} \tag{2.20}$$

These integrals are defined in opposite directions, but if they are both evaluated in a counterclockwise direction as shown in Figure 2.7c, $\int_{\Gamma_1} = \int_{\Gamma_2}$.

2.1.3.2 Crack Tip Opening Displacement

The CTOD is an elastic plastic fracture parameter originally proposed by Wells and it has several definitions. The two common definitions are the displacement at the original crack tip and the 90° intercept which are illustrated in Figure 2.8a and 2.8b respectively.

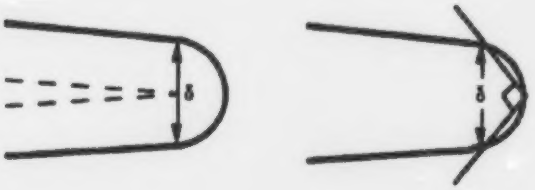

Figure 2.8 - (a) Displacement at the original crack tip and (b) 90° intercept (Anderson, 1995)

If the crack blunts into a semicircle, the above two methods are identical.

It has been proven that the CTOD parameter is related to the *K*, *G* and *J* fracture parameters by the following equations.

$$\mathrm{CTOD} = \delta \approx \frac{G}{\sigma_{yield}} = \frac{K^2}{E\sigma_{yield}} \quad \text{(LEFM)} \tag{2.21a}$$

$$\mathrm{CTOD} = \delta \approx \frac{J}{\sigma_{yield}} \quad \text{(EPFM)} \tag{2.21b}$$

2.1.4 LEFM Versus EPFM

The flow chart illustrated by Figure 2.9 summarizes the various fracture mechanics parameters and when they are applicable.

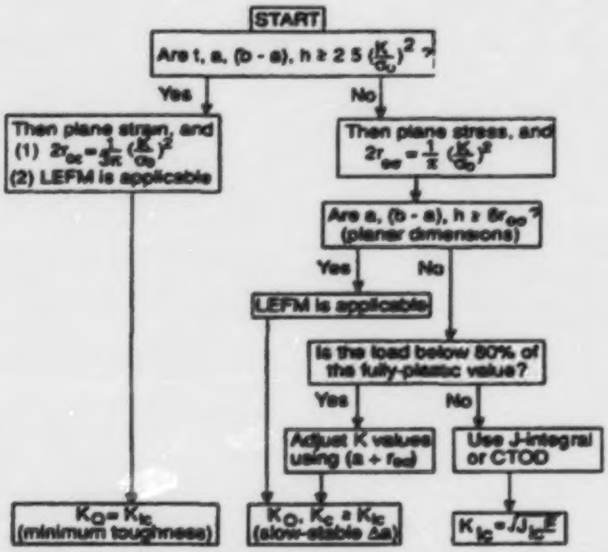

Figure 2.9 - Fracture mechanics flow chart (Dowling, 1993)

If the first criterion at the top of the flow chart is valid, then plane strain conditions exist and LEFM is applicable. The value obtained for the stress intensity factor (K_Q) is equal to the minimum toughness (K_C) which represents the worst case scenario. If the first criteria is not met, then plane stress conditions exist and a second less severe criteria is evaluated to determine if LEFM is applicable. The resulting stress intensity factor (K_Q) is somewhat greater than K_C; however the K_C value is often used in this situation recognizing that some extra conservatism is thus included. If the second criterion is not met, the LEFM plastic zone adjustment or the more applicable EPFM methods such as the *J*-integral or the CTOD must be used.

2.2 Fatigue

2.2.1 Introduction

A typical textbook definition of fatigue is the "… initiation and propagation of microscopic cracks into macro cracks by the repeated application of stresses" (Kulak et al., 1993). That is, a crack is initiated and slowly propagates under the action of cyclic loading until its critical size is reached at which point failure occurs. The number of cycles required to initiate and propagate a fatigue crack to a critical size are referred to as the fatigue crack initiation life (N_i) and the fatigue crack propagation life (N_f) respectively. Therefore the total fatigue life (N_T) is equal to the sum of the initiation and propagation lives; that is,

$$N_T = N_i + N_f \tag{2.22}$$

The point at which fatigue crack initiation has occurred and when fatigue crack propagation starts is still a subject of controversy. For engineering purposes, "… a crack may be assumed to initiate when it is about 1 to 2 mm in length and subsequent growth to the critical size is characterized by the crack growth models" (ENDURE, 1995).

For an ideal material with no initial flaws or imperfections the fatigue crack initiation life usually represents the majority of the total fatigue life. However if a pre-existing flaw or crack exists, the initiation life is very small and the fatigue crack propagation life represents the majority of the total life.

The majority of the flaws that occur in all fabricated metallic structures are a result of the steel manufacturing and fabrication process. The major source of flaws in fabrication is from the welding process; however, it is neither a practical nor economical option to eliminate welding from the fabrication process. This fact has led to the use of a damage tolerance design approach. That is, "… flaws are assumed to exist at the beginning of service life and hence only the propagation phase comprises the life" (ENDURE, 1995). This represents a conservative design approach and the size of the assumed flaw (crack) is determined from the quality control and/or the inspection programs. For this reason, knowledge of fatigue crack propagation is of great importance.

2.2.2 Fatigue Loading

Before any fatigue crack propagation analysis is conducted, one must first accurately determine the loading scenario that the structural component will experience. In most cases, the loading scenario used is a simplified version of the actual in-service stress history. Any loading may be classified as either constant amplitude or variable amplitude loading and are discussed below.

2.2.2.1 Constant Amplitude Loading

Constant amplitude loading is the simplest load history representation and is illustrated in Figure 2.10.

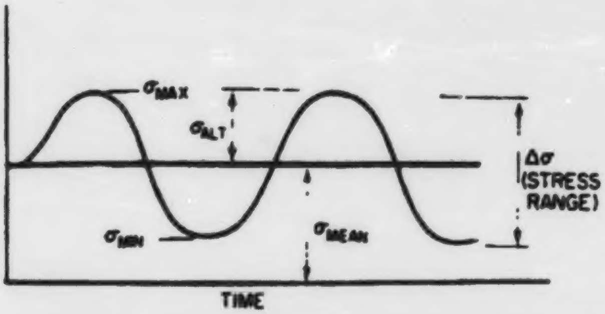

Figure 2.10 - Constant amplitude loading (Barsom, 1987)

The load is usually represented as a sinusoidal stress-time pattern of constant amplitude and fixed frequency, applied for a specified number of cycles. Referring to Figure 2.10, some necessary definitions and symbols can be introduced as follows:

σ_{max} = maximum stress in the cycle

σ_{min} = minimum stress in the cycle

σ_{mean} = mean stress = $\dfrac{\sigma_{max} + \sigma_{min}}{2}$

$\Delta\sigma$ = stress range = $\sigma_{max} - \sigma_{min}$

R = stress ratio = $\dfrac{\sigma_{min}}{\sigma_{max}}$

Any two of the above can adequately describe the constant amplitude loading.

Some common stress amplitude patterns are completely reversed stressing ($R = -1$), zero to tension stressing ($R = 0$) and tensile to tensile load ($0 \leq R \leq 1$) as illustrated in Figure 2.11a, 2.11b and 2.11c respectively.

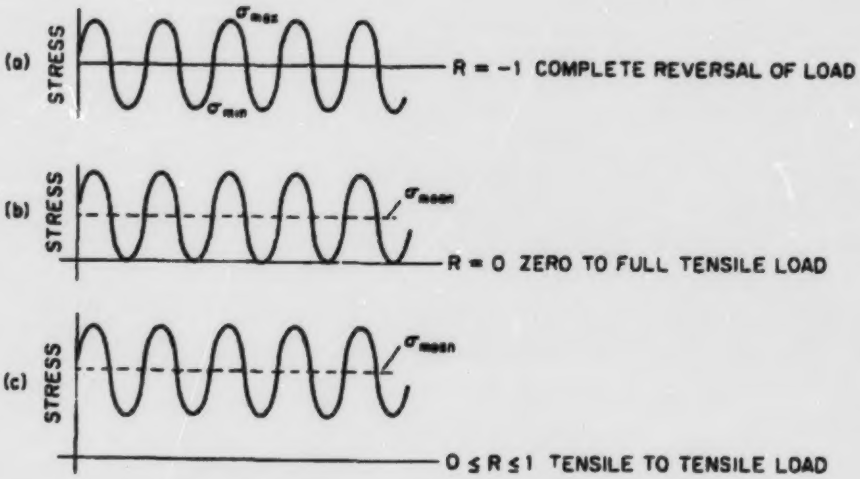
(a)
STRESS
σ_{max}
σ_{min}
R = −1 COMPLETE REVERSAL OF LOAD
(b)
STRESS
σ_{mean}
R = 0 ZERO TO FULL TENSILE LOAD
(c)
STRESS
σ_{mean}
0 ≤ R ≤ 1 TENSILE TO TENSILE LOAD

Figure 2.11 - Common stress amplitude loading patterns (Barsom, 1987)

Constant amplitude loading is simple to describe, unfortunately very few structures or components have loading occur in this manner. Therefore constant amplitude loading is limited to rotating machinery, such as turbomachinery, propellers and helicopter blades, as well as piping components of nuclear power structures.

2.2.2.2 Variable Amplitude Loading

For the majority of structural components the loading scenario is classified as variable amplitude loading. Variable amplitude loading sequence may either be a repetition of cyclic stresses, semi-random or completely random as illustrated in Figure 2.12a, 2.12b and 2.12c, respectively.

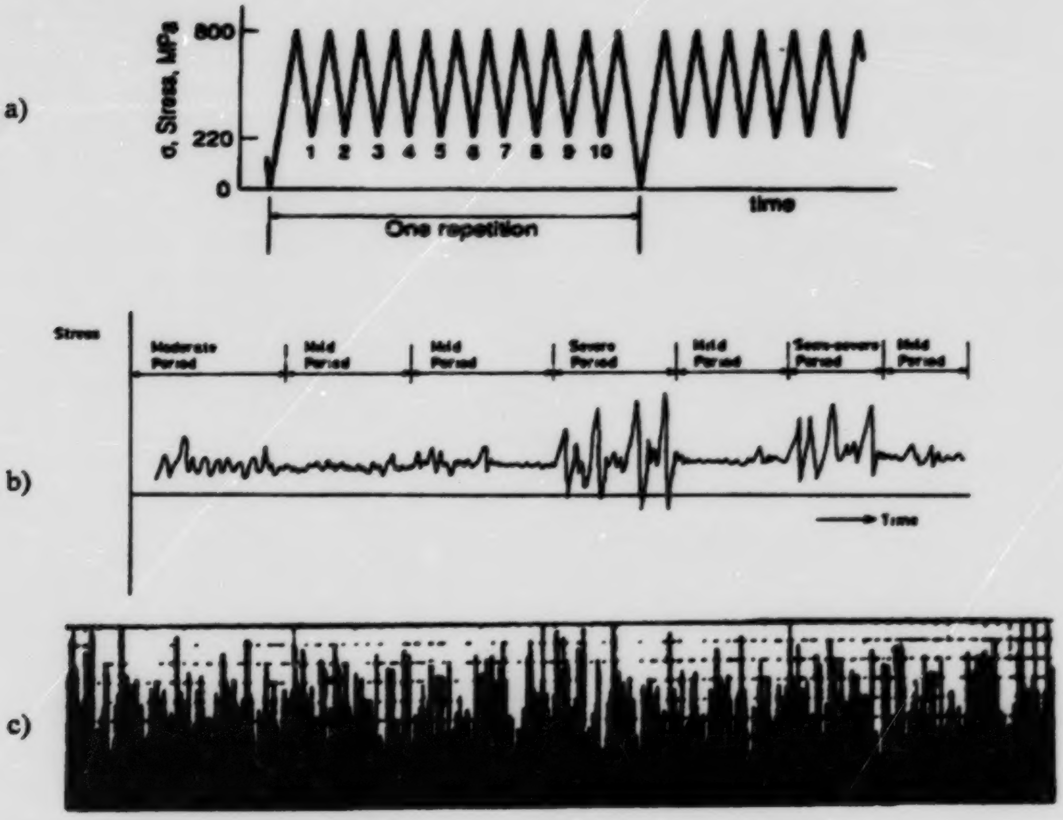

Figure 2.12 - (a) Repeated (Dowling, 1993), (b) Semi-random (Broek, 1995) and (c) Completely random loading scenarios (Fuchs, 1980)

Repeated variable amplitude loading is the simplest loading type and involves describing one 'block' of uncomplicated variable load applied repetitively during the structures life. In contrast, completely random variable loading involves "... very complex functions in which the probability of the same sequence and magnitude of stress ranges recurring during a particular time interval is very small" (Barsom, 1987). Most structure's load sequence is not completely random in nature but rather semi-random. Typical examples are airplanes, ships, offshore structures, railroad rails etc. The load sequence on ships and offshore structures depend upon waves that are different from month to month and location to location. They are semi-random because high loads are clustered in certain periods (storms) rather than randomly scattered throughout the stress-time history.

For constant amplitude loading it is obvious how to define a cycle; however, for highly irregular variations of load with time, such as Figure 2.12c, it is not obvious how individual events should be isolated and defined. As a result many counting methods have been proposed and include peak count, mean-crossing peak count, range pair mean count and rainflow counting. After years of debate it has been generally agreed that the rainflow counting method gives the best representation for fatigue (Broek, 1995).

2.2.3 Fatigue Life Curve

The fatigue behavior of a material is graphically illustrated with the aid of a stress-life (S-N) curve as shown by Figure 2.13.

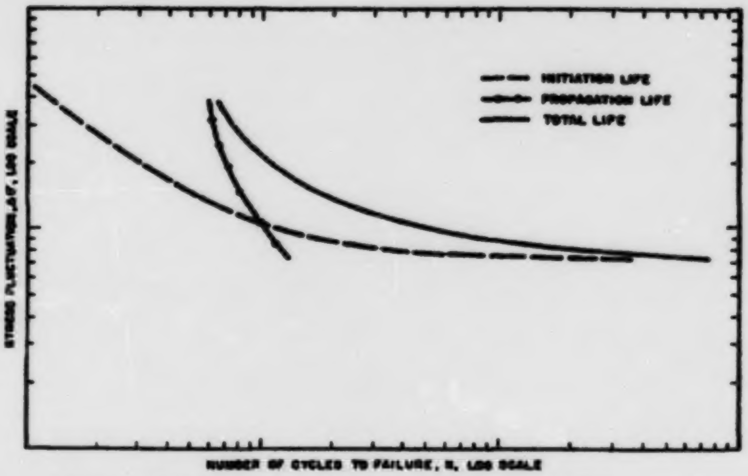

Figure 2.13 - Stress-life curve (Barsom, 1987)

The curve is obtained by testing a number of specimens at various stress levels under sinusoidal loading conditions and is composed of an initiation and a propagation component. The fatigue tests are conducted on smooth unnotched specimens that make it practically impossible to distinguish between the crack initiation and propagation phase. Thus, the S-N curve usually represents only the total fatigue life of a specimen as shown by the solid line of Figure 2.13.

A typical S-N curve for some materials appears to become flat for large number of cycles representing a distinct stress level below which fatigue failure will not occur. This limit is called the *fatigue limit* or the *endurance limit.*

A given S-N curve is valid for the specific conditions under which it was tested. One may extrapolate the results from a S-N curve to include the influence of other factors provided that sufficient knowledge of how they affect the S-N curve is known. These factors include member geometry, chemical environment, cyclic frequency, temperature, residual stress and mean stress.

2.2.4 Fatigue Rate Curve

A typical fatigue rate curve, commonly referred to as a *da/dN* versus *ΔK* curve, is illustrated by Figure 2.14

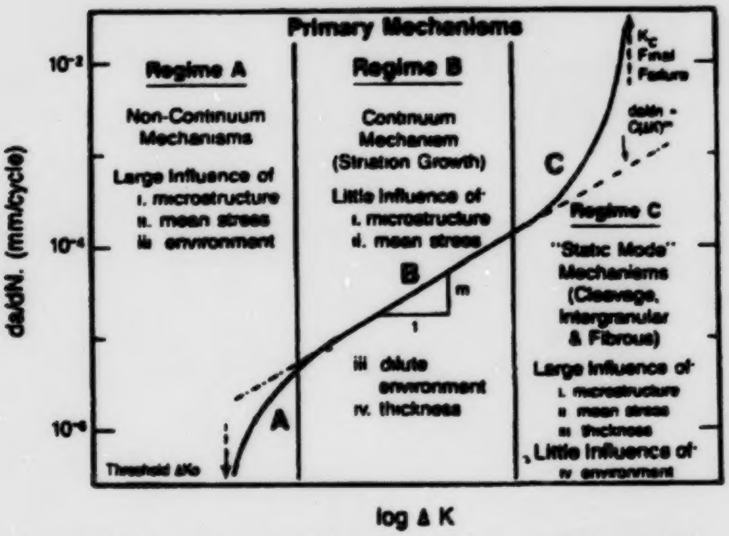

Figure 2.14 - Typical *da/dN* versus *ΔK* curve (Rice, 1988)

The curve is defined by Regions A, B and C which are commonly referred to as region I, II and III respectively.

2.2.4.1 Description of Region I

Region I represents the early development of a fatigue crack and the crack growth rate, *da/dN*, is typically of the order 10^{-6} mm/cycle or smaller. This region is extremely sensitive and is largely influenced by the microstructure features of the material such as grain size, the mean stress of the applied load, the operating temperature and the environment present.

The most important feature of this region is the existence of a stress intensity factor range below which fatigue cracks should not propagate. This value is defined as the fatigue crack growth threshold and is represented by the symbol ΔK_{th}. Its value is experimentally determined by using the decreasing K test as described in ASTM E647 – "*Standard Test Method for Measurement of Fatigue Crack Growth Rates*". The above mentioned factors affect the value of ΔK_{th}, but from "... the available data for long fatigue cracks subjected to constant amplitude cyclic loading in various room temperature laboratory atmospheres suggest that the stress ratio is the most important factor affecting the magnitude of ΔK_{th}" (Dowling, 1993).

2.2.4.2 Description of Region II

Region II represents the intermediate crack propagation zone where the "... length of the plastic zone ahead of the crack tip is long compared with the mean grain size, but much smaller than the crack length" (Wang, 1994). The use of LEFM concepts is acceptable and the data follows a linear relationship between log da/dN and log ΔK. The crack growth rate is typically on the order of 10^{-6} to 10^{-3} mm/cycle, which corresponds to the majority of the test data results from ASTM E647. This region corresponds to stable crack growth and the influence of microstructure, mean stress, ductility, environment and thickness are small. The influence of the mean stress is probably the most significant and usually results in closely spaced lines parallel to each other. The mean stress effect is greater for some material than others.

2.2.4.3 Description of Region III

Region III represents the fatigue crack growth at very high rates, $da/dN > 10^{-3}$ mm/cycle, due to rapid and unstable crack growth just prior to final failure. The da/dN versus ΔK curve becomes steep and asymptotically approaches the fracture toughness K_C for the material. The corresponding stress level is very high and causes a large plastic zone near the crack tip as compared with the specimen geometry. Because large scale yielding occurs, the influence of the nonlinear properties of the material cannot be ignored.

Therefore, the use of LEFM is not entirely correct and nonlinear fracture mechanics should be applied to this stage. The mean stress, materials microstructure and thickness have a large influence in this region and the environment has little influence. Fatigue crack propagation analysis is very complex in this region but often ignored because it has little importance in most fatigue situations. The reason being that the fatigue crack growth rates are very high and little fatigue life is involved.

Part B – State-of-the-Art Review of Fatigue Crack Propagation Models

2.3 Introduction

The common approach for fatigue crack growth analysis is to describe the data by a differential equation, which is referred to as a fatigue crack growth law or model. By integrating the equation one can obtain the crack length versus number of cycles (*a-N* curve) and predict the number of cycles required for the crack to grow from an initial to final size. The differential equation used to describe the data is often of the form

$$\frac{da}{dN} = \mathrm{f}(\Delta K, R) \tag{2.23}$$

The right hand side of Equation 2.23 describes the fatigue rate data relationship, usually with empirical curve fitting parameters. The main disadvantage is that the fatigue crack growth model parameters have no physical significance, but are representative of the curve fitting technique used to describe the *da/dN* versus *ΔK* curve. As a result, "… there are probably as many equations as there are researchers in the field" (Broek, 1995). Thus if the fatigue crack growth model 'fits' the data properly, it may be used in conducting a fatigue crack growth analysis. However, "… no equation can fit all data, so that religious adherence to one equation is not advisable" (Broek, 1995). All the models are valid in that they describe a particular set of fatigue crack growth data and can be used to predict crack growth rates in situations similar to those used to collect the data. "It is sometimes possible to fit the same set of data to apparently contradictory laws but, owing to the inherent scatter in fatigue crack growth data, it is not possible to decide which law is the most correct" (Frost, 1971).

It is practically impossible to discuss every available model because of the large number which exist in literature. Therefore, the remainder of this section will discuss the models, which are promising and/or commonly used.

2.4 Constant Amplitude Loading Models

The fatigue crack growth analysis of a component that is subjected to a constant amplitude load (K increasing) is the simplest to perform because no load history has to be considered. Numerous fatigue crack growth models exist which are capable of representing the fatigue rate data; however, they vary in the factors they consider and the number of curve fitting parameters required. The following discussion will introduce various fatigue crack growth models used strictly for constant amplitude loading and their advantages and limitations will be examined.

2.4.1 Paris Model

A simple and well known method for predicting fatigue crack propagation is a power law described by Paris and Erdogan (1963), commonly known as the Paris law. The equation represents the first application of fracture mechanics to fatigue and is given by the relationship

$$\frac{da}{dN} = C_P(\Delta K)^{m_P} \tag{2.24}$$

where C_P is the intercept and m_P is the slope on the log-log plot of da/dN versus ΔK. Equation 2.24 represents a straight line on the log-log plot of da/dN versus ΔK and thus describes region II of the fatigue rate curve.

The Paris law is simple to use and requires the determination of two curve fitting parameters which are easily obtained. As long as the data follows a straight line relationship, the Paris law is commonly used.

The limitation of the Paris law is that it is only capable of describing data in region II. If the data exhibits a threshold (region I) or an accelerated growth (region III) Paris law cannot adequately describe these regions. Depending upon the analysis being undertaken, this approximation may not be adequate. Finally, Paris law does not consider the effect of stress ratio and it depends upon the material used. For steels tested at various stress ratios, a family of straight lines parallel to each other are produced. This means that the value of m_P is the same for all stress ratios but the value of C_P is specific for a particular stress ratio. Therefore one must ensure that the fatigue rate data used is for the stress ratio of interest.

2.4.2 Walker Model

The major limitation of Paris's law is its inability to account for the stress ratio and in 1970 Walker improved the Paris model by including the effect of stress ratio. Walker proposed a parameter, $\overline{\Delta K}$, which is an equivalent zero to maximum ($R = 0$) stress intensity factor that causes the same growth rate as the actual K_{max} and R combination. It is expressed by the relationship

$$\overline{\Delta K} = K_{max}(1-R)^{\gamma_w} \tag{2.25}$$

where $K_{max} = \dfrac{\Delta K}{(1-R)}$. Thus Equation 2.25 becomes

$$\overline{\Delta K} = \frac{\Delta K}{(1-R)^{1-\gamma_w}} \tag{2.26}$$

Therefore Walker's law is represented by

$$\frac{da}{dN} = C_w\left(\overline{\Delta K}\right)^{m_w}$$

$$\text{or} \qquad \frac{da}{dN} = C_w\left[\frac{\Delta K}{(1-R)^{1-\gamma_w}}\right]^{m_w} \tag{2.27}$$

For $R = 0$, Equation 2.27 becomes equal to

$$\frac{da}{dN} = C_w(\Delta K)^{m_w} \tag{2.28}$$

which is equivalent to the Paris law with $C_P = C_W$ and $m_P = m_W$.

The significance of this equation is that a log-log plot of *da/dN* versus ΔK should result in a single straight line regardless of the stress ratio for which the data was obtained. The ability to account for this results in the introduction of a third curve fitting parameter γ_w. γ_w is determined by trial and error and its value is the one that best consolidates the data along a single straight line on the log-log plot of *da/dN* versus $\overline{\Delta K}$. It is possible that no value of γ_w may be found and in this situation Walker's equation cannot be used. If the value of γ_w is equal to one, $\overline{\Delta K}$ equals ΔK which indicates that the stress ratio has no effect on the data.

In summary, Walker's law is a modification of Paris's law that accounts for the stress ratio effect at the expense of introducing a third curve fitting parameter.

2.4.3 Forman Model

Although Walker improved the Paris model by taking account of the stress ratio, neither models could account for the instability of the crack growth when the stress intensity factor approaches its critical value. Forman improved Walker's model by suggesting a new model which is capable of describing region III of the fatigue rate curve and includes the stress ratio effect. Forman's law is given by the relationship

$$\frac{da}{dN} = \frac{C_F(\Delta K)^{m_F}}{(1-R)K_C - \Delta K} = \frac{C_F(\Delta K)^{m_F}}{(1-R)(K_C - K_{max})} \tag{2.29}$$

where K_C is the fracture toughness for the material and thickness of interest. Equation 2.29 indicates that as K_{max} approaches K_C, da/dN tends to infinity. Therefore Forman's equation is capable of representing stable intermediate growth (region II) and the accelerated growth rates (region III).

Forman's equation is capable of representing data for various stress ratios by computing the following quantity for each data point.

$$Q = \frac{da}{dN}\left[(1-R)K_C - \Delta K\right] \tag{2.30}$$

If the various ΔK and R combinations fall together on a straight line on a log-log plot of Q versus ΔK, Forman's equation is applicable and may be used.

Comparing Equation 2.29 and 2.30, Forman's equation may be represented as

$$Q = C_F(\Delta K)^{m_F} \tag{2.31}$$

2.4.4 Modified Forman Models

Forman's equation is capable of representing data of various stress ratios for region II and III. Further modifications of Forman's expression to represent region I, II and III have been accomplished by including the threshold stress intensity parameter ΔK_{th}.

Hartman and Schijve (1970) proposed the following equation.

$$\frac{da}{dN} = \frac{C_{HS}(\Delta K - \Delta K_{th})^{m_{HS}}}{(1-R)K_C - \Delta K} \tag{2.32}$$

Another version of the Forman equation is

$$\frac{da}{dN}=\frac{C_{MOD}(\Delta K)^{m_{MOD}}\left(\Delta K-\Delta K_{th}\right)^{0.5}}{(1-R)K_C-\Delta K} \tag{2.33}$$

Both Equation 2.32 and 2.33 produce a sigmoidal shaped curve as illustrated earlier by Figure 2.14 where the curve steepens at both low and high growth rates. That is, an asymptote not only occurs as K_{max} approaches K_C but also as ΔK approaches ΔK_{th}. One disadvantage in using these equations is that the value of "… ΔK_{th} is sensitive to R and a specific value of this parameter in the equation is generally needed for any given R value" (Dowling, 1993). Also, the correct value of K_C for the given thickness must be used.

2.4.5 Collipriest Model

Collipriest (1972) proposed a crack growth law capable of describing all three regions, includes the stress ratio effect and is given by the relationship

$$\frac{da}{dN}=C\left(K_C\Delta K\right)^{m/2}\mathrm{EXP}\left[\ln\left(\frac{K_C}{\Delta K_O}\right)^{m/2}\mathrm{ARCTANH}\left(\frac{\ln\left[\dfrac{\Delta K^2}{(1-R)K_C\Delta K_O}\right]}{\ln\left[\dfrac{(1-\mathrm{R})K_C}{\Delta K_O}\right]}\right)\right] \tag{2.34}$$

The model appears complicated with a number of parameters; however, it is one of the available models used in the numerical fatigue analysis program ENDURE that will be discussed later.

2.4.6 McEvily Model

McEvily proposed to relate the crack advance per cycle in the striation mode to the crack tip opening displacement and to include the threshold effect, which leads to the relationship

$$\frac{da}{dN}=\frac{4A}{\pi\sigma_y E}\left(\Delta K^2-\Delta K_{th}^2\right) \tag{2.35}$$

This expression is useful only for the lower portion of the fatigue rate curve and for inert atmospheres, "... A can be expressed as $A = 2\sigma_y / E$, a parameter thought to be related to the rate of strain hardening" (McEvily, 1974), so that

$$\frac{da}{dN} = \frac{8}{\pi E^2}\left(\Delta K^2 - \Delta K_{th}^2\right) \tag{2.36}$$

When aggressive environments are present, the value of A increases which in turn increases the rate of crack growth. The above equation "... provides a baseline for growth rates below 1 x 10^{-6} m/cycle under $R = 0$ conditions" (McEvily, 1974).

To include the stress ratio effect and region III of the fatigue rate curve, the following modification to Equation 2.36 is suggested

$$\frac{da}{dN} = \frac{4A}{\pi \sigma_y E}\left(\Delta K^2 - \Delta K_{th}^2\right)\left(1 + \frac{\Delta K}{K_C - K_{MAX}}\right) \tag{2.37}$$

where

$$\Delta K_{th} = \frac{1.2\left(\Delta K_{th_o}\right)}{1 + 0.2\left(\frac{1+R}{1-R}\right)} \tag{2.38}$$

and ΔK_{th_o} is the ΔK value for $R = 0$.

The equation is based on a simple physical model rather than a purely empirical fit and "... the expression distinguishes between the two components of crack advance; the ductile striation component, the other the static mode component. It is noted that the number of adjustable parameters goes to zero for tests in non-aggressive environments for ΔK values large with respect to K_{th}" (McEvily, 1974).

2.4.7 Pook and Frost Model

Pook and Frost attempted to create a fatigue crack growth equation that has some physical significance. They hypothesized that "… crack growth occurs under cyclic loading not as a consequence of any progressive structural damage but merely because unloading resharpens the crack tip at each cycle and this sequence is responsible for the formation of striations" (Chell, 1979). Therefore the increment of crack growth in each cycle can be related to the changing crack tip geometry during its opening and closing and a simple model based on this is given by the relationship

$$\frac{da}{dN} = \frac{9}{\pi}\left(\frac{\Delta K}{E}\right)^2 \qquad \text{(plane stress)} \qquad (2.39)$$

$$\frac{da}{dN} = \frac{7}{\pi}\left(\frac{\Delta K}{E}\right)^2 \qquad \text{(plane strain)} \qquad (2.40)$$

They found that the prediction of the plane stress equation and experimental data plotted in terms of $\Delta K/E$ against da/dN are in good agreement at crack growth rates around 3×10^{-5} mm/cycle. However, experimental crack growth rates are underestimated at high growth rates and overestimated at low growth rates.

It is interesting to note that a similarity between the above equation and McEvily's equation (non-aggressive environment) exists in the $(\Delta K/E)^2$ term. Also, it has been pointed out by Rice that "… any continuum mechanics theory of crack growth will result in a $(\Delta K/E)^2$ dependence unless a characteristic dimension is introduced" (Frost, 1971).

2.4.8 Zheng and Hirt Model

Lal and Weiss (1978) proposed a static fracture model, where during each cycle, the crack was advanced by a distance over which the maximum normal stress exceeded the critical fracture stress of the metal as illustrated by Figure 2.15.

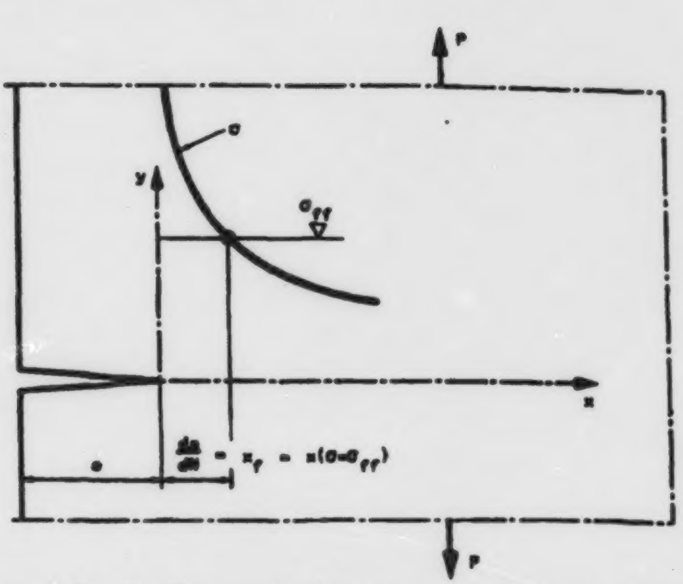

Figure 2.15 - Assumption of the amount of incremental fatigue crack propagation (Zheng and Hirt, 1983)

Their model was moderately successful in predicting fatigue crack growth except it did not account for the crack tip blunting phenomena and their model used material constants that had no physical significance.

Zheng and Hirt (1983) improved the Lal and Weiss model by modifying the static fracture portion and obtained material constants that are defined by the tensile properties of the metal. Briefly, Zheng and Hirt found that upon loading the crack opens elastically and the crack tip becomes blunt, which occurs at a stress intensity threshold denoted as K_{th}. To derive his model, Zheng and Hirt used the fracture parameter $\Delta K_{eff} = K_{max} - K_{th}$ instead of the normal convention that $\Delta K = K_{max} - K_{min}$ since no crack growth occurs below K_{th}. Using this new parameter and the assumption made by Lal and Weiss in Figure 2.15, Zheng and Hirt's model is derived as follows:

$$\frac{da}{dN} = x_f = x\left(\sigma = \sigma_{ff}\right) \tag{2.41}$$

Now from LEFM, the stress in the direction of the applied load along the crack (x-axis) is expressed as

$$\sigma_{yy} = \frac{K_I}{\sqrt{2\pi x}} \tag{2.42}$$

and at the location x_f in Figure 2.15,

$$x_f = \frac{K_I^2}{2\pi\sigma_{ff}^2} \tag{2.43}$$

Combining equation 2.43 and 2.41 and using the new fracture parameter ΔK_{eff}

$$\frac{da}{dN} = \frac{1}{2\pi\sigma_{ff}^2} K_{eff}^2 = \frac{1}{2\pi\sigma_{ff}^2}\left(K_{max} - K_{th}\right)^2 \tag{2.44}$$

The theoretical strength of metallic materials, σ_{ff}, is equal to $\sqrt{E\sigma_f\varepsilon_f}$ where $\sigma_f = \sigma_u(1+RA)$ and $\varepsilon_f = -\ln(1-RA)$ are the materials fracture strength and fracture ductility, respectively, σ_u is the materials ultimate stress and *RA* is the specimens reduction in area at fracture in the tension test. Therefore

$$\frac{da}{dN} = \frac{1}{2\pi E\sigma_f\varepsilon_f}\left(K_{max} - K_{th}\right)^2 \tag{2.45}$$

When $R = 0$, $\Delta K = K_{max}$ and $K_{th} = \Delta K_{th}$ which gives

$$\frac{da}{dN} = B\left(\Delta K - \Delta K_{th}\right)^2 \tag{2.46}$$

where $B = \dfrac{1}{2\pi E\sigma_f\varepsilon_f}$ which is determined from the tensile properties of the metal.

For situations where $R \neq 0$, it has been determined that Equation 2.46 may be used if ΔK_{th} is defined as

$$\Delta K_{th} = \Delta K_{th_0}(1-R)^{\gamma} \qquad (2.47)$$

where ΔK_{th_0} is the crack propagation threshold value for stress ratio equal to zero and γ is a constant between zero and one.

Zheng and Hirt determined that Equation 2.46 is valid when $da/dN \leq 10^{-3}$ mm/cycle which corresponds to regions I and II (for the materials he tested). The experimental and predicted results for various metals can be found in Table 2 of Zheng and Hirt's paper (Zheng and Hirt, 1983).

This appears to be an attractive model because it is capable of predicting fatigue crack growth in regions I and II and the parameters are easily obtained and appear to have some physical significance.

2.4.9 Wang Model

Wang et al. (1994) proposed a damage accumulation theory, which considers the plastic component of the J integral as a damage factor resulting in a simple formula for the fatigue crack growth rate.

The proposed damage accumulation theory assumes

1. The total plastic strain energy density absorbed by the material is a constant prior to reaching its ultimate state. This constant is a parameter that can be determined by tests.

2. The elastic strain energy density stored by the material does not cause damage and is released upon unloading.

Thus, the plastic strain energy accumulated in the material will cause the damage of the material and will lead to failure of the material. This plastic damage only occurs after the maximum elastic component has been reached.

The complete derivation of the fatigue crack growth rate equation shown below is found in the article by Wang.

$$\frac{da}{dN} = \alpha \frac{K_{max}^4}{\overline{\sigma}_y^2}\left[\frac{1}{1-\xi^2} - \frac{1}{1-(R\xi)^2}\right]\left[\frac{1}{\sqrt{1-\xi^2}} - \frac{1}{\sqrt{1-(R\xi)^2}}\right]^2 \tag{2.48}$$

where $\xi^2 = \dfrac{K_{max}^2}{2K_{nf}^2}$

$K_{nf} = \sigma_y \sqrt{\pi a}$

α = a constant determined according to the material and loading condition

σ_y = local yielding strength

$\overline{\sigma}_y$ = average local yielding strength

Based on the research to obtain Equation 2.48, Wang concluded that the crack growth rate is not simply a function of *ΔK*, but a function of average local yielding strength, fracture toughness and amplitude of the applied effective stress intensity factor in regions II and III. The model was verified by using the test results published in ASTM STP 789 by Miller and Gallagher (1981). The test data and the proposed formula were found to be in reasonably good agreement.

2.4.10 Miller and Gallagher's Review of Fatigue Crack Growth Rate Models

This section will discuss the above mentioned article written by M.S. Miller and J.P. Gallagher which presents the results of a round robin life prediction effort. Each participant reviewed a set of baseline data containing specimens test parameters (load, stress ratio, crack length interval) and fatigue crack growth rate data for varying stress ratios. The material used was 2219-T851 Aluminum and each participant was allowed to use an equation of their choice to predict specimen lives for constant amplitude loading which was chosen by the task group chairman. The predictions consisted of both the entire crack growth interval and a shorter interval contained within the larger one.

Nine different methods were used to predict the fatigue life. Each method is capable of modeling all three regions of the crack growth rate curve. Table 2.1 provides a summary of the models used.

Table 2.1 - Fatigue crack growth rate descriptions (Miller et al., 1981)

Participant/ FCGR Description No.	Form	Corresponding Appendix
(1)	$\frac{da}{dN} = C_1 \overline{\Delta K}^{C_2}$	I
(2)	$\frac{da}{dN} = P_1 \frac{(\Delta K - \Delta K_t)^{P_2}}{(\Delta K_c - \Delta K)^{P_3}}$	II
(3)	$\frac{1}{da/dN} = \frac{A_1}{(\Delta K)^{p_1}} + A_2 \left[\frac{1}{(\Delta K)^{p_2}} - C' \right]$	III
(4)	$\frac{da}{dN} = C(K_{max})^m \left[(K_{max} + K_e)(1 - R_{eff}) + {}^{\circ}K \right]^2$	IV
(5)	$\log_{10} \left(\frac{da}{dN} \right) = P_1 \exp(P_2 x) + P_3 \exp(P_4 x) + P_5$	V
(6)	$\frac{da}{dN} = {}_{10}\{C_1 \sinh[C_2(\log \Delta K + C_3)] + C_4\}$	VI
(7)	$\frac{da}{dN} = {}_{10}\{C_1 \sinh[C_2(\log \Delta K + C_3)] + C_4\}$	. . .
(8)	$\frac{da}{dN} = e + (v - e) \left[-\ln \left(1 - \frac{\Delta K}{K_b} \right) \right]^{1/b}$	VII
(9)	tensile ligament instability model	VIII
(10)	table lookup procedure	IX

These models range in complexity and number of parameters that must be determined. A complete description for each model is provided in the appendices of the article. They also provide information of "... (1) measures of accuracy of the fatigue crack growth rate fit, (2) methods used to establish the descriptions coefficients (or constants) and (3) methods of integrating *da/dN = f(ΔK,R)* for those cases where such information is available" (Miller et al., 1981). Therefore only a brief description of each model will be presented in this section.

Model 1 is a modified Paris power-law equation where

$$\overline{\Delta K} = \frac{\Delta K_{eff} - \Delta K_o}{1 - \left(\frac{K_{max}}{K_C} \right)^2} \tag{2.49}$$

and $K_{eff} = (1 - P_{op} / P_{max}) K_{max}$. The ratio P_{op} / P_{max} is calculated from a crack closure model under plane strain conditions and the coefficients C_1, C_2, K_C and ΔK_O are derived from least squares procedures.

Model 2 is a five parameter model where the constants ΔK_t and ΔK_C define the asymptotes at low and high ΔK respectively. P_1 shifts the crack growth rate curve up or down and P_2 and P_3 influence curvature.

In Model 3, the parameters n_1 and n_2 represent the slopes of the data in Region I and II respectively. $C^{'}$ is calculated from the exponent n_2 by the relationship

$$C^{'} = \frac{1}{K_C (1 - R)^{n_2}} \tag{2.50}$$

The coefficients A_1 and A_2 are then determined by multiple linear regression analysis.

Model 4 is another modified Paris equation, which accounts for environmental effects on the crack growth rate. The values of C and m are defined by the modulus of elasticity (units of pounds per square inch) by $C = E^2 (10^{-23})$ and

$$m = 1.442 \ln \left[\frac{10^{7.5}}{E} \right] \tag{2.51}$$

K_e is the environmental parameter and is defined by

$$K_e = K_{econst}\left[\frac{\left(K_{\max} - K_{eo}\right)}{\left(K_{plat} - K_{eo}\right)}\right] \tag{2.52}$$

and $K_e = 0$ when $K_{\max} < K_{eo}$. The point at which K_e becomes constant is represented by K_{plat}. The effective stress ratio is given by

$$R_{eff} = \frac{K_{\min} + \Delta K_o}{K_{\max}} \tag{2.53}$$

where ΔK_o is the threshold value. The term $*K$ fits the upper end of the growth rate data and is given by the relationship

$$*K = \alpha e^{\beta(K_{\max})} \tag{2.54}$$

where α and β are fitting constants.

Model 5 is a five parameter model and the coefficients P_1 through P_5 are determined by the least squares method and x is the base ten logarithm of the stress intensity factor range ΔK.

Model 6 and 7 are the same and were used by two separate participants. It is a hyperbolic sine equation and the parameters C_1 through C_4 are determined by least squares fitting techniques.

Model 8 is a four parameter model where K_b is the normalizing parameter for ΔK, k is the shape parameter, e is the threshold parameter and v is the characteristic value of the shape parameter.

Model 9 is a tensile ligament instability model and "… predicts crack growth behavior by assuming that instability mechanisms induce separation of microstructural tensile ligaments at the crack tip" (Miller et al., 1981). The model includes Poisson's contraction, stress relaxation and environmental surface attack. The numbers of fitting parameters are minimal and have some physical meaning.

Model 10 is based on a table lookup procedure. That is, values of *da/dN* and *ΔK* for each stress ratio are obtained from a smoothed curve through the *da/dN* versus *ΔK* data. The appropriate *da/dN* values are obtained by first determining the *ΔK* value for a crack length interval and obtaining the *da/dN* value by linear interpolation of the table values.

Table 2.2 presents the life prediction ratios for the full interval, Table 2.3 presents the life prediction ratios for the shortened crack length interval and Table 2.4 presents the mean and standard deviation for the sets of life prediction ratio.

Table 2.2 - Life prediction ratios for the full interval (Miller et al., 1981)

	Participant FCGR Description No.									
Specimen No.	1	2	3	4	5	6	7	8	9	10
2219-3	0.96	0.70	0.81	0.77	1.01	1.01	0.99	0.99	1.30	1.03
2219-4	1.04	0.73	0.77	0.82	0.85	0.86	0.89	1.00	1.31	0.94
2219-5	0.71	0.56	0.99	0.65	1.01	1.01	0.91	0.81	0.95	0.91
2219-6	0.40	0.41	1.77	0.74	1.09	1.10	0.83	...	0.55	0.91
2219-11	1.20	0.85	0.89	0.95	0.98	1.00	1.03	1.16	1.50	1.08
2219-20	0.84	0.66	0.70	0.64	0.65	0.66	0.67	...	1.29	0.64
2219-56	0.87	0.82	1.05	0.96	0.95	1.03	1.02	1.03	1.04	0.99
2219-58	0.68	0.69	0.97	0.68	0.97	0.80	0.88	0.96	1.01	0.88
2219-52	0.89	0.66	0.86	0.86	1.04	0.89	23.29	0.95	0.85	1.07
2219-54	0.83	0.70	0.84	0.67	1.11	0.92	0.96	...	1.01	1.00
2219-60	0.90	0.90	1.17	0.66	0.86	0.79	0.95	.	1.47	1.10
2219-19	2.48	1.47	2.22	0.74	1.60	2.61	1.59	...	2.06	1.71
2219-27	1.54	0.93	1.34	0.45	0.99	1 68	0.97	...	1.25	1.02
2219-37	1.13	0.48	0.94	0.98	0.94	0.91	1.00	...	0.54	0.92
2219-CCP-9	0.95	0.73	0.84	...	0.87	...	0.15	...	1.21	0.87
2219-CCP-11	1.26	0.96	1.10	...	1.14	...	0.24	..	0.55	1.14

Table 2.3 - Life prediction interval for the shortened interval (Miller et al., 1981)

	Participant FCGR Description No.									
Specimen No.	1	2	3	4	5	6	7	8	9	10
2219-3	0.93	0.68	0.80	0.72	1.01	1.02	0.99	0.98	1.33	1.05
2219-4	1.15	0.82	0.84	0.91	0.93	0.95	0.98	1.11	1.22	0.99
2219-5	0.67	0.54	1.04	0.62	1.04	1.03	0.92	0.80	0.83	0.91
2219-6	0.37	0.39	1.90	0.75	1.12	1.13	0.84	. .	0.50	0.93
2219-11	1.16	0.83	0.85	0.92	0.94	0.96	0.99	1.12	1.24	1.00
2219-20	1.17	0.96	1.00	0.89	0.98	0.99	0.99	1.02	1.87	0.93
2219-56	0.79	0.75	0.72	0.86	0.91	0.92	0.96	0.95	0.88	0.92
2219-58	0.65	0.68	0.95	0.64	0.99	0.79	0.86	0.94	1.04	0.86
2219-52	0.86	0.65	0.85	0.88	1.09	0.87	6.52	0.95	0.89	1.16
2219-54	0.86	0.75	1.10	0.68	1.18	1.00	0.99	1.20	1.10	1.01
2219-60	0.95	1.04	1.18	0.67	0.87	0.73	0.95	. .	1.41	0.92
2219-19	3.21	2.19	2.23	0.52	1.73	3.40	1.80	. .	1.55	1.97
2219-27	1.77	1.21	1.14	0.27	0.93	1.85	0.95	.	0.79	1.04
2219-37	0.58	0.46	0.89	0.80	0.96	0.91	0.97	0.97	0.71	0.93
2219-CCP-9	1.04	0.80	0.91	...	0.95	0.95	0.17	2.79	0.30	0.95
2219-CCP-11	1.27	0.97	1.11	...	1.15	1.16	0.21	3.40	0.37	1.16

Table 2.4 - Life prediction mean and standard deviation (Miller et al., 1981)

	Participant FCGR Description No.									
	1	2	3	4	5	6	7	8	9	10
Full crack growth interval										
Mean	0.95	0.72	1.00	0.76	0.96	0.97	2.32	0.99	1.05	0.96
Standard	0.27	0.16	0.27	0.15	0.12	0.24	5.81	0.10	0.32	0.12
Short crack growth interval										
Mean	0.95	0.77	1.02	0.73	1.00	1.02	1.22	1.35	0.96	0.98
Standard	0.34	0.22	0.28	0.17	0.09	0.26	1.49	0.83	0.41	0.09
Group number	IV	IV	II	IV	I	III	II	II	IV	I

The life prediction ratio is equal to the ratio of predicted specimen life (N_p) to actual measured specimen life (N_a). Therefore a predicted ratio less than one underestimates the specimens life (conservative) and a ratio greater than one overestimates the specimen life (unconservative). In Table 2.4 the group numbers are defined as

Group I - 90 to 100% of life prediction ratios within 20% of 1.00
Group II - 80 to 90% of life prediction ratios within 20% of 1.00
Group III - 70 to 80% of life prediction ratios within 20% of 1.00
Group IV - less than 70 % of life prediction ratios within 20% of 1.00

Based on the above results, it can be concluded that most fatigue crack growth rate models will accurately predict fatigue crack growth rates under constant amplitude loading. It also highlights the most effective fatigue crack growth models, which were $\log_{10}(da/dN) = P_1 \exp(P_2 x) + P_3 \exp(P_4 x) + P_5$ and the table lookup procedure. It is interesting to note that the more accurate fatigue crack growth models required an individual data fit for each stress ratio data set whereas the least accurate models used one collective data fit for all stress ratios.

2.4.11 Dowling and Begley Model

The previously discussed fatigue crack growth models have the common fracture parameter ΔK which means that the equations assume LEFM is always valid. Equation 2.1 states the limits on the applicability of LEFM and if this condition is violated during fatigue crack growth, the use of the stress intensity factor is not admissible. For situations of fatigue crack growth under large scale yielding conditions, where the stress intensity factor is no longer valid, Dowling and Begley suggested to use the ΔJ integral as the fracture parameter. They fit the growth rate data to a power law expression by using ΔJ given by the relationship

$$\frac{da}{dN} = C_{DB} \Delta J^{m_{DB}} \tag{2.55}$$

This equation is very similar to the Paris equation in that it 'fits' the data in region II and does not include the stress ratio effect; however, it is used in situations where fatigue crack growth occurs under large scale yielding conditions.

2.5 Summary of Constant Amplitude Loading Models

A total of nineteen constant amplitude fatigue crack growth models were discussed and each varied in the approach used, number of calibration parameters and complexity. Most models used empirical curve fitting parameters obtained from the results of fatigue testing; however, three models were discussed that have no empirical parameters but rather are based on the materials tensile properties.

The majority of the models, if calibrated properly, adequately predict the fatigue life of a component. The selection of the appropriate model is usually based on the analyst's experience and personal preference. This thesis will consider the previously discussed models during the experimental data analysis section, with more emphasis on those models that are simple to use and/or have few curve fitting parameters.

2.6 Variable Amplitude Loading Models

Although constant amplitude loading does occur in practice, usually in rotating machinery, the majority of structures are subjected to variable amplitude loading. During this type of loading it has been well established that various load interactions occur which may significantly alter the growth behavior of a crack. The constant amplitude loading fatigue crack growth rate models previously discussed do not account for these load interactions and thus may not accurately represent the fatigue crack growth process. The various load interactions that occur will be discussed in the next section followed by some fatigue crack propagation laws that are used to predict the crack growth of components subjected to variable amplitude loading.

2.6.1 Load Interactions

In a variable amplitude loading scenario, stresses of differing magnitude occur and affect the crack growth rate depending upon their sequences. Three load sequences, which have a significant effect on the fatigue crack growth rate, are a tensile overload, compressive underload and a tensile overload followed by a compressive underload which are commonly referred to as crack retardation, crack acceleration and reduction in crack retardation, respectively. It is because of these interactions, which are highly dependent upon the loading sequence, that variable amplitude loading is more complex than constant amplitude loading. Another factor which complicates the situation is that the load sequence must be known so that the correct order may be applied during analysis; however, variable amplitude loading is difficult, if not impossible, to predict.

The simplest type of variable amplitude loading is the occurrence of high peak loads interspersed in a constant amplitude history. When the peak load is tensile, the crack growth immediately following the overload is slower than the 'normal' growth rate. This continues for a number of cycles until the original growth rate is resumed. This behavior for multiple and a single overload is illustrated by Figure 2.16a and 2.16b respectively.

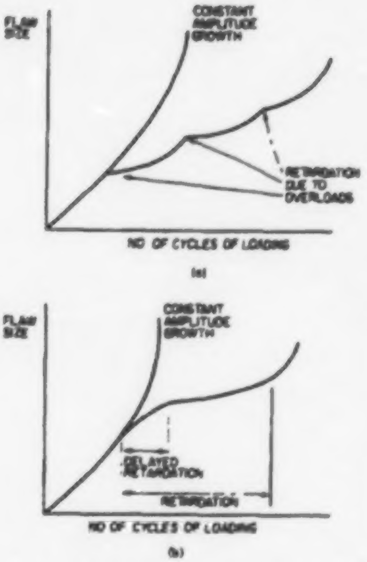

Figure 2.16 - Retardation (a) Multiple overloads and (b) Single overloads (Barsom, 1995)

The physical interpretation is that a tensile overload introduces a larger compressive residual stress field in the vicinity of the crack tip compared to before the overload. This retards the crack growth by helping to keep the crack tip closed during the subsequent relatively smaller loads. This continues until the crack has grown through the overload residual stress field and the original stress field is restored. The amount of retardation is described by the overload ratio, OLR, which is equal to the magnitude of the overload stress to the 'normal' peak stress value. The higher the overload ratio the greater the retardation and for overload ratios greater then two or three, crack arrest may occur.

When a compressive underload is interspersed in constant amplitude loading, the crack growth rate following the underload will be greater than that of the constant amplitude load. The crack growth acceleration is short lived and the 'normal' constant amplitude growth rate is restored quickly as illustrated by curve 'd' in Figure 2.17.

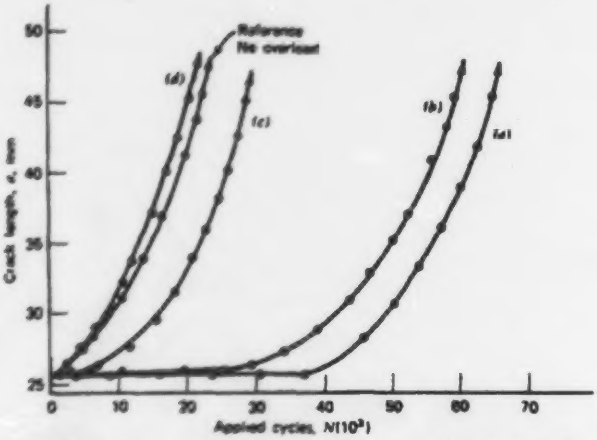

Figure 2.17 - Crack growth behavior for (a) Tension overload (b) Compression-tension overload (c) Tension-compression overload and (d) Compression underload (Fuchs, 1980)

If a compressive underload immediately follows a tensile overload, the amount of retardation is reduced but not eliminated. On the other hand, a compressive underload applied prior to overloading has only a little change on the amount of crack retardation.

Figure 2.17 illustrates the relative effect of the previously discussed load interactions that are encountered. The overload sequence effects will be of greater importance when they occur predominately in one direction. Less effect is expected "... if overloads occur in both directions, if the history is highly irregular or if the overloads are relatively mild" (Dowling, 1993).

Numerous attempts have been made to develop a fatigue crack growth law which includes the load interactions and they will be discussed in the following sections. The majority of the fatigue models neglect the crack acceleration effect because of the dominance of the crack retardation.

2.6.2 Use of Constant Amplitude Loading Fatigue Crack Growth Models

The simplest approach to fatigue crack growth for variable amplitude loading is to neglect all sequence effects and determine the crack growth on a cycle by cycle basis in conjunction with a constant amplitude fatigue crack growth law. This method neglects the sequence effects that generally provide a conservative estimate of crack growth life sufficient for preliminary analysis.

The advantages of this approach are that it is relatively simple, inexpensive and not very time consuming. If it has been previously determined that the load sequences effects cancel each other or are entirely unpredictable, this may be the best method to use because nothing would be gained by conducting a more detailed analysis.

2.6.3 Wheeler Model

Wheeler (1972) proposed a model that accounts for retardation by introduction of a retardation parameter, ϕ_R. Wheeler's model is applicable to any fatigue crack growth equation of the form $da/dN = f(\Delta K, R)$. He considers any retardation effects by including a retardation parameter such that $da/dN = \phi_R f(\Delta K, R)$ where

$$\phi_R = \begin{cases} \left(\dfrac{R_y}{a_p - a}\right)^{\gamma} & , \quad a + R_y < a_p \\ 1 & , \quad a + R_y \geq a_p \end{cases} \tag{2.56}$$

and R_y is the extent of the current yield zone, $a_p - a$ is the distance from the crack tip to the elastic-plastic interface and γ is the shaping exponent. These terms are illustrated in Figure 2.18.

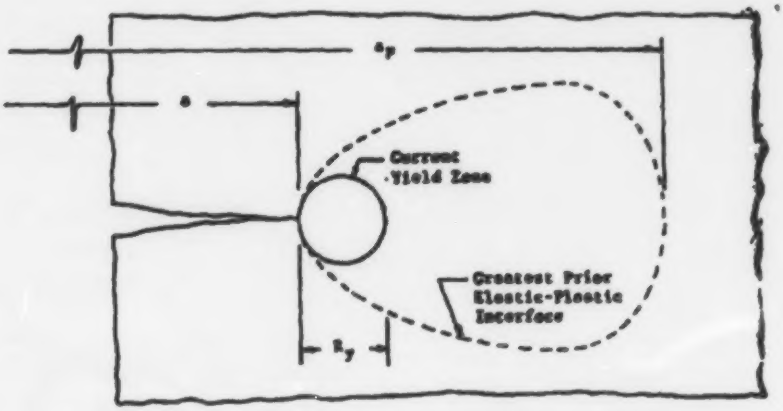

Figure 2.18 - Crack tip yield zones (Wheeler, 1972)

The solid line represents the yield zone due to the current applied load and the dotted line is the extent of yielding due to some prior overload. When the crack has propagated through the overload zone, the current yield zone is equal to the greatest elastic-plastic interface and $\phi_R = 1$. This corresponds to no retardation and thus the fatigue crack growth rate reduces to that of constant amplitude loading, $da/dN = f(\Delta K, R)$. The plastic zone size is calculated by using an appropriate equation. One such equation was previously discussed in Section 2.1.2.3 and Wheeler (1981) suggests to use the relationship

$$R_y = \frac{1}{\pi\, 4\sqrt{2}}\left(\frac{K_I}{\sigma_y}\right)^2 \tag{2.57}$$

for a plane strain condition.

The shaping exponent, γ, is determined by empirically fitting the variable amplitude loading test data and it generally depends upon the material and the nature of the load spectrum that is being considered. Therefore, once a value of γ has been obtained it should only be used to predict fatigue life for components of similar material and load spectrum type. If a different load spectrum type is to be applied γ must be re-calibrated otherwise serious errors will result.

2.6.4 Willemborg Model

Willemborg advanced Wheeler's model by determining the amount of retardation as a function of the stress intensity factor necessary to cancel the effect of the overload plastic zone. It does not require any empirical parameters; only the material yield stress must be determined. The modified stress intensity factor, which includes retardation, is given by the relationship

$$K_r = \left(K_{\max}\right)_{OL}\left(1-\frac{\Delta a}{Z_{OL}}\right)^{1/2} - K_{\max i} \tag{2.58}$$

where $\left(K_{\max}\right)_{OL}$ is the maximum stress intensity factor during the overload cycle, Δa is the amount of crack growth since the overload cycle, Z_{OL} is the overload plastic zone size and $K_{max i}$ is the maximum stress intensity factor for cycle i. Johnson proposed the overload plastic zone size be calculated by using the relationship

$$Z_{OL} = \frac{1}{\beta\pi}\left[\frac{(K_{\max})_{OL}}{\sigma_y}\right]^2 \tag{2.59}$$

Once the current yield zone has extended through the overload zone ($\Delta a = Z_{OL}$) the value for K_r is set equal to zero. The effective stress intensity factor is used and defined as $\Delta K_{eff} = K_{\max\,eff} - K_{\min\,eff}$ where $K_{\max\,eff} = K_{\max i} - K_r$ and $K_{\min\,eff} = K_{\min i} - K_r$. If one desires to use a fatigue crack growth law which is a function of both ΔK and R, one must use an effective overload ratio defined by

$$R_{eff} = \frac{K_{\min\ eff}}{K_{\max\ eff}} \tag{2.60}$$

Therefore Forman's equation in conjunction with Willemborg's model will become

$$\frac{da}{dN} = C_F \frac{\left(\Delta K_{eff}\right)^{m_F}}{(1-R)K_C - \Delta K_{eff}} \tag{2.61}$$

2.6.5 Elber Model

Elber introduced the crack closure concept to analyze crack propagation under variable amplitude loading. It is based on the observation that the faces of fatigue cracks close before all the tensile load is removed. Previously, it was assumed that a crack is closed under compressive loads and open under tensile load. The crack closure under tensile load is due to residual deformation in the wake of the crack.

Elber observed that for a stress-displacement curve (Figure 2.19)

1. Slope AB is linear and equal to that of the uncracked body
2. Slope CD is linear and equal to that of the cracked body
3. Nonlinear line BC is the transition from fully open and fully closed crack

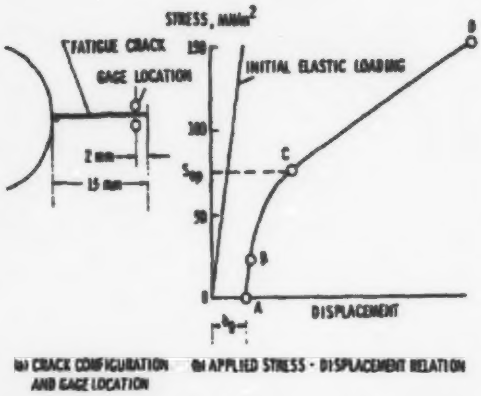

Figure 2.19 - Crack closure results for fatigue crack propagation (Elber, 1971)

Therefore, assuming that crack propagation can only occur for the portion of the loading cycle for which the crack is fully open, Elber proposed a parameter defined as

$$\Delta K_{eff} = K_{max} - K_{op} \tag{2.62}$$

where K_{op} is the stress intensity factor corresponding to a fully open crack. He also introduced an effective stress intensity ratio defined as

$$U = \frac{\Delta K_{eff}}{\Delta K} = \frac{K_{max} - K_{op}}{K_{max} - K_{min}} \tag{2.63}$$

Using the above expressions, any existing fatigue crack growth relationship could be utilized by simply replacing ΔK by $U\Delta K$. Elber proposed a modified Paris equation

$$\frac{da}{dN} = C_p \Delta K_{eff}^{m_p} = C_p (U\Delta K)^{m_p} \tag{2.64}$$

The difficulty is in determining the appropriate K_{op} value required to obtain U. Elber determined the relationship

$$U = 0.5 + 0.4R \qquad -0.1 \le R \le 0.7 \tag{2.65}$$

which is based on tests for aluminum 2024-T3. Other relationships for various materials have been obtained and reported in the literature.

The significance of this model is that crack closure appears to be a significant factor in causing load interactions. In the crack closure model, "... crack growth retardation following an overload is not visualized as a consequence of residual compressive stresses ahead of the crack tip, but rather as the result of a wake of residual local deformation left behind the crack tip as it propagates" (Collins, 1993).

Some limitations of the model are that the relationships for U and K_{op} must be determined for the specific material, loading type and region on the fatigue rate curve. Further, the definition of the closure load is somewhat arbitrary and is the subject of on going research. Finally, "... the complex way in which σ_{op} (K_{op}) must be determined for each load cycle and the step by step counting method of generating the crack growth curve requires a large computer program and long running times" (Chell, 1979).

2.6.6 Barsom Model

Barsom's objective was to obtain a single stress intensity parameter capable of describing the crack growth rate under both constant and variable amplitude loading. For this approach, it is required that the variable amplitude load spectra be represented by a continuos unimoidal distribution function (for example; Rayleigh probability density curves or log-normal functions) and the loading condition should result in a relatively smooth continuous crack length versus number of cycles curve.

If the above requirements are satisfied, Barsom proposed the relationship

$$\frac{da}{dN} = A_B\left(\Delta K_{rms}\right)^{m_B} \tag{2.66}$$

where A_B and m_B are constants and

$$\Delta K_{rms} = \sqrt{\frac{\sum_{i=1}^{k} \Delta K_i^2}{n}} \tag{2.67}$$

The ΔK_{rms} parameter represents the square root of the mean of the squares of the individual load cycles in a spectrum.

This method is extremely simple because it only requires the curve fitting parameters A_B and m_B to be determined (similar to Paris coefficients) along with the value for ΔK_{rms} which is determined from the variable amplitude load spectra. The load interactions are not included but are assumed to occur often, and thus this method determines the average fatigue crack growth rate. In other words, an equivalent constant amplitude load is determined from the variable amplitude spectra. Therefore the most accurate predictions can be made for a large number of random cycles closely spaced together.

Barsom verified his model by testing various bridge steels (A36, A588-A, A588-B, A514-B, A514-E and A514-F) under variable amplitude load spectra having Rayleigh probability density curves of $\sigma_{rd} / \sigma_{rm}$ values equal to 0 (constant amplitude), 0.5 and 1.0 as illustrated by Figure 2.20.

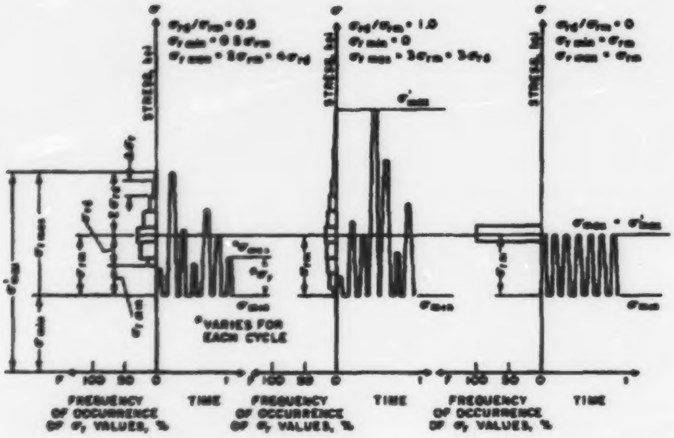

Figure 2.20 - Stress spectra (Imhof et al., 1973)

The ratio $\sigma_{rd} / \sigma_{rm}$ is equal to the standard deviation divided by the peak value of the distribution. The major disadvantages of this model are that the load spectrum of the structure must be accurately known and follow certain relationships.

2.6.7 McEvily Model

In Section 2.4.6, McEvily proposed a fatigue crack growth law for constant amplitude loading. Upon examining the details of Barsom's model, he extended his constant amplitude loading model to include variable amplitude loading as follows.

For constant amplitude loading

$$\frac{da}{dN}=\frac{C}{\sigma_y E}\left(\Delta K^2-\Delta K_{th}^2\right)\left(1+\frac{\Delta K}{K_C-K_{MAX}}\right) \tag{2.68}$$

McEvily determined that the crack growth rate was independent of mean stress for crack growth less than 10^{-4} inch/cycle and thus the contribution due to static modes in Equation 2.68, that is, the $\frac{\Delta K}{K_C-K_{max}}$ term can be neglected. Now by considering an average rate of crack growth under a variable load, $(da/dN)_{avg}$ "... can be taken to be equal to the average contribution from each of the cycles over the increment of crack growth considered" (Barsom, 1976).

$$\left(\frac{da}{dN}\right)_{avg}=\frac{C}{\sigma_y E}\sum_{i+N}^{i+N+\Delta N}\frac{\Delta K_i^2}{\Delta N}-\Delta K_{th}^2 \tag{2.69}$$

The quantity $\frac{\sum \Delta K^2}{\Delta N}$ is the square of ΔK_{rms} so Equation 2.69 becomes

$$\left(\frac{da}{dN}\right)_{avg}=\frac{A}{\sigma_y E}\left(\Delta K_{rms}^2-\Delta K_{th}^2\right) \tag{2.70}$$

The above equation is similar in nature to Barsom's model and includes the threshold value.

2.6.8 Ahn's Model

Ahn and Mendel (1994) proposed a probabilistic fatigue life model which is derived from the differential equation governing the fatigue process and contains a single parameter (Barsom's root mean square stress range) which has a direct physical meaning pertinent to the fatigue process. The differential equation used was the Paris equation; however, it is possible to develop the following formulation on any other. The Paris model was chosen because of its simplicity.

Briefly, Ahn defined the number of cycles requiring a unit crack increment (ΔN_i) as the random variable and L as the number of cycles necessary to cause fatigue failure. Therefore

$$L = \Delta N_1 + \Delta N_2 + \ldots + \Delta Nm \tag{2.71}$$

where m is the number of unit increments chosen. For constant amplitude loading, Paris's equation is

$$\frac{\Delta a}{\Delta N} = C\left(Y\Delta\sigma\sqrt{\pi a}\right)^m \tag{2.72}$$

which gives the number of cycles ΔN needed for a crack increment Δa at any point along the crack. Substituting Equation 2.72, for ΔN, into Equation 2.71 gives

$$L = \frac{1}{(\Delta\sigma)^m}\left(\frac{\Delta a}{A\pi^{m/2}Y^m}\right)\left(\frac{1}{a_o^{m/2}} + \ldots + \frac{1}{\left(a_o + \left(M^* - 1\right)\Delta a\right)^{m/2}}\right) = B(\Delta\sigma)^m \tag{2.73}$$

Therefore if one knows the stress range $\Delta\sigma$, the number of cycles to cause fatigue failure (L) is known.

For a variable amplitude load, $\Delta\sigma$ varies in an unknown manner and the ΔN_i's and L are random variables. To determine the value of $\Delta\sigma$, Barsom's root mean square method is employed. That is, by using the relationship $\Delta K = Y\Delta\sigma\sqrt{\pi a}$, the root mean square approach gives

$$\Delta\sigma_{rms} = \left(\frac{1}{n}\sum_{i=1}^{n}\Delta\sigma_i^2\right)^{1/2} \tag{2.74}$$

where $\Delta\sigma_{rms}$ completely characterizes the crack propagation rate. Using the above expression in conjunction with a Gaussian distribution gives

$$p(l/\Delta\sigma_{rms})\alpha\left(\frac{1}{\Delta\sigma_{rms}}\right)l^{-1/m-1}\exp\left(-\frac{l^{-2/m}B^{2/m}}{2\Delta\sigma_{rms}^{2}}\right)dl \tag{2.75}$$

where α denotes 'proportional to'. This expression represents a likelihood model for fatigue life. An unconditional or predictive distribution is determined as follows

$$p(l)=\int_{0}^{\infty}p(l/\Delta\sigma_{rms})\pi(\Delta\sigma_{rms})d\sigma_{rms} \tag{2.76}$$

The area under this curve represents the probable fatigue life of the component and this method is good for narrow banded random processes.

2.6.9 Variable Amplitude Load Fatigue Crack Growth Predictions

As it has been shown so far, fatigue crack growth analysis for a variable amplitude load spectrum is more difficult than that of constant amplitude loading. To asses the capability of using constant amplitude fatigue crack growth rate to predict the crack growth behavior of center cracked panels subjected to random flight-by-flight spectrum loading, ASTM task group E24.06.01 was formed. The group members were asked to make crack growth predictions for 13 center cracked tension specimens, without prior knowledge of the test results, using any fatigue crack growth model of their choice. Six different models were used and some included load interactions and others did not. A description of the models used and the results of the task group are the subject of the book ASTM STP 748 and will be briefly discussed for the remainder of this section.

Initially, each participant was provided with the material baseline constant amplitude crack growth rate data, specimen dimensions, the initial crack sizes for each test and the random spectrum load tables. The baseline data consisted of a *da/dN* versus ΔK plot for load ratios R = 0.1, 0.2, 0.3 and 0.7 with the maximum stress kept at 138.1 MPa. The fracture toughness was determined to be 70.85 MPa. The material used was a 6.35 mm thick 2219-T851 aluminum plate. The random spectrum data was representative of a typical fighter aircraft and generated by a computer program employing a random noise theory. Details for the above data are provided in the first article of the ASTM publication (Chang, 1981a).

2.6.9.1 C. M. Hudson Model

Hudson used a root mean square approach, similar to that proposed by Barsom, for predicting the fatigue crack growth under aircraft random spectrum loading. This approach is relatively simple and neglects load interaction effects. It requires analyzing the loading history for each specimen to determine the root mean square maximum and minimum stresses. The predictions are then made by assuming the tests had been conducted under constant amplitude loading at the root mean square maximum and minimum stress levels. This method provides an 'average' fatigue crack growth rate, and if the influence of the load interactions are small, provides good results. Since the loading is random in nature, it is reasonable that the load interactions will offset one another. "For non-random loading sequences where relatively few high load cycles cause long delays in fatigue crack growth, this approach will probably not be applicable" (Hudson, 1981).

The maximum and minimum root mean square stress levels were calculated by using the relationships

$$S_{\max\ rms} = \left[\frac{1}{N}\sum_{i=1}^{N}\left(S_{\max}\right)^{2}\right]^{0.5} \tag{2.77}$$

and

$$S_{\min\ rms} = \left[\frac{1}{N}\sum_{i=1}^{N}\left(S_{\min}\right)^{2}\right]^{0.5} \tag{2.78}$$

where S_{max} and S_{min} are the maximum and minimum stresses of the random load spectrum and N is the total number of S_{max} or S_{min} values. Now the root mean square stress ratio is calculated by

$$R_{rms} = \frac{S_{\min\ rms}}{S_{\max\ rms}} \tag{2.79}$$

The root mean square maximum and minimum stress intensity factors are calculated from Equation 2.71 and 2.72 respectively in conjunction with the correction factor for a center cracked specimen. This gives

$$K_{\max\ rms} = S_{\max\ rms}\sqrt{\pi\, a \sec\left(\frac{\pi\, a}{W}\right)} \tag{2.80}$$

and

$$K_{\min\ rms} = S_{\min\ rms}\sqrt{\pi\, a \sec\left(\frac{\pi\, a}{W}\right)} \tag{2.81}$$

where a is the crack length and W is the specimen width. Therefore the root mean square stress intensity range is

$$\Delta K_{rms} = K_{\max\ rms} - K_{\min\ rms} \tag{2.82}$$

Hudson used the above root mean square parameters in conjunction with Forman's equation to predict fatigue crack growth rates. That is,

$$\frac{da}{dN} = \frac{C\Delta K_{rms}^{m}}{\left(1 - R_{rms}\right)K_C - \Delta K_{rms}} \tag{2.83}$$

where K_C is the elastic fracture toughness. The above equation was numerically integrated from the initial flaw size to the critical flaw size.

2.6.9.2 J.C. Newman Jr. Model

Newman used a crack closure approach for predicting the fatigue crack growth life. The method is based on a concept like the Dugdale model, but was modified to leave plastically deformed material in the wake of the advancing crack tip. The crack opening stress (σ_{op}), as a function of crack length and load history was calculated from the analytical model. Then, the effective stress intensity factor range, as proposed by Elber, was calculated. Details of the model are provided by Newman (1981).

The fatigue crack growth law was given by the relationship

$$\frac{da}{dN} = C_1 \left[\frac{\Delta K_{eff}}{1 - \left(\frac{K_{max}}{C_3} \right)^2} \right]^{C_2} \tag{2.84}$$

where $\Delta K_{eff} = \left(\sigma_{max} - \sigma_{op} \right) Y \sqrt{\pi a}$. The parameters C_1 to C_3 were determined from the constant amplitude load data by using a least squares regression.

The predictions Newman provided to the task group were based on Equation 2.78. After the results were known, he modified the fatigue crack growth law and re-predicted the results with the following equation

$$\frac{da}{dN} = C_1 \Delta K_{eff}^{C_2} \left[\frac{1 - \left(\frac{\Delta K_O}{\Delta K_{eff}} \right)^2}{1 - \left(\frac{K_{max}}{C_3} \right)^2} \right] \tag{2.85}$$

where

$$\Delta K_O = C_3 \left(1 - C_4 \frac{\sigma_O}{\sigma_{max}} \right) \tag{2.86}$$

and

$$K_{max} = \sigma_{max} Y \sqrt{\pi a} \tag{2.87}$$

In addition, he re-predicted the results using a linear cumulative damage rule. The predictions with this approach were good, which indicated that retardation and acceleration nearly canceled each other out for most of the load spectra. Table 2.5 represents the results for the three methods used by Newman.

Table 2.5 - Comparison of experimental and predicted crack growth under spectrum loading (Newman, 1981).

						Closure Model		
Spectrum Type	Scale Factor	Specimen	c_i, mm	c_f, mm	Test N_T Cycles	$\alpha = 2.3$ $\frac{N_P}{N_T}$	$\frac{N_P{}^a}{N_T}$	LCD.[b] $\frac{N_P}{N_T}$
Air-to-Air Fighter	0.2	M81	4.06	13.0	115 700	1.20	1.01	1.27
	0.3	M82	3.81	35.4	58 585	0.71	0.67	0.85
	0.4	M83	3.81	23.3	18 612	0.66	0.64	0.89
Air-to-Ground Fighter	0.2	M84	4.00	55.9	268 908	1.48	1.47	1.09
	0.3	M85	3.66	44.1	95 642	0.96	0.89	0.81
	0.4	M86	3.87	32.8	36 397	0.72	0.65	0.70
Navigation Fighter	0.3	M88	3.81	45.8	380 443	1.47	2.52	0.73
	0.4	M89	3.81	38.4	164 738	1.06	1.47	0.62
Composite Mission Fighter	0.2	M90	3.87	51.6	218 151	1.14	1.17	1.09
	0.3	M91	3.81	36.1	65 627	0.85	0 78	0.87
	0.4	M92	3.81	29.5	22 187	0.74	0.69	0.88
Composite Mission Transport	0.2	M93	6.35	13.6	1,354 024	1.02	0.76	3.00
	0 3	M94	6.54	9.5	279 000	0.76	1.25	1.81
					Mean	0.98	1.12	1.12
					Standard deviation	0.28	0.50	0.63

[a] Predictions submitted in the ASTM Task Group E24.06.01 round-robin analysis.

[b] Linear-cumulative damage (no retardation and no acceleration) predictions from Johnson (this publication, pp. 85–102).

2.6.9.3 W. S. Johnson Model

Johnson used a multi-parameter yield zone (MPYZ) model for predicting the fatigue crack growth under aircraft random spectrum loading. The MPYZ model accounts for crack growth retardation, acceleration and underload effects by decreasing or increasing the stress ratio used in a modified Forman crack growth equation. It is assumed that the load interactions are a result of the residual stress intensity due to plastic deformation at the crack tip.

For the present study, Johnson used a slightly altered form of the Forman equation given by the relationship

$$\frac{da}{dN} = \frac{C\Delta K^{n}}{\left(1 - R^{eff}\right)^{m} K_{C} - \Delta K} \tag{2.88}$$

where $m = 1$ at $R \geq 0$ and $m = 2$ at $R < 0$. The full stress intensity range (ΔK) is used; that is, the stress range includes the compressive portions. R^{eff} accounts for the three load interaction effects by adjusting its value during each cycle. Therefore, the procedure used to determine the proper value of R^{eff} to account for retardation, acceleration and underload effects is discussed. The parameters C and n are determined from the supplied constant amplitude load data. Finally, if the value of ΔK is less than ΔK_{th}^{*}, then equation 2.82 is not applicable and no crack growth results. The threshold for each cycle is

$$\Delta K_{th}^{*} = \left(1 - R^{eff}\right)\Delta K_{th} \tag{2.89}$$

where ΔK_{th} is obtained from data for $R = 0$. The effective stress ratio is defined by the relationship

$$R^{eff} = \frac{K_{min} - K_{R}}{K_{max} - K_{R}} = \frac{K_{min}^{eff}}{K_{max}^{eff}} \tag{2.90}$$

where K_R is the residual stress intensity and will be positive or negative depending on whether there is retardation or acceleration, respectively. The maximum allowable stress ratio that can be used is

$$R_{\max} = \left[\frac{0.2Z_{OL}}{t}\right] + 0.6 \tag{2.91}$$

where Z_{OL} is the plastic zone diameter for the applied $K_{\max}$.

The value of K_R to be used in Equation 2.84 is difficult to obtain and involves numerous equations. These will not be reproduced in this report as they are defined by Johnson (1981).

2.6.9.4 J.L. Rudd and R.M. Engle Jr. Model

Rudd and Engle used Walker's crack growth rate equation where the compressive loads were set equal to zero and the tensile load retardation effect was accounted for by a generalized Willemborg model. Specifically, the equation

$$\frac{da}{dN} = C\left[\frac{\Delta K}{(1-R)^{1-\gamma}}\right]^{n} \tag{2.92}$$

was used and the parameters determined from the constant amplitude data. This equation was numerically integrated on a cycle by cycle basis. The effect of compressive underload applied immediately after a tensile overload was ignored. Retardation was accounted for by replacing ΔK by the following effective value

$$(\Delta K)_{eff} = \frac{(K_{\min})_{eff}}{(K_{\max})_{eff}} \tag{2.93}$$

The effective $K_{\max}$ and $K_{\min}$ values are defined by Rudd et al. (1981).

2.6.9.5 Chang et al (Model One)

Chang et al. (1981b) used Walker's crack growth rate equation where the compressive loads were set equal to zero and the tensile load retardation was not accounted for. That is, for $\Delta K > \Delta K_{th}$

$$\frac{da}{dN} = C\left[\frac{\Delta K}{(1-R)^{1-r}}\right]^{n} \tag{2.94}$$

and for $\Delta K \leq \Delta K_{th}$, da/dN is equal to zero. The stress intensity threshold value is defined by

$$\Delta K_{th} = (1-R)\Delta K_{th0} \tag{2.95}$$

This procedure is similar to that of Walker's and neglects load interaction effects.

2.6.9.6 Chang et al (Model Two)

This model also utilizes Walker's crack growth rate equation; however, the load interaction effects are accounted for by the Willenborg/Chang model. This load interaction model is the same as the one used by Rudd and Engle and is discussed in detail by Chang et al. (1981b).

2.6.9.7 Results and Discussion

The results obtained by the six different fatigue crack growth models are presented in Table 2.6

Table 2.6 - Random spectrum round-robin analysis summary (Chang, 1981a)

Test No.	Mission Type	Test Life, cycles; (c_i to c_f, in.^{a})	Analytical Predictions, cycles; (N_{pred}/N_{test})					
			JC(1)	CMH	JN	WSJ	JR	JC(2)
M-81	Fighter (A-A)^b	115 700	140 720	246 000	115 800	137 000	213 110	168 720
	DLS^c = 20 ksi^d	(0.16 to 0.501)	(1.21)	(2.13)	(1.01)	(1.18)	(1.84)	(1.46)
M-82	Fighter (A-A)	58 585	44 525	79 000	39 125	57 000	74 055	53 312
	DLS = 30 ksi	(0.15 to failure)	(0.76)	(1.35)	(0.67)	(0.97)	(1.26)	(0.91)
M-83	Fighter (A-A)	18 612	14 703	25 359	11 940	19 700	25 944	17 309
	DLS = 40 ksi	(0.15 to failure)	(0.79)	(1.36)	(0.64)	(1.06)	(1.39)	(0.93)
M-84	Fighter (A-G)^e	268 900	302 816	395 292	396 230	342 000	496 284	368 662
	DLS = 20 ksi	(0.158 to failure)	(1.13)	(1.47)	(1.47)	(1.27)	(1.85)	(1.37)
M-85	Fighter (A-G)	95 642	73 644	99 368	84 850	90 020	131 868	91 816
	DLS = 30 ksi	(0.144 to failure)	(0.77)	(1.04)	(0.89)	(0.94)	(1.38)	(0.96)
M-86	Fighter (A-G)	36 367	23 275	29 789	23 820	30 000	45 034	29 093
	DLS = 40 ksi	(0.153 to failure)	(0.64)	(0.82)	(0.65)	(0.82)	(1.24)	(0.80)
M-88	Fighter (I-N)^f	380 443	281 528	475 292	959 700	589 000	810 900	528 816
	DLS = 30 ksi	(0.150 to failure)	(0.74)	(1.25)	(2.52)	(1.55)	(2.13)	(1.39)
M-89	Fighter (I-N)	164 738	95 548	155 294	242 380	223 000	288 900	184 507
	DLS = 40 ksi	(0.150 to failure)	(0.58)	(0.94)	(1.47)	(1.35)	(1.75)	(1.12)
M-90	Fighter Composite	218 151	231 240	430 225	255 090	270 400	401 140	290 140
	DLS = 20 ksi	(0.153 to failure)	(1.06)	(1.97)	(1.17)	(1.24)	(1.84)	(1.33)
M-91	Fighter Composite	65 627	51 845	93 473	51 165	66 000	97 679	65 630
	DLS = 30 ksi	(0.15 to failure)	(0.79)	(1.42)	(0.78)	(1.01)	(1.49)	(1.01)
M-92	Fighter Composite	22 182	17 080	31 446	15 370	22 800	34 000	21 738
	DLS = 40 ksi	(0.15 to failure)	(0.77)	(1.42)	(0.69)	(1.03)	(1.53)	(0.98)
M-93	Transport Composite	1 359 000	2 419 020	..	1 031 200	1 470 000	3 599 000	1 780 290
	MSS^g = 14 ksi	(0.25 to 0.54)	(1.78)	...	(0.76)	(1.08)	(2.65)	(1.31)
M-94	Transport Composite	279 000	426 870	...	348 550	257 000	628 074	318 060
	MSS = 19.6 ksi	(0.258 to 0.38)	(1.53)	. .	(1.25)	(0.92)	(2.25)	(1.14)
Average (N_{pred}/N_{test}) ratio			(0.96)	(1.38)	(1.07)	(1.11)	(1.74)	(1.13)
Standard deviation			(0.36)	(0.42)	(0.33)	(0.20)	(0.42)	(0.22)

^{a}1 in. = 25.4 mm.
^{b}A-A = Air-to-Air.
^{c}DLS = Design limit stress
^{d}1 ksi = 6.9 MPa.
^{e}A-G = Air-to-Ground.
^{f}I-N = Instrumentation and Navigation.
^{g}MSS = Maximum spectrum stress

The ratios of the predicted life to the test life (N_{pred}/N_{test}) were calculated. Ratios smaller than 1.0 are considered to be conservative predictions and ratios greater than 1.0 are unconservative. The average prediction ratio and the standard deviation for each model are presented.

The fact that six participants all used different fatigue crack growth models reconfirms the fact that there is no standard methodology used to perform the fatigue crack growth life predictions for structures under random loading. The average prediction ratio of the 76 life predictions was 1.28 (slightly unconservative) and the standard deviation was 0.45, which suggests that the different methods used did not greatly affect the results. Table 2.7 presents the average prediction ratios for each test case.

Table 2.7 - Summary of prediction ratios for each test case (Chang, 1981a)

Test No.	Mission Type	Test Life, cycles	N_{pred}/N_{test}
M-81	Fighter (A-A)[a] DLS[b] = 20 ksi[c]	115 700	1.47 ± 0.43
M-82	Fighter (A-A) DLS = 30 ksi	58 585	0.99 ± 0.27
M-83	Fighter (A-A) DLS = 40 ksi	18 612	1.03 ± 0.3
M-84	Fighter (A-G)[d] DLS = 20 ksi	268 908	1.43 ± 0.24
M-85	Fighter (A-G) DLS = 30 ksi	95 642	0.99 ± 0.21
M-86	Fighter (A-G) DLS = 40 ksi	36 367	0.83 ± 0.22
M-88	Fighter (I-N)[e] DLS = 30 ksi	380 443	1.60 ± 0.64
M-89	Fighter (I-N) DLS = 40 ksi	164 738	1.20 ± 0.41
M-90	Fighter Composite DLS = 20 ksi	218 151	1.44 ± 0.38
M-91	Fighter Composite DLS = 30 ksi	65 627	1.08 ± 0.31
M-92	Fighter Composite DLS = 40 ksi	22 182	1.07 ± 0.34
M-93	Transport Composite MSS[f] = 14 ksi	1 359 000	1.52 ± 0.73
M-94	Transport Composite MSS = 19.6 ksi	279 000	1.42 ± 0.51

[a] A-A = Air-to-Air.
[b] DLS = Design limit stress.
[c] 1 ksi = 6.9 MPa.
[d] A-G = Air-to-Ground.
[e] I-N = Instrumentation and Navigation.
[f] MSS = Maximum spectrum stress.

There is a trend for unconservative predictions for crack lives exceeding 10^5 cycles and excellent prediction results for crack lives below 10^5 cycles.

The conclusions of this study are as follows.

1. Reasonable prediction for specimens subjected to random spectrum loading were obtained from constant amplitude crack growth rate data and crack growth prediction methods which account for load interaction effects.
2. Trade off between computation cost and predictive accuracy should be considered in choosing the model to be used.
3. Improvement of predictive accuracy requires low value ΔK crack growth rate data.

2.7 Summary of Variable Amplitude Loading Models

A total of thirteen variable amplitude fatigue crack growth models were discussed and each varied in the approach used, number of calibration parameters and complexity. The majority of the models, if calibrated properly, adequately predict the fatigue life of a component. The selection of the appropriate model is usually based on the analyst's experience and personal preference. This thesis will consider the previously discussed models during the experimental data analysis section, with more emphasis on those models that are simple to use and/or have few curve fitting parameters.

Chapter 3

Experimental Method

3.1 Introduction

The experimental fatigue program consisted of both constant and variable amplitude loading on a simple crack geometry to obtain some baseline data for 350WT steel. This data was analyzed to determine the significance of crack growth retardation and help identify a suitable fatigue crack growth model.

All fatigue crack growth tests were conducted in accordance with ASTM Standard No. E647 entitled "*Standard Test Method for Measurement of Fatigue Crack Growth Rates*". This standard discusses a general fatigue crack growth testing procedure which suggests various specimen configurations, apparatus, crack measurement and data analysis methods. The standard is only concerned with conditions under which linear elastic fracture mechanics is valid and the results are expressed in terms of the stress intensity factor range, ΔK. The details of the experimental program will now be discussed.

3.2 Test Material

The material used in this study is 350WT Category 5 steel, which is primarily used in the hull of the Halifax class frigates which varies in thickness from 5 to 12 mm. This steel has a minimum required yield strength of 350 MPa, fracture toughness of at least 40J at -40 degrees Celsius and is readily weldable. This steel is also commonly used in applications such as bridges, pressure vessels and offshore structures.

DREA provided the author with a 1250 mm x 610 mm x 7 mm (4.1 feet x 2 feet) sheet of steel from which to prepare the required test samples. An optical metallography test was performed on this steel and the carbon fraction was determined to be equal to 0.09. The

Halifax Dockyard Lab performed a chemical analysis and the results are presented in Table 3.1.

Table 3.1 - Chemical composition of 350WT steel

0.075	Carbon	0.22 max
0.034	Chromium	-
0.016	Cobalt	-
0.010	Copper	-
1.250	Manganese	0.80 - 1.50
0.006	Molybenum	-
0.300	Niobium	-
0.008	Nickel	-
0.009	Phosphorus	0.03 max
0.230	Silicon	0.15 - 0.40
0.052	Vanadium	-
0.004	Sulfur	0.03 max

The material properties for the 350WT steel are shown in Table 3.2

Table 3.2 – Material properties of 350WT steel

σ_y	450 MPa
σ_u	524 MPa
RA	71%
E	205 GPa
ν	0.3

* (Fleet Technology Ltd., 1997)

3.3 Test Specimen

3.3.1 Configuration and Dimensions

The ASTM E647 Standard (Clause 1.5) allows any test specimen configuration to be used, provided that well-established stress intensity correction factor calibrations are available and that specimens are of sufficient planar size to remain predominantly elastic during testing. Commonly used configurations include compact tension, center cracked and three point bend specimens. It was determined that a center cracked specimen would be used for this experimental program because the configuration is ideal for thin specimens and the required test apparatus could be readily obtained. The dimensions and layout of the test specimen are shown in Appendix A.

The specimen's width and bolt hole layout were predetermined by the test fixture that was to be used. The ASTM Standard Clause 6.2.2 requires that the minimum distance between the innermost row of bolt holes for a specimen width greater than 75 mm be equal to 1.5W (W = specimen width). A specimen length of 300 mm was used because it provided sufficient length to satisfy clause 6.2.2 with a distance of 2.0W between the innermost row of bolt holes (1.7W between edges of grips). The steel thickness provided by DREA was 7 mm; however, the fixture opening could not accommodate this. As a result, the specimen thickness was reduced to 5.35 mm and 5.06 mm to be used in the constant amplitude loading and variable amplitude loading phases, respectively. The smaller thickness is beneficial because it would reduce the required load.

Clause 7.1.2 (Note 10) recommends that the center crack length should be at least 0.2W when using the compliance method to monitor crack extension so that accurate crack length determinations can be obtained. Although the compliance method would not be used, a starter notch of 0.2W (20 mm) was chosen because this length would provide sufficient crack growth rate data, the testing time would be of a reasonable length and the required load magnitudes would be within the limits of the load cell.

In summary, the specimen dimensions are approximately 300 mm x 100 mm x (5.35 or 5.06) mm with a starter notch of length 20 mm. The final dimensions of each specimen are provided in Appendix A.

3.3.2 Specimen Preparation

The specimens were laid out on the sheet of 350WT steel provided by DREA as shown in Figure 3.1.

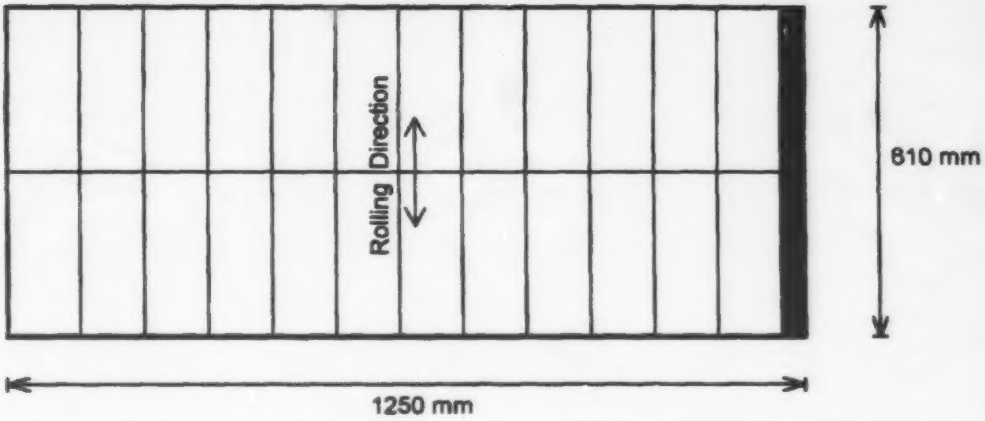

Figure 3.1 – Layout of specimens

As a result, the specimen crack orientation is in the L – T direction where L is the longitudinal rolling direction and T is the width (i.e. transverse direction). The first letter indicates the direction of the applied loading and the second letter indicates the direction of crack growth.

The sheet of steel in Figure 3.1 was cut in half with a vertical bandsaw to obtain two strips with dimensions 1250 mm x 305 mm x 7 mm. Next, the horizontal bandsaw was used to cut twelve 101 mm wide sections from each strip. The length of each specimen was then reduced to 300 mm by cutting off a 5 mm end section with the horizontal bandsaw. Twelve specimens were selected and their thickness was reduced to approximately 5.35 mm or 5.06 mm with the milling machine. They were then 'finished' with the surface grinder to ensure the specimen was 'flat'.

The grip holes were laid out and drilled according to the dimensions shown in Appendix A. A one-eighth inch diameter hole was drilled in the center of each specimen to allow the starter notch to be machined. The notch was machined at the Halifax Dockyard machine shop by the electrical discharge machining (EDM) process. The width of the EDM notch was 0.254 mm (0.010 in).

The specimen's surface, where the fatigue crack was expected to propagate, was polished to provide a clear image of the crack tip when observed through the microscope. This was accomplished by first sanding the surface with progressively 'finer' grades of sandpaper; that is 320, 400 and then 600 grit paper. The polishing process was completed by using a mixture of 5 micron aluminum oxide powder and water, applied over the specimens surface with a rotary buffering pad.

3.4 Test Apparatus

An Instron model 8501 servo-hydraulic testing machine was used to perform the fatigue testing. The machine has a digital control panel (model 8500^{+}) and the load cell capacity is ± 100KN under dynamic loading conditions (200KN static). The Instron, control panel and load cell are shown in Figure 3.2.

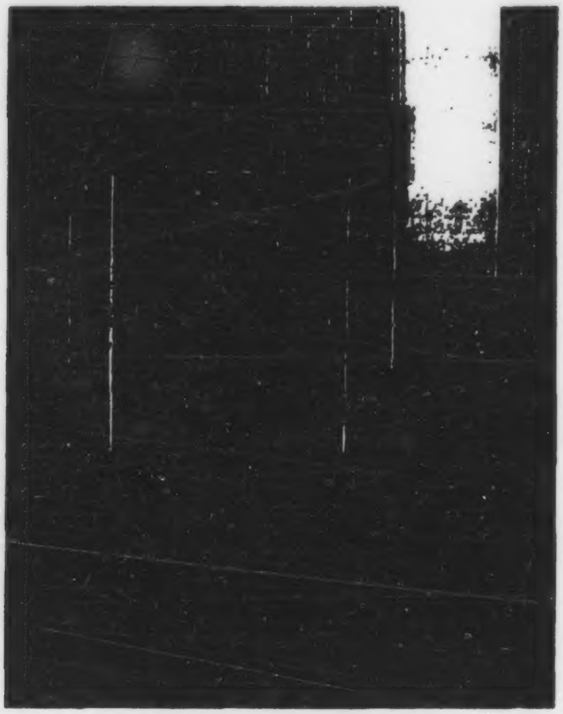

Figure 3.2 – Loading apparatus

The fixtures used to grip the specimens are shown in Figure 3.3

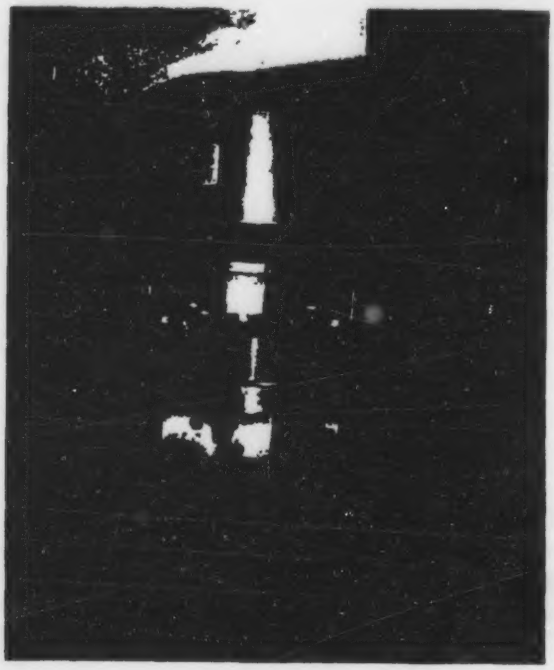

(a)

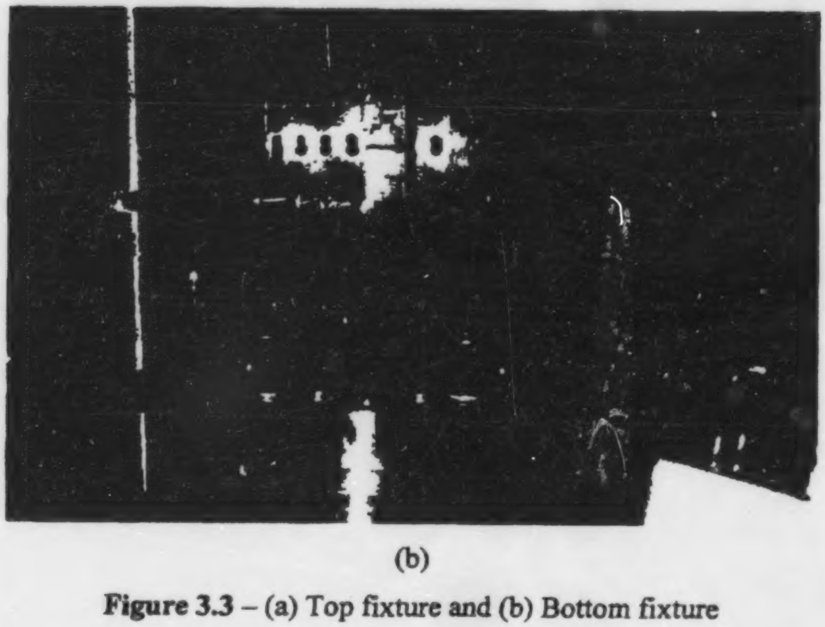

(b)

Figure 3.3 – (a) Top fixture and (b) Bottom fixture

The top and bottom fixtures are bolted to the load cell and actuator base plate, respectively. Extreme caution was used when attaching the fixtures to the Instron to ensure that the alignment is as accurate as possible because relatively large bending moments can be introduced for a minimal misalignment. These bending moments may affect the experimental results and cause failure of the bolts that fasten the fixture to the Instron load cell and actuator.

Two plates (grips) are bolted together on each end of the specimen as shown by Figure 3.4a. This arrangement is then attached to both the top and bottom fixture by two large pins that are inserted through both the fixture and specimens grip as shown by Figure 3.4b.

A Mitutoyo travelling microscope (10x magnification) with a resolution of 0.01 mm was used to measure the fatigue crack growth length. The crack length was required to be measured on only one side because the specimen is sufficiently thin ($B/W < 0.15$). Figure 3.5 shows the microscope and its supporting frame.

(a)

(b)

Figure 3.4 – (a) Specimen grips and (b) Grip to fixture connection

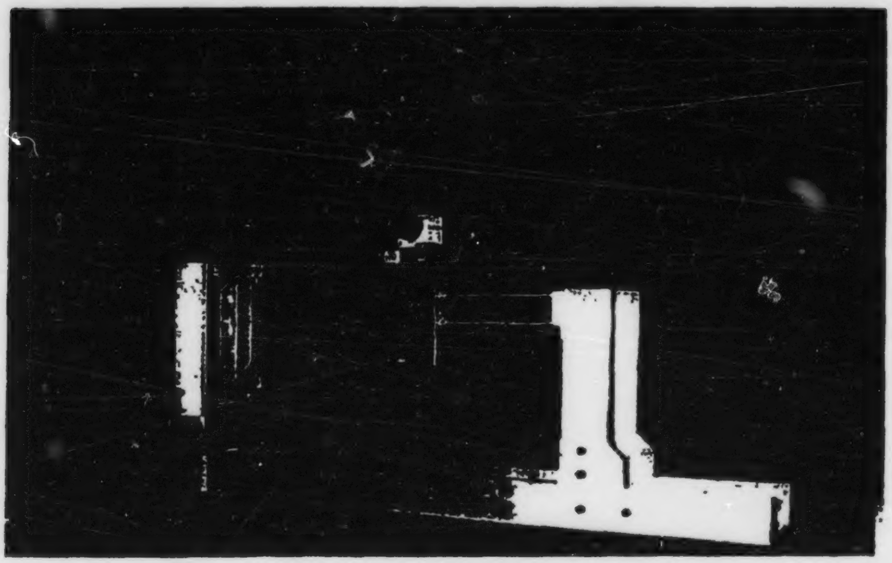

Figure 3.5 – Travelling microscope and its supporting frame

Figure 3.6 and Figure 3.7 illustrate the complete experimental setup and close up of the experimental setup respectively.

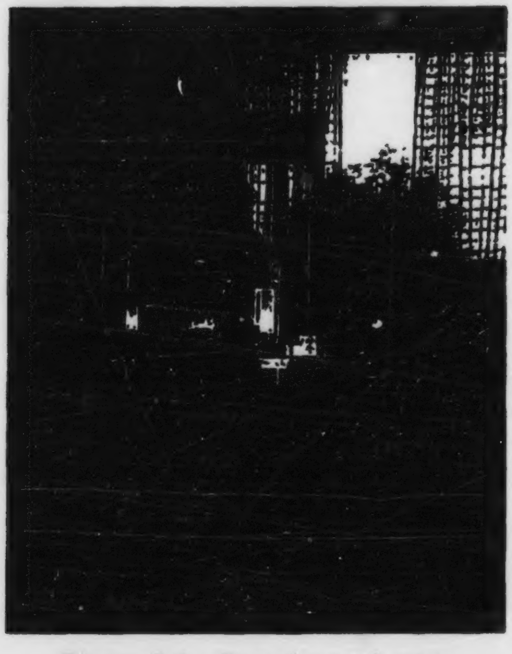

Figure 3.6 – Experimental setup

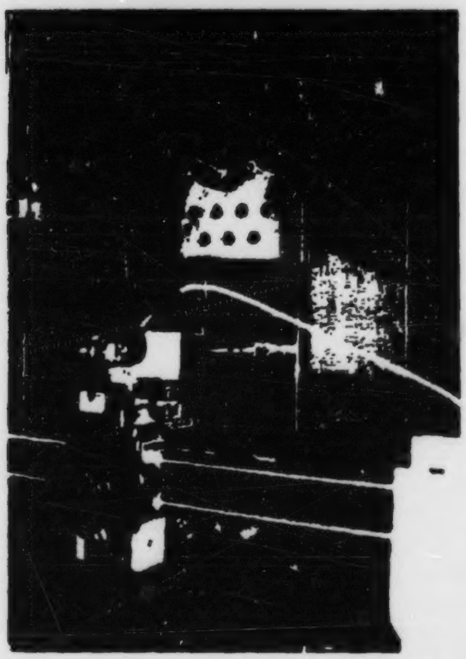

Figure 3.7 – Close up of experimental setup

3.5 Test Procedure

The experimental fatigue program was conducted in accordance with ASTM E647 and consisted of both a constant amplitude and variable amplitude loading phase. The details of the loading scenario for each specimen are described in Appendix A.

Before the above loading scenarios are applied, the specimen must first undergo fatigue precracking, which provides a sharpened fatigue crack of adequate size and straightness. This ensures that the effect of the machined starter notch is removed (Clause 8.3). The fatigue-precracking load was not to be greater than the specimens starting fatigue load and in most cases was equal to the initial constant amplitude load. The standard requires that the minimum fatigue precrack length for this specimen configuration to be 1.0 mm. Fatigue precracking was continued until the minimum 1.0 mm was reached and the crack appeared to be propagating at the same rate from both sides of the starter notch.

Following the fatigue precracking, the specimens were subjected to their required loading scenario. The crack length measurements were made as a function of the elapsed number of cycles at intervals such that the d*a*/dN data was nearly evenly distributed with respect to ΔK.

Measurements were continued until the specimen appeared to be near failure. At this point, the travelling microscope was removed and the specimen loaded until failure.

Chapter 4

Experimental Results and Data Analysis

4.1 Introduction

This chapter presents the experimental results for the constant amplitude and variable amplitude loading tests. These results were analyzed with the various fatigue crack propagation models described in the literature review to determine the most suitable models. Most of the models were considered; however, only the most applicable models are discussed in the following sections.

When selecting a model, there is no absolute or 'correct' methodology and the choice generally depends upon the user's preference and prior experiences. A rule of thumb is to choose a model that best satisfies the objectives of the required analysis. Some general remarks regarding the selection of a model are as follows.

1. Select a model that coincides with the expected type of loading that the structure will experience; that is, constant amplitude or variable amplitude loading.
2. Determine which fracture parameter should be used; that is, *K*, *G*, *J* or *CTOD*. If it is determined that *EPFM* will be the dominating condition, a fracture parameter based on *LEFM* should not be used.
3. For variable amplitude loading, the selection of a model should consider which load sequence effects are expected to be present. For example, if retardation is expected to be significant, a model solely based upon crack growth acceleration should not be used.
4. Evaluate the influence of the environmental effect on fatigue crack growth. If the structure is to be exposed to a harsh environment (i.e. salt water) during its service lifetime, a model based on an air environment should be used cautiously.

5. In accordance with the above factors, the trade off between the computational cost and the prediction accuracy should be considered when selecting a model. If the objective of the analysis is to obtain an approximate life estimate, resources should not be wasted by using a complicated model that requires the calibration of numerous parameters.

It is the author's opinion that an ideal model should be simple, have few empirical parameters and provide fairly accurate results in the least amount of time.

As discussed in Section 2.1.1, the failure of a cracked component may occur by either collapse (yielding) of the remaining cross-sectional area or fracture, which are competing conditions, and the one satisfied first will prevail. That is, the fatigue crack will propagate until either the stress in the remaining cross-section reaches the materials yield stress or the value of K_{max} exceeds the materials fracture toughness, K_C. At the time, the fracture toughness of the 350WT steel was unknown; however, it was determined that its value would be large, since the specimens thickness was small and thus plane stress conditions would prevail. Therefore, the specimens were expected to fail by yielding as shown by Figure 4.1.

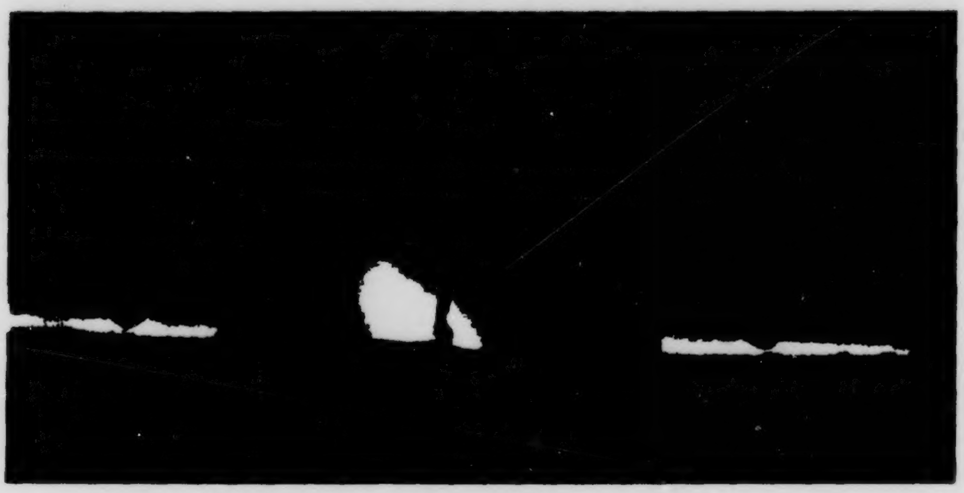

Figure 4.1 Typical specimen failure (note yielding at edges)

4.2 Data Reduction

During the fatigue tests, the crack length and corresponding number of elapsed cycles were measured and recorded. The resulting crack length data is plotted versus the corresponding number of elapsed cycles to obtain an '*a* versus N' curve. The usefulness of this graph, however, is limited because it depends upon the initial crack length, stress range and specimen geometry. Therefore, it is necessary to further process the test results to obtain quantities that are independent of these parameters. This is accomplished by using the stress intensity factor defined by Equation 2.3 which is capable of reducing the data for any crack length, specimen geometry and stress range to a single term parameter. The crack growth rate is determined from the slope of the crack length versus number of cycles (*a* versus N) curve and is plotted against the corresponding value of the stress intensity factor range (ΔK) on a log-log scale. This is commonly referred to as a fatigue rate or 'd*a*/dN versus ΔK' curve.

Both the secant and incremental methods are used in this thesis to obtain the d*a*/dN versus ΔK curve from the '*a* versus N' data. The secant method is a simple and generally suitable approach if the crack length is measured at fairly short intervals and exhibits little scatter. This method calculates the growth rate between adjacent data points as

$$\left(\frac{da}{dN}\right)_j \approx \left(\frac{\Delta a}{\Delta N}\right)_j = \frac{a_j - a_{j-1}}{N_j - N_{j-1}} \qquad (4.1)$$

The corresponding ΔK value is calculated from the average crack length during the interval.

$$\Delta K_j = Y\Delta\sigma\sqrt{\pi a_{avg}} \qquad (4.2)$$

The incremental method involves fitting a second-order polynomial (parabola) to sets of (2n + 1) successive data points and is useful for data with scatter. The ASTM E647 standard recommends a value of n = 3 which is referred to as the seven point incremental polynomial method. The form of the equation for the local fit is given by

$$a_i = b_o + b_1\left(\frac{N_i - C_1}{C_2}\right) + b_2\left(\frac{N_i - C_1}{C_2}\right)^2 \qquad (4.3)$$

where

$$-1 \le \left(\frac{N_i - C_1}{C_2}\right) \le +1 \qquad (4.4)$$

and b_0, b_1, and b_2 are the regression parameters that are determined by the least squares methods. The parameters $C_1 = ½(N_{i-n} + N_{i+n})$ and $C_2 = ½(N_{i+n} - N_{i-n})$ are used to scale the input data to avoid numerical difficulties when determining the regression parameters. The crack growth rate is equal to the derivative of the parabolic fit (Equation 4.3), that is

$$\left(\frac{da}{dN}\right)_{a_i} = \frac{b_1}{C_2} + \frac{2b_2(N_i - C_1)}{C_2^2} \qquad (4.5)$$

The corresponding ΔK value is computed with the fitted crack length, a_i, which is calculated from Equation 4.3.

Appendix B illustrates an example of the data reduction procedure used for each test specimen. That is, the experimental data is recorded in the data sheet, from which the d*a*/dN and ΔK terms are evaluated by the secant and incremental method for both the left and right crack. These results are then plotted on an '*a* versus N' and 'd*a*/dN versus ΔK' graph.

4.3 Constant Amplitude Loading Test Results

A total of six constant amplitude loading tests were performed to obtain some baseline data at various stress ratios for the 350WT steel. Table 4.1 summarizes the average crack lengths and number of cycles to failure for each test.

Table 4.1 -- Constant amplitude test summary

Specimen Number	Stress Ratio	a_i (mm)	a_f (mm)	a_y (mm)	# of Cycles a_i to a_f	# of Cycles a_i to a_y	# of Cycles a_i to failure
CAL 1	0.10	11.46	26.83	-	72104	-	-
CAL 2	0 10	11.28	38.92	39.5	165000	165500	166391
CAL 3	0.10	11.14	35 74	39.1	147500	150400	151210
CAL 4	0.20	11 17	38.24	39.2	189000	189500	190714
CAL 5	0.30	11.17	35.44	38.9	275000	281000	282871
CAL 6	0.40	15 03	34.71	39.0	186000	194800	197324

Notes: All crack lengths are the average value of the right and left crack measurements

a_i = crack length when started recording test data

a_f = crack length when stopped recording test data

a_y = crack length when remaining cross-section started to yield

During each test, the crack length and corresponding number of elapsed cycles were measured from a_i to a_f. No data was recorded past a crack length of a_f because large yield zones were beginning to form at the crack tip, making it difficult to accurately determine the crack length. The test was continued until the crack stopped propagating and the remaining cross-section of the specimen yielded. The corresponding crack length (a_y) and number of elapsed cycles were recorded. Once the specimen had yielded, the loading was maintained until the specimen failed into two sections and the number of elapsed cycles to failure was recorded. The number of cycles between the crack length, a_y, and failure is small and represents the time required for the 'necking' (failure) of the yielded section to occur.

Three tests were conducted at a stress ratio (R) of 0.10 and one test for each stress ratio equal to 0.20, 0.30 and 0.40. The test results for specimen number CAL 1 are incomplete because one of the bolts connecting the bottom fixture to the actuator's baseplate failed when the crack had only propagated to a length of 26.83 mm. It was determined that the bolt failed because the test setup was misaligned which introduced relatively large bending stresses on the connection and thus the test specimen. Consequently, the results from this test are questionable and will not be considered in the analysis section. To ensure that this problem did not re-occur, all subsequent tests were performed only after careful alignment of the test setup was completed.

The '*a* versus N' and corresponding fatigue rate curve (d*a*/dN versus ΔK) for each test specimen are presented in Appendix C. Referring to the '*a* versus N' curves, the data points for the right and left crack tips are nearly indistinguishable for any given number of elapsed cycles. This confirms that the crack propagated from each side of the center notch at similar rates as expected. For the fatigue rate curves, the values of d*a*/dN and ΔK were obtained and plotted for both the right and left crack tip using the secant and incremental polynomial methods. Both data reduction methods were used to obtain the best results. Referring to the fatigue rate curves, little difference exists between the values obtained by the two methods because of the 'lack of scatter' in the '*a* versus N' data. It is interesting to note that the fatigue rate curve for each specimen contains a 'point of inflection' corresponding to a value of ΔK approximately equal to 23 MPa $m^{1/2}$, which divides the curve into two sections. The section below and above the point of inflection will herein be referred to as the lower and upper curve, respectively.

Figure 4.2 and Figure 4.3 illustrates the '*a* versus N' curves and fatigue rate curves (using average crack length of left and right measurements) for specimens CAL 2 and CAL 3, respectively. The fatigue rate curves are nearly identical, regardless of the fact that the '*a* versus N' curves are different, illustrating the importance of the fatigue rate curve for fatigue analysis.

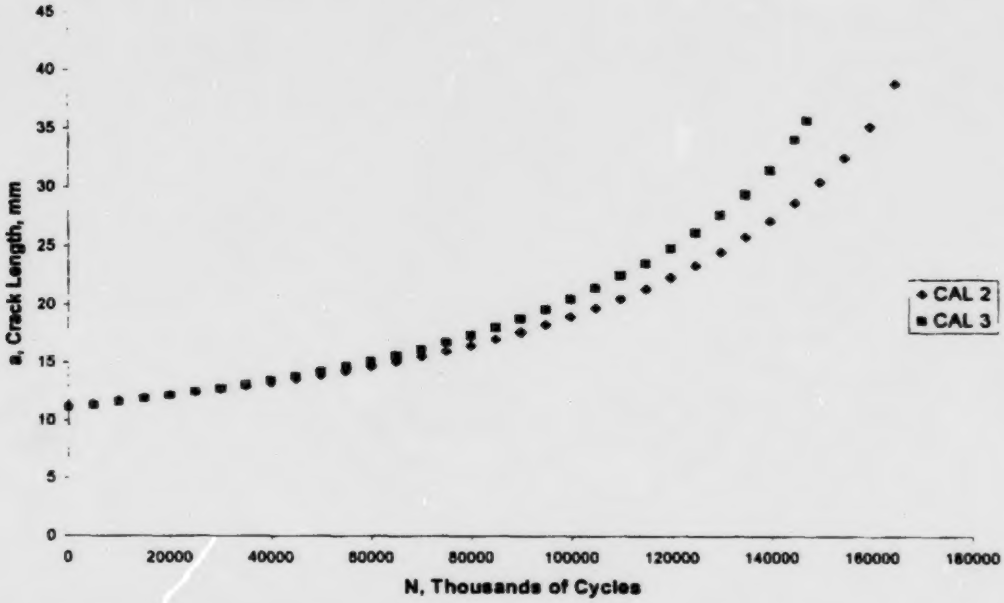

Figure 4.2 – Crack length versus number of cycles for specimens CAL 2 and CAL 3

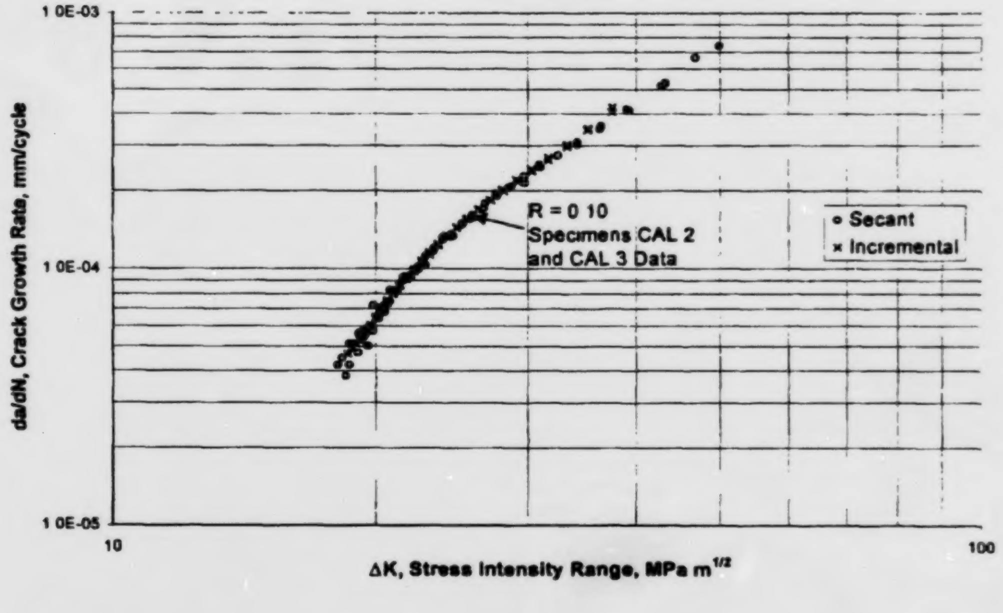

Figure 4.3 – d*a*/dN versus ΔK for specimens CAL 2 and CAL 3

Figure 4.4 illustrates the plots of the fatigue rate curves for specimens CAL 2 to CAL 6. This figure illustrates that the fatigue response of the 350WT steel is dependent upon the stress ratio parameter, R, (ratio of σ_{min} to σ_{max}) by an amount representative of the degree of shift between the respective fatigue rate curves. The curves corresponding to a stress ratio equal to 0.10 are located in the lower right hand portion of Figure 4.4 and the curve for a stress ratio equal to 0.40 is shifted 'upwards' and nearly parallel to the R = 0.10 curves. The fatigue rate curves corresponding to a stress ratio equal to 0.20 and 0.30 are bounded by the 0.10 and 0.40 curves. The amount of variance between the stress ratio curves appears to be significant for this material and will be further considered during the fatigue analysis.

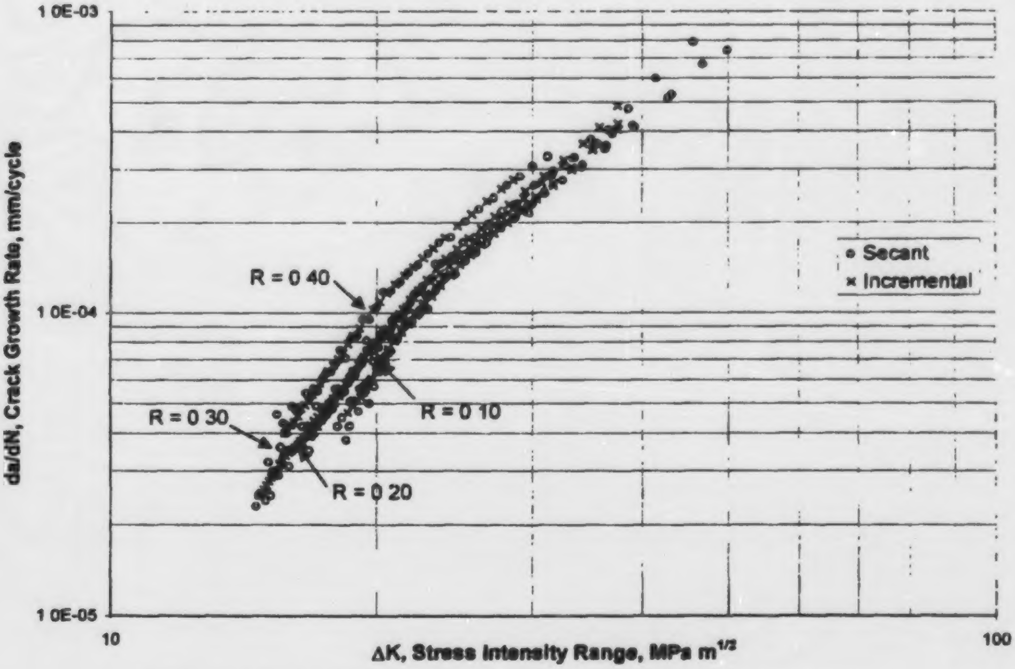

Figure 4.4 – d*a*/dN versus ΔK for specimens CAL 2 to CAL 6

4.4 Constant Amplitude Loading Data Analysis

This section will discuss the analysis of the constant amplitude loading experimental data using the various fatigue crack propagation models discussed during the literature review. Only the most attractive models will be presented in the following sections.

4.4.1 Paris Model

4.4.1.1 Parameter Evaluation

A simple and well-known method for predicting fatigue crack propagation is the Paris model defined by the relationship

$$\frac{da}{dN} = C(\Delta K)^m \tag{4.6}$$

By taking the logarithm of each side, one obtains

$$\log\frac{da}{dN} = m\log(\Delta K) + \log C \tag{4.7}$$

which is of the form $y = mx + b$. The parameters m and C represent the slope and intercept of a straight line on a logarithmic plot of 'd*a*/dN versus ΔK'. Therefore, the Paris model is most applicable for fatigue rate curves that follow a linear relationship.

In the previous section, it was discussed that the constant amplitude loading fatigue rate curves differ depending upon the loading stress ratio and have a point of inflection at a ΔK value of approximately 23 MPa $m^{1/2}$. The corresponding upper and lower curves are nearly linear in nature. As a result, it was determined that the best results would be obtained by determining the Paris coefficients for the upper and lower portion of the curve separately (two curve model), for each stress ratio value. For comparison, the Paris coefficients were determined for each individual stress ratio considering the entire fatigue rate curve (one curve model) and for all the stress ratio data grouped together (for both the one and two curve models).

A least-squares regression was applied to the appropriate data to obtain the best fit straight line from which the Paris parameters were calculated. The results are presented in Table 4.2.

Table 4.2 – Summary of the Paris model parameters

Stress Ratios	R	One Curve Model		Two Curve Model			
		m	C	m_{lower}	C_{lower}	m_{upper}	C_{upper}
Individual	0.10*	2.94	1.02E-08	4.22	2.04E-10	2.41	6.35E-08
	0.20	3.06	7.84E-09	3.99	5.09E-10	2.53	4.81E-08
	0.30	3.22	4.77E-09	3.71	1.17E-09	2.59	3.79E-08
	0.40	3.27	5.36E-09	4.075	5.26E-10	2.64	4.11E-08
Grouped	0.10 - 0.40**	3.08	7.46E-09	3.36	3.32E-09	2.92	1.26E-08

* The parameters for this stress ratio are based on a combination of the data for specimen CAL 2 and 3

** One set of data was used for each stress ratio to prevent a biased answer. For the 0.10 stress ratio, the test results from specimen CAL 3 were used.

The one curve model is described by Equation 4.6 and the two-curve model is based on the expression given by Equation 4.8.

$$\frac{da}{dN} = \begin{cases} C_{lower}(\Delta K)^{m_{lower}} & \text{, for } \Delta K \leq 23\text{ MPa m}^{1/2} \\ C_{upper}(\Delta K)^{m_{upper}} & \text{, for } \Delta K > 23\text{ MPa m}^{1/2} \end{cases} \tag{4.8}$$

4.4.1.2 Predictions for Crack Length a_i to a_f

The above Paris coefficients were obtained from the data recorded between crack lengths a_i and a_f as outlined in Table 4.1. To ensure that these values are correct and to illustrate the difference between the various approaches, the appropriate models are evaluated and their results are compared in this section. The results are graphically illustrated in Figure 4.5 to 4.9 and are summarized in Table 4.3 and 4.4.

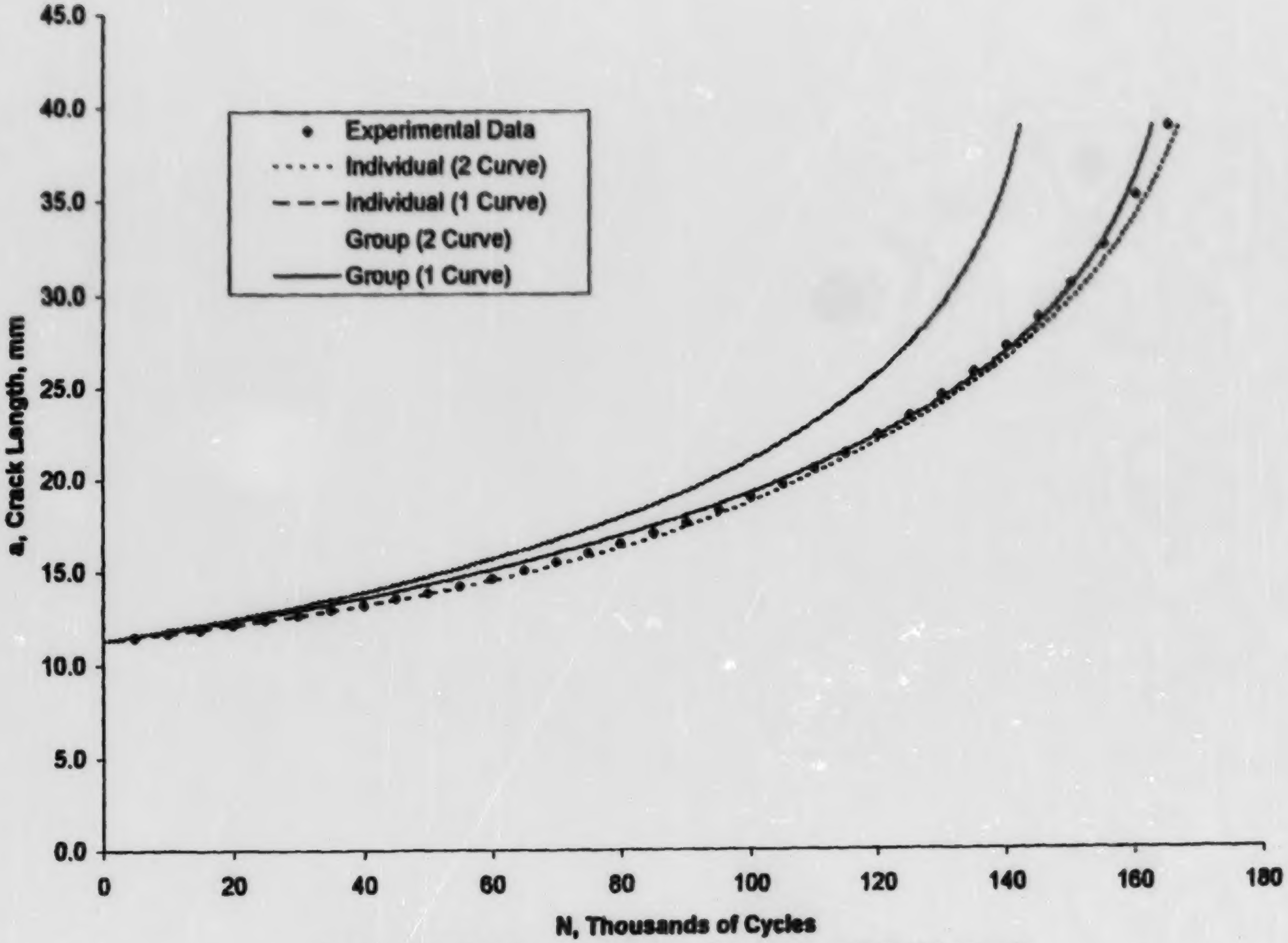

Figure 4.5 - Paris based predictions for specimen CAL 2 (a_i to a_f)

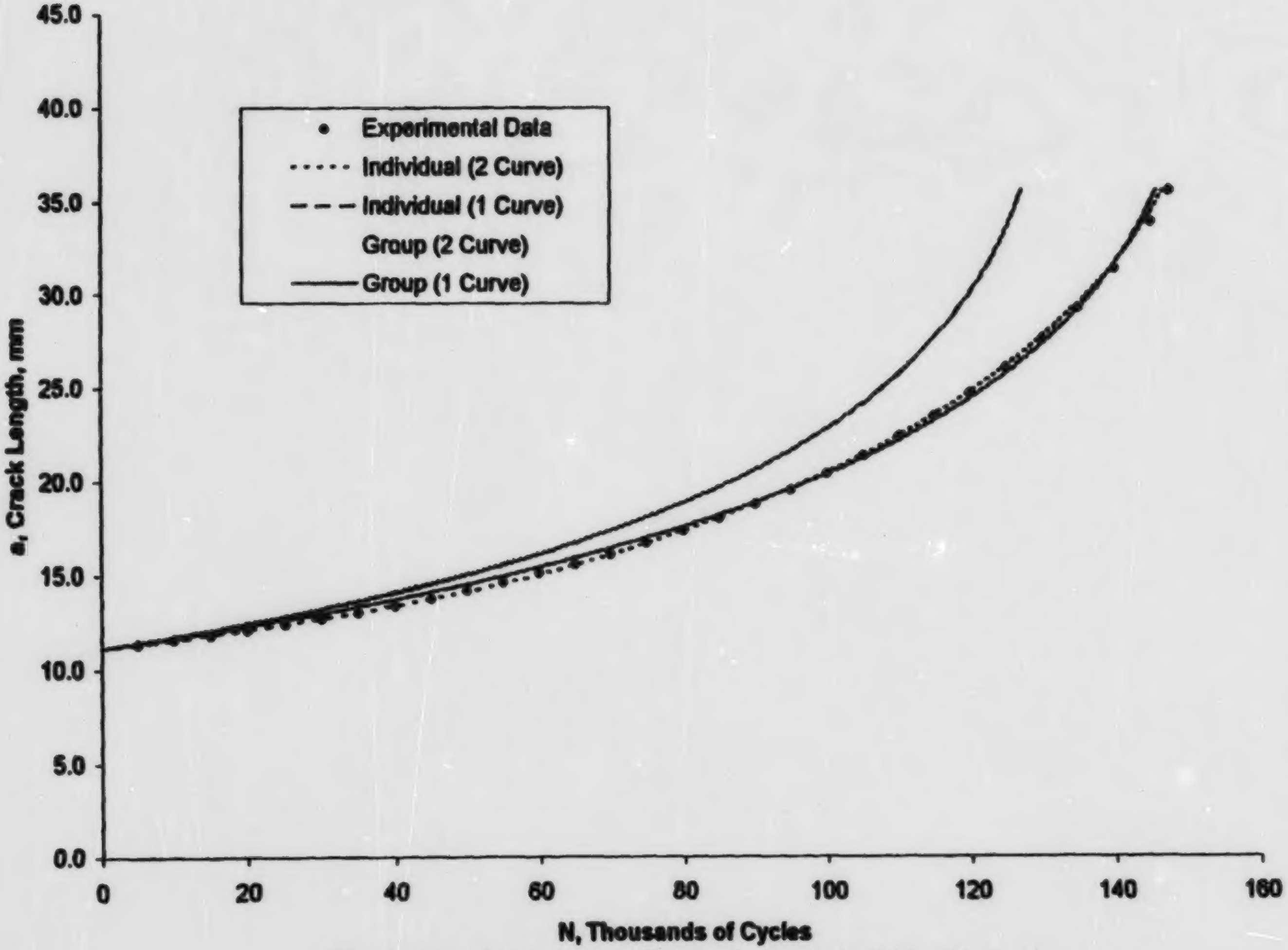

Figure 4.6 - Paris based predictions for specimen CAL 3 (a_i to a_f)

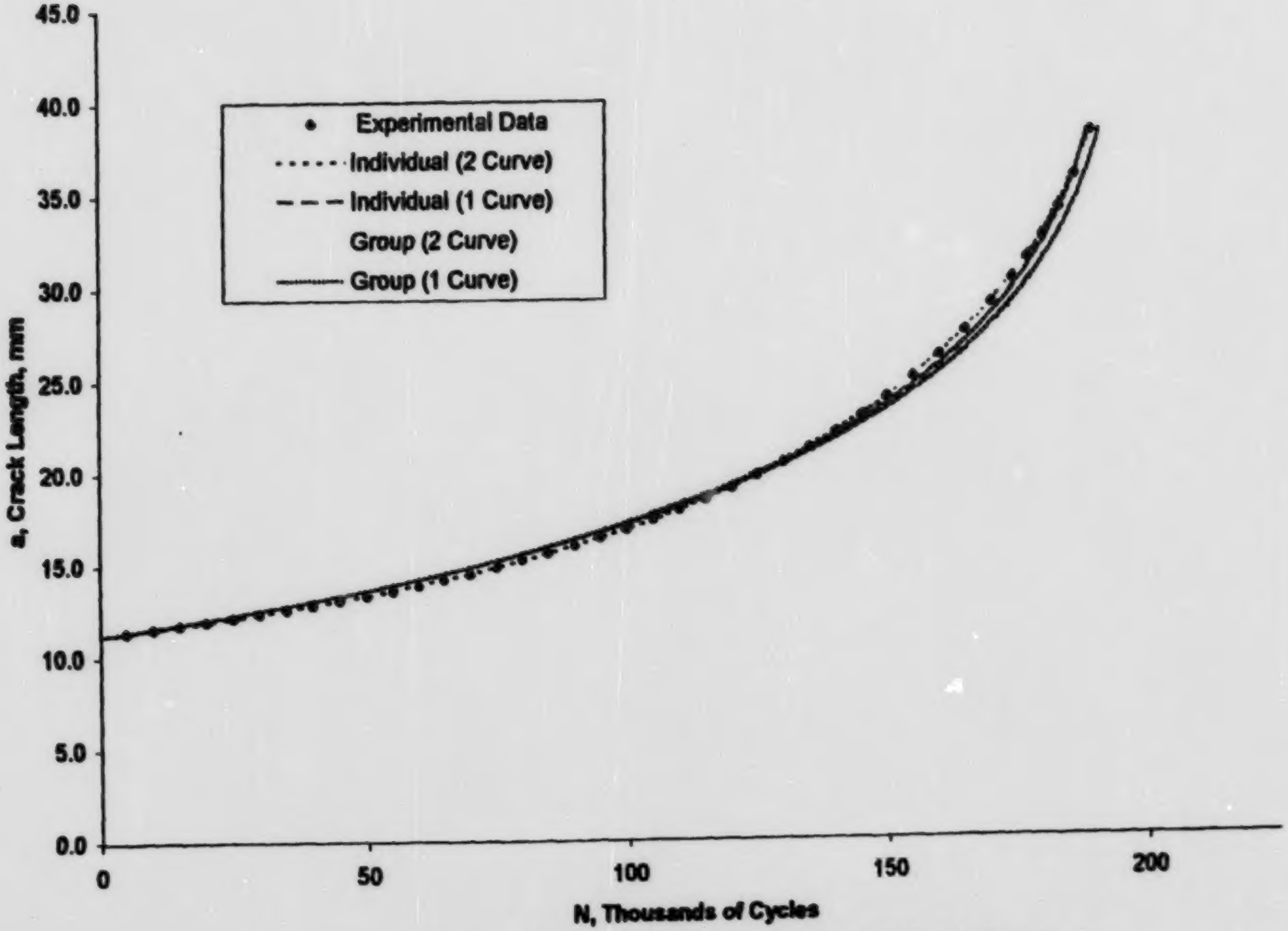

Figure 4.7 - Paris based predictions for specimen CAL 4 (a_i to a_f)

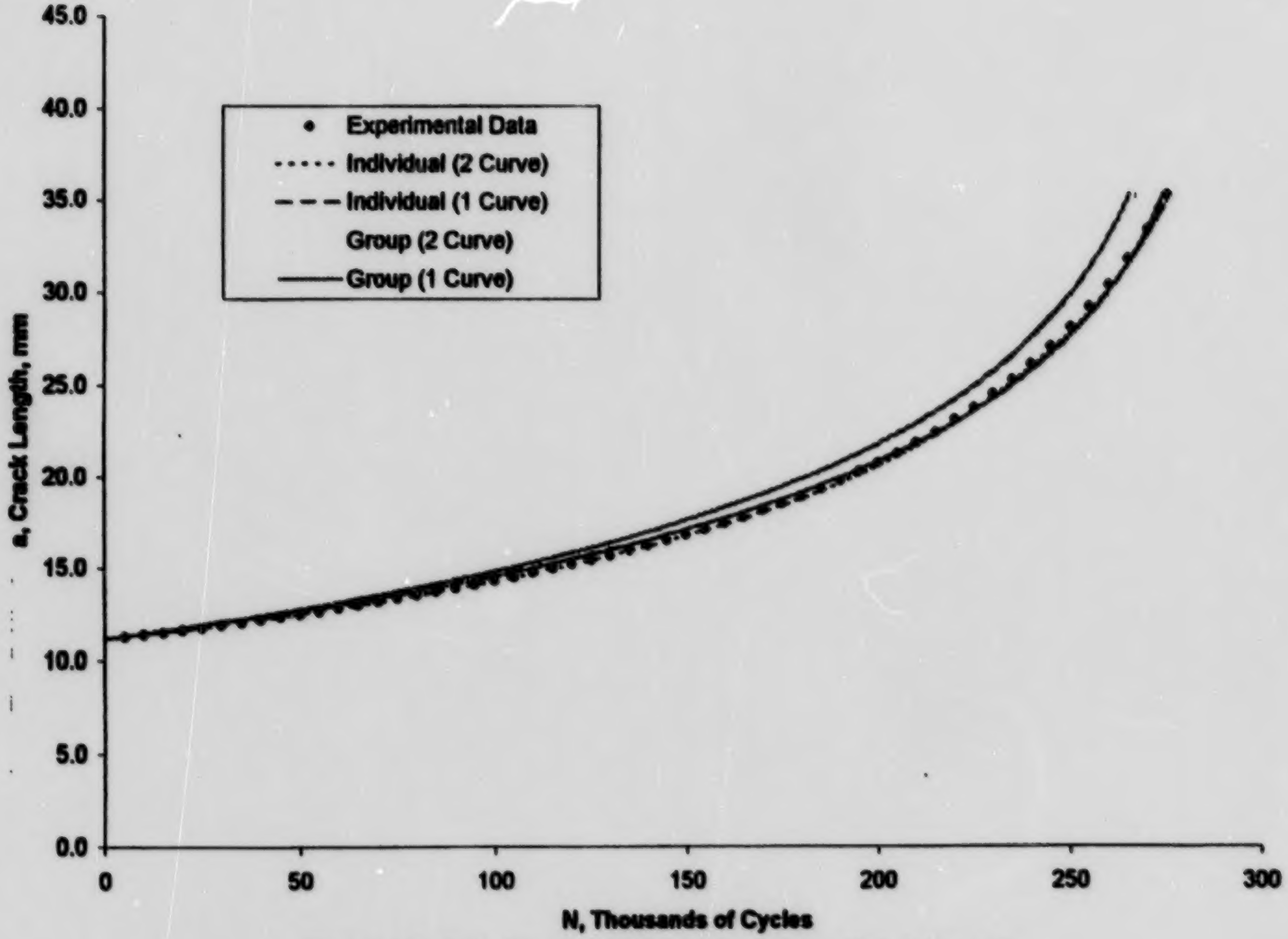

Figure 4.8 - Paris based predictions for specimen CAL 5 (a_i to a_f)

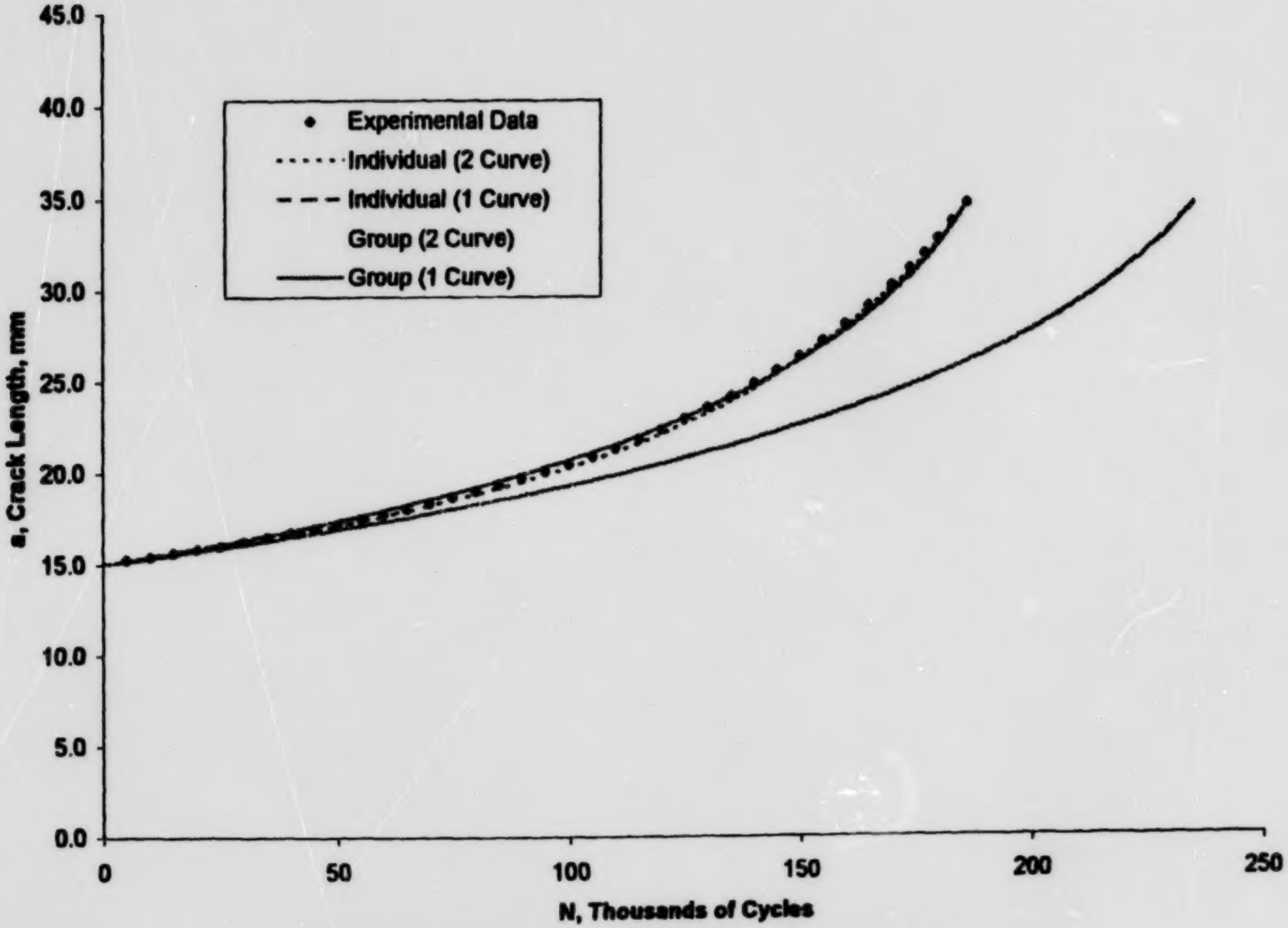

Figure 4.9 - Paris based predictions for specimen CAL 6 (a_i to a_f)

Table 4.3 – Summary of Paris predictions for crack length a_i to a_f

Specimen [illegible]	[illegible]	[illegible]	[illegible]	[illegible]	[illegible]
CAL 2	165000	162500	166500	142100	141200
CAL 3	147500	145700	146600	127100	126100
CAL 4	189000	190500	188700	188200	187500
CAL 5	275000	274000	275600	265200	267100
CAL 6	186000	186100	186150	235000	234700

Table 4.4 – Percent errors of Paris predictions for crack length a_i to a_f

Specimen Number	N Experiment	Individual R Parameters		Grouped R Parameters	
		N (1 Curve)	N (2 Curve)	N (1 Curve)	N (2 Curve)
CAL 2	165000	1.5	-0.9	13.9	14.4
CAL 3	147500	1.2	0.6	13.8	14.5
CAL 4	189000	-0.8	0.2	0.4	0.8
CAL 5	275000	0.4	-0.2	3.6	2.9
CAL 6	186000	-0.1	-0.1	-26 3	-26.2

The above results were calculated by numerically integrating the appropriate Paris model in small step sizes using an Excel spreadsheet. The step size was taken as a crack increment of one percent of the current crack size and an example calculation was described by Broek (1995). For constant amplitude loading, this procedure has been shown to give excellent results with very little error.

It is evident from the previous figures and tables that the predictions based on an individual stress ratio produce the best results. The magnitudes of errors for the predictions based on the 'grouped' data are significant and help quantify the influence of the stress ratio parameter. It is interesting to point out that the results using the grouped parameters for specimens CAL 4 and 5 (R = 0.20 and 0.30 respectively), are more accurate than those of specimens CAL 2, 3 and 6 (R = 0.10, 0.10 and 0.40 respectively). This conforms to the fact that the Paris coefficients obtained from the 'grouped' data are only an average of the four stress ratios. Therefore, one would expect better predictions for the middle stress ratio's (R = 0.20 and 0.30) as compared to the extreme values (R = 0.10 and 0.40).

The results of the two curve Paris model are more accurate than those obtained for the one curve model as highlighted in Table 4.4. Based on these results, it appears that there is not much difference between the one and two curve models. However, close inspection of Figures 4.5 to 4.9 reveal that a subtle difference exists. That is, the two curve model's '*a* versus N' predictions mimic the curve shape of the experimental data. In contrast, the one parameter model '*a* versus N' predictions consistently start 'above' and end 'below' the experimental data curve, crossings over at approximately the halfway point. Thus, the two-curve model accurately predicts the experimental data results; whereas, the one curve model closely approximates the results.

In summary, the stress ratio effect is significant in the 350WT steel, resulting in better predictions when the Paris coefficients are obtained for the individual stress ratios. Furthermore, the two-curve Paris model better represents the experimental data results than the one curve model.

4.4.1.3 Failure Predictions

The previous section dealt with comparing various approaches to predict the fatigue life between two known crack lengths using the Paris model. It was concluded that the two curve model with coefficients obtained for individual stress ratios produced the best results. Practically, a fatigue analysis is performed to evaluate the remaining fatigue life of a component once a crack has been identified. This section will predict the total fatigue life of each specimen assuming that the initial crack was discovered at a length equal to a_i.

It was discussed, that the failure of a cracked component may occur by either collapse (yielding) of the remaining cross-sectional area or by fracture, which are competing conditions, and the one satisfied first will prevail. For the specimens in question, the value of K_c is large and failure is anticipated to occur by yielding of the remaining uncracked cross-section. The stress in a center-cracked specimen with crack length '2a' is equal to

$$\sigma = \frac{P}{A} = \frac{P_{max}}{B(W-2a)} \tag{4.9}$$

where B and W are the specimen thickness and width respectively. Letting the value of $\sigma = \sigma_y$ and rearranging Equation 4.9, one can obtain the following expression for the crack length corresponding to yielding of the uncracked cross-section.

$$a_y = \frac{1}{2}\left[W - \frac{P_{max}}{\sigma_y B}\right] \tag{4.10}$$

The static tensile yield strength of the material is equal to 450 MPa; however, the fatigue loading is cyclic in nature resulting in the possibility of material strain hardening. This data was unavailable so the yield stress of 450 MPa was used to predict 'a_y' and the strain hardened yield stress was back calculated based on the crack length at which yielding occurred during the experiment. The results are presented in Table 4.5.

Table 4.5 – Predictions of crack length when yielding occurs

Specimen Number	a_y Exp.	a_y σ_y = 450 MPa	% Error Exp. & 450	Calculated σ_y From Exp. Results
CAL 2	39 5	38.8	1.77	480
CAL 3	39.1	38.3	2.05	481
CAL 4	39.2	38.4	2.04	481
CAL 5	38 9	38.2	1.80	479
CAL 6	39.0	38.3	1.79	478

Note: All crack lengths in mm and stresses in MPa

Based on a yield stress of 450 MPa, the predicted crack lengths for yielding are between 1.75 and 2 percent under-predicted. The required yield stress to predict the experimental crack lengths (for yielding) is approximately equal to 480 MPa. This value is believed to account for the materials cyclic strain hardening. Table 4.6 presents various predictions based on the two curve Paris model with the coefficients obtained for each individual stress ratio and Table 4.7 presents the percentage errors.

Table 4.6 – Predictions for a_i to a_y

Specimen Number	Number of cycles for a_i to a_y			a_i to failure
	Exp.	σ_y = 450 Mpa	σ_y = 480 Mpa	Exp.
CAL 2	165500	166400	167100	166391
CAL 3	150400	149670	150440	151210
CAL 4	189500	188890	189750	190714
CAL 5	281000	280810	281860	282871
CAL 6	194800	193920	195220	197324

Table 4.7 – Comparison of analysis

Specimen Number	% Error - a_i to a_y		% Error - a_i to failure		% Error
	Exp. & 450	Exp. & 480	Exp. & 450	Exp. & 480	Yield & Failure
CAL 2	-0.5	-1.0	0.0	-0.4	0.5
CAL 3	0.5	0.0	1.0	0.5	0.5
CAL 4	0.3	-0.1	1.0	0.5	0.6
CAL 5	0.1	-0.3	0.7	0.4	0.7
CAL 6	0.5	-0.2	1.7	1.1	1.3

From the above tables, it can be stated that the predictions for a crack length a_i to a_y based on a yield strength of 450 MPa gives good results, which are slightly on the conservative side. The results based on the yield strength of 480 MPa give better results, though, on the nonconservative side. Once the crack length is equal to a_y, a relatively small number of cycles are required for the specimen to fail. This results in the predictions for a crack length a_i to failure, based on a yield strength of 450 MPa, to be in error by approximately one percent on the conservative side. When dealing with fatigue predictions, percent error less than 5% are considered acceptable, while 1% error is considered as an excellent prediction.

4.4.2 Walker Model

The major limitation of Paris's model is its inability to account for the stress ratio effect and thus it was required to obtain the coefficients for each individual stress ratio. Walker proposed a model to incorporate the effect of the stress ratio as

$$\frac{da}{dN} = \frac{C_W}{(1-R)^{n_W}}(\Delta K)^m \tag{4.11}$$

This method requires that the fatigue rate curves be parallel to each other; that is, they have the same value for 'm' as that determined for the Paris law. To determine the value of C_W and n_W, one must plot the value of 'log C' and 'log (1 – R)' where 'C' is the same value obtained from the Paris model for each individual stress ratio. If Walker's model is to be applicable, the resulting curve should be linear, and the slope of the curve is equal to n_W and the y-intercept is equal to $\log(C_W)$. Figure 4.10 and 4.11 represent the plot of 'log C versus log (1 – R)' for the one and two curve models respectively.

A summary of the Walker model predictions are shown in Table 4.8.

Table 4.8 – Predictions for interval a_i to a_f using Walker model

Specimen Number	# Cycles Experimental	Walker (# Cycles)		% Error	
		1 Curve	2 Curve	1 Curve	2 Curve
CAL 2	165000	77650	234350	53	-42
CAL 3	147500	69460	197280	53	-34
CAL 4	189000	83720	488220	56	-158
CAL 5	275000	93390	1196400	66	-335
CAL 6	186000	63170	1547860	66	-732

Note: Predictions are for crack length a_i to a_f

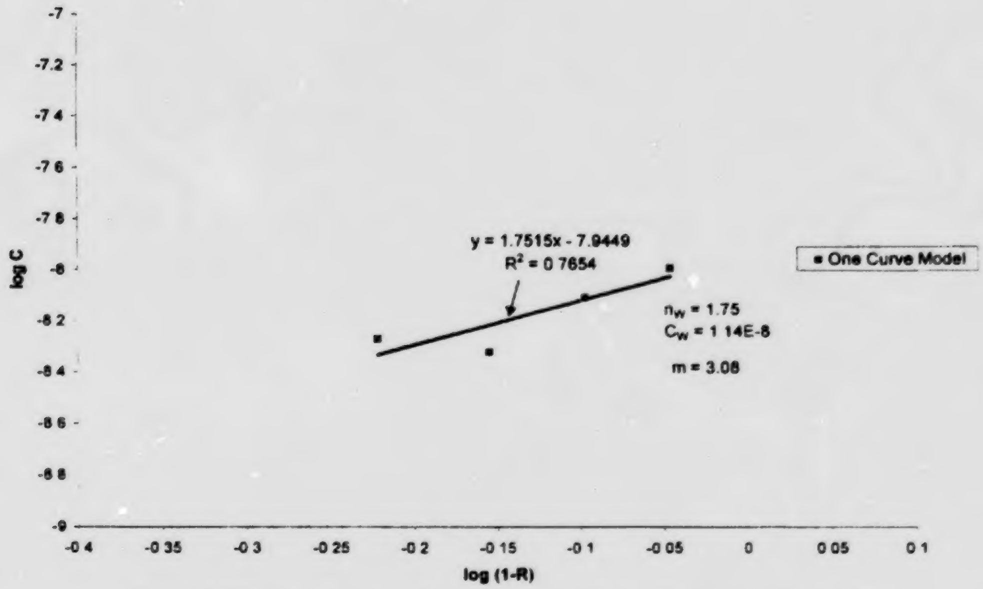

Figure 4.10 – log C versus log (1 – R) graph for the one curve model

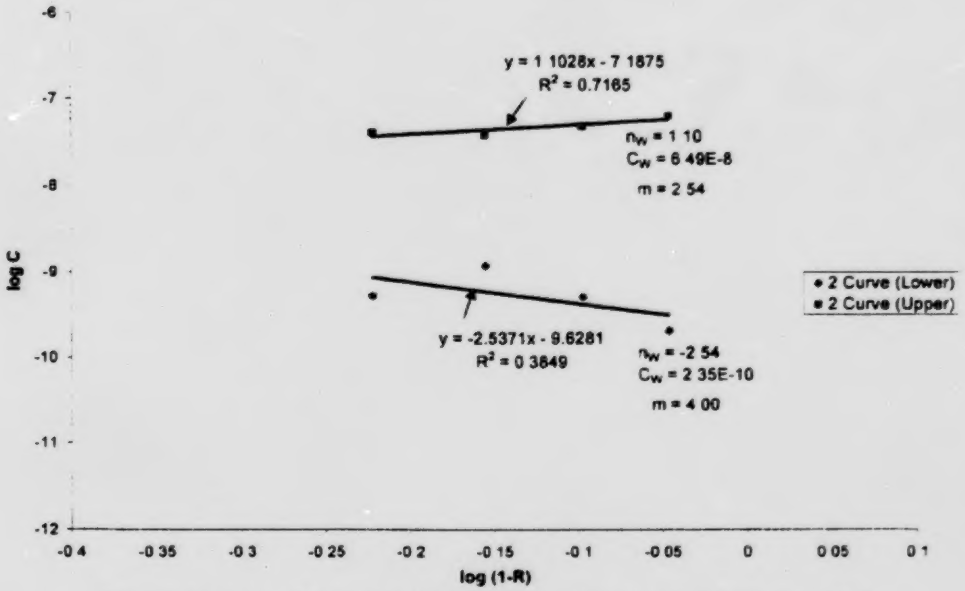

Figure 4.11 – log C versus log (1 – R) graph for the two curve model

From Table 4.8, it is obvious that Walker's model does not adequately account for the fatigue behavior of this particular material. First, Walker's model requires that the various stress ratio fatigue rate curves are parallel to each other. The results for the 350WT are offset from one another and not always parallel. Secondly, the results from Figure 4.10 and 4.11 are not linear (as required), indicated by the low R^2 values.

The one curve model consistently underpredicts the experimental results by approximately 55 to 65 percent. The two curve model results vary, with the largest errors occurring for the higher stress ratios which is due to the fact that the value for $n_{W\,lower}$ is negative. Generally, however, this value is positive, resulting in the term '$(1-R)^{n_w}$' being less than unity; whereas, a negative value of n_W results in the term being greater than unity. For a stress ratio of 0.40 and n_W equal to ± 2.54, the term '$(1-R)^{n_w}$' is equal to 0.27 and 3.66 respectively, which is a difference in magnitude of 13.5 times. In summary, it was found that Walker's model does not provide accurate fatigue predictions for the 350WT steel.

4.4.3 Fatigue Models Based on Tensile Properties of Material

The main limitation for a majority of constant amplitude fatigue crack models is that they require the calibration of usually two or more empirical parameters. These parameters are obtained from the results of fatigue tests, which are expensive and time consuming to perform. Several models have been proposed that do not rely on empirical curve fitting parameters, but rather the results of a simple tensile test. Such models are appealing and their application to the 350WT steel experimental fatigue results will be examined.

Three models were identified and discussed in the literature review section, that have parameters obtained from the tensile properties of the material. These models are

1. Pook and Frost $$\frac{da}{dN} = \frac{9}{\pi}\left(\frac{\Delta K}{E}\right)^2$$

2. McEvily $$\frac{da}{dN}=\frac{8}{\pi E^2}\left(\Delta K^2-\Delta K_{th}^2\right)$$

3. Zheng and Hirt $$\frac{da}{dN}=\frac{1}{2\pi E\sigma_f\varepsilon_f}(\Delta K-\Delta K_{th})^2$$

All three models rely on the square of the stress intensity factor range and have a E^2 term (in model 3, the E^2 value is implicit in the $E\sigma_f\varepsilon_f$ expression). Model 1 does not consider the threshold parameter, whereas model 2 and 3 do. It is interesting to point out that model 2 considers the square of the ΔK and ΔK_{th} terms individually; whereas, model 3 considers the square of the difference between the ΔK and ΔK_{th} terms.

Model 1 and 2 requires the value of the modulus of elasticity; whereas, model 3 additionally requires the fracture strength and fracture ductility. The fracture strength ($\sigma_f = \sigma_u\{1 + RA\}$) and fracture ductility ($\varepsilon_f = -\ln\{1 - RA\}$) are determined from the ultimate stress (σ_u) and the reduction in area at fracture in the tension test (RA). The tensile properties for the 350WT steel are as follows: E = 205 000 MPa, σ_u = 524 MPa and RA = 71%.

The exponent on the ΔK term is two for all models and the terms based on the tensile properties are

1. Pook $$C=\frac{9}{\pi E^2}=6.8\times10^{-11}$$

2. McEvily $$C=\frac{8}{\pi E^2}=6.1\times10^{-11}$$

3. Zheng and Hirt $$C=\frac{1}{2\pi E\sigma_f\varepsilon_f}=\frac{92.4}{\pi E^2}=7.0\times10^{-10}$$

Models 1 and 2 have similar values; however, the coefficient for model 3 is nearly an order of magnitude different.

Figures 4.12 graphically illustrates the difference between the predictions of the three models for an arbitrarily chosen threshold value of 20 MPa $m^{1/2}$. Model 1 is a straight line; whereas, the lower portions of the model 2 and 3 curves are asymptotic to the threshold value at a fatigue growth rate (d*a*/dN) of approximately 1 x 10^{-6} mm/cycle. If the threshold value was equal to zero, model 2 and 3 would be a straight line extending downward from the curves upper portion, similar to model 1. It is interesting to note that model 2 and 3 behave similarly until a value of d*a*/dN = 1 x 10^{-5} mm/cycle, and then deviate as d*a*/dN increases. This behavior is accounted for by the difference in the tensile coefficient, C, as well as the stress intensity factor expressions. That is, model 2 uses $\left(\Delta K^2 - \Delta K_{th}^2\right)$ whereas model 3 uses $\left(\Delta K - \Delta K_{th}\right)^2$.

Comparing the curves in Figure 4.12 to the experimental results shown in Appendix C, one may conclude that the model proposed by Zheng and Hirt appears to best represent the data. This is because at a stress intensity factor range greater than 30 MPa $m^{1/2}$, the fatigue crack growth rate is on the order of 1 x 10^{-3} mm/cycle to 1 x 10^{-4} mm/cycle, which is similar to the experimental results. Therefore, the number of cycles required to propagate the crack between a_i and a_f will hereafter be evaluated with Zheng and Hirt's model only, since the other models would produce relatively larger errors.

To use Zheng and Hirt's model, the threshold values are required and are determined from the 'K-decreasing procedure' described in ASTM Standard E647. This test was not performed during the experimental program; therefore, the threshold values are unknown. Theoretically, the threshold value represents the value below which fatigue crack growth is zero. In practice, this point corresponds to the ΔK value defined at a fatigue growth rate of approximately 1 x 10^{-7} mm/cycle to 1 x 10^{-8} mm/cycle. Therefore, the 'd*a*/dN versus ΔK' experimental results were extrapolated to a value of 1 x 10^{-8} mm/cycle to obtain an approximate value for the threshold parameter. It was found, that the threshold value corresponds to approximately 10 to 11 MPa $m^{1/2}$ depending upon the stress ratio. Therefore, a value of 11 MPa $m^{1/2}$ was used for a stress ratio of 0.10, 10.5 MPa $m^{1/2}$ for a

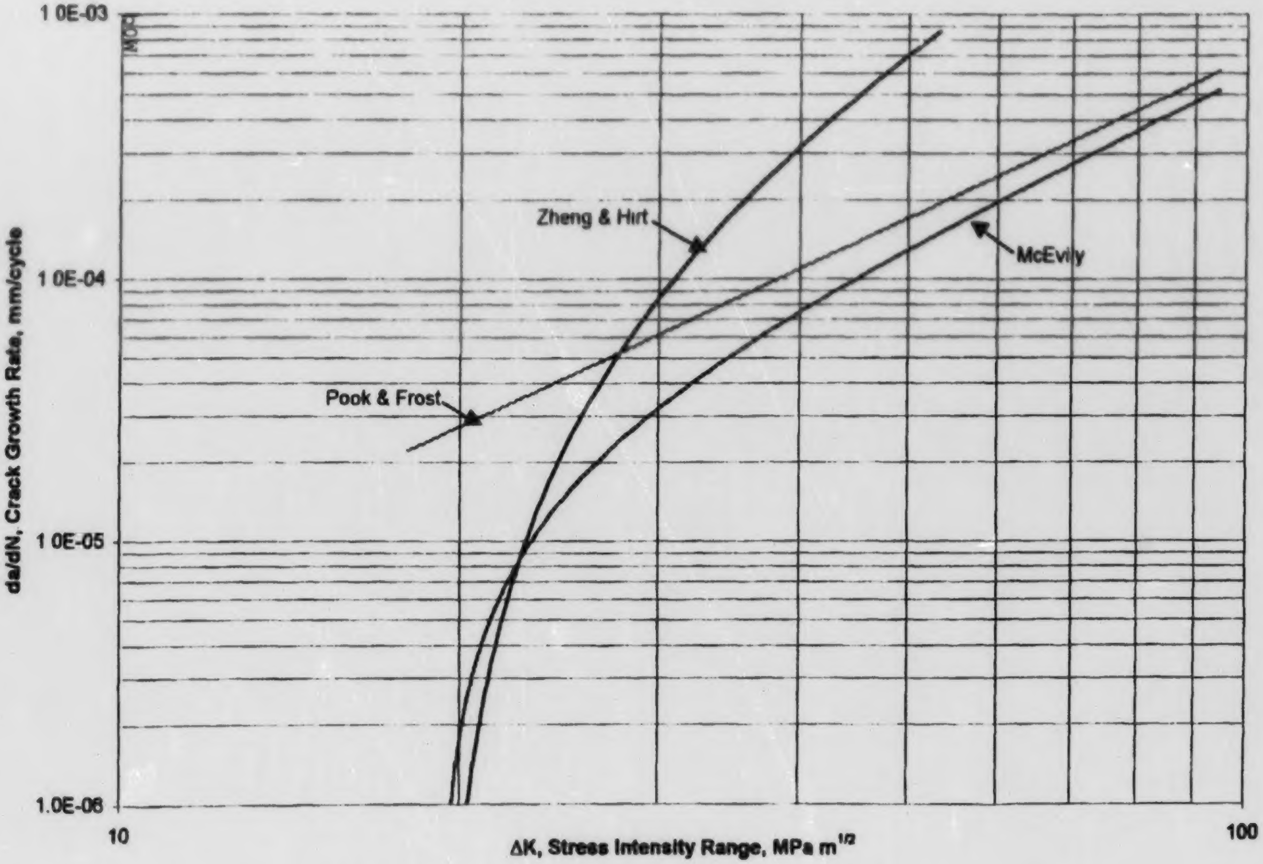

Figure 4.12 - Comparison of fatigue models based on material tensile properties

stress ratio of 0.20/0.30 and 10 MPa $m^{1/2}$ for a stress ratio of 0.40. For comparison, the Zheng and Hirt equation with the appropriate parameters is plotted with the experimental results for each stress ratio, shown in Appendix D.

The results based on Zheng and Hirt's model are presented in Table 4.9.

Table 4.9 – Predictions for crack growth interval a_i to a_f based on Zheng and Hirt's model

[illegible]	[illegible]	[illegible]	[illegible]	[illegible]
CAL 2	165000	11	162200	1.7
CAL 3	147500	11	142000	3.7
CAL 4	189000	10 5	195200	-3 3
CAL 5	275000	10 5	274900	0.0
CAL 6	186000	10	191700	-3.1

These results are relatively good and only require the determination of the material's tensile properties and the threshold values. The threshold values used to obtain the above results were extrapolated from the fatigue test results and are only approximate. Therefore, it is necessary to examine the influence of the threshold value on the accuracy of Zheng and Hirt's model. This was accomplished by increasing/decreasing the threshold value used in Table 4.9 by a certain percentage and determining the percent error of Zheng and Hirt's model with respect to the experimental values as graphically illustrated by Figure 4.13. This figure indicates that the threshold value should be accurately known, since an incorrect value will give relatively large errors.

In summary, Zheng and Hirt's model adequately predicts crack growth as shown in Table 4.9, but requires the threshold value to be accurately known. As a result, Zheng and Hirt model requires a tensile and a fatigue threshold test. The tensile test is readily performed; however, the fatigue threshold test is more time consuming, but less fatigue crack

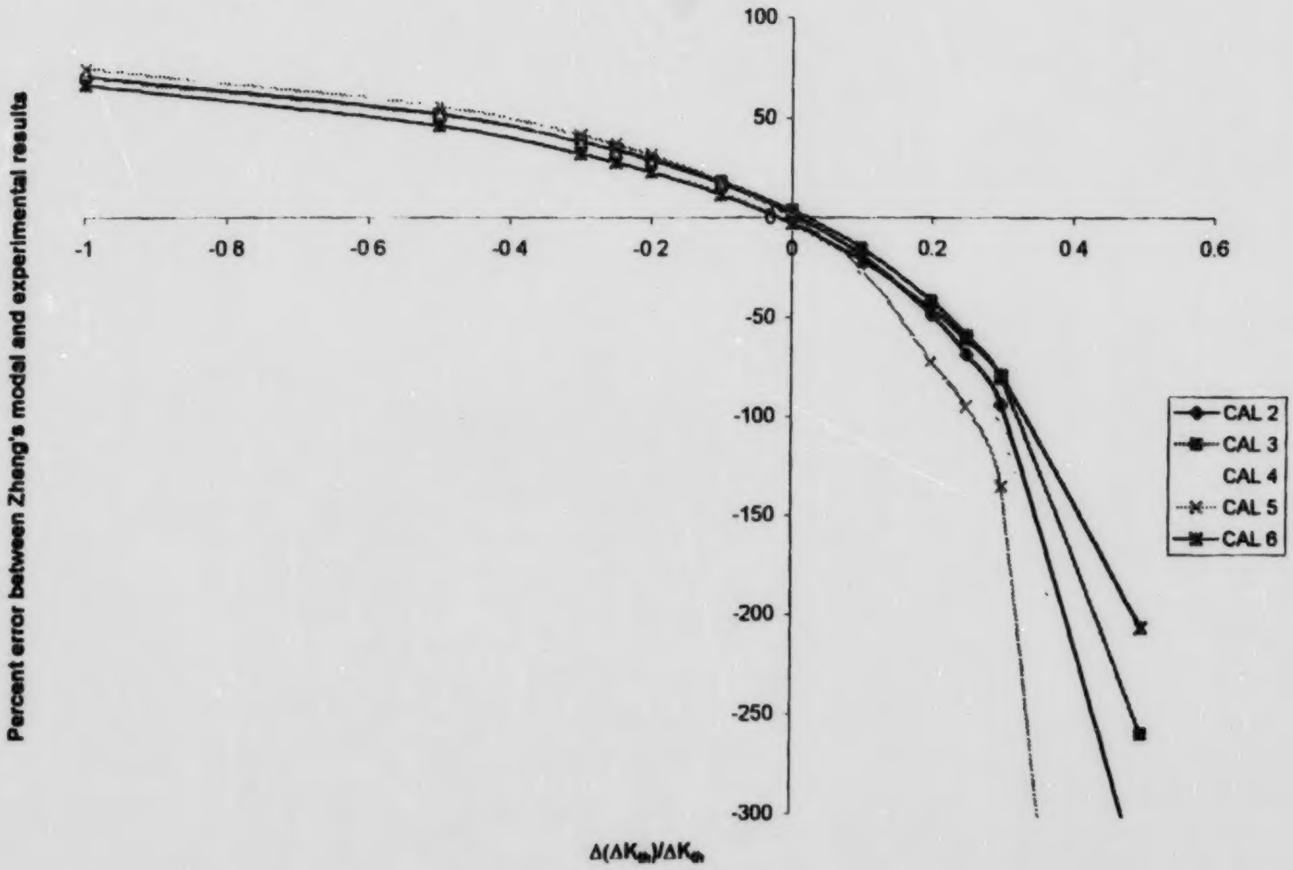

Figure 4.13 - Evaluation of threshold effect on Zheng and Hirt model prediction accuracy

propagation testing. Therefore, Zheng and Hirt model is considered to be attractive because it can adequately predict fatigue with relatively little experimental work to calibrate the model.

4.4.4 Summary of Constant Amplitude Models

The Paris model was evaluated and shown to adequately predict fatigue crack growth with the use of a two curve model defined by Equation 4.8. The influence of stress ratio was determined to be significant; therefore for best results, the Paris coefficients were obtained for each individual stress ratio.

Walker's law was then examined as a model that could account for the stress ratio effect with one set of parameters. The model was calibrated, however, did not adequately represent the data and resulted in unacceptable errors.

Various other models that were discussed in the literature review were also considered, but not discussed in this section, since they involved greater than two curve fitting parameters and were more complicated and time consuming to calibrate. They may have provided excellent results, similar to the Paris equation, but the required effort to use the model is thought to be much greater.

One exception to the above comments, are the three models whose parameters are based on the results of a simple tensile test rather than fatigue testing. Among those models, it was shown that the model proposed by Zheng and Hirt was able to accurately predict the fatigue results, based on a threshold value that was extrapolated from the experimental data. Figure 4.13 compared the influence of threshold value on the accuracy of Zheng and Hirt's model and shows that the threshold must be accurately known.

4.5 Variable Amplitude Loading Test Results

A total of six variable amplitude tests were performed to investigate the effect of periodic single tensile overloads interspersed in a constant amplitude loading scenario. For all tests, the constant amplitude load corresponded to a stress ratio of 0.10 and the overload range (ΔP_{OL}) was obtained by multiplying the constant amplitude load range by the appropriate overload ratio ($\Delta P_{OL}/\Delta P$). The value for $P_{min(OL)}$ is kept equal to the minimum value of the constant amplitude loading and the value for $P_{max(OL)}$ is calculated as '$\Delta P_{OL} + P_{min(OL)}$'. Details of the specimen loading scenarios are shown in Appendix A.

Table 4.10 summarizes the average crack lengths and number of cycles to failure for each test specimen.

Table 4.10 – Variable amplitude test summary

Specimen Number	OL Ratio	# of OL in Test	[illegible]	[illegible]	[illegible]	[illegible]	# of Cycles a_i to a_y	# of Cycles a_i to failure
Val 1	1.25	2	11.19	35.11	39.10	146000	150000	150756
Val 2	1 25	3	11.35	34 56	39.24	165000	171250	172022
Val 3	1.50	2	11.25	34.43	38.53	167500	171800	172498
Val 4	1.50	3	11.23	34.26	38.66	193000	198400	199108
Val 5	1.75	2	11 25	35.19	39.21	223000	227750	228433
Val 6	1.75	2	11.17	34.48	38.50	255000	259400	260024

Notes: All crack lengths are the average value of the right and left crack measurements

a_i = crack length when started recording test data

a_f = crack length when stopped recording test data

a_y = crack length where yielding occurs (crack stops propagating)

The '*a* versus N' and fatigue rate curve (d*a*/dN versus ΔK) for each test specimen are shown in Appendix E. The overloads were applied at a crack length of 15 and 25 mm and 15, 20 and 25 mm for the two and three overload tests, respectively. As with the constant amplitude results, the crack propagated from each side of the center notch at similar rates as indicated by the '*a* versus N' curves. Both data reduction methods were used to obtain the fatigue rate curves, resulting in little difference between the respective curves (See Appendix E), which confirms the 'lack of scatter' in the data.

Figure 4.14 illustrates the difference between the fatigue rate curves for constant and variable amplitude loading scenarios where the constant amplitude curve is a linear trendline based on the R = 0.10 data of Figure 4.3. The variable amplitude data for specimen number VAL 6 was used for comparison because it had the largest overload ratio, which best illustrates the influence of a periodic tensile overload interspersed in a constant amplitude loading scenario. The initial portion of the experimental data and R = 0.10 curve coincide; however, immediately following the overload, the variable amplitude fatigue crack growth rate increases for a very short period and then decreases by an amount dependent upon the magnitude of the overload. Once the minimum d*a*/dN value is reached, the fatigue crack growth gradually increases until the equilibrium constant amplitude growth rate is re-established.

Tests having the same loading scenarios (i.e. the same stress and overload ratios) should produce similar fatigue rate curves. This is the situation for the tests with overload ratios of 1.25 and 1.50, but not 1.75. Figure 4.15 compares the experimental fatigue rate curves for specimens VAL 5 and VAL 6, both having two overloads (OLR = 1.75), applied at crack lengths of 15 and 25 mm. The response for both specimens is nearly identical until the second overload, where the curves deviate as shown. The crack growth rate during the second overload for specimen VAL 5 decreases to a value of 1.5×10^{-4} mm/cycle and then gradually increases to the equilibrium rate (for R = 0.10); whereas, the crack growth rate for specimen VAL 6 decreases to a value of 1.9×10^{-5} mm/cycle before returning to the equilibrium rate. This represents almost an order of magnitude in difference between the minimum fatigue crack growth rates during the second overload. This peculiarity is a result of the second overload for specimen VAL 5 being incorrectly applied as described below.

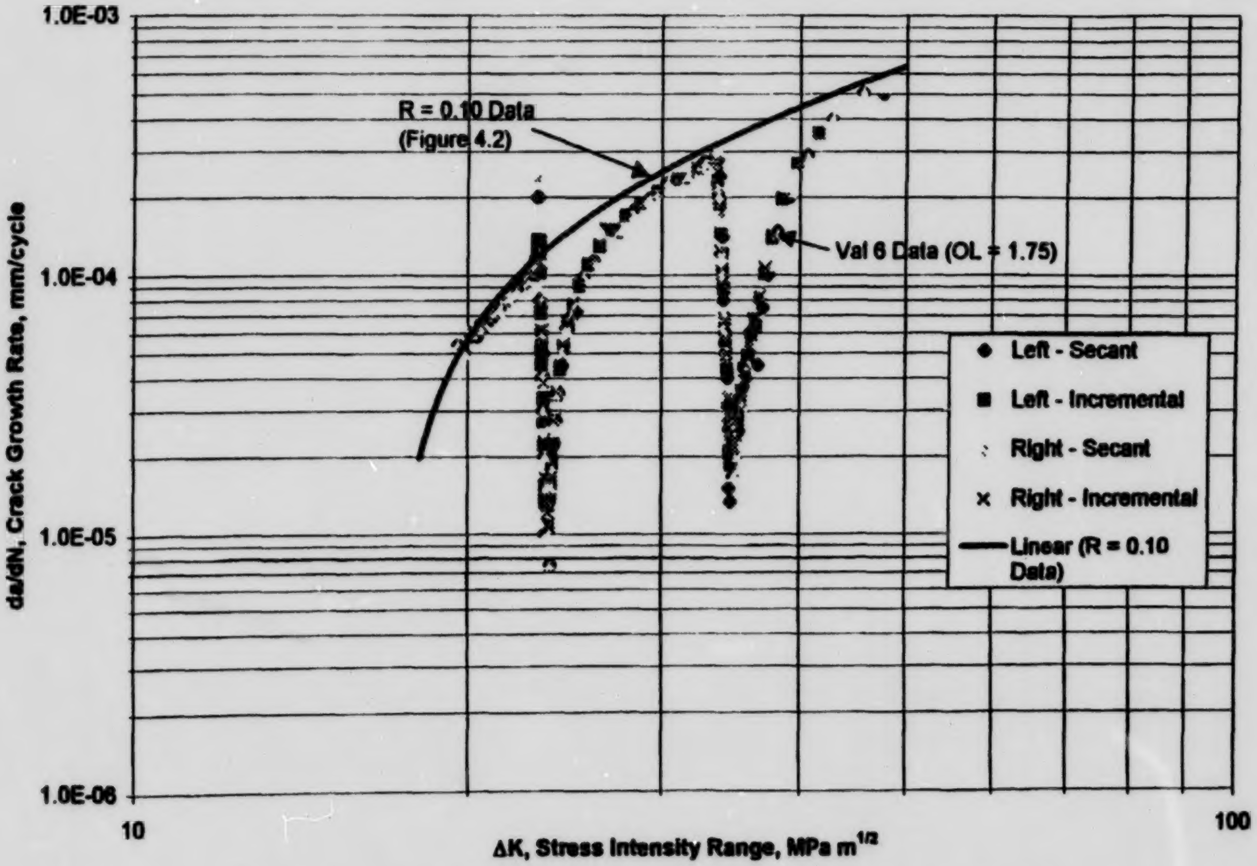

Figure 4.14 - Comparison of constant and variable amplitude data for R = 0.10

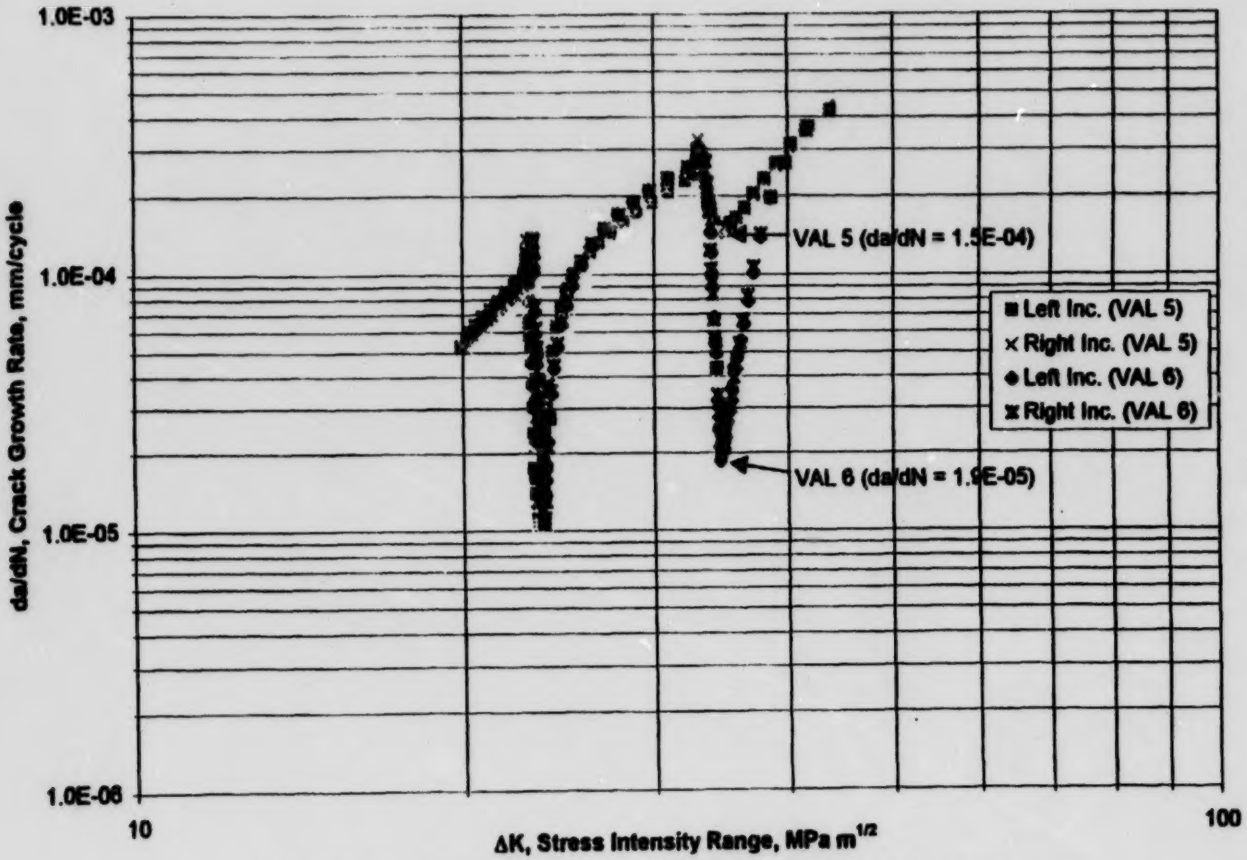

Figure 4.15 - Comparison of specimens VAL 5 and VAL 6 fatigue rate curves

During the experiment, the loading sequence is defined by programming the control panel with the mean loading level and the corresponding amplitude. To apply the overload, these values were changed from their constant amplitude values. However, during the second overload for specimen VAL 5, the mean and amplitude values were reversed. As a result, the load was increased to the correct maximum load of 95475 N and also decreased to the correct minimum load of 5700 N which represent three quarters of the required overload cycle. At this point the load should have increased back to the mean level; however, since the mean and amplitude were reversed, the load was directed to continue decreasing below 5700 N. The machine stopped at 5000 N as the lowest load limit of 5000 N (programmed into the control panel) was exceeded. At this point, it was decided to continue testing by applying the load to the required mean level by manually controlling the machine. However, due to an anomaly in the program, a compressive load of 115 KN was applied, forcing the machine to stop as the capacity of the load cell was exceeded. Again, the machine was re-started and was directed to apply the original constant amplitude loading. As a result, one can consider that the overload cycle consisted of a maximum load of 95475 N followed by a minimum load of –115 KN. This represents a tensile overload immediately followed by a compressive underload. As previously discussed in Section 2.6.1, when a compressive underload immediately follows a tensile overload, the amount of retardation is reduced but not eliminated. This phenomenon occurred for specimen number VAL 5.

One of the objectives of this work, as mentioned earlier, was to investigate the influence of single tensile overloads interspersed in a constant amplitude loading scenario. The results for the second overload in specimen VAL 5 was a mistake and is discussed in this section, qualitatively. As a result of the anomaly with applying the overloads, and therefore lack of sufficient data, no quantitative investigation is possible. The only conclusions that can be reached is that a compressive underload following a tensile overload reduces the degree of retardation significantly.

4.6 Variable Amplitude Loading Data Analysis

This section will discuss the analysis of the variable amplitude loading experimental data with the various fatigue crack propagation models discussed during the literature review. Only the most practical models will be presented in the following section.

4.6.1 Predictions By Using Constant Amplitude Model

This section will use the two curve Paris model described by Equation 4.8 with the parameters tabulated in Table 4.2 for a stress ratio of 0.10. This procedure neglects load interactions and will provide an indication of the amount of retardation resulting from the tensile overload. The fatigue predictions for the crack growth interval a_i to a_f are presented in Table 4.11.

Table 4.11 – Summary of Paris predictions for crack length interval a_i to a_f

Specimen Number	#Cycles Experimental	# Cycles Predicted	% Error
VAL 1	146000	129700	11.2
VAL 2	165000	127000	23.0
VAL 3	167500	121600	27.4
VAL 4	193000	122300	36.6
VAL 5	223000	129000	42.2
VAL 6	255000	122900	51.8

It can be concluded from Table 4.11 that the use of a constant amplitude model cannot adequately predict the crack growth for a single tensile overload interspersed in a constant amplitude loading scenario. As expected, the greater the number and magnitude of the overloads, the higher the error. These results indicate that the amount of retardation is significant and must be accounted for by other modeling approaches.

The predicted and experimental '*a* versus N' curves are graphically illustrated in Figure 4.16 to 4.19. The constant amplitude model accurately predicts the crack growth behavior until the first overload is applied. At this point the experimental '*a* versus N'

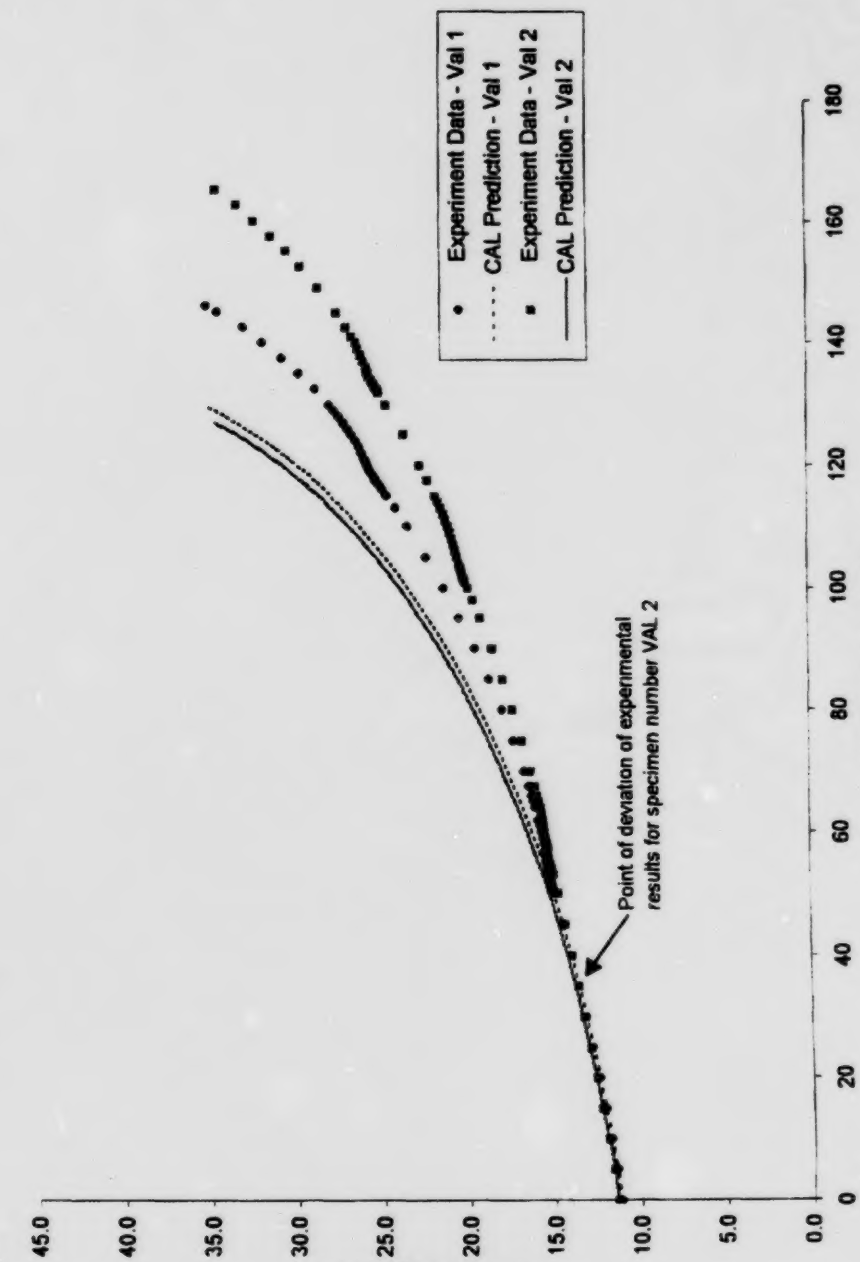

Figure 4.16 - Paris predictions for specimens VAL 1 and VAL 2

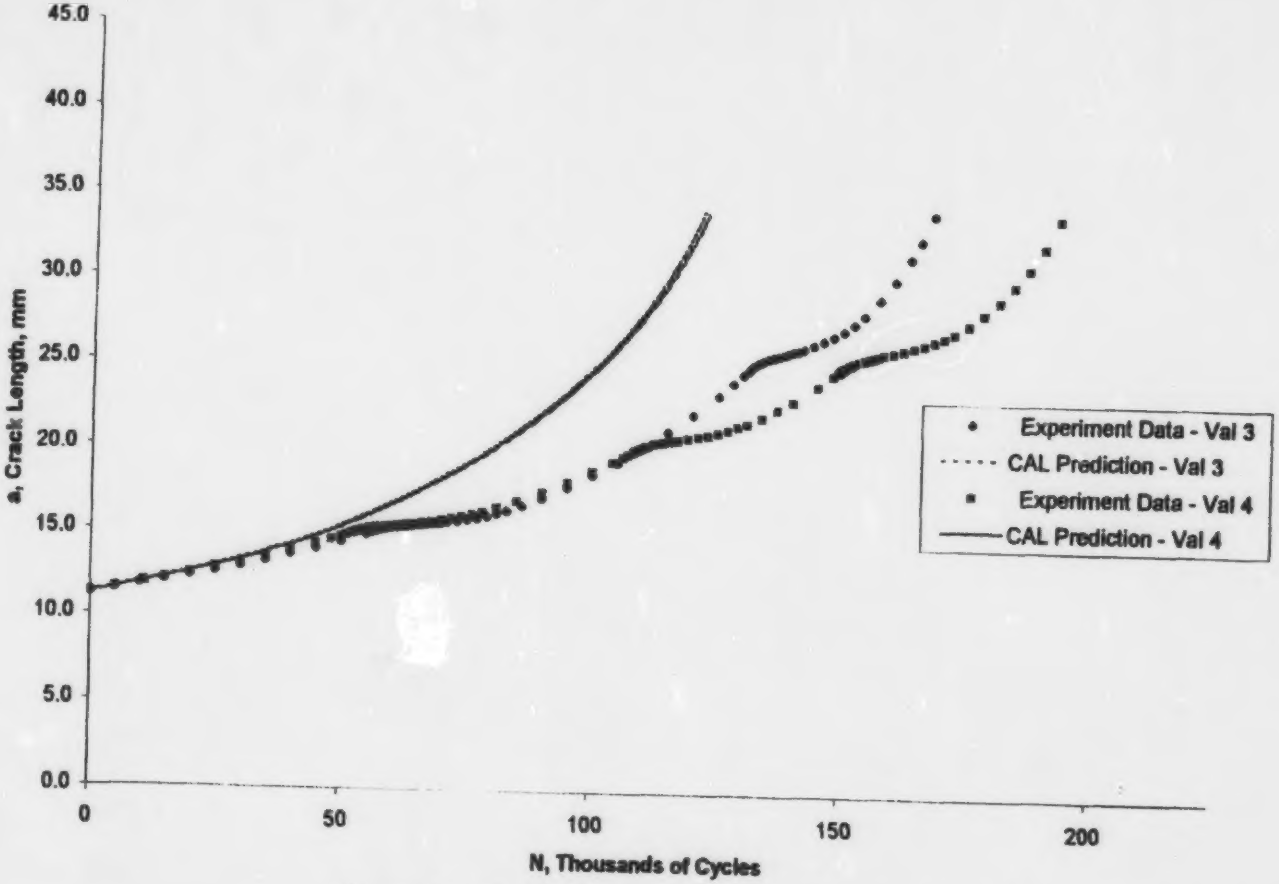

Figure 4.17 - Paris predictions for specimens VAL 3 and VAL 4

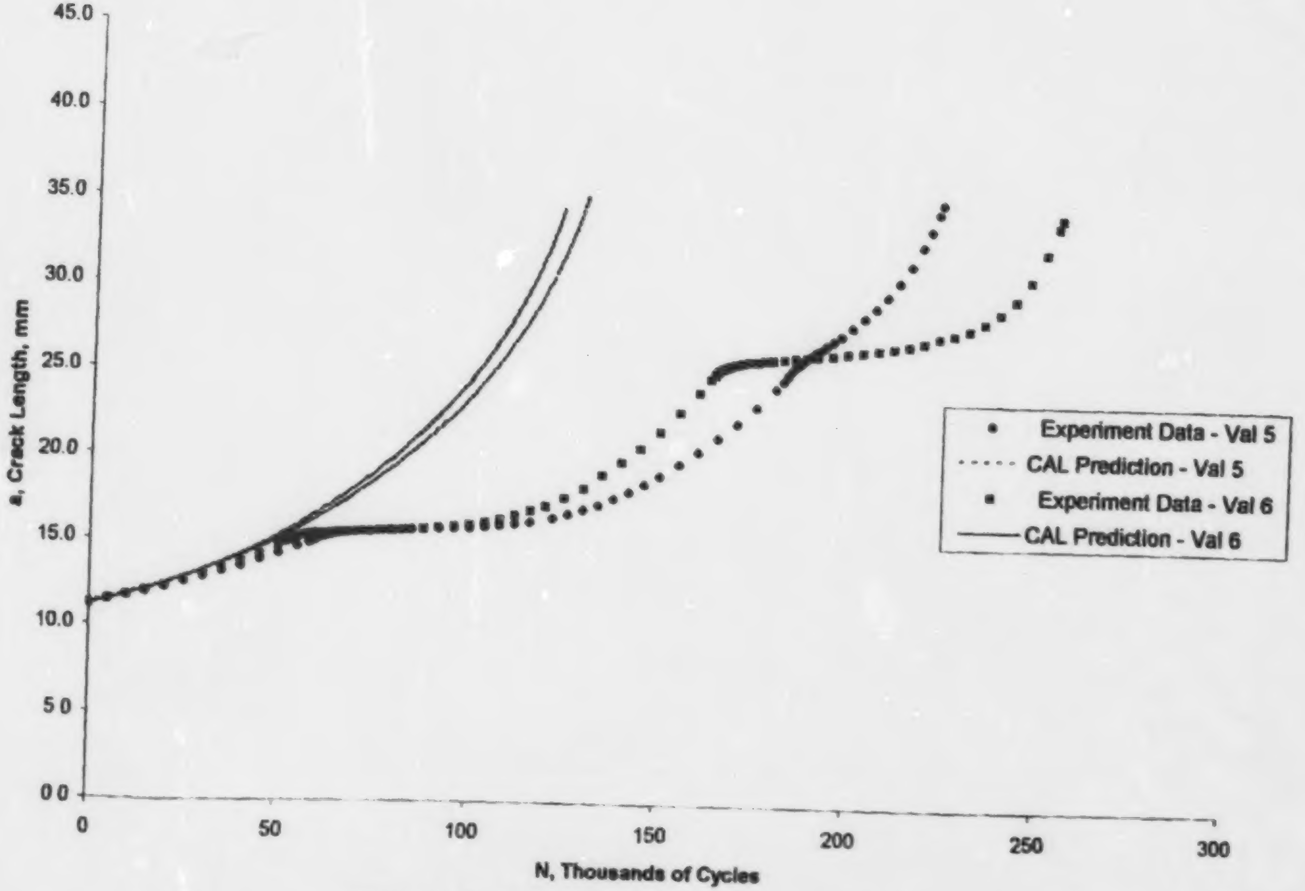

Figure 4.18 - Paris predictions for specimens VAL 5 and VAL 6

curve *flattens out* in the horizontal direction, due to the reduction in the fatigue crack growth rate. After a certain number of cycles, the 'equilibrium' crack growth rate is resumed and the '*a* versus N' curves are parallel to one another but offset by a certain distance. This distance represents the magnitude of retardation resulting from the applied overload. During the experimental program, all the overloads were applied far enough apart so that the steady state crack growth rate was obtained prior to the application of the next overload.

The trends between the predicted and experimental '*a* versus N' curve are the same, with the exception of specimen number VAL 2. Consider the results for specimen number VAL 3 and VAL 4 shown by Figure 4.17; the constant amplitude predictions are nearly identical indicating that the behavior of the two specimens should be the same. The experimental curves are consistent up to approximately 100 000 cycles, where specimen number VAL 4 deviates due to a second applied overload, as expected. Examining the third overload and beyond, the two curves are offset by a certain distance and parallel to one another. Thus, the experimental results for specimen numbers VAL 3 and VAL 4 follow the predictions of the Paris constant amplitude model.

Next, the results for specimen number VAL 5 and VAL 6 shown by Figure 4.18 will be compared. The constant amplitude model is capable of differentiating the responses of the two specimens. The prediction indicates that the crack growth rate for specimen number VAL 6 will be greater than VAL 5 after approximately 50 000 cycles. This trend is also present in the experimental results as the two curves start to deviate at approximately 50 000 cycles. The first overload is then applied and after a number of elapsed cycles (approximately 100 000), the crack growth rate for specimen number VAL 6 becomes greater than VAL 5 as expected from the Paris model. The difference between the trends for the two curves at the second overload is due to the loading error discussed in the previous section. That is, the amount of retardation for specimen number VAL 5 is reduced due to the compressive underload immediately following the tensile overload. Nonetheless, the experimental observations for specimens VAL 5 and VAL 6 are very similar, as expected, up until the second overload.

Finally, the response for specimens VAL 1 and VAL 2, illustrated by Figure 4.16 will be considered. For these specimens the constant amplitude predictions differ, indicating that the crack growth rate for specimen number VAL 2 will be greater than VAL 1. This trend is observed in the experimental results until approximately 35 000 cycles as indicated by Figure 4.16. At this point, the '*a* versus N' curve for specimen VAL 2 crosses underneath the curve for specimen VAL 1. In this case, VAL 2's data is considered suspicious, as upon comparing the predicted and experimental curves for specimen number VAL 1, after 35 000 cycles, the curves appear to follow the same trend except the presence of the offset. This indicates that the experimental data for VAL 1 are reliable. On the other hand, the predicted and experimental curves for specimen VAL 2 do not follow the same trend (not having the same curvature). Based on the above discussion, it is believed that the experimental curve for VAL 2 should lie above that of VAL 1, similar to that of the predicted curves. The data analysis and fatigue prediction calculations were reevaluated, and were deemed as reliable. The ensuing difference is postulated to be the result of an experimental error (i.e. misalignment), incorrect measurements or presence of high residual stresses in the test specimen. In all, the experimental results for VAL 2 are questionable and will be dealt with caution for the remainder of this thesis.

4.6.2 Delay Model

It was previously discussed, that after an overload there is a "… period of abnormally low rate, or zero rate, of fatigue crack growth between a decrease in load level and the establishment of a rate of growth commensurate with that for constant amplitude loading at the prevailing (lower) load" (Wei et al., 1974). The corresponding number of elapsed load cycles represents the amount of retardation, hereafter called *delay*. The common approach in literature is to define delay, N_D, as a period of zero crack growth, immediately following the overload (Wei et al., 1974; Close et al., 1989). To determine N_D, a horizontal zero-growth (zero slope) line is drawn at the crack length corresponding to where the overload was applied, as shown in Figure 4.19. Then, a line is drawn and extrapolated from the steady state crack growth curve that follows the overload. The distance between the intercept of this line and the zero-growth line to the point corresponding to the application of the overload is considered as the number of delay cycles, N_D.

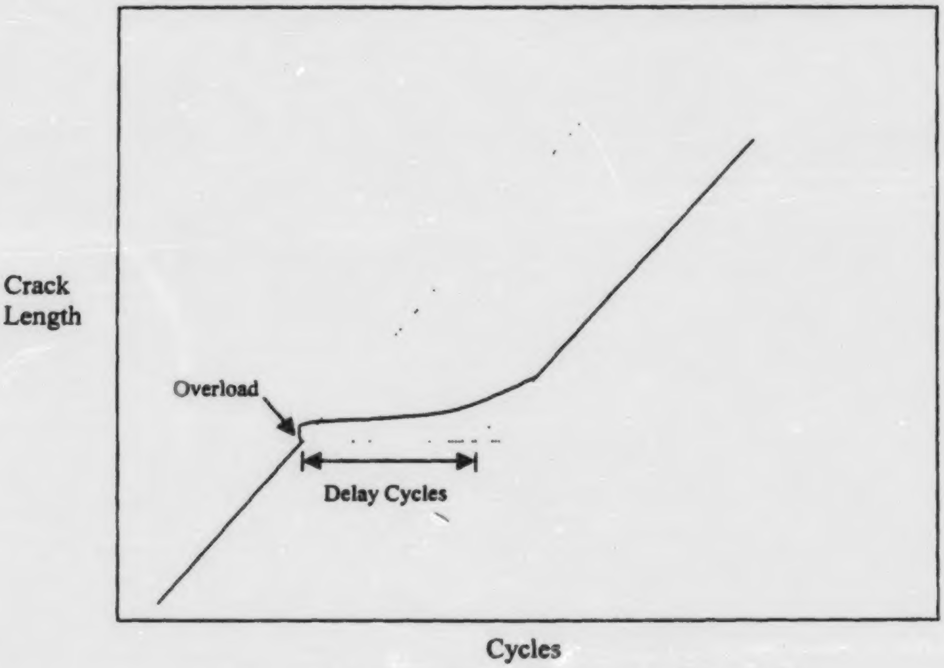

Figure 4.19 – Definition of number of delay cycles

This graphical method is equivalent to the relationship suggested by Goel et al (1994). That is, $N_D = N_{OL} - N_{CA}$ where N_{OL} is the number of cycles of overload between a_{OL} and a_f and N_{CA} is the number of cycles of corresponding constant amplitude load tests between a_{OL} and a_f.

Table 4.12 shows the average number of delay cycles for each test specimen.

Table 4.12 – Number of delay cycles after overload

[redacted]	[redacted]	[redacted]	[redacted]
VAL 1	8200	1.25	8200*
VAL 2	12700	1.25	
VAL 3	23000	1.50	23300**
VAL 4	23500	1.50	
VAL 5	47000	1.75	66000***
VAL 6	66000	1.75	

* Based only on specimen VAL 1 results

** Weighted average {i.e. 2 overloads * (23000) + 3 overloads * (23500) }

*** Based on specimen VAL 6 and first overload of specimenVAL 5

The average number of delay cycles per overload is the average of either the two or three overloads that were applied during each test. The average is used because the amount of delay per overload is nearly the same within a test, regardless of when it is applied. The weighted average number of delay cycles based on the overload ratio value is shown in the last column of Table 4.12. The average for overload ratio of 1.25 was assumed to be equal to that of specimen number VAL 1 because the results for specimen number VAL 2 are questionable as previously discussed. The average for an overload ratio of 1.50 is the weighted average of specimen number VAL 3 and 4. The average for an overload ratio of 1.75 was based on the results of specimen VAL 6 and only the first overload of specimen VAL 5, which was also equal to approximately 66 000 cycles.

Plotting the number of delay cycles versus overload ratio (i.e. $\Delta K_{(OL)}/\Delta K_{Base}$) on semi-log paper provides a linear relationship ($R^2 = 1$) as shown in Figure 4.20. This relationship is extrapolated to predict the number of delay cycles for higher overload ratio values. These predictions are graphically illustrated in Figure 4.21. Therefore, for overload ratios of 2.00, 2.25 and 2.50, the predicted number of delay cycles per overload are 187500, 532000 and 1.5 million, respectively.

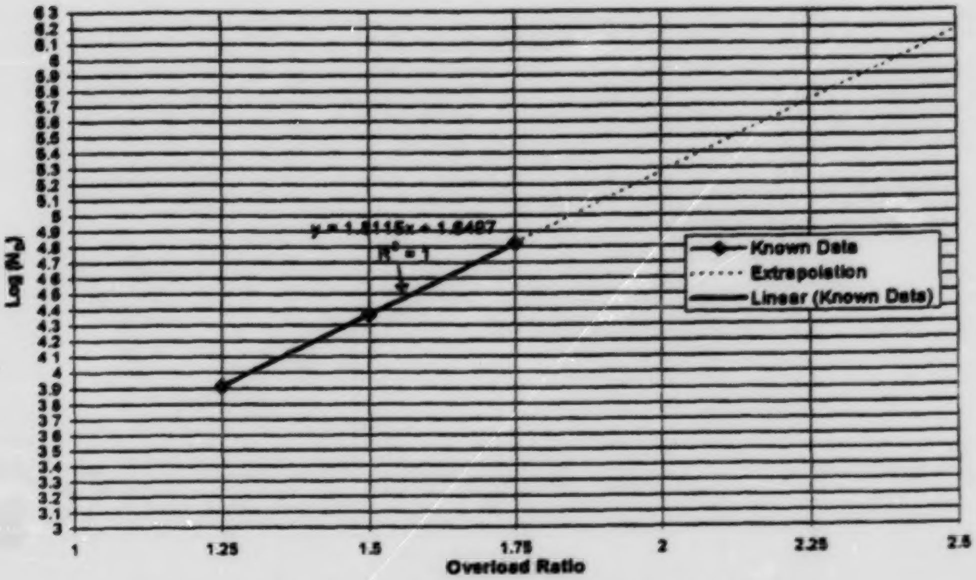

Figure 4.20 – Number of delay cycles versus overload ratio

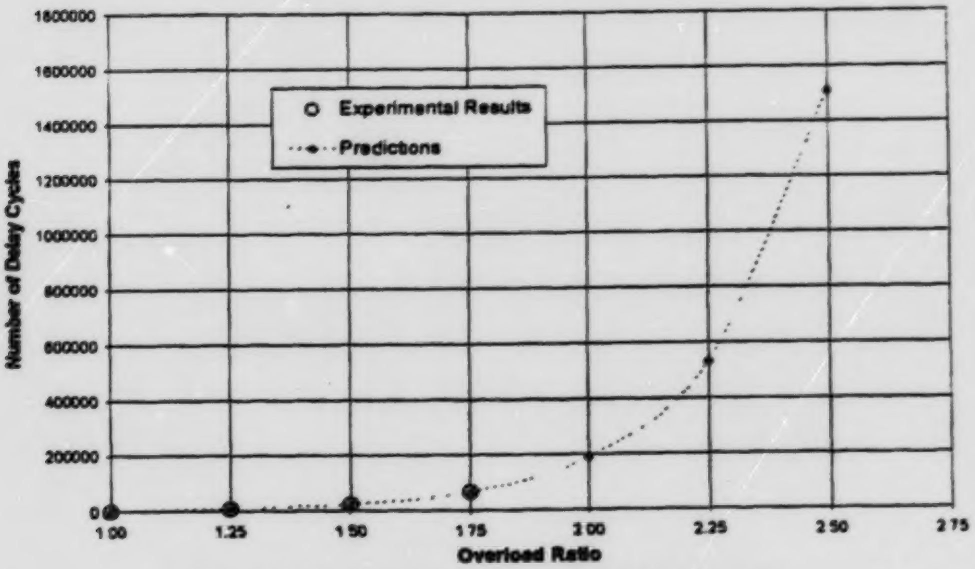

Figure 4.21 – Predictions for number of delay cycles

$$N_{if} = \left[\int_{a_i}^{a_f} \begin{cases} C_{lower} (\Delta K)^{m_{lower}} & \text{, for } \Delta K \leq 23 \text{ MPa m}^{1/2} \\ C_{upper} (\Delta K)^{m_{upper}} & \text{, for } \Delta K > 23 \text{ MPa m}^{1/2} \end{cases} \right] + N_{OL} * 10^{(\alpha + \beta)} \tag{4.12}$$

where N_{if} is the number of cycles required to propagate a crack from a_i to a_f, 'N_{OL}' is the number of overloads which have been previously applied and 'α' and 'β' are obtained from a linear regression of the experimental delay values shown in Figure 4.20. The fatigue predictions based on this method are presented in Table 4.13.

Table 4.13 – Predictions based on the delay model for crack length interval a_i to a_f

[illegible]	[illegible]	[illegible]	[illegible]	[illegible]	[illegible]
VAL 1	1.25	2	146,000	146,100	-0 1
VAL 2	1.25	3	165,000	151,600	8 1
VAL 3	1.50	2	167,500	168,200	-0.4
VAL 4	1.50	3	193,000	192,180	0 4
VAL 5	1 75	2	223,000	261,000	-17.0
VAL 6	1 75	2	255,000	254,900	0 0
VAL 6	2 00	2	-	500,000	-
VAL 6	2 25	2	-	1,200,000	-
VAL 6	2 50	2	-	3,100,000	-

The predictions are in excellent agreement with the experimental data, except for specimens VAL 2 and VAL 6. As mentioned, the experimental data for specimen VAL 2 are questionable and the error for specimen VAL 5 is due to the fact that the second overload was followed by a compressive underload which reduces the amount of delay. Predictions were made for specimen VAL 6 for overload ratios of 2.00, 2.25 and 2.50 as shown. This is based on the assumption that the extrapolated relationship of Figure 4.20 is valid. These predictions indicate that the fatigue life for a specimen increases exponentially with increasing magnitudes for the overload values. Wei and Shih (1974) found that this relationship was typical for this type of loading scenario.

In summary, the above delay model is valid for single tensile overloads that are applied far enough apart such that the steady state constant amplitude crack growth rate is re-established. It appears to provide excellent results and looks promising as a valuable prediction method for such loadings. However, more work regarding the verification of the method (i.e. the linear plot of Figure 4.20) should be conducted for various overload ratios and for different values of the baseline ΔK. The two curve Paris model was used in applying Equation 4.12; however, any constant amplitude model could be used in its place.

4.6.3 Wheeler Model

Wheeler proposed a model to predict the fatigue life of a component subjected to variable amplitude loading by considering the size of the plastic zone ahead of the crack tip expressed by the relationship $da/dN = \phi_R C(\Delta K)^m$. The retardation parameter, ϕ_R, is defined by Equation 2.56 and is equal to the ratio of the current yield zone size to the distance from the crack tip to the overload yield zone boundary. This ratio is multiplied by an exponent referred to as the "shaping exponent", which has no physical significance and its value is determined by a trial and error procedure. The plastic zone diameter is calculated using the relationship

$$R_y = \frac{1}{\alpha\pi}\left(\frac{K_{max}}{\sigma_y}\right)^2 \qquad (4.13)$$

in which $\alpha = 1$ (from theory of elasticity) for a plane stress condition, and $\alpha = 3$ (Irwin's estimate) for a plane strain condition.

The two curve Paris model defined by Equation 4.8 was used in conjunction with the Wheeler retardation parameter, ϕ_R, to predict the results for specimens VAL 1 to 6. The yield zone size was estimated based on the plane stress assumption ($\alpha = 1$). The fatigue predictions for crack length intervals a_i to a_f are shown in Table 4.14.

Table 4.14 – Wheeler model fatigue predictions

[illegible]	[illegible]	[illegible]	[illegible]	[illegible]	[illegible]
VAL 1	1.25	4.5	146000	143450	1.7
VAL 2	1.25	4.5	165000	148400	10.1
VAL 3	1 5	3	167500	166600	0.5
VAL 4	1.5	3	193000	190750	1.2
VAL 5	1.75	2.65	223000	250200	-12 2
VAL 6	1.75	2.65	255000	242700	4.8

The model provides good predictions, with the exception of specimens VAL 2 and VAL 5, whose data are questionable as discussed earlier. A different shaping exponent was required for each overload ratio, determined by a trial and error procedure. The value was selected based on the number that provided the best fit of the experimental data. This obviously limits the usefulness of the model because the shaping exponent has to be determined from the experimental data for each specific loading scenario, requiring a huge database of test data.

The plastic yield zone size was determined by using $\alpha = 1$ in Equation 4.13. If the value of $\alpha = 3$ had been used, the number of predicted cycles would still be very similar to those tabulated in Table 4.14, except a different value of the shaping exponent would have to be used. This implies a lack of physical significance of the Wheeler model, as the results are highly dependent upon the empirically determined shaping exponent.

4.6.4 Willemborg Model

Willemborg's model expresses the magnitude of retardation as a function of the stress intensity factor required to cancel the effect of the plastic zone created by an overload. This approach requires the determination of the plastic zone size ahead of the crack tip and does not rely on any arbitrary empirical parameters.

The expression to determine the plastic zone size is given by Equation 4.13. Using the Von Mises yield criterion, the 'α' value required to calculate the plastic zone diameter, along the path of crack propagation ($\theta = 0$), for plane stress and plane strain conditions would be equal to 1 and 6.25, respectively. A three dimensional nonlinear finite element analysis for the test specimen shown in Appendix A was conducted, and the value of α was found to be equal to 3. A parametric study on the correlation between the value of α and the Willemborg fatigue life predictions will now be performed.

The Willemborg approach was used to determine the crack growth rate from a_i to a_f for specimen VAL 1 (OLR = 1.25). A value of $\alpha = 1$ was used to determine the plastic zone size and the model predicted approximately 131000 cycles. This prediction is not much better than those of the constant amplitude loading model predictions, which ignore the retardation effect. If a value of $\alpha = 3$ or 6.25 was used, the corresponding plastic zone size would be smaller as well as the magnitude of the stress intensity factor required to cancel the effect of the plastic zone created by the overload. This would result in fewer number of cycles than predicted with $\alpha = 1$, thus a larger margin of error.

Next, the Willemborg model was used to predict the fatigue crack growth from a_i to a_f for specimen VAL 6 (OLR = 1.75). The results for a value of α equal to 1 and 3 are illustrated by Figure 4.22. It is predicted that the amount of retardation after the first overload is greater than the second overload. This is contrary to the experimental results, which indicates that the amount of retardation is the same regardless of the crack length at which the overload was applied. Using the plastic zone size associated with a value of $\alpha = 3$, correctly predicts the amount of retardation for the first overload but not the second overload. Using $\alpha = 1$, correctly predicts the second overload but overpredicts the first. Figure 4.22 also shows the prediction based on the plastic zone size associated, with a value of $\alpha = 3$ and 1 for the first and second overload, respectively. Clearly this provides the best estimate; however, using a combination of 'α' values to determine the

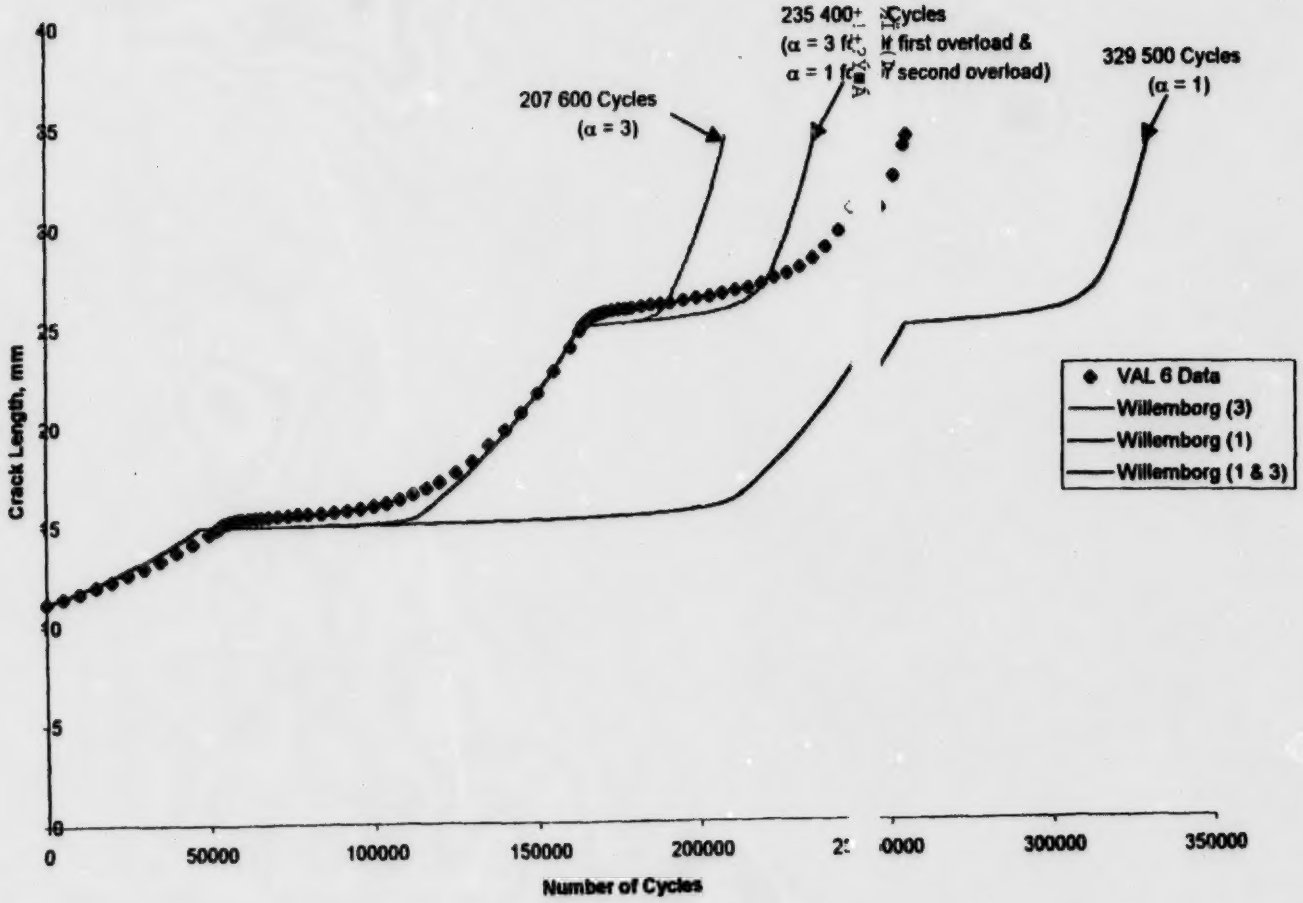

Figure 4.22 - Willemborg predictions for $\alpha = 3$, $\alpha = 1$ and $\alpha = 3$ & 1

plastic zone size is not justifiable. As a result, the Willemborg model does not appear to reliably predict the retardation following a single tensile overload.

4.6.5 Summary of Variable Amplitude Models

The two curve Paris model was used to predict the fatigue life for the specimens subjected to single tensile overloads applied periodically throughout the loading scenario. This constant amplitude prediction was not accurate, indicating that the retardation effect is significant and must be considered. It is interesting to note, as indicated by Figure 4.15, that a compressive overload immediately following a tensile overload has a significant effect on the amount of retardation.

A model based on adding a predicted number of delay cycles to those of the constant amplitude loading predictions was also evaluated. It involved establishing a relationship between the number of delay cycles and the overload ratio for a particular baseline ΔK value shown by Figure 4.20. The constant amplitude model used was the two curve Paris model; however, it was concluded that any adequate model, such as the model proposed by Zheng and Hirt, may be used.

The Wheeler model was evaluated and found to accurately predict the fatigue life; however, it required the determination of an empirical shaping exponent. This parameter was found to be strongly dependant upon the specimens overload ratio and had to be determined by a trial and error procedure. The optimum value was obtained for each specimen overload ratio; however, such values did not appear to follow any predictable trend. Finally, the Willemborg model was examined and determined to be inconsistent and inadequate for predicting the experimental results.

Various other models that were discussed in the literature review section were also considered, but not discussed in this section, as they required calibration of greater than two parameters and thus, demanding large number of experimental fatigue testing and hence time. One exception is the root mean square approaches used by Ahn et al (1995), Hudson (1981), and Barsom (1976), which require only the knowledge of the loading scenario and the Paris constant amplitude parameters. However, they are most suitable for random variable amplitude loading with frequently applied overloads and not for single or infrequent overloads, which differ from the conditions covered in this study.

Chapter 5

Numerical Analysis

5.1 Introduction

"Computers have had an enormous influence in virtually all branches of engineering, and fracture mechanics is no exception" (Anderson, 1995). Traditionally if the value of an unknown fracture parameter was required, one would have to obtain it by experimental methods. Presently, a variety of numerical techniques are available to solve fracture mechanics problems which include finite difference, finite element and boundary integral methods. The finite element approach is the most common method and will be used in this section. Most fracture mechanics finite element packages also offer a module to predict a component's fatigue crack growth life by using the results of a fracture mechanics evaluation.

Various fracture and fatigue software packages are available; most notably, ANSYS, NISA/ENDURE and FAST. Based on the author's qualitative evaluation of the various software packages, NISA/ENDURE and FAST appear to be the most versatile programs. Their theory, advantages, disadvantages, limitations and accuracy will be investigated in the next sections both qualitatively and quantitatively. Both software packages will then be used to predict the results of the experimental program.

5.2 Fracture Parameter Evaluation

5.2.1 Introduction

It was discussed in Section 2.1.2.1 that the stress intensity factor is defined as

$\Delta K = Y\Delta\sigma\sqrt{\pi a}$ where Y is the geometric correction factor defined by an empirical equation applicable to a specific crack configuration and geometry. These equations are available in various fracture mechanics handbooks for certain experimental configuration's; such as the center cracked specimen, edge cracked specimen, compact tension specimen and three point bend specimen.

Knowing the value of the crack tip stress intensity factor for a range of crack lengths is essential for a fatigue crack propagation analysis. If the analysis is to be conducted for a geometry with an unknown geometric correction factor calibration, the fatigue analysis cannot be performed. Traditionally, one would have to either idealize the structure as a geometry with a known correction factor or develop an empirical correction factor relationship for the geometry in question. The latter option is time consuming and difficult to perform. As a result, numerical methods have been developed that are capable of determining the stress intensity factor range for any geometry.

The advantage of computational fracture mechanics is that accurate results can be obtained for any complex geometry in a fraction of time and cost. The capabilities of FAST and NISA/ENDURE fracture mechanic programs will be discussed in the following sections.

5.2.2 FAST-I

The acronym FAST stands for Fracture Analysis of STructures and FAST-I is the module capable of calculating the crack tip stress intensity factor for both mode I and II loading. The program was developed at the Technical University of Nova Scotia and is an extension of the existing finite element program APES (Axisymmetric/Planar Elastic Structures) that was developed at the David Taylor Naval Ship Research and Development Center. It is used for linear elastic fracture mechanics applications, however, an elasto-plastic version of the program also exists.

The FAST-I data file has to be created manually because there is no pre-processor available with the program. This process becomes extremely tedious, time consuming, and prone to mistakes even for the simplest models. Numerous models were examined as a part of this study; therefore, a Fortran program capable of converting the data file created by the preprocessor DISLAY-III (the .NIS file) to the proper FAST-I data input file format was developed by the author. The Fortran program is listed in Appendix F and the FAST-I data file format is described in the FAST user manual (Mufti et al., 1985).

The program uses a twelve-node isoparametric element with an 'enriched' twelve-node isoparametric element to represent the crack tip singularity, both of which will be discussed in the following sections. The advantage of these elements is that only a few elements are required to accurately model the cracked component and to *directly* calculate the stress intensity factor. Another advantage of the FAST-I program is that the mesh in the vicinity of the crack can be readjusted automatically to extend the crack by increments of Δa and the corresponding stress intensity factors are automatically evaluated. This enables the calculation of multiple stress intensity factors from one finite element model. The stress intensity factor parameters for the corresponding crack length and stress values are summarized in the output file **Tabl**. A filename **Inform** is also created which contains a tabular summary of the '*a* versus *ΔK*' values that are used as an input file for the fatigue crack growth module.

5.2.2.1 Conventional Twelve-Node Isoparametric Element

Figure 5.1 illustrates a typical twelve-node isoparametric element defined in natural coordinates.

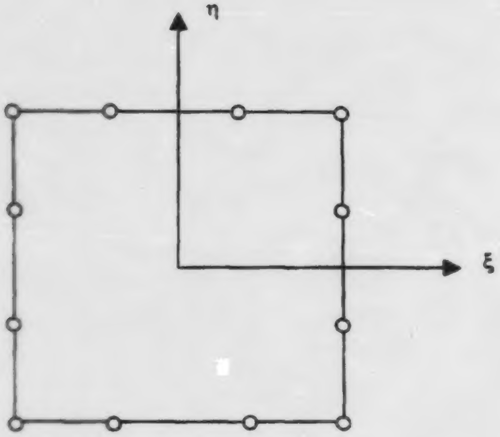

Figure 5.1 – Twelve node isoparametric element

The element displacement assumption is defined as

$$u = \sum_{j=1}^{12} N_j(\xi,\eta) u_j$$

$$v = \sum_{j=1}^{12} N_j(\xi,\eta) v_j \qquad (5.1)$$

where u and v are the x and y displacement components respectively and $N_j(\xi,\eta)$ is the elements shape function which can be found in the APES manual (Gifford et al., 1981).

The elements geometry is defined by

$$x = \sum_{j=1}^{12} N_j(\xi,\eta) x_j$$

$$y = \sum_{j=1}^{12} N_j(\xi,\eta) y_j \qquad (5.2)$$

which varies the same as the displacement assumption; therefore, the element is isoparametric.

Since the displacement varies cubically, the strains and stresses, which are the first derivative of the displacement component, vary quadratically. This is a significant improvement over lower order elements, such as the triangular element for which stresses are constant over the element, and also quadrilateral elements which vary linearly. As a result, a relatively coarse twelve node isoparametric element mesh is capable of providing accurate results, compared to a finer mesh composed of lower order elements.

5.2.2.2 Enriched Twelve-Node Isoparametric Element

Equation 2.2 predicts the stress value at the crack tip to become infinitely large, otherwise referred to as a stress singularity. As a result, the conventional twelve-node isoparametric element is not very accurate near the crack tip.

Gifford and Hinton (1979) modified the displacement function defined by Equation 5.2, by adding extra terms that account for crack tip singularity. This procedure is commonly referred to as 'enriching' an element.

The enriched elements displacement function is defined as

$$\begin{aligned} u(\xi,\eta) &= \sum_{j=1}^{12} N_j u_j + \left[K_I \left(f_1 - \sum_{j=1}^{12} N_j f_{1j} \right) + K_{II} \left(g_1 - \sum_{j=1}^{12} N_j g_{1j} \right) \right] \\ v(\xi,\eta) &= \sum_{j=1}^{12} N_j v_j + \left[K_I \left(f_2 - \sum_{j=1}^{12} N_j f_{2j} \right) + K_{II} \left(g_2 - \sum_{j=1}^{12} N_j g_{2j} \right) \right] \end{aligned} \tag{5.3}$$

where *f* and *g* are functions depending on the crack geometry.

An enriched element is used if any one of its nodes correspond to the crack tip node. The stress intensity factors K_I and K_{II} are directly calculated from the above displacement function.

5.2.3 ENDURE – Fracture Mechanics Module

The finite element program NISA (Numerically Integrated elements for System Analysis) contains a post-processor ENDURE (1997), which is capable of fatigue crack initiation, fatigue crack propagation and fracture mechanics analysis. The fracture mechanics option evaluates the value of the stress intensity factor (K), strain energy release rate (G) and the J integral (J) for the three possible modes of loading (I, II and III) for a given geometric shape and crack size. The parameters can be evaluated according to LEFM or EPFM theory.

In NISA, the fracture parameters are calculated in an indirect manner. The first step is to conduct a finite element analysis (linear or nonlinear) for the structure subjected to a unit load. The pre-processor DISPLAY-III is used to create the finite element model and the finite element run is completed using the NISA static analysis option. For a 2-D analysis, the eight-node isoparametric element is used. It is similar to the twelve node isoparametric element except it has midside nodes as compared to quarter side nodes. The element displacement assumption is defined as

$$u = \sum_{j=1}^{8} N_j(\xi,\eta) u_j$$

$$v = \sum_{j=1}^{8} N_j(\xi,\eta) v_j \qquad (5.4)$$

where *u* and *v* are the x and y displacement components respectively and $N_j(\xi,\eta)$ are the elements shape functions which can be found in any finite element textbook. The element's geometry is defined by

$$x = \sum_{j=1}^{8} N_j(\xi,\eta)x_j$$

$$y = \sum_{j=1}^{8} N_j(\xi,\eta)y_j \tag{5.5}$$

which varies the same as the displacement; therefore, the element is isoparametric.

This element can be used throughout the model; however as with the twelve-node isoparametric element, results are not very accurate at the crack tip since the crack tip singularity is not emulated. NISA is capable of handling large numbers of elements, so one option is to make the mesh surrounding the crack tip extremely fine. This will increase the number of elements and the required execution time. For better efficiency, a special quarter node element surrounding the crack tip may be used which is capable of modeling the crack tip singularity.

The crack tip element is shown by Figure 5.2.

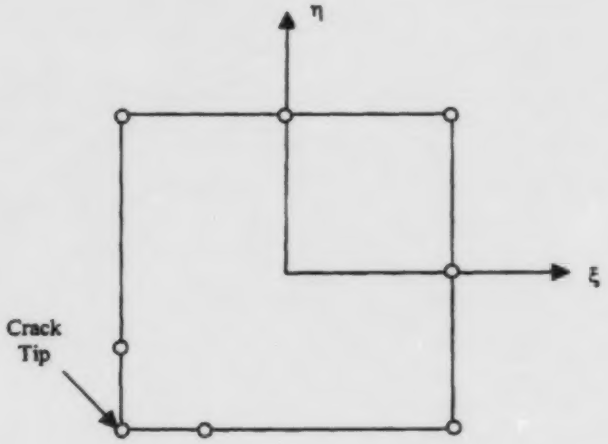

Figure 5.2 – NISA's crack tip element

It is similar to the eight-node isoparametric element, except the mid-side nodes on the two sides corresponding to the crack tip are moved to the quarter point location. This produces a singularity of the type $1/\sqrt{r}$, which matches exactly the singular stress field near the crack tip.

Following a unit load finite element analysis, the input data file for ENDURE is created which provides the information that is required for postprocessing the finite element results to evaluate the required fracture parameters. Endure uses the finite element analysis results in conjunction with either the crack tip opening displacement (CTOD) method, the virtual crack extension (VCE) method, the modified crack closure integral (MCCI) method or the J integral method to calculate the fracture parameters. More details on the ENDURE data file format or the theory for the above methods can be found in the ENDURE manual (1997).

5.2.4 Quantitative Comparison of FAST-I and ENDURE

The strength of the finite element method is in its ability to solve a variety of problems with unknown analytical solutions with relative ease. This is accomplished by approximating the behavior of the structure in question with 'elements' having specifically defined mathematical properties. These properties are usually different than the actual behavior; however, as the number of elements increases (finer mesh) so does the solution accuracy. Theoretically, the finite element approximation will converge to the exact solution by making the mesh increasingly 'finer'.

This section will compare the efficiency and accuracy of the two programs in evaluating the stress intensity factor. An example problem will be examined to determine the best method, which will be used later in this thesis to analyze the experimental results. The example used is a model of the 'typical' experimental test specimen described in Appendix A with the properties shown in Table 5.1.

Table 5.1 – Example problem properties

Length (L)	300 mm
Width (W)	100 mm
Thickness (B)	5.35 mm
Crack Length (2a)	20 mm
Yield Stress (σ_y)	450 MPa
Modulus of Elasitcity (E)	205 000 MPa
Poisson Ratio (ν)	0.30
Maximum Stress (σ_{max})	1 MPa
Minimum Stress (σ_{min})	0 MPa
Stress State	Plane Stress

FAST-I is an older program that was created in the early 1980's when computer resources were not as abundant as in the present time. As a result, the program is capable of solving a model with a maximum wavefront of forty. This limitation restricts the model mesh size, thereby limiting the extent of a convergence study.

Due to this limitation, it was determined that the mesh size in the vicinity of the crack tip, for the given problem, prior to mesh refinement, had to be on the order of 10 mm by 10 mm. It was found that the best results were obtained by refining the mesh in the vicinity of the crack with a ratio of 1.25:10 as shown by Figure 5.3.

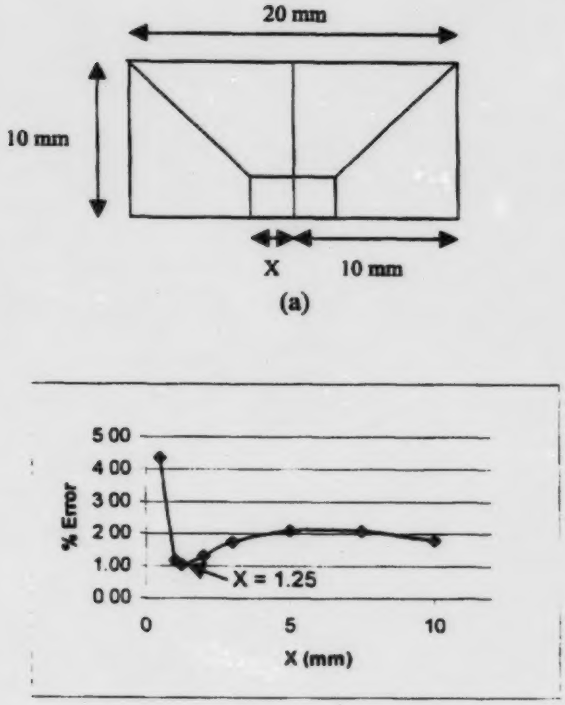

(b)

Figure 5.3 – (a) Mesh layout and (b) Accuracy of ΔK with respect to correct value

Further refinement of the mesh in the vicinity of the crack tip, resulted in either large margins of error (due to excessive distortion of the elements), or the wavefront exceeded the limit of forty which halted program execution.

The finite element program NISA is not limited by the number of elements; thus, the corresponding mesh can be made increasingly 'finer' until the solution has converged. It has been determined that all the methods (mentioned in the last section) can provide acceptable results by using the quarter node elements surrounding the crack tip.

The example problem was analyzed and the results for various mesh densities are presented in Table 5.2.

Table 5.2 – Comparison of fracture parameter evaluations

[illegible]	[illegible]	[illegible]	[illegible]	[illegible]	[illegible]
7	5.7474	5.9616	6.1852	-3.7	-7.6
40	5.7474	5.8071	5.5028	-1.0	4.3
316	5.7474	-	5.7496	-	0.0

Comparing the results for the 7 and 40 element models, the FAST-I results are consistently better. Both values overpredict the theoretical value and show a converging trend. On the other hand, the results for the ENDURE model overpredict and underpredict the theoretical value, respectively. For models with greater than approximately forty elements, the FAST-I program cannot execute. The NISA/ENDURE program is not limited by the number of elements and, therefor, converges at approximately 316 elements.

Table 5.3 compares the execution time between the two programs.

Table 5.3 – Comparison of execution time (in seconds)

[illegible]	[illegible]	[illegible]	[illegible]	[illegible]
7	4	25	29	2
40	6	70	76	5
316	13	450	463	-

It is evident that the required execution time for the FAST-I program is superior to that of NISA/ENDURE.

In summary, the results obtained from the FAST-I program are more accurate and require less computational effort compared to those of NISA/ENDURE. However, FAST-I is limited in the number of elements that it can accommodate, which may create problems in converging to the exact solution. Finally, FAST-I has no pre-processor and thus requires significant user effort for mesh creation.

5.3 Fatigue Life Evaluation

5.3.1 Introduction

The evaluation of the number of cycles required to propagate a crack from an initial to final value requires the solution of the governing differential equation. The general form of the equation is given by the relationship

$$\frac{da}{dN} = f(\Delta K, R) \tag{5.6}$$

and the number of cycles to propagate a crack from an initial to final crack length is obtained by integrating both sides as follows

$$N_{if} = \int_{N_i}^{N_f} dN = \int_{a_i}^{a_f} \frac{da}{f(\Delta K, R)} \tag{5.7}$$

The term $f(\Delta K, R)$ usually involves a complicated dependency upon the crack length, a, resulting in no closed form solution and must be solved by a numerical integration technique. This process requires knowledge of the empirically defined parameters and an input table of crack length versus stress intensity factor (a vs. ΔK). The table is obtained from either the finite element methods described in the previous sections or known empirical equations. For a through the thickness center-cracked plate, the empirical equation is given by the relationship

$$Y = \sqrt{\sec\left(\frac{\pi a}{W}\right)} \tag{5.8}$$

The complexity of the fatigue life evaluation program depends upon the options available; such as, type of loading descriptions, numerical solution techniques, built in stress intensity factor solutions and graphics. The fatigue programs FAST-II and ENDURE (fatigue module) will be discussed in the following sections.

5.3.2 FAST-II

The FAST-II program was developed at the Technical University of Nova Scotia (TUNS) in 1986 and calculates the fatigue life of a component based on the Paris, Walker and Forman fatigue crack growth models. The program requires an input file containing tabulated '*a* versus ΔK' data for the stress range of interest, which can be obtained from the FAST-I module. However, FAST-II is an independent program because the user has the option of creating the corresponding input file based on empirical equations or the results from other fracture parameter programs.

The program runs interactively asking the user to enter the name of the input file, the model's empirical parameters, the crack interval of concern and the model to be used. Depending upon the model chosen, a function is fitted through the points from the input table by either Newton's or the least-squares methods. Once the appropriate function is obtained, the fatigue crack growth model is numerically evaluated by an adaptive quadrature integration scheme. The program provides a table containing the total number of cycles for the crack interval as well as intermediate values.

5.3.3 ENDURE – Fatigue Module

The ENDURE fatigue module calculates the fatigue life of a component based on either the Paris, Walker, Forman, Collipriest or Elber fatigue crack growth models. The program also requires tabulated '*a* versus ΔK' data for a stress range of 1 MPa, which can be obtained from either the results of a fracture mechanics analysis, manually created using a known empirical solution or from the programs internal stress intensity factor functions (for certain crack geometries). In addition, an input file is required which provides information about the type of analysis to be performed, material data, crack data, location of stress intensity factor input file and location of the loading scenario file.

The numerical technique employed to solve the fatigue crack growth equations is unknown since the manual does not disclose its detail, and cannot be determined by examining the code since it is not in the public domain. The output from the fatigue analysis consists of five files that contain d*a*/dN versus crack length data, life versus crack length data, d*a*/dN versus ΔK data, applied load histroy data and load history from the rainflow counting method.

5.3.4 Quantitative Comparison of FAST-II and ENDURE

This section will compare the efficiency and accuracy of the two programs in question with respect to evaluating a component's fatigue life. The example that will be evaluated is Example Problem 11.4 from the book by Dowling (1993). It consists of a center-cracked plate of AISI 4340 steel with a width of 76 mm, thickness of 6 mm and a center crack total length of 2 mm. It is subjected to constant amplitude tension-tension loading of minimum and maximum load equal to 80 KN and 240 KN, respectively. The task is to predict the number of cycles to propagate the crack from an initial crack length of 1 mm to a final crack length of 15.8 mm. The Paris coefficients have been determined to be $C = 1.095 \times 10^{-9}$ mm/cycle and $m = 3.24$. The estimates for the required number of fatigue cycles are presented in Table 5.4.

Table 5.4 – Comparison of fatigue life predictions

[illegible]	[illegible]
Closed Form Integration	86200
Simpson Rule (Spreadsheet)	75500
1% Method (Spreadsheet)	75350
ENDURE - User Supplied Data	77830
ENDURE - Built in Function	77400
FAST-I	76239

Neglecting the closed form approximation, the various approaches provide a fatigue life estimate range of approximately 75000 to 78000 cycles which represents a difference of approximately four percent. Examining the above results, one may question the need for the fatigue programs because the spreadsheet solution produces similar results. The main difference between the two approaches is that the spreadsheet solution requires a known empirical geometric correction factor relationship; whereas, the fatigue programs obtain this relationship based on an empirical fit of the input '*a* versus ΔK' data. Therefore, for problems with an unknown geometric correction factor relationship, the spreadsheet method fails.

The time required to create the appropriate input data files and execute the fatigue programs are similar for simple constant amplitude loading scenarios. This is, however, the only loading scenario available with FAST-II; whereas, ENDURE is capable of deterministic and probabilistic load representation. The deterministic loads are either i) peak-valley or range-mean matrix type, ii) cumulative exceedence curves, and iii) sequential variable amplitude histories; whereas, the probabilistic load representation is described by the power spectral density statistical function.

In summary, both fatigue life prediction programs produce similar results, are simple to use and require similar amounts of effort for input file preparation and program execution. The main advantage of the ENDURE fatigue module is that it has certain internal geometric correction factors and has more capability with respect to load representation.

5.4 Constant Amplitude Loading Predictions

This section will use the previously discussed numerical methods to predict the fatigue life for the experimental results of specimens CAL 2 through CAL 6. This requires first determining the stress intensity fracture parameter for various crack lengths followed by evaluation of the fatigue crack propagation model. The results are presented and discussed in the next two sections.

5.4.1 Fracture Parameter Analysis

Prior to performing the fatigue life estimate, the stress intensity fracture parameters for various crack lengths must be determined. The programs FAST-I and ENDURE were discussed and it was shown that FAST-I is more efficient due to its element formulation and solution time, however, it is limited in handling large mesh sizes. In contrast, ENDURE is unlimited in mesh size and was shown to converge to the correct solution. The objective of this section is to determine the stress intensity factors for various crack lengths as accurately as possible. As a result, only the ENDURE program will be used during this analysis.

A numerical analysis was performed on a model with the material properties and dimensions shown in Table 5.1, which are the same as those expected for the experimental test specimens. The initial half crack length was to be equal to 10 mm and the specimens were calculated to fail by yielding at a crack length between 37.5 and 40 mm. Therefore, the stress intensity factors were to be evaluated for the crack length range of 5 to 42.5 mm to include the expected crack propagation range. It was determined from a preliminary analysis (to be discussed in the next section) that the NISA produced '*a* versus ΔK' values, used in the ENDURE fatigue module data file, gave excellent results for crack length increments of 2.5 mm. As a result, sixteen finite element models were constructed to accommodate sixteen different crack lengths, and the results are presented in Table 5.5. These value are compared to those obtained from the following analytical expression

$$\Delta K = \sqrt{\sec\left(\frac{\pi a}{W}\right)}\Delta\sigma\sqrt{\pi a} \tag{5.9}$$

Table 5.5 – '*a* versus ΔK' values obtained through NISA/ENDURE for the model described in Table 5.1

[illegible]	[illegible]	[illegible]	[illegible]
5.0	3.9880	3.9890	0.0
7.5	4.9225	4.9246	0.0
10.0	5.7474	5.7496	0.0
12.5	6.5196	6.5219	0.0
15.0	7.2724	7.2745	0.0
17.5	8.0299	8.0314	0.0
20.0	8.8127	8.8138	0 0
22.5	9.6415	9.6432	0.0
25.0	10 5391	10.5437	0.0
27 5	11.5337	11.5451	-0.1
30 0	12.6627	12.6872	-0.2
32.5	13.9789	14.0263	-0.3
35.0	15.5627	15.6484	-0.6
37.5	17.5457	17.6922	-0.8
40.0	20.1657	20.4103	-1.2
42.5	23.9154	24 3209	-1.7

Note: ΔK evaluated for stress range of 1 MPa, W = 100 mm and B = 5.35 mm.

The mesh had 316 elements conforming to the convergence study discussed in Section 5.2.4. The numerical results are within 2% error of the values determined by Equation 5.9. The geometric correction factor defined by Equation 5.8 is an approximate expression that is within 2% of the exact answer, for values of '2a/W' less than 0.90. Due to this error, it was decided that further refinement of the mesh for the larger crack lengths, to reduce the error, would be unjustified since the values that they are compared to have the same order of error. The 'ΔK versus a' graphs for Equation 5.9 and the ENDURE results are illustrated in Figure 5.4.

The model studied above differs slightly in its length, width and thickness from those of the actual experimental test specimens shown in Appendix A. To precisely model the experimental test specimens, one would have to modify the previous model 80 times (5

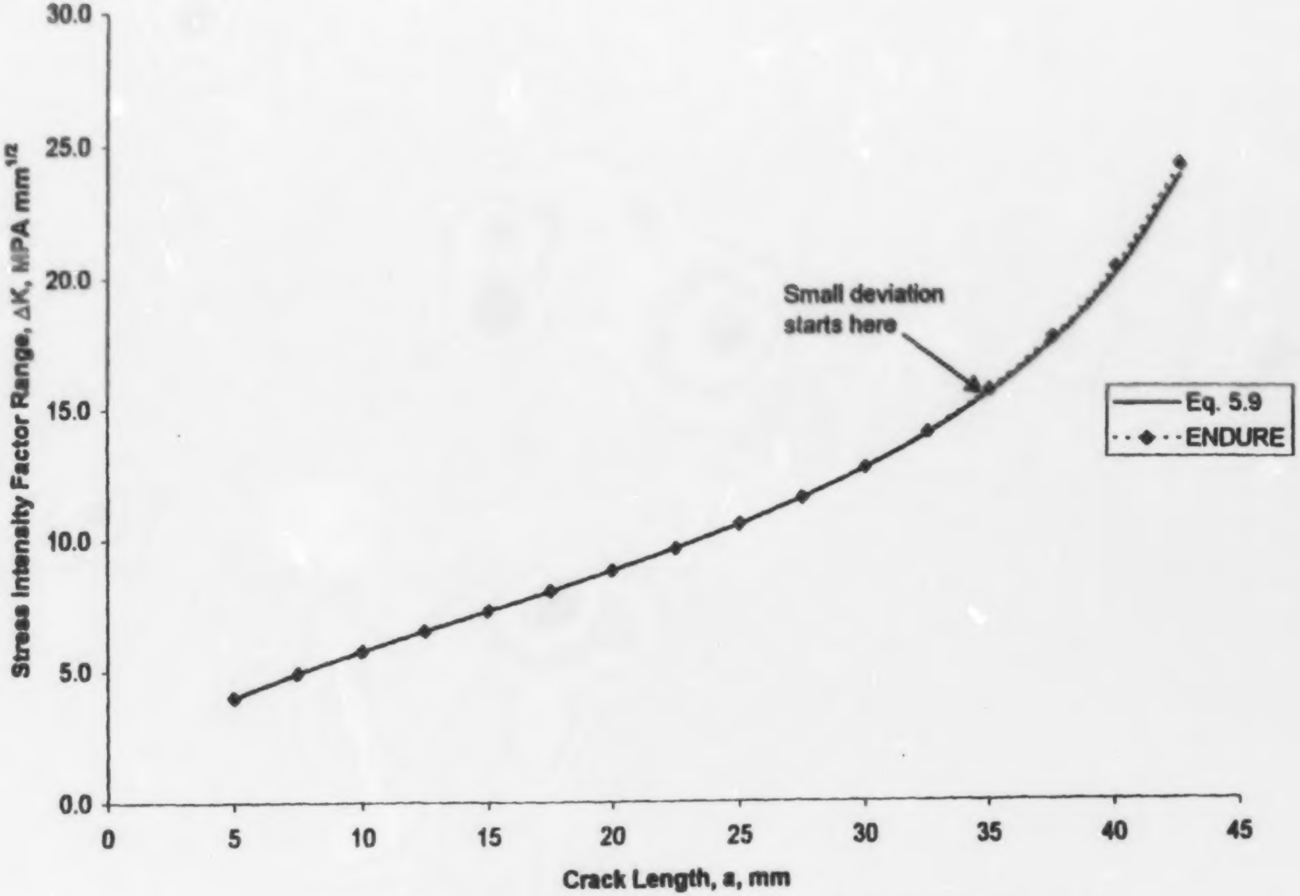

Figure 5.4 - Comparison of 'ΔK versus a' values calculated by ENDURE and Equation 5.9

specimens times 16 models per specimen). This would require approximately 50 hours (80 specimens * {30 min/specimen to remodel + 463 s/model to execute}). Therefore, a parametric study was conducted to determine the influence of the change of length, width and thickness of the plates. The results will indicate whether one needs to conduct a new set of analysis, or use the model constructed earlier.

For this situation with a through the thickness center cracked plate, the ratio of stress intensity factor ranges for a 'current' to 'old' specimen for the same crack length, *a*, based on Equation 5.9 is

$$\frac{\Delta K_{current}}{\Delta K_{old}} = \frac{\sqrt{\sec\frac{\pi a}{W_{current}}} * \Delta\sigma_{current}\sqrt{\pi a}}{\sqrt{\sec\frac{\pi a}{W_{old}}} * \Delta\sigma_{old}\sqrt{\pi a}} \tag{5.10}$$

Equation 5.10 indicates that the length and thickness of a specimen has no influence on the value of the stress intensity factor. This was also verified numerically by changing the length of the model from 300 mm to 299.72 mm and its thickness from 5.35 mm to 5.07 mm, to correspond with those of specimen number CAL 6. The calculated stress intensity factor was equal to 5.7496 MPa mm$^{1/2}$, which is identical to the values shown in Table 5.5. It is therefore concluded that the small differences in length and thickness have no effect on the calculation of the stress intensity factor.

The remaining parameter that is different between the 'old model' and the experimental test specimens is the width. According to Equation 5.10, the width will have an effect on the stress intensity factor equal to the ratio of the geometric correction factors. To verify this relationship, the 'original model' for crack lengths of 10 and 35 mm was remodeled according to the dimensions of specimen number CAL 6 (has biggest change in width) shown in Appendix A. The results are shown in Table 5.6.

Table 5.6 – Numerical verification of width influence

[redacted]	[redacted]	[redacted]	[redacted]	[redacted]	[redacted]
10	5.7496	5.7447	5.7448	0.1	0.0
35	15.6484	15.3687	15.3660	1.8	0.0

Note: Stress range of 1 MPa was used

The results from Table 5.6 confirms that the difference in specimen width can be accounted for by multiplying the stress intensity factor by the ratio of the 'current' to 'old' geometric correction factors as shown by Equation 5.10. If this provision is not followed, the error between a model of width 100 and 101.74 mm is small for the shorter crack length but becomes more significant for the larger crack lengths.

As a result of the above investigation, the difference in width is the only significant factor affecting the value of the stress intensity factor range between the 'old model' and the experimental test specimens. Therefore, instead of spending unnecessary effort (approximately 50 hours in this case) to remodel the test specimens to determine their stress intensity factor values, the results from the 'old model' will be multiplied by the corresponding geometry correction factor ratio. This process is admissible as long as the empirical geometry correction factor equation is known. Otherwise, the above method could not be applied and the geometry would have to be remodeled.

Using the above procedure, the 'a versus ΔK' relationship calculated by ENDURE (Table 5.5 values multiplied by the geometry correction factor ratio) are presented in Table 5.7.

Table 5.7 – Numerically obtained '*a* versus ΔK' relationship for experimental test specimens

5.0	3.9888	3.9888	3.9888	3.9889	3.9882
7.5	4.9238	4.9238	4.9238	4.9240	4.9222
10.0	5.7479	5.7481	5.7479	5.7485	5.7447
12.5	6.5188	6.5191	6.5188	6.5198	6.5129
15.0	7.2693	7.2698	7.2693	7.2711	7.2598
17.5	8.0234	8.0242	8.0234	8.0260	8.0085
20.0	8.8018	8.8030	8.8018	8.8058	8.7798
22.5	9.6260	9.6277	9.6260	9.6317	9.5942
25.0	10.5191	10.5216	10.5191	10.5273	10.4741
27.5	11.5105	11.5139	11.5105	11.5219	11.4471
30.0	12.6385	12.6433	12.6385	12.6545	12.5495
32.5	13.9572	13.9640	13.9572	13.9800	13.8316
35.0	15.5488	15.5586	15.5488	15.5816	15.3687
37.5	17.5443	17.5588	17.5443	17.5929	17.2787
40.0	20.1792	20.2018	20.1792	20.2550	19.7692
42.5	23.9277	23.9659	23.9277	24.0560	23.2436

Note: Based on a stress range of 1 MPa

The above results are graphically compared to those obtained from Equation 5.9 and those for the 'original model' with a width of 100 mm in Figures 5.5 through 5.9. These figures illustrate that the stress intensity factors for various crack lengths are accurately determined by the numerical package NISA/ENDURE. The results of Table 5.7 will now be used in conjunction with the fatigue programs ENDURE and FAST-II, to predict the fatigue life for each of the constant amplitude specimens.

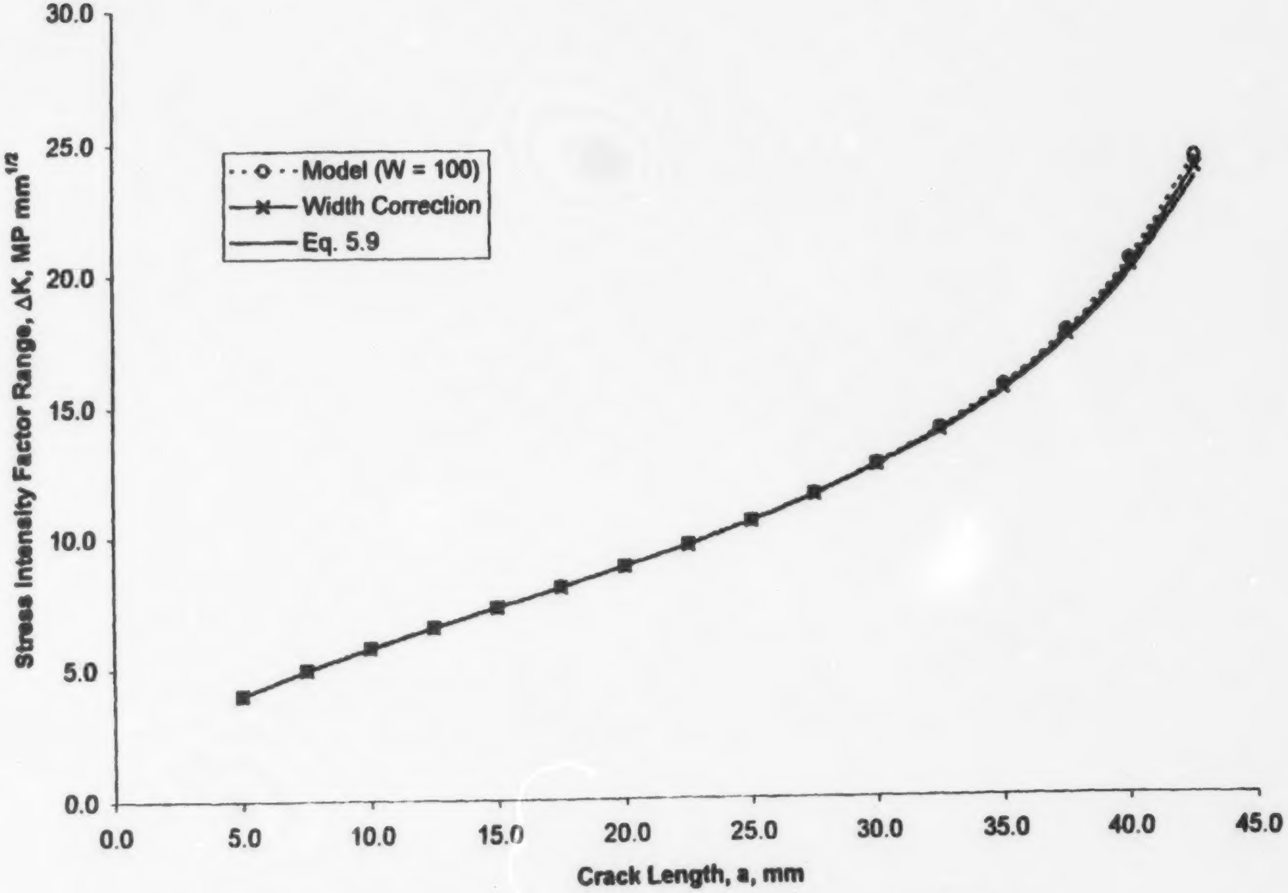

Figure 5.5 - Comparison of 'ΔK versus a' values for specimen CAL 2

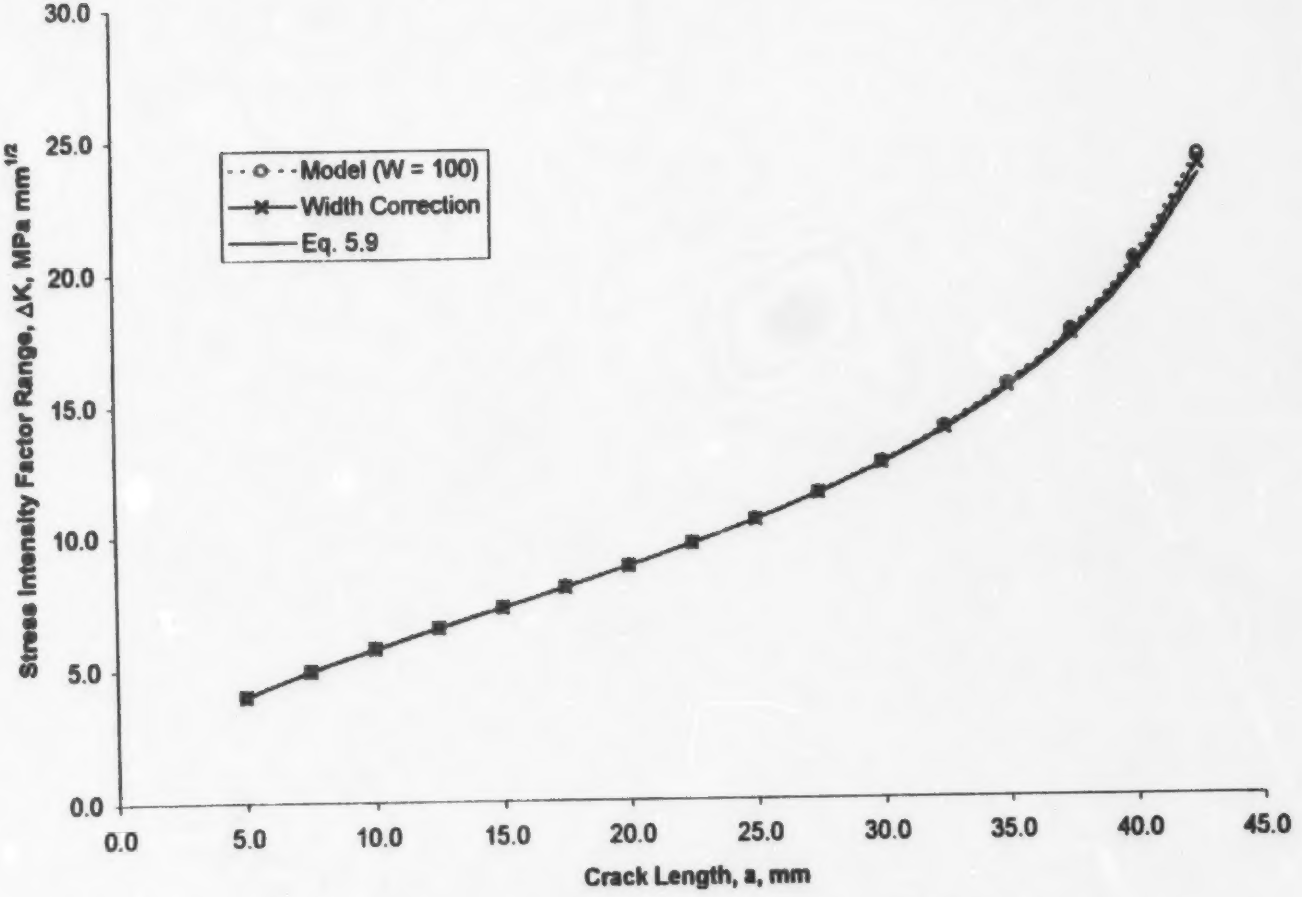

Figure 5.6 - Comparison of 'ΔK versus a' values for specimen CAL 3

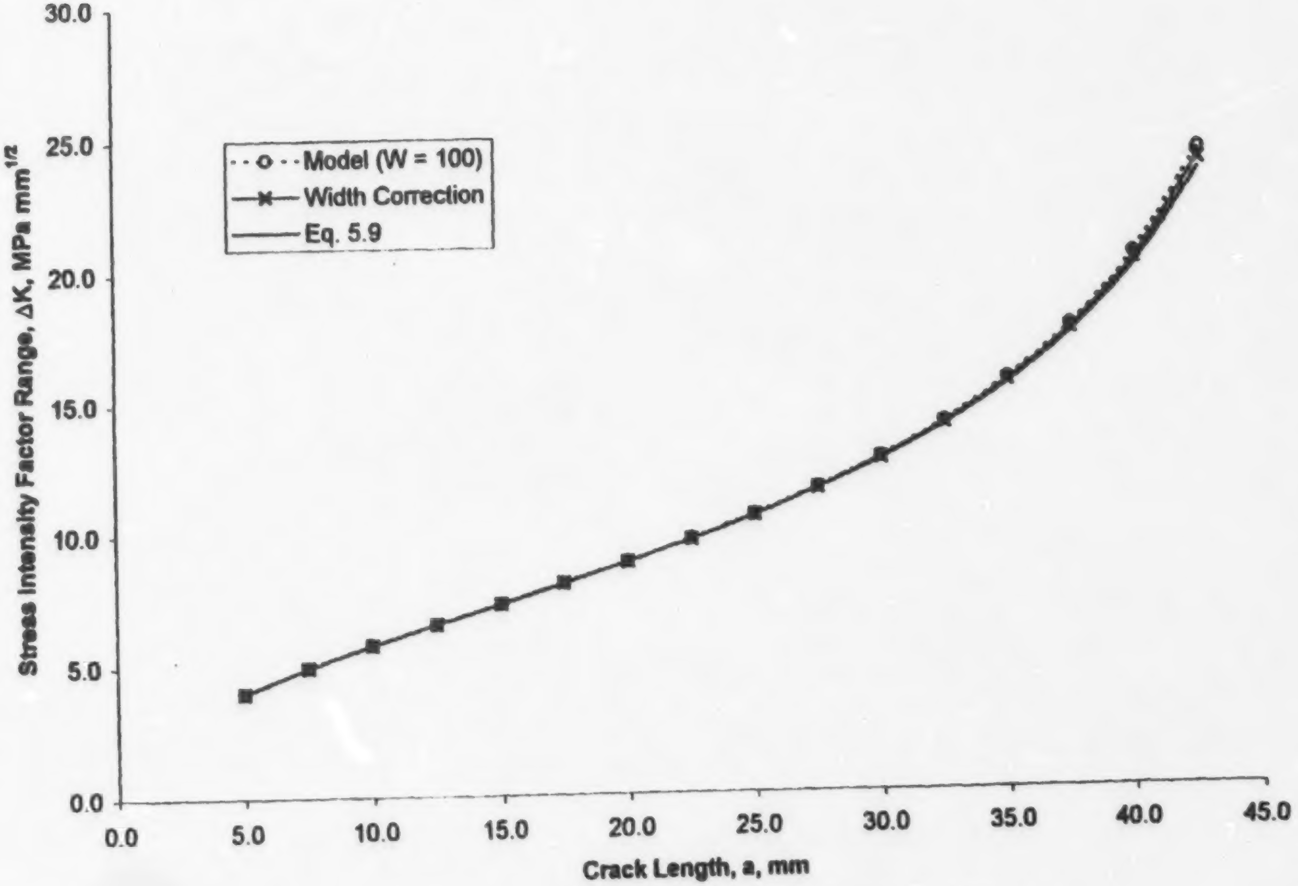

Figure 5.7- Comparison of 'ΔK versus a' values for specimen CAL 4

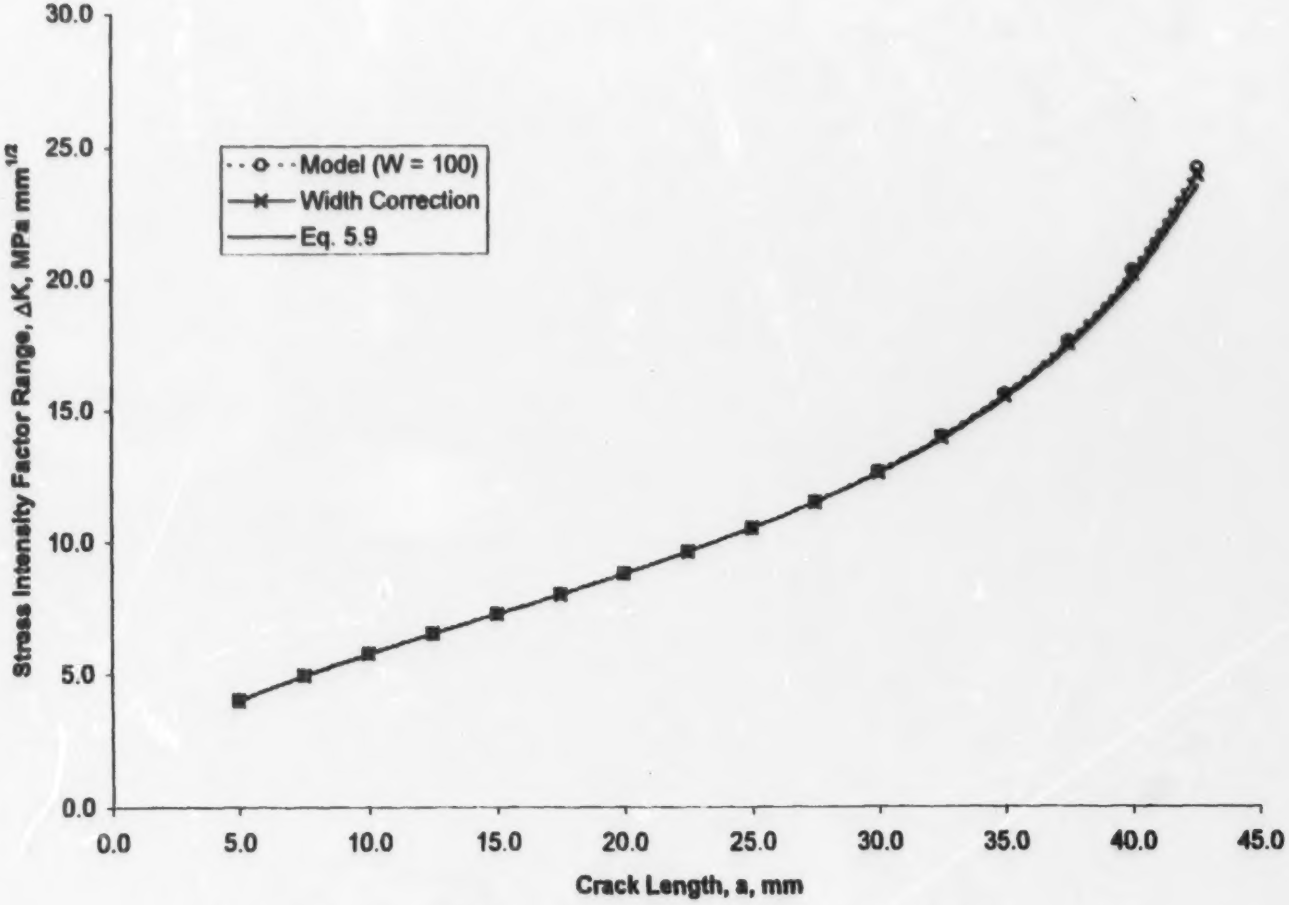

Figure 5.8 - Comparison of 'ΔK versus a' values for specimen CAL 5

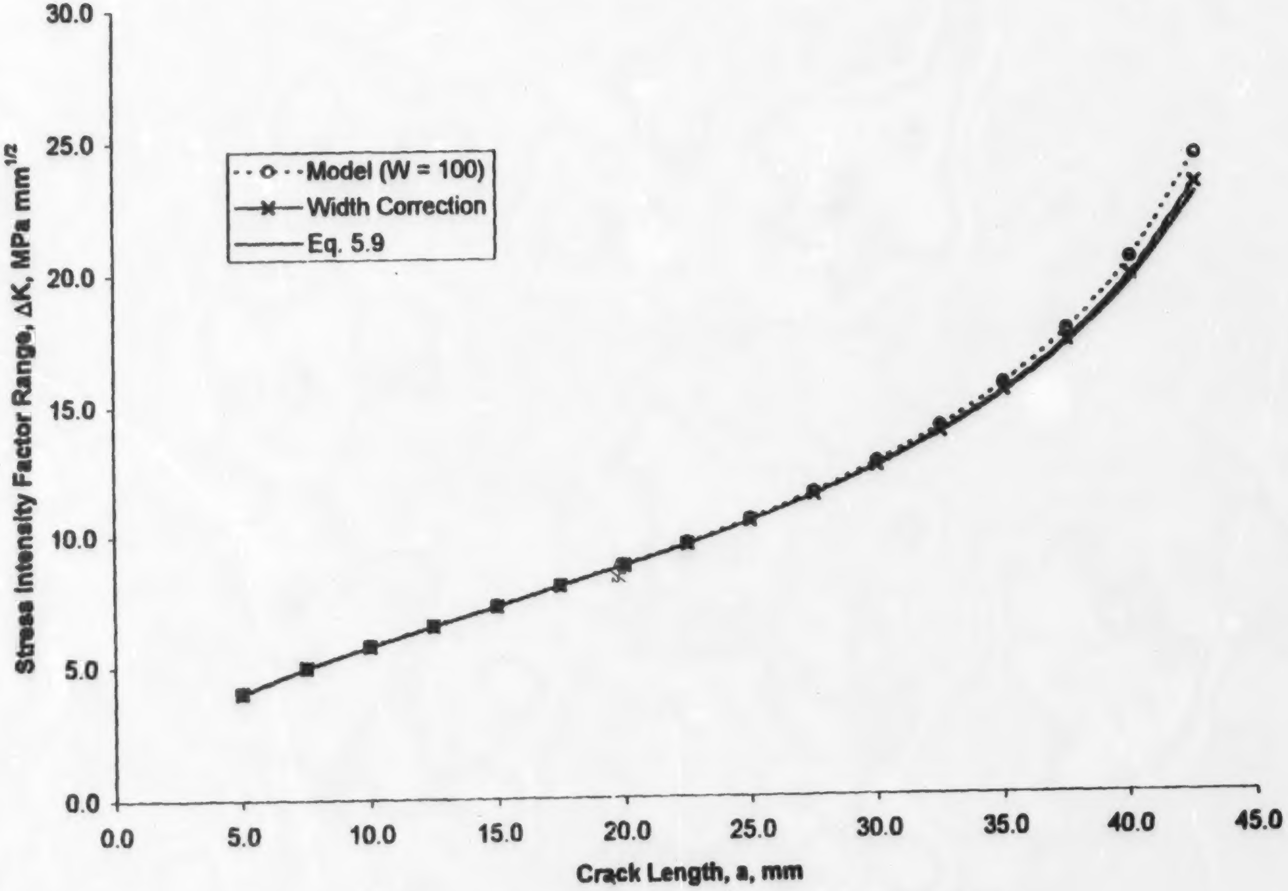

Figure 5.9 - Comparison of 'ΔK versus a' values for specimen CAL 6

5.4.2 Fatigue Life Analysis

The results of the previous section will be used to predict the fatigue life for the constant amplitude loading specimens for a crack length a_i to a_f reported in Table 4.1. The ENDURE program has the option of using a user specified '*a* versus ΔK' input data file or various internal '*a* versus ΔK' relationships for common crack configurations and geometry. The through-the-thickness center-cracked specimen is available as an internal option and only requires the specimens width. Both methods will be used in this fatigue analysis and their results will be compared.

Prior to the numerical fracture parameter evaluation, it was determined that the '*a* versus ΔK' input data file gave excellent results for crack length increments of 2.5 mm. This was established by analyzing an example problem and comparing the ENDURE 'curve fit' results to the known available analytical solution. The problem examined consisted of a finite element model of a center cracked plate with width of 100 mm, thickness of 5.35 mm and $\Delta\sigma = 1$ MPa. The problem was analyzed with user supplied input files obtained from Equation 5.9 for various crack length increments as well as the internal option. Figure 5.10 compares the curve defined by Equation 5.9 to the 'ΔK versus a' curve fit obtained by ENDURE.

The curves are referenced according to the crack length interval spacing between the values used in the ENDURE input data file, always starting with 5 mm. That is, the 20 mm and 10 mm curves are based on data input values for crack length 5, 25, 45 mm and 5, 15, 25, 35, 45 mm, respectively. From the graph, it is shown that for the curves corresponding to crack increments of 1.0 and 2.5 mm produce results very similar to those obtained by Equation 5.9. As a result, the fracture parameters were determined for crack intervals of 2.5 mm in the previous section because this is sufficient data for ENDURE to obtain an accurate 'ΔK versus a' relationship to be used in the fatigue analysis.

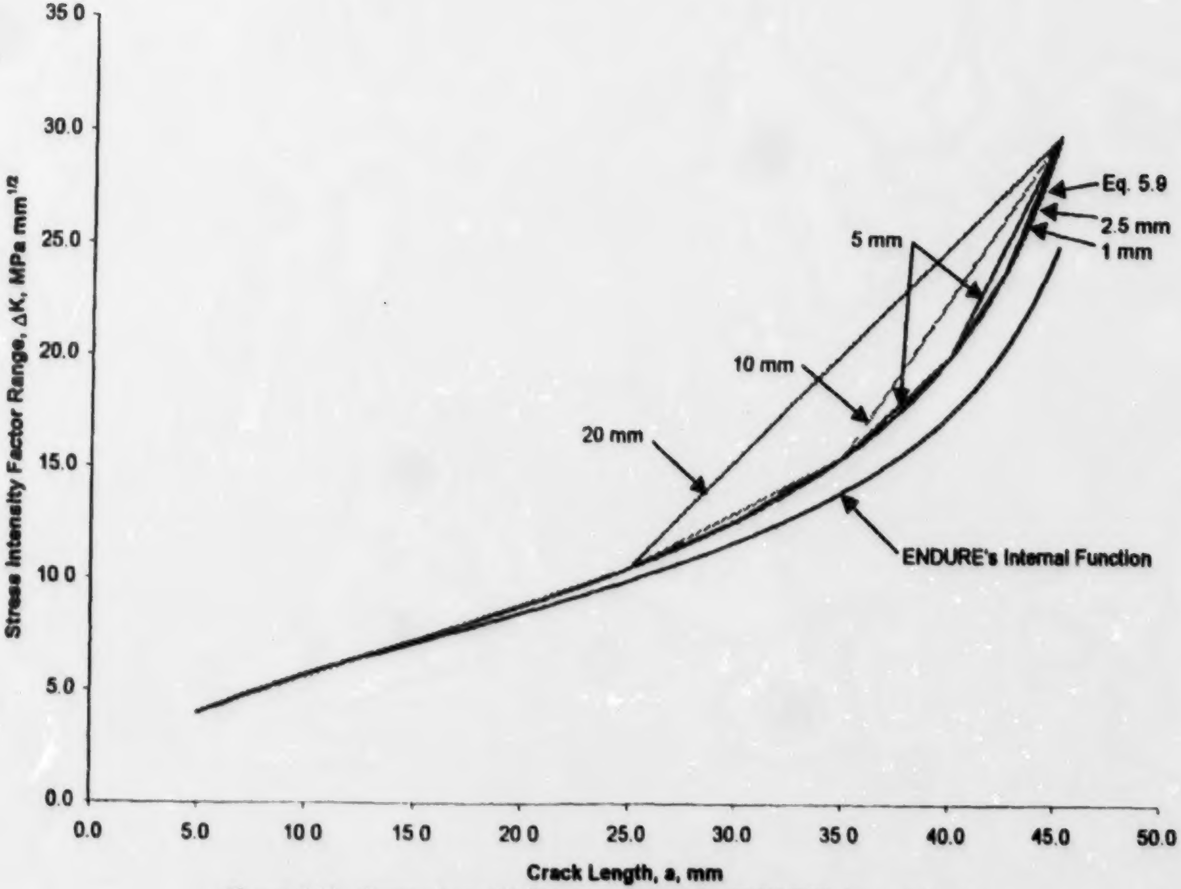

Figure 5.10 - Comparison of 'ΔK versus a' curves for ENDURE's internal function, user supplied data input file and Equation 5.9

Figure 5.10 illustrates that the internal function significantly underestimates the behavior defined by Equation 5.9. No apparent reason is provided in ENDURE's manual for such a difference and it will be shown later in this section that this 'option' does not correctly predict the experimental fatigue results. As a result, it is concluded that an error exists within the fatigue program ENDURE which illustrates the vulnerability of blindly using computer programs without first validating their solutions against known answers. This conclusion is supported by the fact that the ENDURE fracture parameter module predicts results that converge to those of Equation 5.9.

The fatigue life predictions by ENDURE are tabulated in Table 5.8. The results are compared with those obtained from experiments as shown by Table 5.9.

Table 5.8 – ENDURE fatigue life predictions using one and two curve Paris model

[illegible]	[illegible]	[illegible]	[illegible]	[illegible]	[illegible]
CAL 2	165000	161200	164730	178600	181950
CAL 3	147500	144600	145130	159100	159070
CAL 4	189000	189100	186680	209500	206650
CAL 5	275000	271900	272910	300500	285990
CAL 6	186000	184000	183700	210100	211580

Note: Evaluated for crack length interval a_i to a_f shown in Table 4.1

Table 5.9 – Percent error of ENDURE fatigue life predictions using one and two curve Paris models

[illegible]	[illegible]	[illegible]	[illegible]	[illegible]	[illegible]
CAL 2	165000	2.3	0.2	-8.2	-10.3
CAL 3	147500	2.0	1.6	-7.9	-7.8
CAL 4	189000	-0.1	1.2	-10.8	-9.3
CAL 5	275000	1.1	0.8	-9.3	-4.0
CAL 6	186000	1.1	1.2	-13.0	-13.8

The results for the user supplied data input file with values for every 2.5 mm crack length interval are in good agreement with the experimental results. Furthermore, the results for the two curve Paris model are slightly more consistent and accurate than those of the one curve Paris model. The results for the internal option are not accurate due to the 'ΔK versus a' relationship that was used (Figure 5.11).

Comparing the numerical one and two curve parameter model to those obtained by the 1% method spreadsheet solution (Table 4.3 and 4.4), indicates that the spreadsheet predictions are slightly more accurate. This is expected since the spreadsheet results are based on the empirical stress intensity relationship defined by Equation 5.9; whereas, the ENDURE results are based on a curve fit of numerically obtained fracture parameters. Also, different numerical solution techniques are used to evaluate the appropriate fatigue crack growth model.

The fatigue life predictions for FAST-II are presented in Table 5.10.

Table 5.10 – FAST-II fatigue life predictions (2.5 mm crack length intervals)

[illegible]	[illegible]	[illegible]	[illegible]	[illegible]	[illegible]
CAL 2	165000	157865	156766	4.3	5.0
CAL 3	147500	141128	141511	4.3	4.1
CAL 4	189000	185903	184060	1.6	2.6
CAL 5	275000	266062	265836	3.3	3.3
CAL 6	186000	181049	180685	2.7	2.9

The '*a* versus ΔK' input data file supplied to FAST-II were the same values that were used by the ENDURE program. The results are acceptable (within 5%) but not as accurate as those obtained from ENDURE. Re-evaluating the fatigue life with an '*a* versus ΔK' input data file with crack length interval of 1.0 mm (based on Eq. 5.9) provides the results shown in Figure 5.11.

Table 5.11 – FAST-II fatigue life predictions (1.0 mm crack length intervals)

[illegible]	[illegible]	[illegible]	[illegible]
CAL 2	165000	164054	0.6
CAL 3	147500	145943	1.1
CAL 4	189000	193731	-2.5
CAL 5	275000	276289	-0.5
CAL 6	186000	184287	0.9

The results from Table 5.11 are more accurate and bear margins of error as those predicted by ENDURE; however, for an accurate prediction of fatigue life the '*a* versus ΔK' input data file must contain more data points than that produced by ENDURE. From this, it can be concluded that the combination of the 'ΔK versus a' curve fit subroutine and numerical solution of the governing differential equation for ENDURE is more efficient than that of FAST-II. Therefore, the major advantage of ENDURE is that it requires less stress intensity factor values.

The above fatigue analysis was conducted only for the Paris model. The other models available in the two fatigue programs include Walker, Forman, and in ENDURE only, the Elber and Collipriest models. The appropriate parameters for these models were not available and thus the models were not evaluated in this section.

5.5 Variable Amplitude Loading Predictions

The fatigue life for the variable amplitude loaded specimens were predicted by using a constant amplitude model discussed in Section 4.6.1 and the results were presented in Table 4.11. The predictions were unacceptable and the amount of error depended upon the overload ratio and number of overloads applied. Other models that consider the retardation effect were evaluated in Chapter 4 and found to give better results than the constant amplitude models.

The fatigue life prediction programs are limited to the Paris, Walker, Forman, Collipriest or Elber models, which are all formulated for constant amplitude loading scenarios. The use of these constant amplitude models would provide inadequate results, similar to Section 4.6.1.

As a result, the programs will have to be modified to include models capable of predicting the fatigue life subjected to variable amplitude loading. ENDURE is not a public domain code and thus it cannot be modified; whereas, the FAST-II code is available to us, and can be modified to include additional models.

5.6 Summary of Numerical Prediction Methods

The FAST-I and ENDURE fracture parameter programs use the finite element method to model the specimens crack geometry and configuration to evaluate the stress intensity factor. These results are used by the FAST-II and ENDURE fatigue programs, in conjunction with pre-programmed fatigue models, to evaluate the specimen's fatigue life.

It was shown that for the same mesh size and layout, the FAST-I program determines the fracture parameters more accurately and in the least amount of time. However, it is limited by the number of elements that can by used in a model and as a result would not converge to the correct solution. ENDURE is not limited by the number of elements that can be used and thus the mesh size can be made small enough to converge to the correct solution. For this reason, ENDURE was used to obtain the '*a* versus ΔK' values, which were to be used in the fatigue life analysis.

It was determined that the ENDURE fatigue program could accurately predict the required 'ΔK versus a' relationship if the fracture parameters are provided in the input table for crack length increments of 2.5 mm. The fatigue life predictions from FAST-II for the same values are good, but not as accurate as those from ENDURE. It was shown that if the FAST-II input data file contains the stress intensity factor at crack intervals of 1.0 mm, the resulting fatigue predictions are just as accurate as those of ENDURE.

Finally, it was discussed that the numerical programs are unable to accurately predict the fatigue life for constant amplitude loading scenarios with interspersed single tensile overloads. This is due to the fact that the programs contain constant amplitude loading models that were shown in Section 4.6.1 to be inadequate. As a result, models capable of accounting for the retardation effect should be implemented in the fatigue programs; thus, extending their capabilities.

Chapter 6

Conclusions and Recommendations

6.1 Conclusions

Numerous constant and variable amplitude fatigue crack growth models are available that vary significantly in the approach taken, number of required calibration parameters, complexity and time required to perform a fatigue analysis. The most promising and commonly used models were discussed with regards to their advantages, disadvantages and limitations with application to various structures. Despite the numerous fatigue models available, no all-encompassing universally accepted model exists. An experimental fatigue program was performed on a center crack specimen configuration (350WT steel) for both constant and variable amplitude loading scenarios. The following conclusions are made based on the findings of this report.

1. The constant amplitude loading data indicated that this material is quite sensitive to the loading stress ratio. The variable amplitude loading data indicated that following a tensile overload, the crack growth rate is retarded by a significant amount.

2. The amount of retardation is reduced if a compressive underload immediately follows the tensile overload.

3. A two curve Paris model was calibrated for the individual stress ratios and was determined to provide excellent results for the constant amplitude loaded specimens. The one curve Paris model gave reasonable results, but not as good as the two curve model. The Paris model required the calibration of two parameters that must be obtained by experimentation or from established databases.

4. A tensile fatigue crack growth model proposed by Zheng was evaluated and shown to reasonably predict the experimental specimen's fatigue life. The model only requires a simple tensile test to be performed and knowledge of the threshold values.

5. The periodically applied single tensile overload interspersed in a constant amplitude loading scenario resulted in crack growth retardation by an amount dependant upon the number and magnitude of the applied overloads. It was shown that the constant amplitude loading models were inadequate to predict the fatigue life of the specimens subjected to this loading scenario. As a result, various models, which consider the retardation effect during their analysis, were evaluated. A new model, referred to as the 'delay model' was proposed. It was determined that the proposed model, which was based on predicting the amount of retardation after an overload, gave the best results and appears promising.

6. It was determined that the finite element fracture mechanics programs, FAST-I and NISA/ENDURE are capable of predicting the fracture parameters for various crack lengths effectively and accurately. FAST-I was found to be a more efficient program due to its type of higher order elements; however, it cannot accommodate large number of elements in its present format. This restricts the mesh size and thus accuracy.

7. The FAST-II and ENDURE fatigue life evaluation programs provide accurate results for the constant amplitude loaded specimens. However, the programs are limited to constant amplitude models and thus were not capable of accurately predicting the fatigue life for the variable amplitude loaded specimens.

6.2 Recommendations

The experimental program in this thesis was the beginning stage of a systematic investigation into fatigue crack propagation subjected to various loading scenarios. This stage dealt with constant amplitude loading as well as examining tensile overloads. Further investigation should be undertaken to include:

a. Stress intensity threshold value testing (a parameter required for the Zheng model)
b. Single tensile/compressive and compressive/tensile overloads
c. Multiple tensile/tensile, tensile/compressive and compressive/tensile overloads
d. A structures in-service (realistic) loading scenario and
e. Further testing to verify the 'delay model' predictions described in Section 4.6.2 to include the above loading scenarios and varying $\Delta K_{baseline}$ values.

As mentioned, both of the fatigue life evaluation programs, FAST-II and ENDURE, were capable of predicting fatigue life for the constant amplitude specimens but not those for the variable amplitude specimens. The reason is that both programs have no models that are capable of predicting crack growth retardation. The source code for the ENDURE programs is unavailable; whereas, the code for the FAST programs is available. As a result, it is recommended that the following be implemented into the FAST suite of programs.

a. Create a user friendly, interactive processor for FAST-I
b. Improve the post-processing capability of FAST-I
c. Create pre-meshed modules to automatically model commonly used crack configurations and geometry with only a few commands.
d. Increase the capability of FAST-I so that it can handle larger number of elements. This will allow models with finer mesh sizes to be used and thus more accurate solutions can be obtained.
e. Include fatigue crack propagation models within FAST-II that are capable of predicting fatigue life for variable amplitude loading scenarios.

REFERENCES

1. Ahn, Suneung and Max B. Mendel, "A Fatigue Life Model For Crack Propagation Under Variable-Amplitude Load," *Mechanics Research Communications*, Vol. 22, No. 1, pp. 95-101, 1995.

2. Anderson, T.L., Fracture Mechanics: Fundamentals and Applications, Second Edition, CPR Press Inc., Florida, 1995.

3. Barsom, J.M., "Fatigue Crack Growth Under Variable-Amplitude Loading in Various Bridge Steels," *Fatigue Crack Growth Under Spectrum Loads*, ASTM STP 595, American Society for Testing and Materials, 1976, pp. 217-235.

4. Barsom, John M. and Stanley T. Rolfe, Fracture and Fatigue Control in Structures: Applications of Fracture Mechanics, Second Edition, Prentice-Hall Inc., Englewood Cliffs, New Jersey, 1987.

5. Broek, David, The Practical Use of Fracture Mechanics, Kluwer Academic Publishers, Netherlands, 1991.

6. Chang, J.B., "Round-Robin Crack Growth Predictions on Center-Cracked Tension Specimens under Random Spectrum Loading," *Methods and Models for Predicting Fatigue Crack Growth under Random Loading*, ASTM STP 748, J. B. Chang and C.M. Hudson, Eds., American Society for Testing and Materials, 1981a, pp. 3-40.

7. Chang, J.B., Szamossi, M., and Liu, K-W., "Random Spectrum Fatigue Crack Life Predictions With or Without Considering Load Interactions," *Methods and Models for Predicting Fatigue Crack Growth under Random Loading*, ASTM STP 748, J. B. Chang and C.M. Hudson, Eds., American Society for Testing and Materials, 1981b, pp. 115-132.

8. Chell, G. G., *Developments in Fracture Mechanics – 1*, Applied Science Publishers Ltd., London, 1979.

9. Close, C.M. Ward, Blom, A.F. and Ritchie, R.O., "Mechanisms Associated with Transient Fatigue Crack Growth Under Variable-Amplitude Loading: An Experimental and Numerical Study," *Engineering Fracture Mechanics*, Vol. 32, No. 4, pp. 613-638, Great Britain, 1989.

10. Collins, Jack A., Failure of Materials in Mechanical Design: Analysis, Prediction, Prevention, Second Edition, John Wiley & Sons, New York, 1993.

11. Collipriest, J. E. Jr., "An Experimentalist's View of the Surface Flaw Problem", *Physical Problems and Computational Solutions*, J. L. Swedlow, Ed., American Society of Mechanical Engineers, New York, 1972, pp. 43-62.

12. Dowling, Norman E., Mechanical Behavior of Materials: Engineering Methods for Deformation, Fracture, and Fatigue, Prentice Hall, Englewood Cliffs, New Jersey, 1993.

13. Elber, Wolf, "The Significance of Fatigue Crack Closure," *Damage Tolerance in Aircraft Structures*, ASTM STP 486, American Society for Testing and Materials, 1971, pp. 230-242.

14. Endure User's Manual, Engineering Mechanics Research Corporation, Version 6.0, Michigan, 1995.

15. Fleet Technology Limited, *Tensile Properties of CPF Hull Stuctural Materials*, Draft Final Report (Part I), Kanata, Ontario, 1997.

16. Frost, N.E., Pook, L. P. and Denton, K., "A Fracture Mechanics Analysis of Fatigue Crack Growth Data for Various Materials," *Engineering Fracture Mechanics*, 1971, Vol. 3, 109-126.

17. Fuchs, H. O. and R. I. Stephens, Metal Fatigue in Engineering, John Wiley & Sons, New York, 1980.

18. Goel, H.S. and Chand, Satish, "A Fatigue Crack Growth Model for Single Overload Tests," *Transactions of the ASME*, Vol. 116, pp. 168-172, 1994.

19. Gibson, Ronald F., Principles of composite Material Mechanics, McGraw-Hill Inc., New York, 1994.

20. Gifford, L. Nash and Hilton, Peter D., Preliminary Documentation of PAPST Nonlinear Fracture and Stress Analysis By Finite Elements, David W. Taylor Naval Ship Research and Development Center, Bethesda, Maryland, 1981.

21. Hartman, A., and Schijve, J., "The Effects of Environment and Load Frequency on the Crack Propagation law for Macro Fatigue Crack Growth in Aluminum Alloys," *Engineering Fracture Mechanics*, 1970, p. 615.

22. Hudson, C. M., "A Root-Mean-Square Approach for Predicting Fatigue Crack Growth under Random Loading," *Methods and Models for Predicting Fatigue Crack Growth under Random Loading*, ASTM STP 748, J. B. Chang and C.M. Hudson, Eds., American Society for Testing and Materials, 1981, pp. 41-52.

23. Imhof, E. J. and Barsom, J. M., "Fatigue and Corrosion Fatigue Growth of 4340 Steel at Various Yield Strengths," *Progress in Flaw Growth and Fracture Toughness Testing*, ASTM STP 536, American Society for Testing and Materials, 1973, pp. 182-205.

24. Johnson, W. S., "Multi-Parameter Yield Zone Model for Predicting Spectrum Crack Growth," *Methods and Models for Predicting Fatigue Crack Growth under Random Loading*, ASTM STP 748, J. B. Chang and C.M. Hudson, Eds., American Society for Testing and Materials, 1981, pp. 85-102.

25. Kulak, G.L., P.F. Adams and M.I. Gilmor, Limit States Design in Structural Steel, Fifth Edition, Canadian Institute of Steel Construction, Universal Offset Limited, Ontario, 1993.

26. Lal, D. N. and V. Weiss, "A Notch Analysis of Fracture Approach to Fatigue Crack Propagation," *Metallurgical Transactions*, Volume 9A, March 1978, pp. 413-425.

27. Matthews, F.L. and R.D. Rawlings, Composite Materials: Engineering and Science, Chapman & Hall, London, 1994.

28. McEvily, A. J., "Phenomenological and Microstructural Aspects of Fatigue," presented at the Third International Conference on the Strength of Metals and Alloys, 1973, Cambridge, England; published by The Institute and The Iron and Steel Institutes, Publication No. 36, Vol. W, 1974, p. 204-213.

29. Miller, M. S. and Gallagher, J. P., "An Analysis of Several Fatigue Crack Growth Rate (FCGR) Descriptions," *Fatigue Crack Growth Measurement and Data Analysis*, ASTM STP 738, S. J. Hudak, Jr. and R. J. Bucci, Eds., American Society for Testing and Materials, 1981, pp. 205-251.

30. Mufti, A.A., Zamani, N.G. and Russell, L.T., Fatigue Analysis of Structures, Final Report, Technical University of Nova Scotia, 1985.

31. Newman, J. C., Jr., "A Crack-Closure Model for Predicting Fatigue Crack Growth under Aircraft Spectrum Loading," *Methods and Models for Predicting Fatigue Crack Growth under Random Loading*, ASTM STP 748, J. B. Chang and C.M. Hudson, Eds., American Society for Testing and Materials, 1981, pp. 53-84.

32. Paris, P.C. and Erdogan, F., "A Critical Analysis of Crack Propagation Laws," *Journal of Basic Engineering; Transactions,* American Society of Mechanical Engineers, Series D, Vol. 85, Dec. 1963, pp. 528-534.

33. Rice, Richard C., Fatigue Design Handbook, Second Edition, Society of Automotive Engineers, PA, 1988.

34. Rudd, J. L. and Engle, R. M., Jr., "Crack Growth Behavior of Center-Cracked Panels under Random Spectrum Loading," *Methods and Models for Predicting Fatigue Crack Growth under Random Loading*, ASTM STP 748, J. B. Chang and C. M. Hudson, Eds., American Society for Testing and Materials, 1981, pp. 103-114.

35. Shank, M.E., "A Critical Review of Brittle Failure in Carbon Plate Steel Structures Other than Ships." Ship Structure Committee Report SSC-65, National Academy of Science National Research Council, Washington, DC, December, 1953.

36. Wang, Wei and Cheng-Tzu Thomas Hsu, "Fatigue Crack Growth Rate of Metal by Plastic Energy Damage Accumulation Theory," *Journal of Engineering Mechanics*, Vol. 120, No. 4, April 1994, pp. 776-795.

37. Wei, R.P. and Shih, T.T., "Delay in Fatigue Crack Growth," *International Journal of Fracture*, Vol 10, pp. 77-85, 1974.

38. Wheeler, O. E., "Spectrum Loading and Crack Growth," *Journal of Basic Engineering*, March 1972, pp. 181-186.

39. Zheng, Xiulin and Manfred A. Hirt, "Fatigue Crack Propagation in Steels," *Engineering Fracture Mechanics*, Vol. 48, No. 3, June 1983, pp. 965-973.

Appendix A

Specimen Layout, Dimensions and Details of Loading Scenarios

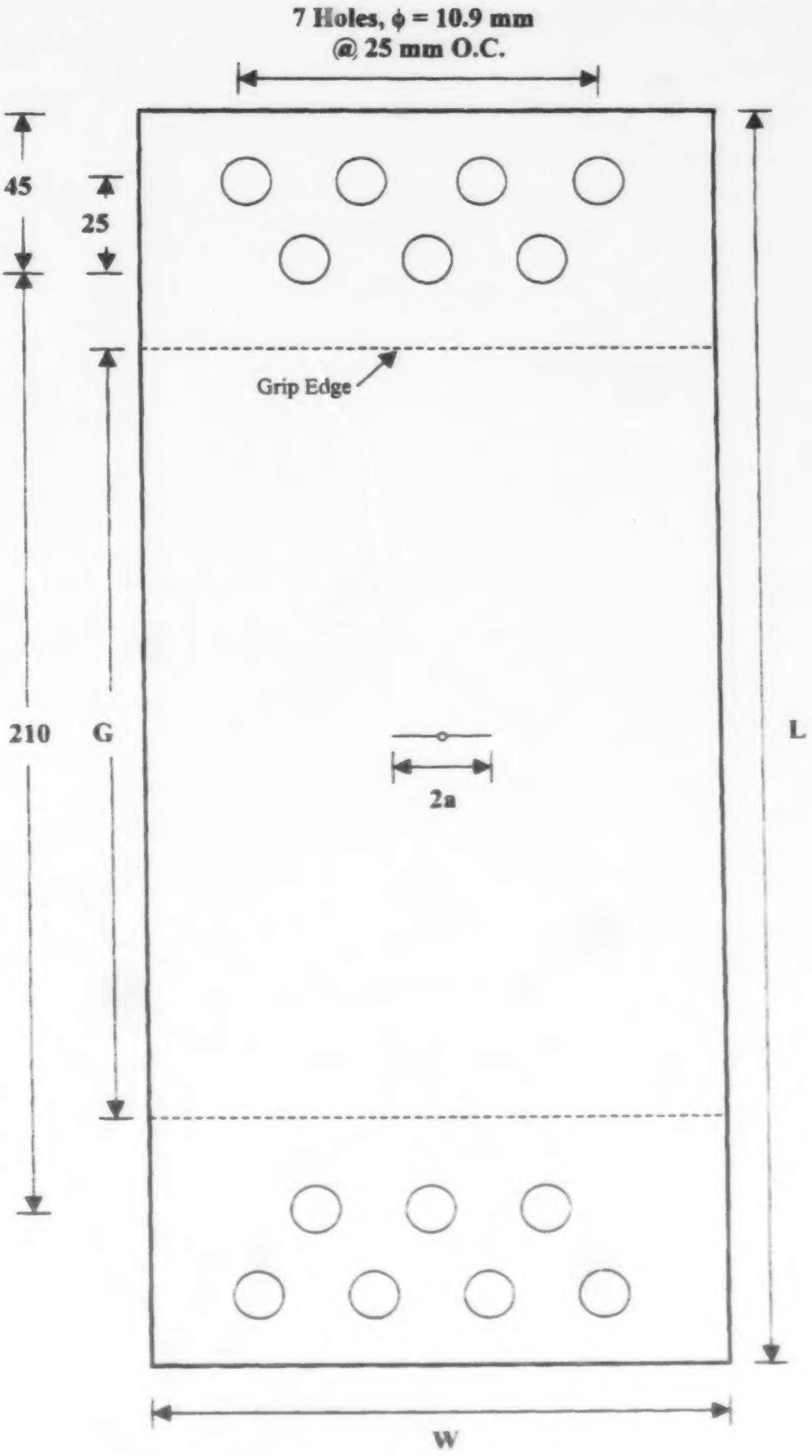

Figure A.1 – Specimen layout

Table A.1 – Specimen dimensions

CAL 1	298.85	100.62	5.37	19.90	169.98
CAL 2	299.72	100.60	5.31	19.90	169.97
CAL 3	297.18	100.54	5.31	19.88	170.00
CAL 4	299.72	100.60	5.34	19.90	169.99
CAL 5	299.72	100.40	5.31	19.87	170.01
CAL 6	299.72	101.74	5.07	19.83	170.00
VAL 1	299.72	101.84	5.06	19.88	170.02
VAL 2	299.72	101.90	5.07	19.85	169.99
VAL 3	298.45	100.58	5.06	19.93	169.98
VAL 4	297.18	100.70	5.06	19.86	170.01
VAL 5	297.18	101.91	5.06	19.88	170.01
VAL 6	298.45	100.55	5.06	19.87	170.00

Table A.2 – Specimen loading scenarios

CAL 1	0.10	-	72700	7200	65500	-	-	-
CAL 2	0.10	-	55000	5500	49500	-	-	-
CAL 3	0.10	-	57000	5700	51300	-	-	-
CAL 4	0.20	-	57000	11400	45600	-	-	-
CAL 5	0.30	-	57500	17250	40250	-	-	-
CAL 6	0.40	-	57500	23000	34500	-	-	-
VAL 1	0.10	1.25	57000	5700	51300	64125	69825	5700
VAL 2	0.10	1.25	57000	5700	51300	64125	69825	5700
VAL 3	0.10	1.50	57000	5700	51300	76950	82650	5700
VAL 4	0.10	1.50	57000	5700	51300	76950	82650	5700
VAL 5	0.10	1.75	57000	5700	51300	89775	95475	5700
VAL 6	0.10	1.75	57000	5700	51300	89775	95475	5700

Note All loads are in Newtons

Appendix B

Example Data Reduction Procedure – Data Sheet, Data Reduction, ‘a versus N’ graph and ‘da/dN versus ΔK’ graph

Specimen No.	**CAL 1**	**(R = 0.10)**		**Load Scenario**			
Width	100.62	mm		**Max**	72700	N	
Thickness	5.37	mm		**Min**	7270	N	
Length	298.85	mm		**Mean**	39985	N	
Initial 2a	19.90	mm					
				Freq.	4	Hz	
Left Edge	0	mm		**R**	0.10		
Left Crack Tip	40.36	mm		**Env.**	Air		
Right Crack Tip	60.26	mm		**Temp.**	Room		
Right Edge	100.62	mm					
	Precracking Data						
	Crack Tip Position		Elapsed				
	Left (mm)	Right (mm)	No. Cycles		**Precracking Load**		
	10.34	10.35	10000		Max	72700	N
	10.48	10.55	12750		Min	7270	N
	10.67	10.74	15500		Mean	39985	N
	10.91	10.98	18250				
	11.16	11.21	21000				
	Fatigue Data						
	Crack Tip Position		Elapsed				
	Left (mm)	Right (mm)	No. Cycles				
	11.44	11.47	23750				
	11.82	11.82	27000				
	12.14	12.15	30000				
	12.49	12.50	33000				
	12.86	12.89	36000				
	13.38	13.43	40000				
	13.95	13.99	44000				
	14.56	14.60	48000				
	15.21	15.26	52000				
	15.88	15.94	56000				
	16.63	16.68	60000				
	17.43	17.48	64000				
	18.35	18.32	68000				
	19.21	19.26	72000				
	20.24	20.25	76000				
	21.28	21.33	80000				
	22.52	22.49	84000				
	23.82	23.82	88000				
	25.23	25.25	92000				
	26.84	26.82	95854	Test Stopped Due to Bolt Failure			

Figure B.1 - Typical experimental data sheet

SPECIMEN NUMBER - CAL 1

LEFT CRACK DATA

Left Measurement (mm)	a (mm)	N (cycles)	Secant Method da/dN (mm/cycle)	Secant Method ΔK (MPa m$^{0.5}$)	Incremental Method da/dN (mm/cycle)	Incremental Method ΔK (MPa m$^{0.5}$)	M.C.C.*
11.44	11.44	0	-	-	-	-	-
11.82	11.82	3250	1.169E-04	23.94	-	-	-
12.14	12.14	6250	1.067E-04	24.35	-	-	-
12.49	12.49	9250	1.167E-04	24.74	1.212E-04	24.94	0.999839
12.86	12.86	12250	1.233E-04	25.16	1.266E-04	25.37	0.999994
13.38	13.38	16250	1.300E-04	25.67	1.368E-04	25.97	0.999995
13.95	13.95	20250	1.425E-04	26.30	1.465E-04	26.63	0.999985
14.56	14.56	24250	1.525E-04	26.97	1.569E-04	27.32	0.999975
15.21	15.21	28250	1.625E-04	27.70	1.681E-04	28.06	0.999954
15.88	15.88	32250	1.675E-04	28.45	1.818E-04	28.84	0.999851
16.63	16.63	36250	1.875E-04	29.27	1.945E-04	29.71	0.999845
17.43	17.43	40250	2.000E-04	30.17	2.096E-04	30.65	0.999857
18.35	18.35	44250	2.300E-04	31.17	2.250E-04	31.67	0.999883
19.21	19.21	48250	2.150E-04	32.23	2.434E-04	32.77	0.999735
20.24	20.24	52250	2.575E-04	33.36	2.641E-04	33.98	0.999775
21.28	21.28	56250	2.600E-04	34.64	2.870E-04	35.32	0.999949
22.52	22.52	60250	3.100E-04	36.08	3.177E-04	36.85	0.999838
23.82	23.82	64250	3.250E-04	37.74	-	-	-
25.23	25.23	68250	3.525E-04	39.59	-	-	-
26.84	26.84	72104	4.177E-04	41.77	-	-	-

RIGHT CRACK DATA

Right Measurement (mm)	a (mm)	N (cycles)	Secant Method da/dN (mm/cycle)	Secant Method ΔK (MPa m$^{0.5}$)	Incremental Method da/dN (mm/cycle)	Incremental Method ΔK (MPa m$^{0.5}$)	M.C.C.*
11.47	11.47	0	-	-	-	-	-
11.82	11.82	3250	1.077E-04	23.96	-	-	-
12.15	12.15	6250	1.100E-04	24.35	-	-	-
12.5	12.5	9250	1.167E-04	24.75	1.226E-04	24.96	0.999958
12.89	12.89	12250	1.300E-04	25.18	1.292E-04	25.40	0.999967
13.43	13.43	16250	1.350E-04	25.72	1.389E-04	26.02	0.999969
13.99	13.99	20250	1.400E-04	26.35	1.482E-04	26.68	0.999975
14.6	14.6	24250	1.525E-04	27.02	1.577E-04	27.37	0.999986
15.26	15.26	28250	1.650E-04	27.75	1.685E-04	28.11	0.999981
15.94	15.94	32250	1.700E-04	28.52	1.801E-04	28.91	0.999981
16.68	16.68	36250	1.850E-04	29.33	1.932E-04	29.76	0.999953
17.48	17.48	40250	2.000E-04	30.23	2.076E-04	30.69	0.999983
18.32	18.32	44250	2.100E-04	31.19	2.240E-04	31.69	0.999980
19.26	19.26	48250	2.350E-04	32.24	2.416E-04	32.79	0.999988
20.25	20.25	52250	2.475E-04	33.40	2.628E-04	34.00	0.999922
21.33	21.33	56250	2.700E-04	34.67	2.871E-04	35.35	0.999912
22.49	22.49	60250	2.900E-04	36.09	3.156E-04	36.86	0.999927
23.82	23.82	64250	3.325E-04	37.72	-	-	-
25.25	25.25	68250	3.575E-04	39.60	-	-	-
26.82	26.82	72104	4.074E-04	41.77	-	-	-

* M C C - multiple correlation coefficient which represent the incremental methods goodness of fit

Figure B.2 – Typical data reduction spreadsheet

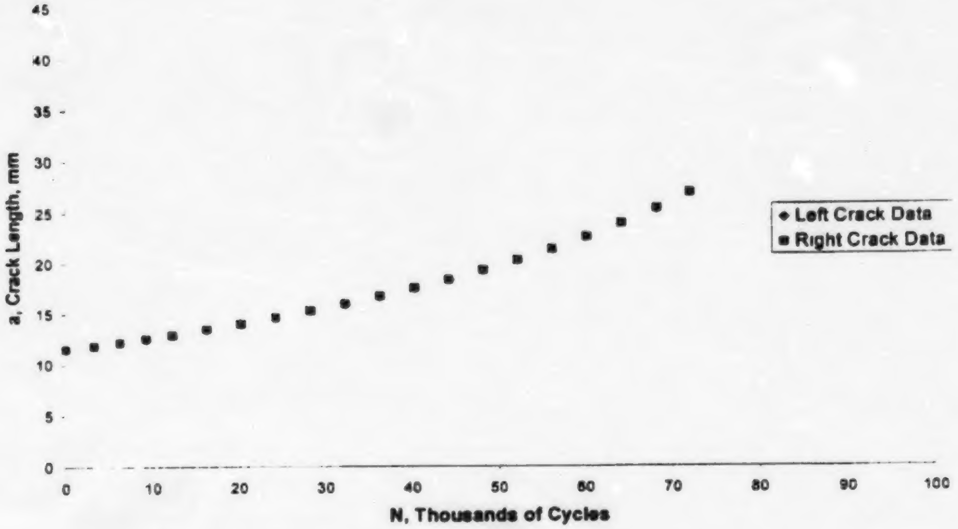

Figure B.3 – Typical *a* versus N graph

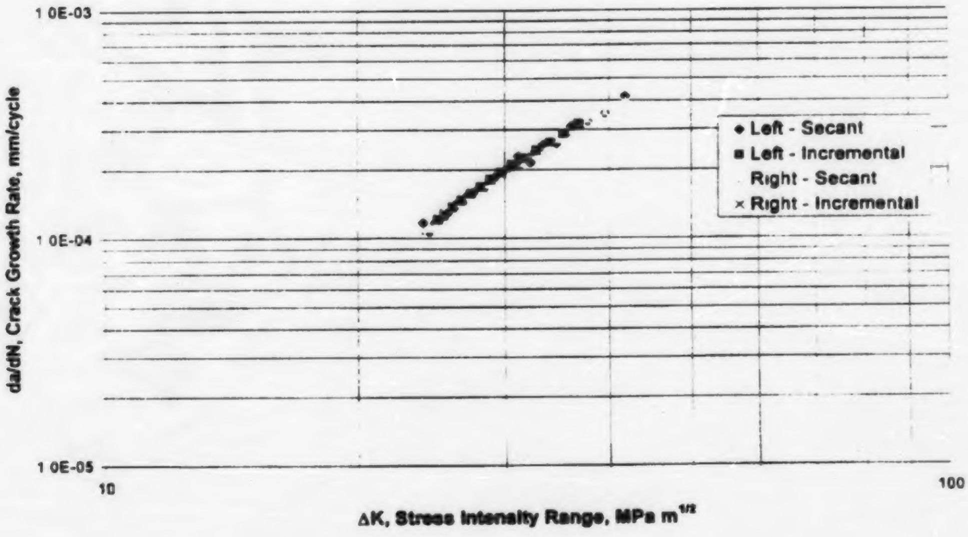

Figure B.3 – Typical d*a*/dN versus ΔK graph

Appendix C

Constant Amplitude Loading Specimens – ‘a versus N’ and ‘da/dN versus ΔK’ graphs

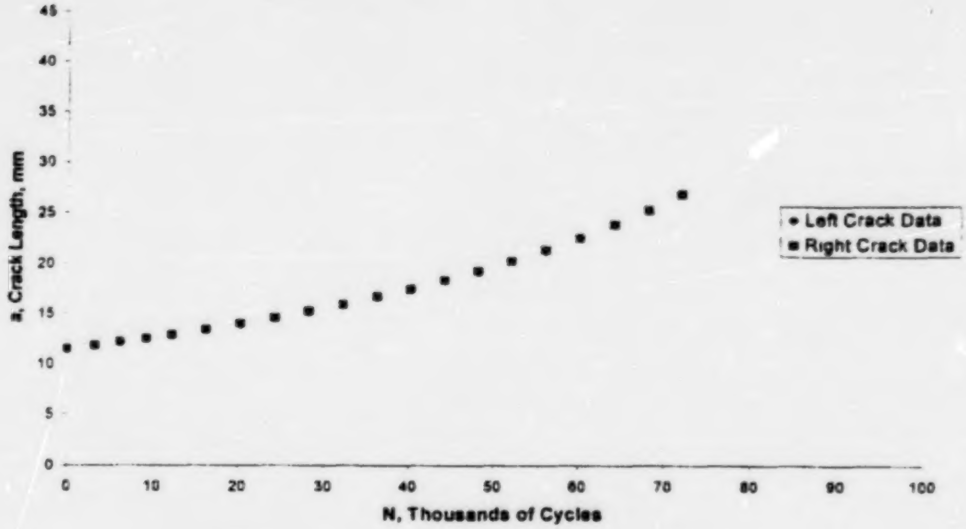

Figure C.1 – Crack length versus cycles for CAL 1

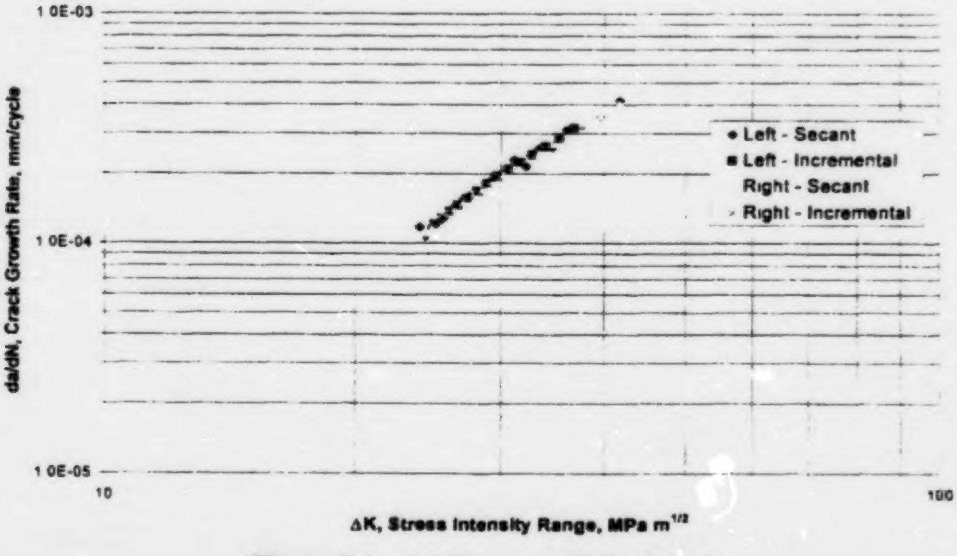

Figure C.2 – d*a*/dN versus ΔK for CAL 1

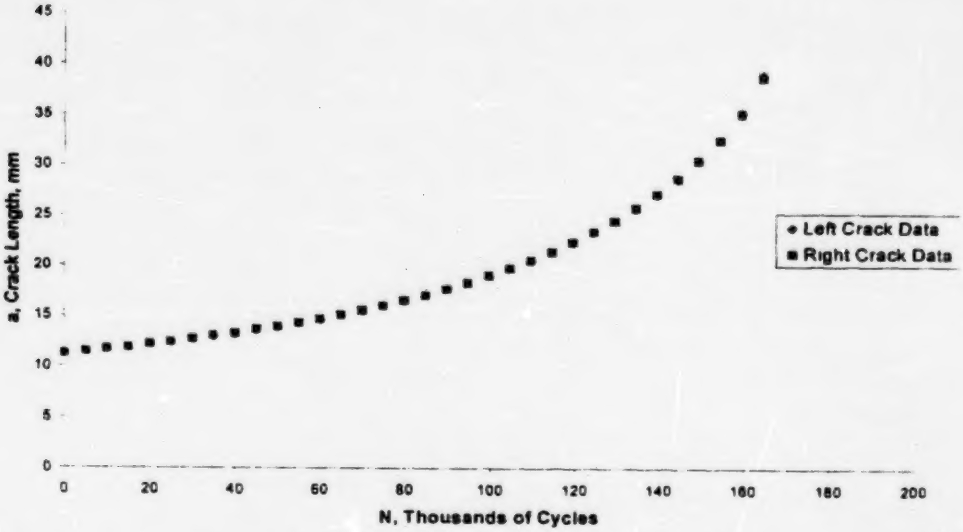

Figure C.3 – Crack length versus cycles for CAL 2

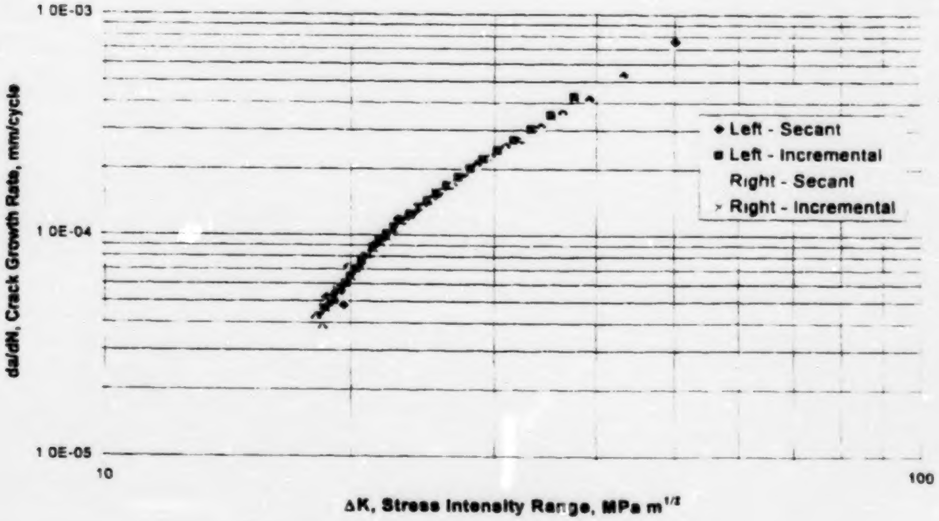

Figure C.4 – d*a*/dN versus ΔK for CAL 2

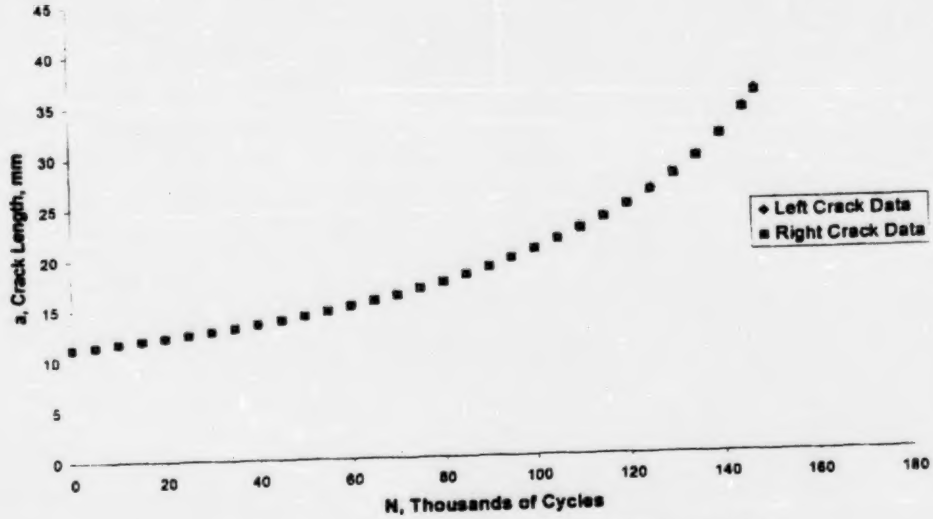

Figure C.5 – Crack length versus cycles for CAL 3

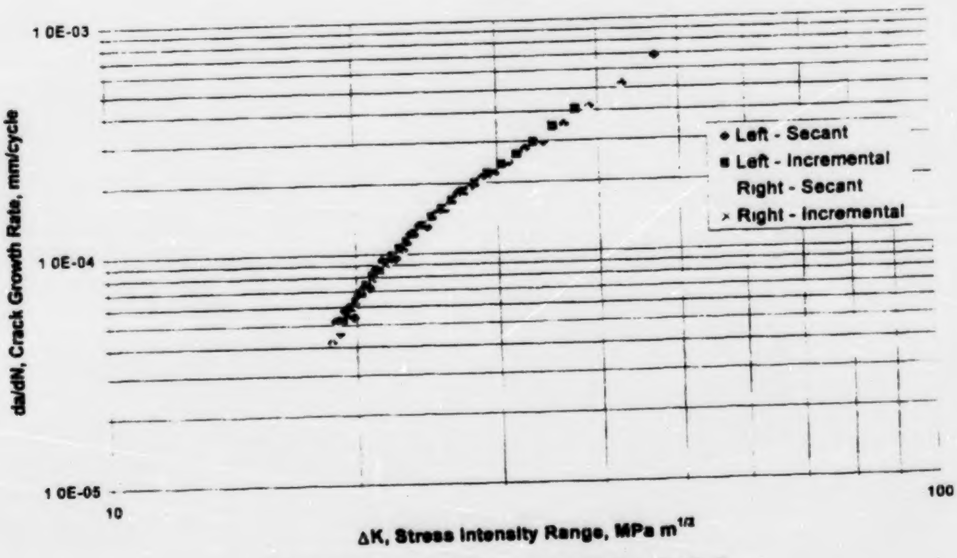

Figure C.6 – d*a*/dN versus ΔK for CAL 3

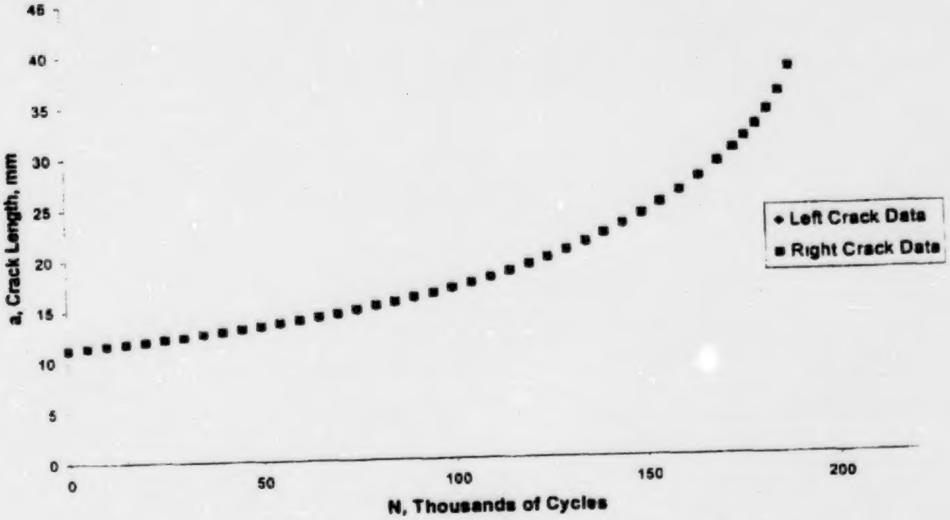

Figure C.7 – Crack length versus cycles for CAL 4

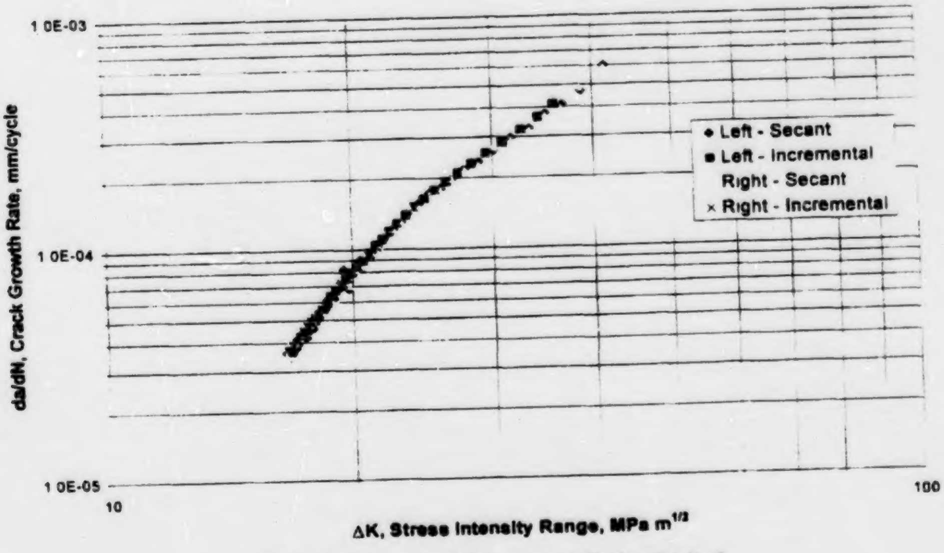

Figure C.8 – d*a*/dN versus ΔK for CAL 4

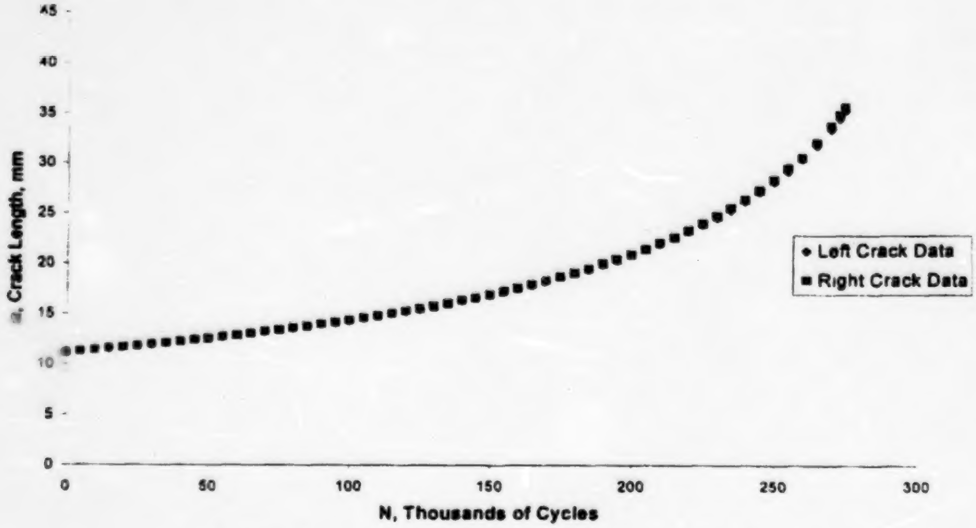

Figure C.9 – Crack length versus cycles for CAL 5

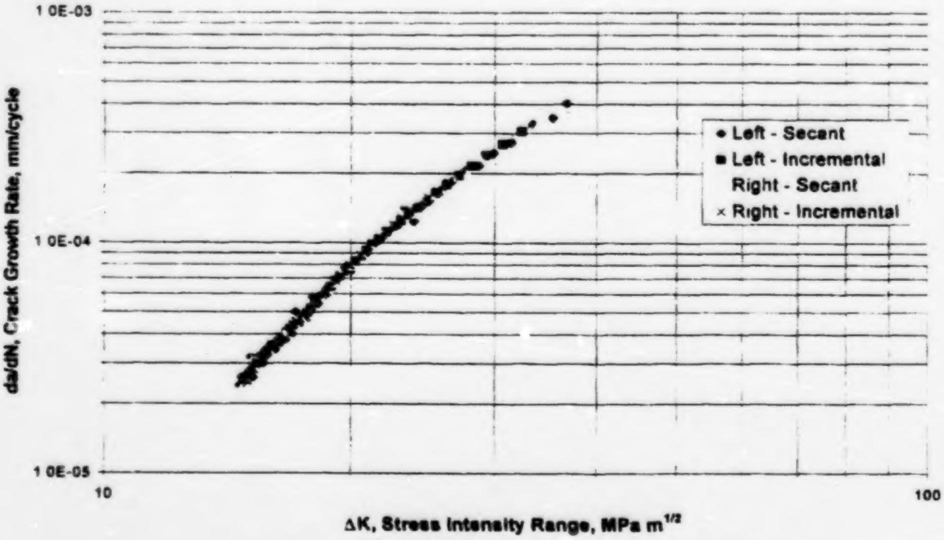

Figure C.10 – d*a*/dN versus ΔK for CAL 5

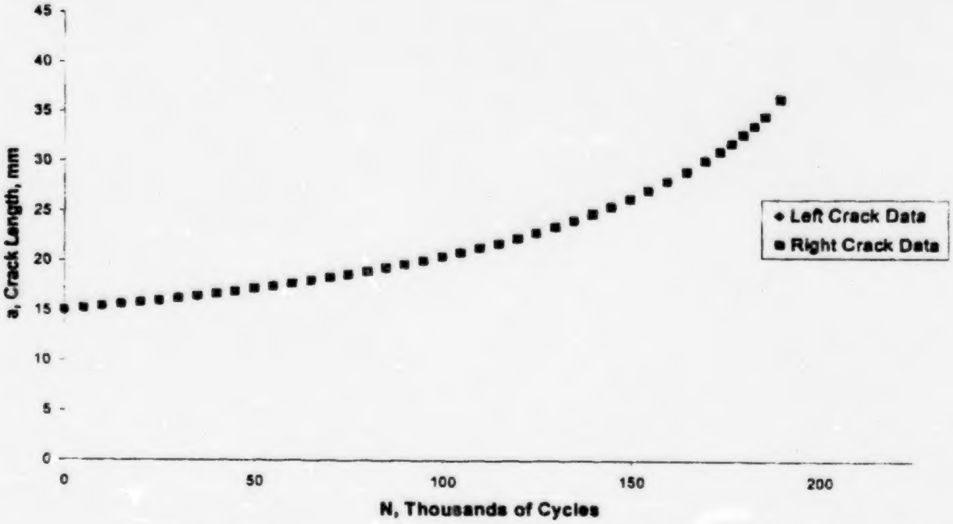

Figure C.11 – Crack length versus cycles for CAL 6

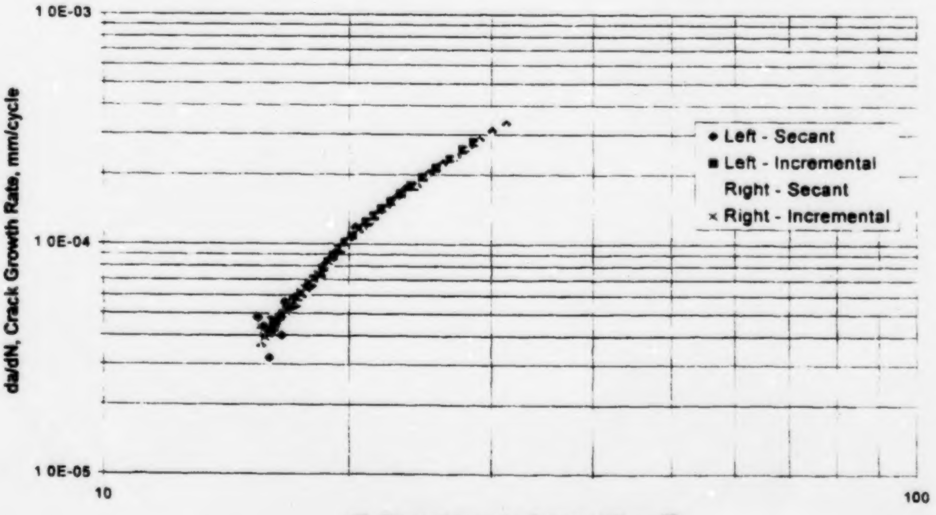

Figure C.12 – d*a*/dN versus ΔK for CAL 6

Appendix D

Experimental Data and Zheng and Hirt's Predictions

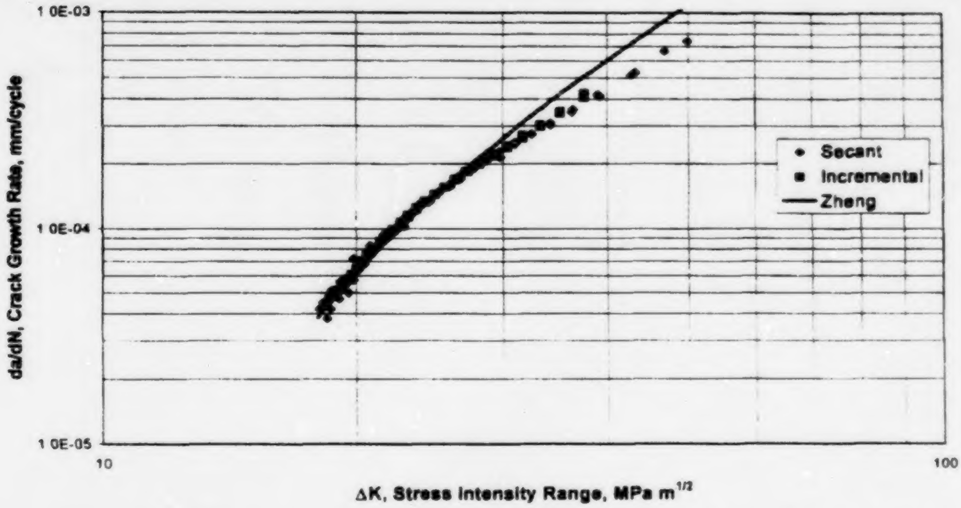

Figure D.1 – Experimental data and Zheng and Hirt's prediction for R = 0.10

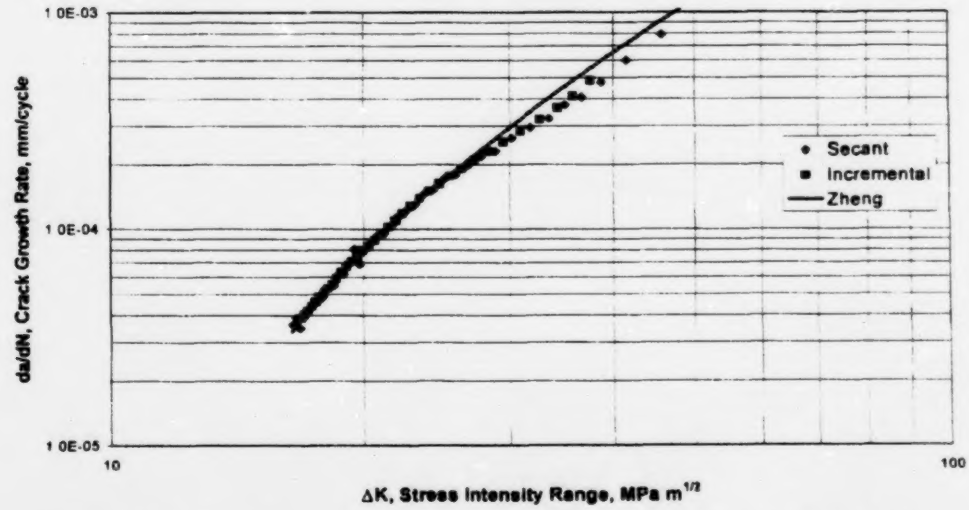

Figure D.2 – Experimental data and Zheng and Hirt's prediction for R = 0.20

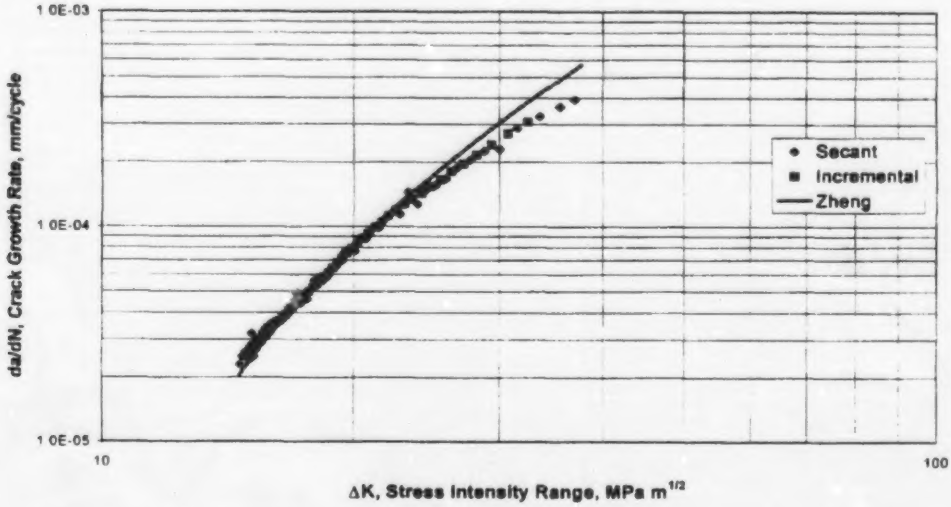

Figure D.3 – Experimental data and Zheng and Hirt's prediction for R = 0.30

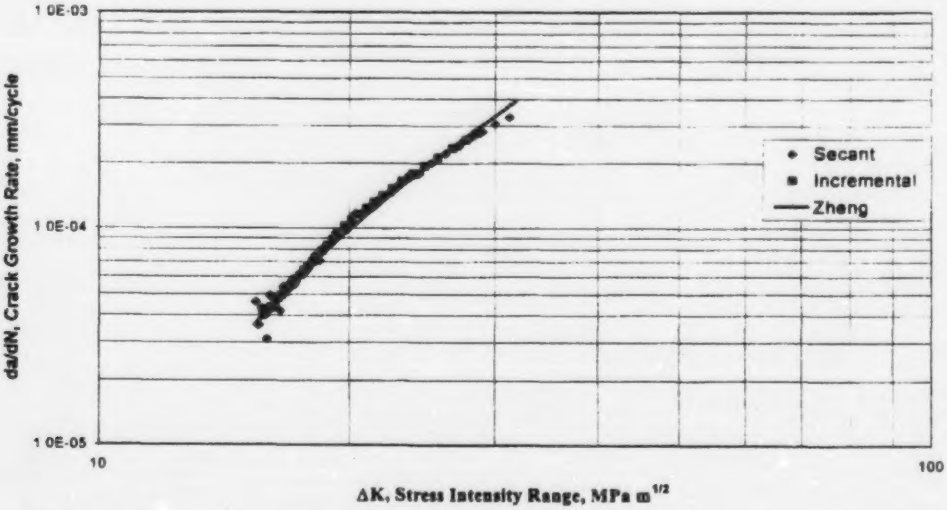

Figure D.4 – Experimental data and Zheng and Hirt's prediction for R = 0.40

Appendix E

Variable Amplitude Loading Specimens – ‘a versus N’ and ‘da/dN versus ΔK’ graphs

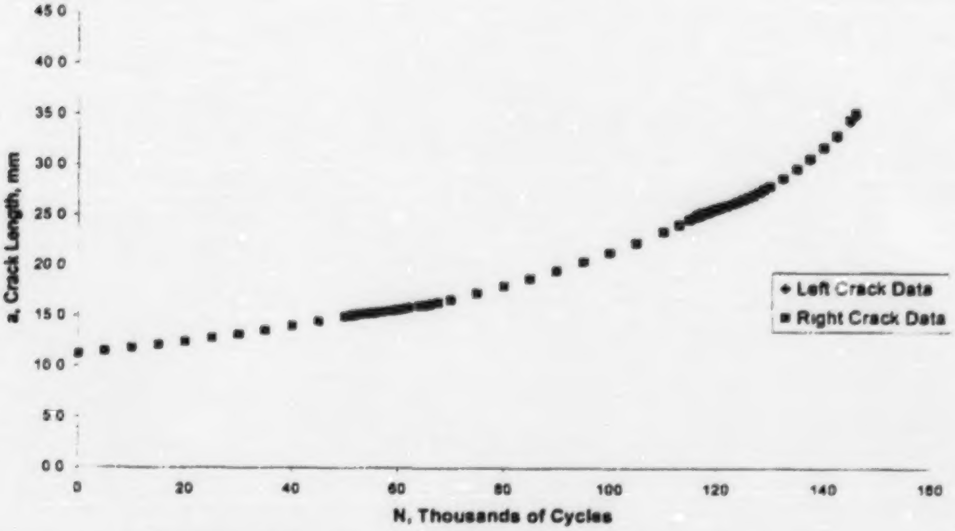

Figure E.1 – Crack length versus cycles for VAL 1

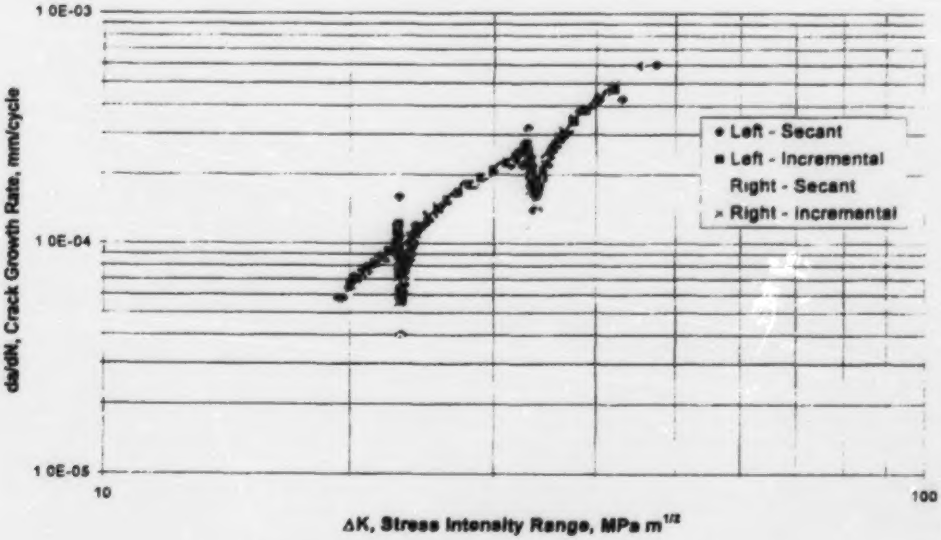

Figure E.2 – d*a*/dN versus ΔK for VAL 1

Crack Length vs. Cycles - VAL 2 (OLR = 1.25)

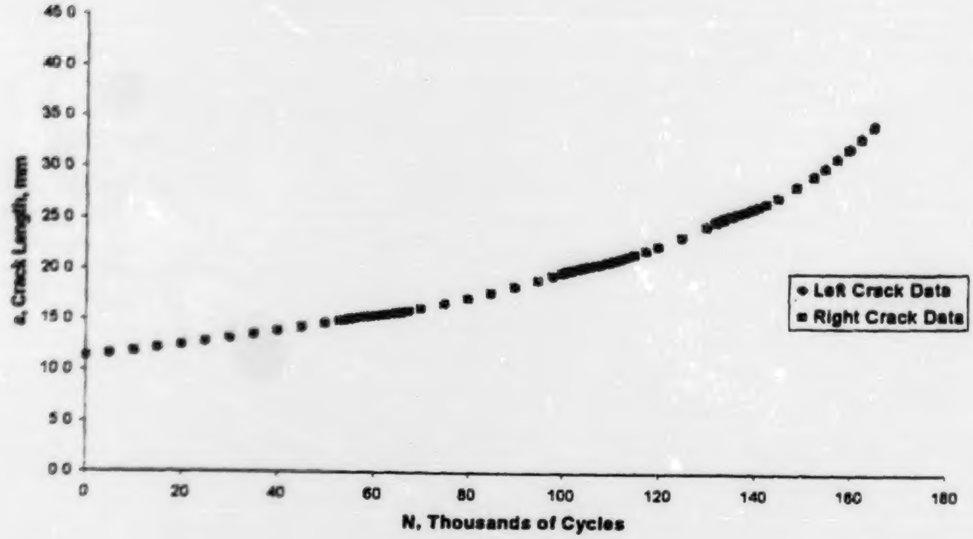

da/dN vs. ΔK - VAL 2 (OLR = 1.25)

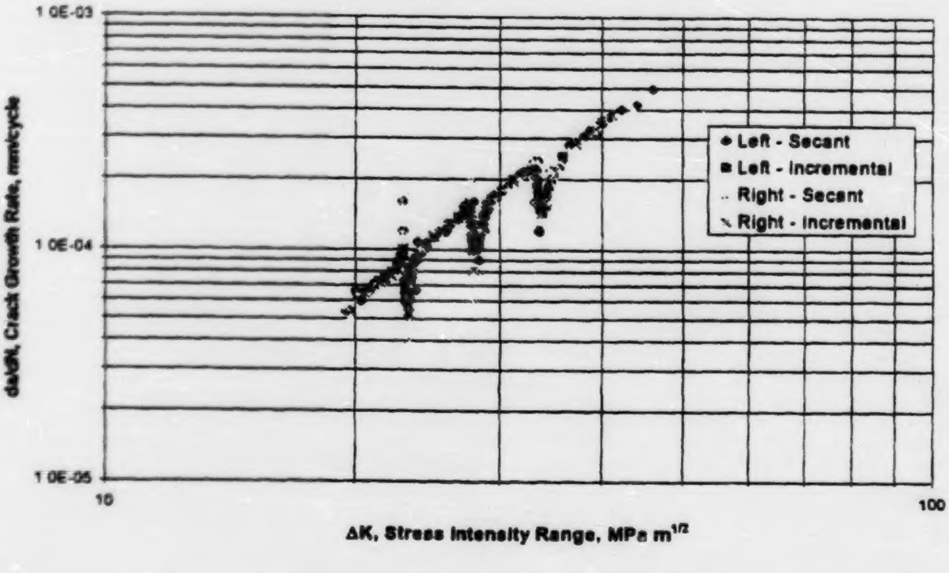

Crack Length vs. Cycles - VAL 3 (OLR = 1.50)

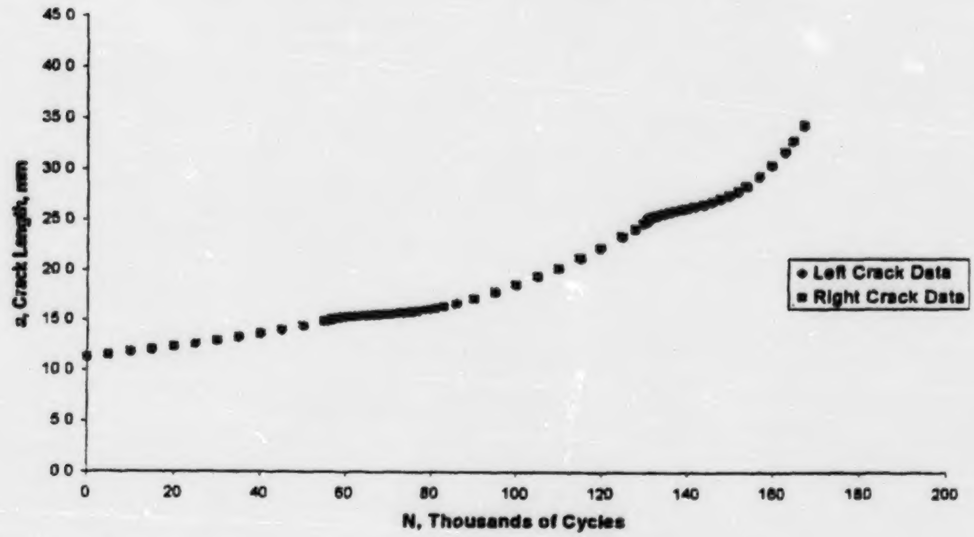

da/dN vs. ΔK - VAL 3 (OLR = 1.50)

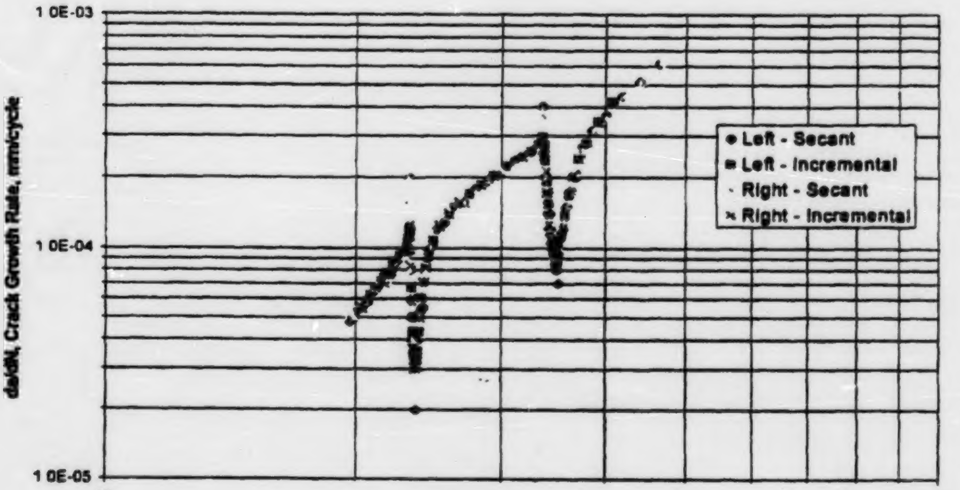

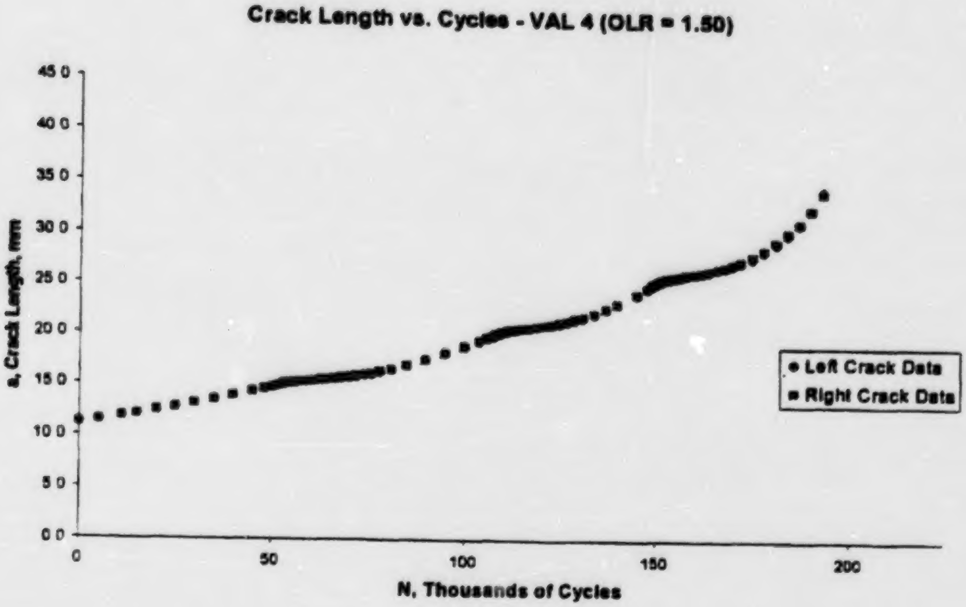

Crack Length vs. Cycles - VAL 4 (OLR = 1.50)

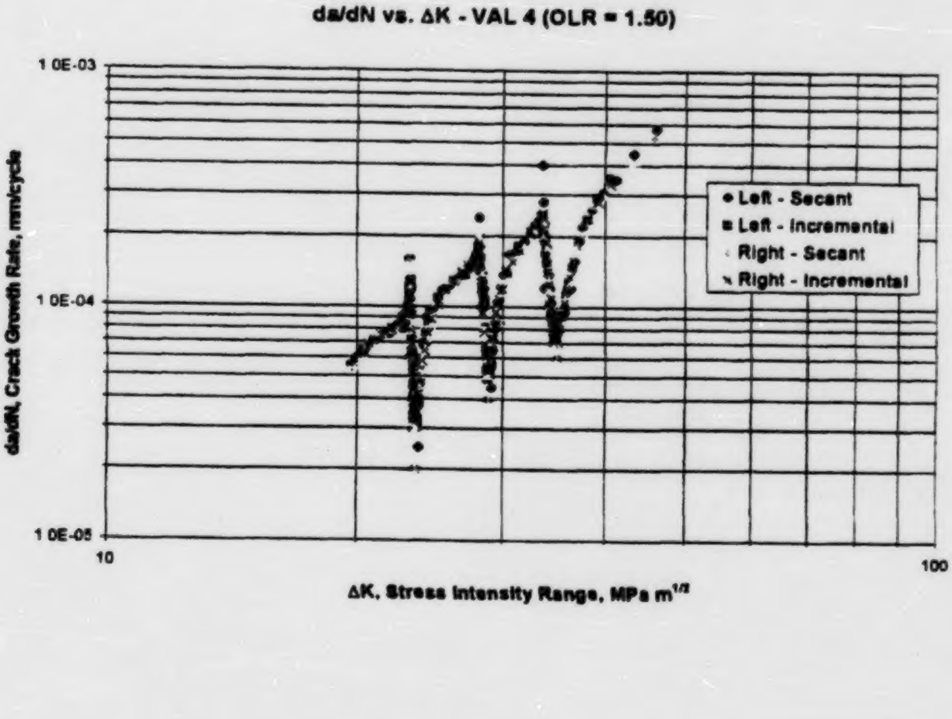

da/dN vs. ΔK - VAL 4 (OLR = 1.50)

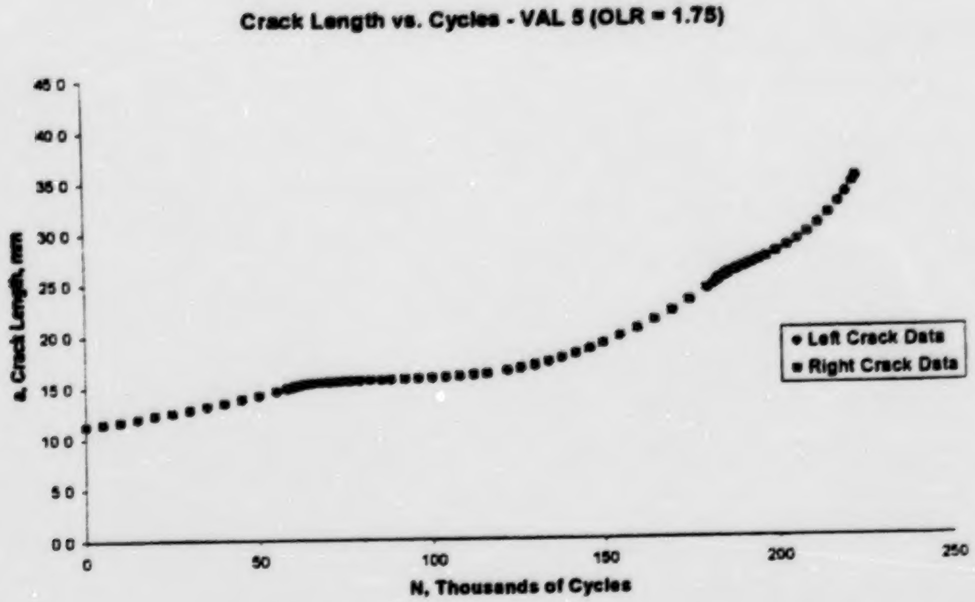
Crack Length vs. Cycles - VAL 5 (OLR = 1.75)
a, Crack Length, mm
45.0
40.0
35.0
30.0
25.0
20.0
15.0
10.0
5.0
0.0
0
50
100
150
200
250
N, Thousands of Cycles
● Left Crack Data
■ Right Crack Data

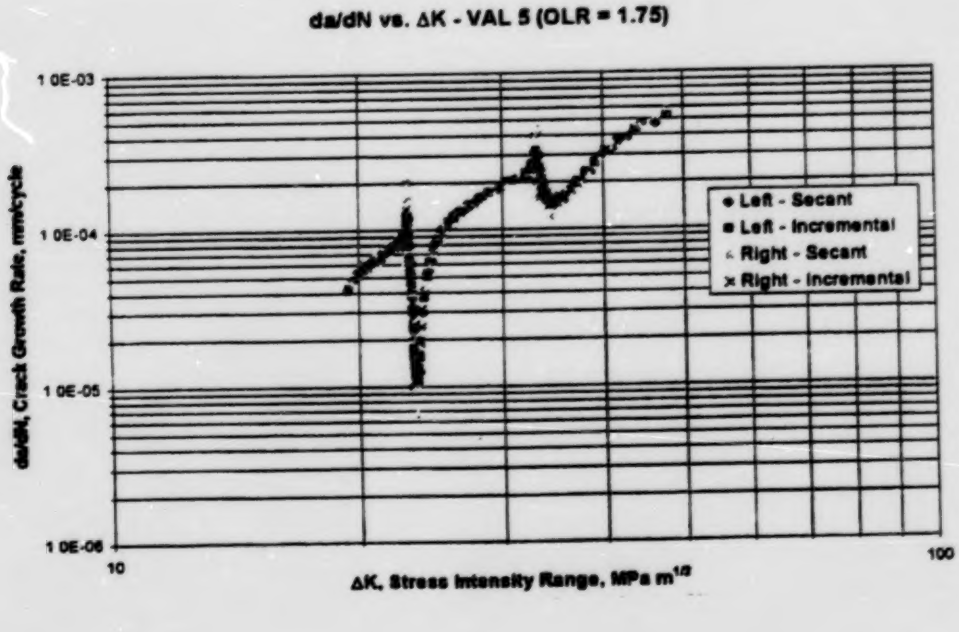
da/dN vs. ΔK - VAL 5 (OLR = 1.75)
da/dN, Crack Growth Rate, mm/cycle
1.0E-03
1.0E-04
1.0E-05
1.0E-06
10
100
ΔK, Stress Intensity Range, MPa m^1/2
● Left - Secant
■ Left - Incremental
▲ Right - Secant
× Right - Incremental

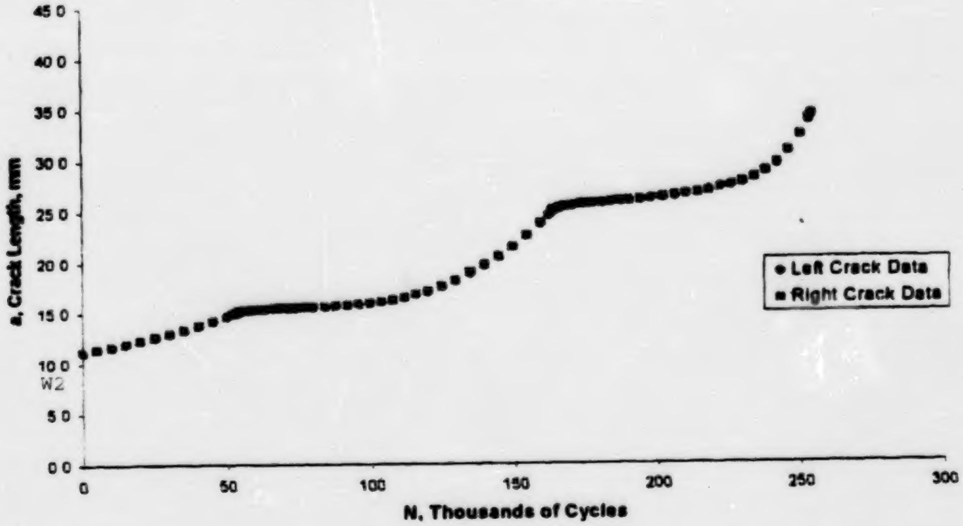

Crack Length vs. Cycles - VAL 6 (OLR = 1.75)

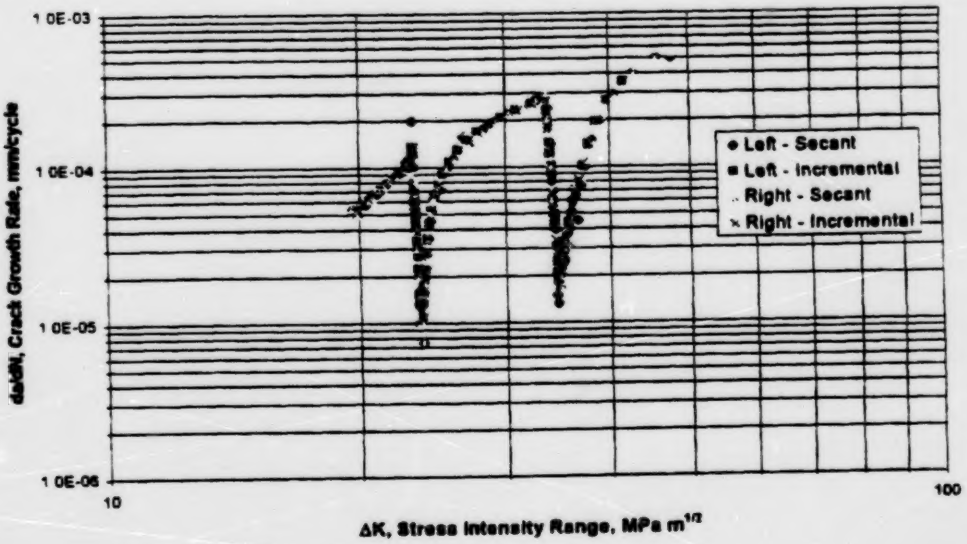

da/dN vs. ΔK - VAL 6 (OLR = 1.75)

Appendix F

Fortran Program used to Convert the NISA (.NIS) File to the FAST-I Input Data File Format

```
C
C    Program to translate the NISA Model File to FAST
C    Input File for Analysis  The NISA file is the
C    output from the preprocessor showing the nodal
C    coordiantes, element numbering and boundary conditions
C
        PROGRAM CONVERT
        PARAMETER (M=700)
        REAL MTL,NEGA,INITIAL
        DIMENSION NN(M),Xc(M),Yc(M),Zc(M)
        DIMENSION EN(M),ELPR(M)
        DIMENSION N1(M),N2(M),N3(M),N4(M)
        DIMENSION N5(M),N6(M),N7(M),N8(M)
        DIMENSION N9(M),N10(M),N11(M),N12(M)
        DIMENSION NNBC(M),DOF(M)
        CHARACTER COMMA*4,D1*1,NAME*10,NAME1*10,JUNK*80,D8,TITLE*80
        CHARACTER DOF*4,D3*3,ANS*1
        INTEGER POSX,POSY,NEGX,NEGY
C
        PRINT *,'Input Total Number of Nodes in Model (#): '
        READ(*,*)NNOD
        PRINT *,'Input Total Number of Elements in Model (#): '
        READ(*,*)NELM
        PRINT *, 'Input Total Number of Boundary Conditions (#): '
        READ(*,*)NBC
        PRINT *,'Input Total Number of Elements under Pressure (#): '
        READ(*,*)NELPR
C
C Read FE model data
C
        PRINT *, 'What is the name of the nisa file to convert? '
        READ (*,*) NAME
        OPEN(10,FILE=NAME,STATUS='UNKNOWN')
C
        DO 10 I = 1,NNOD
          READ(10,20) NN(I),COMMA,Xc(I),D1,Yc(I),
   +         D1,Zc(I),D1,I1
 20    FORMAT (I6,A4,E12 5,A1,E12.5,A1,E12 5,A1,I6)
 10  CONTINUE
C
        READ (10,25) JUNK
 25  FORMAT (A9)
C
        DO 30 I = 1,NELM
          READ(10,40) EN(I),D1,I1,D1,I1,D1,I1,D1,I1
 40    FORMAT(I6,A1,I6,A1,I6,A1,I6,A1,I6)
          READ(10,50) N1(I),D1,N2(I),D1,N3(I),D1,N4(I),D1,
   +         N5(I),D1,N6(I),D1,N7(I),D1,N8(I),D1,
   +         N9(I),D1,N10(I),D1
 50    FORMAT(I6,A1,I6,A1,I6,A1,I6,A1,
   +       I6,A1,I6,A1,I6,A1,I6,A1,
   +       I6,A1,I6,A1)
```

```
          READ(10,52) N11(I),D1,N12(I),D1
 52     FORMAT(I6,A1,I6,A1)
 30   CONTINUE
C
        DO 160 I = 1,NBC
          READ (10,170) NNBC(I),D1,DOF(I),D1,DISP,D8,I6
 170    FORMAT(I6,A1,A4,A1,E12.5,A8,I6)
 160  CONTINUE
C
        DO 260 I = 1,NELPR
          READ (10,262) ELPR(I), D3,I1,D1,I1,D1,I3,D1,PRESS,D1,I6
 262    FORMAT(I6,A3,I1,A1,I1,A1,I3,A1,E9.3,A1,I6)
 260  CONTINUE
C
C     WRITE DATA TO FILE
C
        PRINT *, 'What is the name of the fast output file? '
        READ (*,*) NAME1
C
        OPEN(20,FILE=NAME1,STATUS='UNKNOWN')
C
        PRINT *, 'Enter the number of shifts required '
        READ (*,*) NSHIFT
        PRINT *, 'Enter the number of plots required '
        READ (*,*) NPLOT
        WRITE(20,180) NSHIFT,NPLOT
 180  FORMAT(I2,',',I1)
C
        PRINT *, 'Enter the title '
        READ (*,*) TITLE
        WRITE(20,*) TITLE
C
        PRINT *, 'Type of analysis? 0 = axisymmetric problem'
        PRINT *, '                  1 = plane strain problem'
        PRINT *, '                  2 = plane stress problem'
        PRINT *, '                                          '
        READ (*,*)ISTRN
        PRINT *, 'Enter the number of crack tips in model '
        READ (*,*)NFRAC
        WRITE (20,190) NNOD,NELM,ISTRN,NFRAC,NPLOT
 190  FORMAT(I4,1X,I3,1X,'1 ',I1,1X,'0 0 0 0 -',I1,1X,I1,' 3')
C
        PRINT *, 'What is poissons ratio? '
        READ (*,*) POISSON
        PRINT *, 'What is the modulus of elasticity? '
        READ (*,*) MODULUS
        WRITE(20,200) POISSON
 200  FORMAT(F4.2,'/')
        WRITE(20,210) MODULUS
 210  FORMAT(I6,'/')
C
        PRINT *, 'What is the material thickness? '
        READ (*,*) MTL
```

```
          DO 80 I = 1,NELM
            IF (I  EQ. 1) THEN
                    WRITE(20,90) EN(I),N1(I),N2(I),N3(I),N4(I),
     +                   N5(I),N6(I),N7(I),N8(I),
     +                   N9(I),N10(I),N11(I),N12(I),MTL
 90         FORMAT(I3,I4,I4,I4,I4,I4,I4,I4,I4,I4,I4,I4,I4,' 1. ',
     +           F4 2)
            ELSE
                    WRITE(20,92) EN(I),N1(I),N2(I),N3(I),N4(I),
     +                   N5(I),N6(I),N7(I),N8(I),
     +                   N9(I),N10(I),N11(I),N12(I)
 92         FORMAT(I3,I4,I4,I4,I4,I4,I4,I4,I4,I4,I4,I4,I4,'/')
            ENDIF
 80   CONTINUE
          WRITE (20,*) '0/'
C
          DO 60 I = 1,NNOD
            IF (I  EQ  1) THEN
                    WRITE(20,70) NN(I),Xc(I),Yc(I)
 70         FORMAT(I4,1X,E13 6,1X,E13 6,1X,'0. 0. 0.')
            ELSE
                    WRITE(20,72) NN(I),Xc(I),Yc(I)
 72         FORMAT(I4,1X,E13 6,1X,E13 6,'/')
            ENDIF
 60   CONTINUE
          WRITE (20,*) '0/'
C
          PRINT *, 'Enter the number of nodes moving in +x '
          READ *, POSX
          PRINT *, 'Enter the number of nodes moving in +Y '
          READ *, POSY
          PRINT *, 'Enter the number of nodes moving in -X '
          READ *, NEGX
          PRINT *, 'Enter the number of nodes moving in -y '
          READ *, NEGY
          WRITE (20,252) POSX,POSY,NEGX,NEGY
 252  FORMAT(I2,',',I2,',',I2,',',I2)
C
          IF (POSX .NE  '0')
          DO 111 I = 1,POSX
            PRINT *, 'Enter the +x node number  #',I
            READ (*,*) XPOS(I)
 111  CONTINUE
          ENDIF
          WRITE (20,119)

          PRINT *, 'Enter the positive delta a '
          READ *, POSA
          PRINT *, 'Enter the negative delta a -'
          READ *, NEGA
          WRITE (20,254) POSA,NEGA
 254  FORMAT(F4.2,',-',F4.2)
C
```

```
        DO 220 I = 1,NBC
          IF (DOF(I) .EQ. 'UX  ') THEN
                WRITE(20,232) NNBC(I)
232       FORMAT(I4,1X,'1 0. 0. 0.')
          ELSE
                WRITE(20,234) NNBC(I)
234       FORMAT(I4,1X,'2 0. 0  0 ')
          ENDIF
220  CONTINUE
        WRITE (20,*) '0/'
C
        DO 300 I = 1,NELPR
          XX = ELPR(I)
          IF (I  EQ  1) THEN
                WRITE (20,302) N7(XX),N8(XX),N9(XX),N10(XX),PRESS
302       FORMAT(I4,1X,I4,1X,I4,1X,I4,1X,E9.3,' 0. 0  0. 0')
          ELSE
                WRITE (20 304) N7(XX),N8(XX),N9(XX).N10(XX),PRESS
304       FORMAT(I4,1X,I4,1X,I4,1X,I4,1X,E9 3,'/')
          ENDIF
300  CONTINUE
        WRITE (20,*) '0/'
C
        WRITE (20,*) '0/'
        PRINT *, 'Is their a nodal LOAD present? Y/N '
        READ *, ANS
        IF (ANS  EQ  'Y') THEN
          PRINT *, 'YOU MUST MODIFY FORTRAN PROGRAM TO INCLUDE NODAL LOAD'
          PRINT *, 'OR MANUALLY PUT IT IN THE OUTPUT FILE '
          STOP
        ENDIF
C
        DO 400 I = 1,NFRAC
          PRINT *, 'What is the crack tip number #',I,' = '
          READ *, TIP
          PRINT *, 'What is the corresponding intial crack length'
          READ *, INITIAL
          WRITE (20,402) TIP,INITIAL
402     FORMAT(I4,1X,'1 0  ',F8 4)
400  CONTINUE
C
C
C    This part repeats the file except changes the pressure value
C
C
        WRITE(20,500) NSHIFT,NPLOT
500  FORMAT(I2,',',I1)
C
        WRITE(20,*) TITLE
C
        WRITE (20,510) NNOD,NELM,ISTRN,NFRAC,NPLOT
510  FORMAT(I4,1X,I3,1X,'1 ',I1,1X,'0 0 0 0 -',I1,1X,I1,' 3')
C
```

```
        WRITE(20,520) POISSON
 520  FORMAT(F4.2,'/')
        WRITE(20,530) MODULUS
 530  FORMAT(I6,'/')
C
        DO 540 I = 1,NELM
          IF (I .EQ. 1) THEN
                WRITE(20,542) EN(I),N1(I),N2(I),N3(I),N4(I),
   +                  N5(I),N6(I),N7(I),N8(I),
   +                  N9(I),N10(I),N11(I),N12(I),MTL
 542      FORMAT(I3,I4,I4,I4,I4,I4,I4,I4,I4,I4,I4,I4,I4,' 1. ',
   +        F4.2)
          ELSE
                WRITE(20,544) EN(I),N1(I),N2(I),N3(I),N4(I),
   +                  N5(I),N6(I),N7(I),N8(I),
   +                  N9(I),N10(I),N11(I),N12(I)
 544      FORMAT(I3,I4,I4,I4,I4,I4,I4,I4,I4,I4,I4,I4,I4,'/')
          ENDIF
 540  CONTINUE
        WRITE (20,*) '0/'
C
        DO 550 I = 1,NNOD
          IF (I .EQ. 1) THEN
                WRITE(20,552) NN(I),Xc(I),Yc(I)
 552     FORMAT(I4,1X,E13.6,1X,E13.6,1X,'0  0  0.')
          ELSE
                WRITE(20,554) NN(I),Xc(I),Yc(I)
 554      FORMAT(I4,1X,E13.6,1X,E13.6,'/')
          ENDIF
 550  CONTINUE
        WRITE (20,*) '0/'
C
        WRITE (20,560) POSX,POSY,NEGX,NEGY
 560  FORMAT(I2,',',I2,',',I2,',',I2)
        WRITE (20,570) POSA,NEGA
 570  FORMAT(F4.2,'-',F4.2)
C
        DO 580 I = 1,NBC
          IF (DOF(I) .EQ. 'UX  ') THEN
                WRITE(20,582) NNBC(I)
 582     FORMAT(I4,1X,'1 0  0  0 ')
          ELSE
                WRITE(20,584) NNBC(I)
 584     FORMAT(I4,1X,'2 0  0  0 ')
          ENDIF
 580  CONTINUE
        WRITE (20,*) '0/'
C
        PRINT *, 'What is the minimum stress? '
        READ *, PRESS1
        PRESS = PRESS1
        DO 590 I = 1,NELPR
          XX = ELPR(I)
          IF (I  EQ. 1) THEN
                WRITE (20,592) N7(XX),N8(XX),N9(XX),N10(XX),PRESS
 592     FORMAT(I4,1X,I4,1X,I4,1X,I4,1X,E9.3,' 0. 0  0. 0')
          ELSE
                WRITE (20,594) N7(XX),N8(XX),N9(XX),N10(XX),PRESS
 594     FORMAT(I4,1X,I4,1X,I4,1X,I4,1X,E9 3,'/')
          ENDIF
 590  CONTINUE
        WRITE (20,*) '0/'
C
        WRITE (20,*) '0/'
C
        DO 600 I = 1,NFRAC
          WRITE (20,602) TIP,INITIAL
 602    FORMAT(I4,1X,'1 0  ',F8 4)
 600  CONTINUE
        WRITE (20,*) '/'
C
C
        DO 900 I = 1,33
          PRINT '(/)'
 900  CONTINUE
        PRINT *, 'REMEMBER TO MAUALLY ADD +X,+Y,-X,-Y'
        PRINT '(//)'
        PRINT *, 'CHECK CRACK TIP NODE   ELEMENT NODE NUMBERING'
        PRINT *, 'MUST BEGIN WITH CRACK TIP NODE NUMBER'
        PRINT '(//)'
        PRINT *, 'CHECK ELEMENTS PRESSURE APPLIED CORRESPONDING TO '
        PRINT *, 'N7 TO N10'
        END
```

UNCLASSIFIED
SECURITY CLASSIFICATION OF FORM
(highest classification of Title, Abstract, Keywords)

DOCUMENT CONTROL DATA

(Security classification of title, body of abstract and indexing annotation must be entered when the overall document is classified)

1 **ORIGINATOR** (the name and address of the organization preparing the document.. Organizations for whom the document was prepared, e g Establishment sponsoring a contractor's report, or tasking agency, are entered in section 8)

DalTech, P.O. Box 1000, Halifax, NS

2 **SECURITY CLASSIFICATION** (overall security classification of the document including special warning terms if applicable).

UNCLASSIFIED

3 **TITLE** (the complete document title as indicated on the title page. Its classification should be indicated by the appropriate abbreviation (S,C,R or U) in parentheses after the title).

Experimental and Numerical Investigation into Fatigue Crack Propagation Models for 350WT Steel

4 **AUTHORS** (Last name, first name, middle initial If military, show rank, e.g Doe, Maj John E.)

D. A. Trask

5 **DATE OF PUBLICATION** (month and year of publication of document)

June 2000

6a **NO OF PAGES** (total containing information Include Annexes, Appendices, etc)

200 (approx.)

6b **NO OF REFS** (total cited in document)

39

7 **DESCRIPTIVE NOTES** (the category of the document, e g technical report, technical note or memorandum If appropriate, enter the type of report, e g interim, progress, summary, annual or final Give the inclusive dates when a specific reporting period is covered)

CONTRACTOR REPORT

8 **SPONSORING ACTIVITY** (the name of the department project office or laboratory sponsoring the research and development Include address)

Defence Research Establishment Atlantic
PO Box 1012
Dartmouth, NS, Canada B2Y 3Z7

9a **PROJECT OR GRANT NO** (if appropriate, the applicable research and development project or grant number under which the document was written Please specify whether project or grant).

Project 1.g.c.11

9b **CONTRACT NO** (if appropriate, the applicable number under which the document was written)

W7707-6-3591

10a **ORIGINATOR'S DOCUMENT NUMBER** (the official document number by which the document is identified by the originating activity This number must be unique to this document)

10b **OTHER DOCUMENT NOs** (Any other numbers which may be assigned this document either by the originator or by the sponsor)

DREA CR/98/436

11 **DOCUMENT AVAILABILITY** (any limitations on further dissemination of the document, other than those imposed by security classification)

(x) Unlimited distribution
(   ) Defence departments and defence contractors; further distribution only as approved
(   ) Defence departments and Canadian defence contractors; further distribution only as approved
(   ) Government departments and agencies; further distribution only as approved
(   ) Defence departments; further distribution only as approved
(   ) Other (please specify):

12 **DOCUMENT ANNOUNCEMENT** (any limitation to the bibliographic announcement of this document This will normally correspond to the Document Availability (11) However, where further distribution (beyond the audience specified in (11) is possible, a wider announcement audience may be selected)

UNCLASSIFIED
SECURITY CLASSIFICATION OF FORM

13 ABSTRACT (a brief and factual summary of the document It may also appear elsewhere in the body of the document itself It is highly desirable that the abstract of classified documents be unclassified Each paragraph of the abstract shall begin with an indication of the security classification of the information in the paragraph (unless the document itself is unclassified) represented as (S), (C), (R), or (U) It is not necessary to include here abstracts in both official languages unless the text is bilingual)

Fatigue analysis is a complex and uncertain process due to the numerous factors that may influence the crack growth process. The development of a fatigue model is important for planning inspection intervals, determining required maintenance, conducting a failure analysis and minimizing the problem of crack propagation in future designs. Various models have been proposed; however, no universal or all encompassing model exists.

A state-of-the-art literature review of the available fatigue crack propagation models was conducted to identify their advantages, disadvantages and limitations. Emphasis was placed on models that are simple to evaluate and require few (if any) empirical curve fitting parameters.

An experimental fatigue program was conducted, consisting of both a constant and variable amplitude loading phase on 350WT steel. This is an important structural steel with application to ships, bridges, cranes and towers; all of which are subjected to cyclic loading. The objective of the constant amplitude loading phase was to establish some baseline fatigue data at various stress ratios and to calibrate the available constant amplitude models. The objective of the variable amplitude loading phase was to quantify the magnitude of retardation when periodic tensile overloads are applied in a constant amplitude loading scenario. The fatigue models examined in the literature review were evaluated (spreadsheet method) and the results compared to those obtained from the experiments.

Two fracture-parameter and two fatigue-life prediction software packages were examined and their limitations and advantages were compared. The fracture-parameter progams use the finite element method to calcualate the required parameters for various crack lengths. The fatigue-life prediction programs use the results of the fracture program in conjunction with pre-programmed fatigue models to predict the structures' fatigue life. The test specimens were evaluated with the numerical programs and the results compared to those obtained from the experiments.

14 KEYWORDS, DESCRIPTORS or IDENTIFIERS (technically meaningful terms or short phrases that characterize a document and could be helpful in cataloguing the document They should be selected so that no security classification is required Identifiers, such as equipment model designation, trade name, military project code name, geographic location may also be included If possible keywords should be selected from a published thesaurus e g Thesaurus of Engineering and Scientific Terms (TEST) and that thesaurus-identified If it not possible to select indexing terms which are Unclassified, the classification of each should be indicated as with the title)

Ship
Structures
Fracture
Fatigue
Materials
Experimental testing